PhD Thesis

THE THERMAL MODELING OF TRADITIONAL DOUBLE-SKIN BOX TYPE WINDOWS

Kéthéjú történeti ablakok hőtechnikai modellezése

Dániel Bakonyi
dipl. arch. ing., assistant lecturer

Budapest University of Technology and Economics
Department of Building Constructions

Budapest, 2016

Table of Contents

1 Introduction 3
1.1 Introduction 1
1.2 Research objectives 3
2 Overview of fenestration heat transfer modeling 5
2.1 Glazing area heat transfer 5
2.1.1 Calculation of solar-optical properties....6
2.1.2 Calculation of glazing system heat balance....7
2.2 Component heat transfer....7
2.3 Determination of whole window heat transfer indices 8
2.4 Fenestration heat balance and building level calculations 9
2.4.1 Simple fenestration heat balance models and rating systems....10
2.4.2 Intermediate level fenestration heat balance models 10
2.4.3 Dynamic building energy simulations 11
3 Characterizing the heat transfer in box type windows....12
3.1 Fundamentals....12
3.2 Heat transfer by natural convection in glazing cavities....15
3.2.1 Literature review....15
3.2.2 Flow regimes of IG units and box type windows 25
3.2.3 Critical analysis of Nu correlations for the case of box type windows....27
3.3 CFD model 31
3.3.1 Literature review....31
3.3.2 Governing equation 33
3.3.3 Turbulence model validation 35
3.4 Parameters study – simple cavity....38
3.5 Parameter study – simple glazing system....42
3.6 Whole window heat transfer modeling....44
3.6.1 Measurements....45
3.6.2 Measurement results compared to 2D CFD simulations 48
3.6.3 Three dimensional simulations....53
3.6.4 Comparison of 3D CFD and standard calculations 58
3.7 Evaluation of current fenestration heat transfer calculation methods 60
4 Interaction between fenestration and masonry heat transfer 61
4.1 The treatment of thermal bridges in building heat loss calculations....61
4.2 A new method for improving the simplified calculation method 64
4.2.1 Methodology....65
4.2.2 Investigated building types and parameter sets....66
4.2.3 Monte Carlo simulation results....68
4.2.4 Accuracy and impact....73
4.3 Separating window and masonry calculations....75
4.3.1 The importance of the window-to-wall interface....76

4.3.2 Modification to the new calculation method 80
4.3.3 The accuracy of the new separated calculation method 82
5 The heat balance of box type windows 84
5.1 EPICAC BE – a dynamic fenestration heat balance simulation program 84
5.1.1 Calculating glazing area heat transfer 84
5.1.2 Control algorithms for shading devices 87
5.1.3 Calculating whole window heat transfer. 87
5.1.4 Calculating infiltration and natural ventilation 87
5.1.5 Weather data, models for solar radiation, shading and opaque constructions 88
5.1.6 Calculating zone air moisture balance 89
5.1.7 Calculating internal and HVAC loads, zone air heat balance 89
5.1.8 Occupant thermal comfort model 90
5.1.9 Validation 90
5.2 Case study – the MTA building's windows 91
5.2.1 A brief description of the project 92
5.2.2 Setting up the simulations 94
5.2.3 Simulation Results 97
5.2.4 Discussion 104
5.3 Sensitivity study 104
5.3.1 The Elementary Effects Method 105
5.3.2 Sensitivity analysis results 107
5.3.3 Discussion 111
5.4 Proposed methodology 112
6 Summary 113
6.1 New scientific findings 113
6.1.1 Finding I. 113
6.1.2 Finding II. 113
6.1.3 Finding III. 114
6.1.4 Finding IV. 115
6.1.5 Finding V. 116
6.2 Avenues for further study 117
6.3 Acknowledgements 117
7 Bibliography 119

Nomenclature

Symbol	Description	Unit
a	air permeability	[m^3/hm^2Pa^n]
A	area	[m^2]
ACH	air change rate (air change per hour)	[1/h]
Ar	dimensionless vertical cavity aspect ratio	[-]
c	pressure coefficient	[-]
c_p	specific heat capacity	[J/kgK]
C_p	heat capacity	[J/m^3K]
f	dimensionless temperature	[-]
g	total solar energy transmittance	[-]
Gr	the Grashof number	[-]
h	surface heat transfer coefficient	[W/m^2K]
I	irradiance	[W/m^2K]
H	cavity height	[m]
k	turbulent kinetic energy	[J/kg]
L	cavity thickness	[m]
L_{2D}	two dimensional thermal coupling coefficient	[W/mK]
l	length	[m]
$\dot{m}$	mass source	[kg/s]
M_w	molecular weight	[kg/mol]
n	air flow exponent	[-]
Nu	the Nusselt number	[-]
P	absolute pressure	[Pa]
p	partial pressure	[Pa]
Pr	the Prandtl number	[-]
q	heat flux density	[W/m^2]
Q	heat flux	[W]
$\dot{Q}$	heat source	[W]
R	thermal resistance	[m^2K/W]
R_{univ}	the universal gas constant	[J/molK]
R_v	specific gas constant of water vapor	[J/kgK]
Ra	the Rayleigh number	[-]
SHGC	solar heat gain coefficient	[-]
t	time	[s]
T	temperature	[K]
u	velocity vector	[m/s]
U	thermal transmittance	[W/m^2K]
V	volume	[m^3]
W	cavity width	[m]
y+	dimensionless wall distance	[-]

Greek symbols

α_{sol}	solar absorptance	[-]
β	thermal expansion coefficient	[1/K]
δ	vapor permeability	[kg/msPa]
ε	longwave infrared emissivity	[-]
λ	thermal conductivity	[W/mK]
μ	dynamic viscosity	[kg/ms]
ν	kinematic viscosity	[m^2/s]
ξ	moisture capacity	[kg/kg]
ρ	density	[kg/m^3]
ρ_{sol}	solar reflectance	[-]
σ	the Stefan-Boltzmann constant	[W/m^2K^4]

τ_{sol}	solar transmittance	[-]
τ_{dir}	direct solar energy transmittance	[-]
φ	angle	[°C
ψ	linear heat transfer resistance	[W/mK]
χ	thermal bridge correction factor	[-]
ω	specific dissipation rate	[1/s]

Subscripts

atm	atmospheric
cg	center-of-glazing
cond	conductive
conv	convective
e	external
eg	edge-of-glazing
empd	effective moisture penetration depth
f	frame
g	glazing
I	internal
ins	insulation
inst	installation
L	based on cavity thickness
lw	longwave infrared
op	operative
s	surface
sh	shading
t	turbulent
terr	terrestial
tot	total
T	thermal
w	window

1 Introduction

1.1 Introduction

Most of the windows in central Europe originating from the middle of the 19th century to the middle of the 20th century are double skinned, so called *box type windows* (Kastenfenster in German). They have two layers of usually wooden sashes, each with a single pane of glass. A 10-20 cm thick air cavity is enclosed between them which provides additional thermal resistance to the window. These constructions were the end product of centuries of window development and represented an enormous leap forward in thermal comfort and insulation from previous windows that had only a single piece of glass separating the interior from the exterior environments. Many different sub varieties of such windows exist which are characteristic of the country or region and in some cases even for the decade of the building's construction. The two layers of sashes may both open towards the inside, or in opposite directions, but the essential principle, and the high quality of craftsmanship that went into their making is the same. These windows contribute significantly to the original architectural character of the buildings they are in, and thus their preservation should be a major question in dealing with historical buildings.

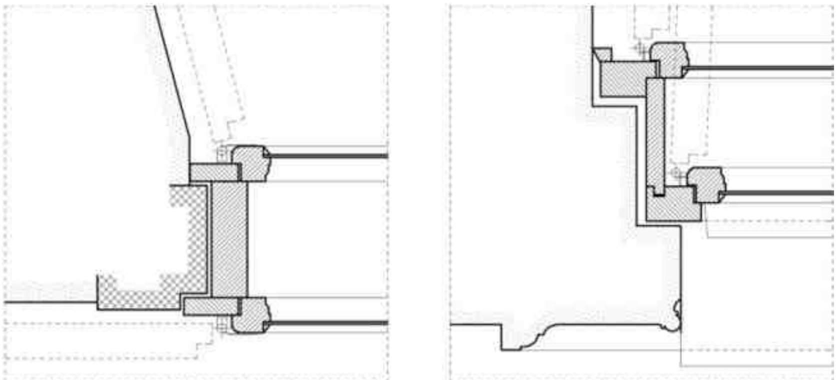

Fig. 1. – Schematic representation of the jamb detail of two typical 19th century box type windows

In the last few decades the preservation and restoration of historic windows in central-Europe and elsewhere was the subject of many studies. The most important structural details of 19th century windows, their common failures and the techniques to mend them are well documented, amongst others in books such as Neumann et al. [132], Gärtner et al. [75], Schrader [149] or Holste et al. [85]. However, though window restoration and refurbishment is mostly the area of specialized practitioners even they base their work largely on rules of thumb and simple design guidelines (such as “HO.09 Runderneuerung von Kastenfenstern aus Holz” [89] in Germany) that can only ever provide generalized solutions for the less demanding cases. Furthermore, the thermal improvement of historic windows, though definitely part of many of the relevant publications, is usually not treated in a systematic fashion. The majority of works is limited to presenting one or two possible solutions leaving little room for optimization.

One of the prerequisites for the preservation of old windows is the ability to plan their retrofit with the same level of detail and precision as with contemporary constructions. Regarding questions of building physics one has to solve problems like quantifying the transmission heat losses, assessing the total energy balance during the heating period or the whole year or checking the resistance to condensation. These tasks are far from trivial since reliable and well documented measurements are scarce and most standards and calculation methods for windows used by the building industry today were developed for contemporary single skin window constructions with insulating glass units (two or more layers of glass held together by spacer bars forming hermetically sealed cavities usually filled with air or some inert gas, henceforth IG units) that differ strongly from traditional windows.

We can list the following main constructional differences between contemporary single-skin and historical box type windows that might affect the way we calculate their behavior:

property	contemporary windows	box type windows
glazing system	• multipane IG units with cavities formed by spacer bars • cavities hermetically sealed • thin high vertical aspect ratio cavity or cavities • fill gas: air, argon, krypton, xenon, … • same internal and external glazing dimensions	• the glazing system is formed by the individual glass panes in the internal and external sashes, the cavity is flanked by the frame (or even the masonry) on the lateral sides, no spacer bars • in- and exfiltration possible through the operating joints between frame and sash • one large low vertical aspect ratio cavity • the main cavity is air filled • internal and external glazing dimensions not necessarily the same (in case of onward opening windows)
frame and sash	• different materials (wood, plastic, aluminum, steel, composite, …) • typical frame thickness: 60-100 [mm] • the same internal and external dimensions	• majority wooden constructions with a very few exceptions made out of metal • total construction thickness: 120-250 [mm] thin individual profiles (41-50 [mm]) • for inward opening windows smaller external dimensions
connection between glazing and sash/frame	• typically inward facing glazing rebates with glazing bead, sealed with rubber gaskets or sealant material • deep and wide glazing rebates to accommodate the large IG units	• outward facing glazing rebate with traditional putty based seal • small (ca. 10/10 [mm]) glazing rebate
airtightness, weather stripping	• typically high airtightness • air in- and exfiltration through the operating joint between frame and sash • one or more layers of rubber gaskets	• typically low airtightness • air in- and exfiltration through the operating joints between frame and sash through the main glazing air cavity • no gaskets (traditionally)
installation	• typically installed in a simple opening with a rebate created only by thermal insulation • installation joint thermally insulated and sealed from both directions	• inward-outward opening type windows either walled-in during construction or installed in separate inward/outward facing rebates, inward opening windows installed in inward opening single or double stepped rebates • installation joint typically uninsulated, seal is created by plaster

Table 1. – structural differences between contemporary single-skin and traditional box type windows

Some structural differences, like the typical thickness of the individual frame elements, pose no difficulty when dealing with box type windows, but others like the widely different cavity size and proportions, the unsealed nature of the cavity or the differences between internal and external dimensions can. It is therefore necessary to investigate the most commonly used fenestration or fenestration related heat transfer models regarding their validity for traditional double-skin box type windows, validate them or identify their possible limitations and propose new and improved calculation methods wherever necessary.

1.2 Research objectives

A comprehensive program for validating existing or establishing new modelling methods and guidelines for double-skin box type windows will have to cover the following main topics:

1. **Investigation of glazing area heat transfer models**
   The different thickness and geometrical proportion of cavities in box type windows can result in a significantly different type of convection than the one found in IG units. In the standard one-dimensional glazing area heat transfer models the equations used to quantify convective heat transfer have to be validated or modified for the different flow regime of box type windows.
2. **Investigation of window component heat transfer models**
   In the standard fenestration heat transfer models the heat transfer in individual window components (sash, jamb, head, dividers, etc.) is usually calculated with the help of two dimensional conduction-only thermal models where the glazing system is modelled in a simplified fashion. The validity of this approach for double-skin box type windows has to be examined with regards to both heat transfer predictions and local temperature field prediction. If necessary have to be modified or replaced.
3. **Investigation of complete window heat transfer models**
   Standard fenestration heat transfer models calculate overall window heat transfer indices (e.g. the overall thermal transmittance Uw) from component level heat transfer results (center of glazing, frame, edge-of-glazing or perimeter, etc.). The accuracy and validity range of these calculations for double-skin box type windows has to be assessed and new formulations have to be devised if necessary.
4. **Investigating the interaction between transmission and in/exfiltration heat transfer in box type windows**
   Unlike contemporary constructions the main glazing cavity of box type window is not hermetically sealed and there is an interaction between heat transmission and infiltration which will normally result in overall heat losses that are smaller than they would have been if the two processes were separate. In building energy simulations however infiltration an heat transmission through windows is treated separately, thereby overestimating the total heating energy demand and overestimating potential energy reductions when replacing double skin windows with single skin windows when this heat exchange effect does not play a role. A new methodology has to be developed for calculating the heat exchange effect in double skin box type windows, possible based on earlier work done on airflow windows.
5. **Investigating the calculations of window-to-wall interface heat transfer**
   In the thick and high conductance masonries of typical historic buildings the thick frames of box type windows result in window-installation thermal bridges that are much more favorable than for the thin frames of contemporary windows. Although this is relatively easy to take into account with detailed thermal bridge calculations, most design decisions are based on simplified calculation of the thermal envelope that account for thermal bridging only by prescribed correction factors. The simplified thermal bridge correction factors' ability of accurately predicting the difference between various window options needs to be investigated. If necessary a new methodology of simple thermal bridge corrections has to be developed.
6. **Investigating hygrothermal models for box type windows**
   Possible hygrothermal problems involving double-skin box type windows include the occurrence of interpane condensation and the prediction of accurate temperature and humidity fields in and around the window installation joints. The condensation resistance of windows is a function of the convective moisture transfer through their joints and the temperature field on their surface and in their interior cavities. Models for predicting the critical glazing surface temperatures of windows have to be examined and validated or modified for the case of box type windows.
   Predictions of mould growth and other hygrothermal phenomena at complicated constructional details are the area of multi-dimensional HAM simulations (the solution of the coupled partial differential equations of heat, moisture and air transport). These simulations generally use very simplified models for the actual window constructions that are adequate only for the thin frames of contemporary windows. The structure of double-skin box type windows pose significant challenges for HAM simulations: temperature stratification, convective heat and moisture sources, lateral diffusion between frame and cavity, etc. New HAM modeling techniques have to be developed to address these issues.
7. **Investigating fenestration heat balance models**

Methods for calculating the heat balance of windows have to be reviewed and calculation guidelines developed for the treatment of double-skin box type windows in building energy calculation with a special emphasis on historic buildings. A new computer program package has to be developed in which the algorithm changes and the new models mentioned in the earlier points can be easily integrated for testing and development.

The combination of all of these topics far exceeds the possible scope of a single doctorate thesis. The works needs to be divided into smaller, manageable parts in a suitable order. The goal of this thesis is only to make the first steps along this road. The thesis will focus mainly on questions of heat transfer, as they are the basis of all the other topics as well. Chapter 2 gives a brief overview of the most commonly used fenestration heat transfer calculations with special regard to their aspects that are important for modelling box type windows. Chapter 3 is an analysis of the convective heat transfer process in box type windows with the help of literature studies, simulations and measurements. It analyzes questions pertaining to points 1 to 3 of this outline. Chapter 4 is an investigation of point 4 where a new methodology is introduced for the analysis and simplified calculation of thermal bridging in well typifyable buildings in general, and their window-to-wall interface in particular. Finally in Chapter 5 a new calculation software and methodology is introduced and tested with the help of sensitivity analysis techniques, for the planning and ranking of retrofit strategies for box type windows in historic buildings.

2 Overview of fenestration heat transfer modeling

The physical processes that determine the thermal performance of windows are more complex than in opaque constructions. Thermal conduction, heat transfer by natural and forced convection as well as both short- and longwave infrared radiation all play an important role. Moreover, windows are inherently highly complex, inhomogeneous and incorporate constructional parts with vastly different dimensions and thermal material properties (e.g. thin metallic spacer bars vs. the bulk of a solid wooden frame). The thermal and solar/optical properties of windows can either be determined by measurement or by calculation. The required measurements (e.g. Hot-Box measurement for the thermal transmittance value [60] [63], integrating-sphere measurement for the solar transmission of glazing layers [10], etc.) are very expensive and time consuming to perform. The wide variety of possible geometries it is possible assemble from a single window profile type and glazing system shows that it would require a huge number of these measurements to be performed to provide designers with a usable database. This makes laboratory measurements impractical as an aid for the everyday practice of fenestration thermal design. Thermal measurements are usually only performed to aid the development of calculation methods, during the development of radically different new fenestration products and to perform an occasional validation of standard calculations.

Recent developments in computing power and numerical calculation methods do enable the modeling of these complex system as a whole in three dimensions without too much simplifications of physical processes, a technique called Multiphysics modeling. Performing fluid flow and more complex Multiphysics simulations by solving the coupled partial differential equations of many physical processes has become a major design tool in many industries. However, In the building industry at least the level of expertise required, the very long time needed to build the models, the still very large raw computational cost and the constant need for model validation all limit the use of very complex models to mainly research purposes.

The everyday practice of fenestration thermal planning has to rely on simple models and calculations based on simplifications and approximations enabled by a deep knowledge of the different heat transfer processes in window constructions. Many models have been developed and refined over several years for the explicit purpose of calculating the usually single-skinned mass produced windows of the contemporary window industry, but there are two main systems codified into systems of standards that are used by most practitioners. The European system is described in a series of CEN standards: EN 410 [52], EN 673 [53], EN 10077-1 [56] and EN 10077-2 [57], while the North-American method is given in ISO 9050 [93], ISO 15099 [97] and NFRC-100 [135]. Despite some significant differences (e.g. in boundary conditions) to a large extent they all follow the same principles and their calculations are divided into the following major steps:

- calculation of center-of-glazing values with one dimensional models,
- calculation of multi-dimensional and frame effects of window/frame components with 2D thermal simulations, and finally
- the combination of glazing and frame component results into whole window performance indices.

2.1 Glazing area heat transfer

Most windows have IG units and most IG units are described by the thermal properties one can measure at their center. The usual assumption is that the effect of spacer and edge seal at the perimeter of the unit only effect heat transfer up to a limited distance from the edge. This area, usually referred to as the edge-of-glass area, is where the interface between glazing and window frame (sash) has a noticeable effect. In the rest of the glazing, the so called center-of-glazing area, heat transfer is approximatively independent of spacer and frame and thus only a function of the IG unit's layers themselves. A further assumption is that the heat transfer of the center-of-glazing area is to a very good approximation one-dimensional. As will be shown in chapter 3 this is usually an acceptable simplification for glazing systems with thin internal cavities.

Center-of-glazing properties are found by either laboratory measurements (which are made relatively easy due to the near one-dimensional nature of the heat flow) or by calculations. For the purpose of this study we will focus on calculations which are themselves divided into solar-optical and heat balance calculations.

2.1.1 Calculation of solar-optical properties

The calculation of the solar optical properties of complex glazing systems requires detailed knowledge of the optical properties of the individual layers (spectral reflectance, absorptance and transmittance) as well as the relative spectral distribution of the incident shortwave solar radiation. The spectral distribution of the solar radiation is available e.g. in the standard ISO 9845-1 [94] or ASTM G173-03 [11] for both direct normal and hemispherical radiation.

The layers of glazing systems are glass panes and other elements such as shading devices. For the purpose of optical calculations we have to differentiate between specular and non-specular layers. Specular layers have near mirror-like reflection and are well described by the law of reflection, whereas for non-specular (scattering) layers more complex descriptions are needed.

Most window glass products are specular and measurements of glazing optical properties are performed at normal incidence and as a function of wavelength between ca. 300 and 2500 [nm]. Data for over 3000 products is available e.g. in the International Glazing Database[1] [160]. The off normal optical properties of glass panes can be calculated with the help of the Fresnel equations if the optical properties and thickness of all their layers are know (see in Furler [73]). This is generally the case for uncoated (e.g. normal float glass) products which are homogeneous and their index of refraction is easily calculated from the normal reflectance, absorptance and transmittance. For coated glass products however the exact thickness and composition of the coating is often a trade secret and can't be determined from measurements at normal angles. Reliable off-normal measurements lay outside the capabilities of even most laboratories as demonstrated by Hutchins et al. [88]. For these glasses other, mostly empirical or semi-empirical, models have to be used to approximate the off-normal properties from the normal properties as described e.g. in Rubin et al [147] and Maestre et al. [123].

Non-specular layers, such as various shading devices, require very complex 3D optical calculations, such as ray-tracing methods, or complex measurements to describe their scattering at various angles. One such measurement is described by Klems [109] to get the so-called Bidirectional Scattering Distribution Function, or BSDF. These functions discretize both the incoming and the outgoing hemispheres and describe the scattering of the layer by giving the reflectance (BRDF) and transmittance (BTDF) for any two discrete directions.

With the necessary data at hand the normal-incidence solar-optical characteristics of glazing systems with only specular layers are calculated according to either the EN 410 [52] or ISO 9050 [93] standards, which both yield very similar results. The presence of non-specular layers necessitates the use of more complex algorithms, such as ray-tracing or the matrix layer method of Klems [107] [108] based on the use of BSDFs. Regardless of the method the actual optical calculation is performed for a discretized set of wavelength bands which are then weighted with the help of the spectral distribution function of the incident solar irradiance. The weighted transmittance and absorptance of the glazing layer can then be used to calculate the total direct solar transmission and the solar radiation absorbed by the individual layers.

Besides the direct transmittance the g value (total solar energy transmittance) or the SHGC value (solar heat gain coefficient) is the performance index most commonly used to describe the solar-optical performance of the glazing system. These describe the ratio of the direct transmittance plus the inward flowing fraction of the absorbed radiation to the total incident radiation. The difference between the two that g value (used mainly in Europe) is defined as a characteristic of the glazing only, while the SHGC value (most commonly used in North America) is defined for the whole window and contains the inward flowing portion of the solar gain absorbed by the opaque part of the window as well[2]. The inward flowing fraction of the absorbed energy is determined either by measurement (see in Klems [110]) or by calculation. The calculation of both the g and SHGC values is given in ISO 15099 [97]. This calculation is done by adding the solar radiation calculated for each layer as a heat source in the

[1] The IGDB is created and maintained by the Window and Daylighting Group of the Lawrence Berkeley National Laboratory (LBNL) in the US with the support of the U.S. Department of Energy.
[2] European and American standards also pose different boundary conditions (ambient temperatures and incident solar radiation, etc.) on the calculation of the g and SHGC values.

heat balance calculation described in the following section and comparing the internal heat fluxes with and without this effect. For most cases the optical calculation is independent on the heat balance, the exception being thermocrome[3] glazing where an iterative approach is needed between the two.

2.1.2 Calculation of glazing system heat balance

The most important standards describing center-of-glazing heat balance calculations are the European EN 673 [53] and the international ISO 10292 [95] and ISO 15099 [97]. ISO 10292 is closely related to EN 673 which does not cover solar gains and is much less accurate than ISO 15099. EN 673 calculates the overall thermal transmittance of the glazing system, Ug [W/m^{2}K], as the inverse of the sum of the heat transfer resistance of the individual layers', cavities' and surfaces' which are in turn calculated for predefined temperature differences. ISO 15099 standard is based on a detailed heat balance method instead. The glazing system is discretized into 2*n nodes representing the front and back faces of each of the n layers in the glazing system. Equations of heat balance accounting for conduction (in the solid layers) as well as radiative and convective heat transfer and absorbed solar gains are written for each face in the system, which are then solved iteratively to give the surface temperature of each point. The temperature difference across airgaps in the glazing system are thus calculated and not prescribed as in EN 673. The convective heat transfer coefficient in the air filled cavities as well as the longwave infrared radiative heat transfer and if required the interior and exterior heat transfer coefficients are all calculated depending on absolute temperature and temperature difference, hence the need for the iterative solution. The overall thermal transmittance of the glazing is derived from the final thermal resistances calculated at the end of the iterative process. Other non-standard calculations also exist, such as the ones described by Winklemann in [168] for the program EnergyPlus [67], but they generally rely on very similar heat balance principles as ISO 15099.

As with the center-of-glazing optical properties the calculation is one-dimensional, heat transfer is perpendicular to the glazing system layers, and stationary. The latter assumption is usually acceptable as thins glazing layers have a relatively low mass compared to other constructions and their transient behavior rarely becomes an issue[4].

2.2 Component heat transfer

Standard describing the heat transfer modeling of window frames are the European EN 10077-2 [57] or the American NFRC 100-2010 [135] as well as the international The ISO 15099 [97] which contains the methods in both of the other standards. The heat transfer of the individual frame, divider etc. elements of windows can't be determined by one dimensional calculations or by measurements. The solution is to use relatively simple two-dimensional heat conduction simulations of the individual frame profile cross sections. However, depending on the window's construction (wood, plastic, aluminum, etc.) convective and radiative heat transfer can still play a significant role in the internal frame cavities. To eliminate the need for Multiphysics modeling frame cavity models are used to approximate both the radiative and convective heat transfer with a virtual solid material and an effective thermal conductivity so that only the stationary heat conduction equations needs to be solved. These models give reasonably accurate results for the overall heat transfer but have their limitations[5] as demonstrated by Gustavsen in his PhD thesis [79]. Gustavsen investigated both CEN and ISO/NFRC cavity models and found neither to be superior to the other.

The heat transfer of window frames is a function of the glazing system (at the previously mentioned edge-of-glass area) and the glazing spacer. Calculating this effect necessitates the inclusion of the glazing system in the two-dimensional frame heat transfer model. The solid part of the glazing system can be easily modelled while for the glazing cavities a virtual solid material with an effective thermal conductivity is used (as was the case with the internal frame cavities). The thermal conductivity of the frame cavity material is calculated based on the result of the center-of-glazing calculation to give the same heat transfer resistance for a given cavity thickness as the combined radiative and convective heat transfer coefficients do in reality.

[3] glazing product with temperature dependent solar-optical properties

[4] With the possible exceptions of many layered thick and heavy glazing systems where the thermal mass of the glazing is significantly increased.

[5] e.g. simple cavity models can't predict vertical temperature stratification

2.3 Determination of whole window heat transfer indices

The heat transfer in windows is inherently three-dimensional but it was thus far approximated only with one- and two-dimensional simulations. A final model is needed to integrate the results of the component level simulations in a whole window performance index. Once again, there are two main approaches to this: a CEN model described in the European EN 10077-1[56] standard and another model used mainly in North-America given in NFRC-100 [135]. The difference lies in how they treat the interaction between frame and glazing/spacer heat transfer and both are described in the ISO 15099 [97] standard as well. The CEN method calculates the edge-of-glass effect with the help of a linear heat transfer coefficient and the glazing perimeter length, while the frame and glazing heat transfer is added with values excluding lateral heat transfer:

$$U_w = \frac{\sum A_g U_g + \sum A_f U_f + \sum l_{eg} \psi_{eg}}{\sum A_g + \sum A_f} \tag{1}$$

where:
- U_w [W/m²K] – the overall window thermal transmittance
- A_g [m²] – the total unobstructed glazing area
- U_g [W/m²K] – the overall one-dimensional glazing thermal transmittance
- A_f [m²] – the frame area
- U_f [W/m²K] – the frame thermal transmittance (with no lateral heat transfer towards the glazing system[6])
- l_{eg} [m] – the glazing perimeter length
- ψ [W/mK] – the linear heat transfer coefficient accounting for the interaction of the frame and glazing system and spacer bars

The NFRC system uses an area-weighted method where the glazing is divided into a center-of-glazing area where heat transfer is assumed to be truly one-dimensional and an edge-of-glass area with a prescribed width of 63.5 [mm] (2 inches) around the glazing perimeter. A thermal transmittance is calculated for all three areas from the two-dimensional simulations and the results are averaged by area-weighting:

$$U_w = \frac{\sum A_{cg} U_{cg} + \sum A_f U_f + \sum A_{eg} U_{eg}}{\sum A_g + \sum A_f + \sum A_{eg}} \tag{2}$$

where:
- U_w [W/m²K] – the overall window thermal transmittance
- A_g [m²] – the center-of-glazing area
- U_{cg} [W/m²K] – the overall one-dimensional glazing thermal transmittance
- A_f [m²] – the frame area
- U_f [W/m²K] – the frame thermal transmittance
- A_{eg} [m²] – the area of the edge-of-glass region
- U_{eg} [W/m²K] – the heat transfer coefficient of the edge-of-glass region

[6] This is calculated wit replacing the glazing system with a very low conductance polyurethane foam panel of the same thickness in the thermal model of the frame.

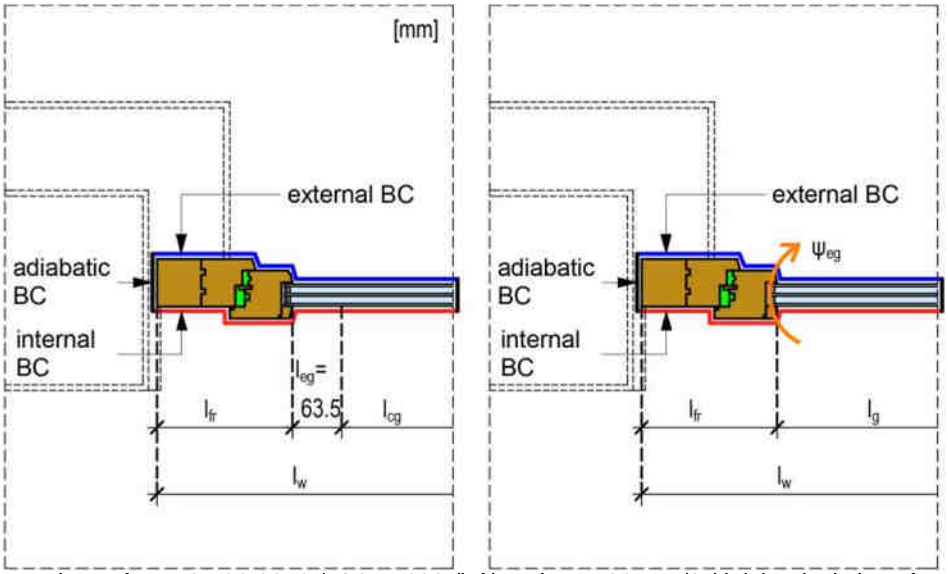

Fig. 2. – comparison of NFRC 100-2010 / ISO 15099 (left) and EN 10077-1/2 (right) calculations for the overall window thermal transmittance

Blanusa et al. [27] have performed a comparison of the CEN and NFRC calculation methods for the same boundary conditions and found that neither one is clearly more accurate than the other in predicting multi dimensional frame heat transfer. The inherent small discrepancies between the two models exist because they both try to approximate three dimensional heat transfer processes (conduction, convection and radiation) with only two dimensional calculations in slightly different ways. These differences only grow larger when the glazing-to-frame area ratio is small and three dimensional effects become more dominant. To address this issue Kumar [112] compared two and three dimensional thermal calculations of window heat transfer and found no significant errors between them, while Gustavsen et al. [80] compared hot-box measurements with calculations according to both methods and found errors of less than 10% for contemporary energy-efficient windows. Both Kumar and Gustavsen have indicated that two dimensional calculations give window-level results that are acceptable, but component-level results and temperature fields can show significant errors due to the three dimensional and convective effects that only tend to cancel out at window level.

2.4 Fenestration heat balance and building level calculations

The methods to calculate fenestration heat balance in standalone or complex building level calculations are much more numerous than the ones for determining the simple performance indices. The most basic building energy calculations simply take the window performance indices as constant properties. This can lead to errors as fenestration heat transfer is a function of the boundary conditions. The convective heat transfer is a function of absolute temperature and a strong function of temperature difference as well as the incidence angle (as demonstrated in e.g. in Bakonyi and Becker [14]). The standard solar-optical properties like τ_{dir} , g or SHGC are determined for normal incidence but are strongly dependent on the angle of incidence of the solar radiation as well as the proportion of direct and diffuse components in the incoming irradiance. Standard performance indices with standardized boundary conditions are intended for the simple comparability of different products, not necessarily for accurate heat balance calculations. More detailed models, e.g. dynamic building energy simulations, try to calculate the windows' thermal performance dynamically, as a function of the varying internal and external boundary conditions. However they still retain the same basic division of one dimensional models for the glazing system completed by additional heat transfer coefficients describing multidimensional heat transfer in the frame and sash profiles (usually precalculated).

In a paper Urbikain et. al [163] present three models to calculate the energy balance of window options. These represent levels of complexity that map well onto other models as well and we can use it as a guide for a literature study. According to the system the tree types of fenestration heat balance calculations are:

- simple models relying on only the constant thermal transmittance and g or SHGC value of windows that calculate their heat balance through a simple relationship using location specific heating degree-hours and some weighted total of incident solar radiation;
- intermediate models that try to incorporate the whole building's effect into the window heat balance in simplified ways, e.g. by calculating a balance temperature and a utilization factor for the solar gains, and try to correct for the angle of incidence dependence of solar gains at least in an approximate fashion;
- detailed dynamic building-simulation models.

According to their findings models of the first kind can only be considered as approximate. Their intermediate and detailed calculations showed reasonably similar results, but the complexity of dynamic simulations and the difficulties in separating their influencing parameters led them to chose the intermediate modelling approach to propose their window rating system.

2.4.1 Simple fenestration heat balance models and rating systems

Simple models can be said to include most fenestration rating systems used around the world, a good summary of which is found in [144] and [91]. Two good examples are the British Fenestration Rating Council's rating system and the Canadian Energy Rating (ER) [144] system. Both systems use a singular equation to represent the heat balance of a window with given U_w and g or SHGC values and an effective leakage rate for a theoretical averaged British or Canadian climate, building type and orientation. The British system focuses solely on the heating season while the Canadian one also provides a cooling energy rating (CER). Skou and Kragh [155] proposed an European labelling scheme that also takes both the heating and cooling seasons into account. They divided the continent into three distinct climate zones and used two reference buildings (one for northern and one for southern countries) and the standard ISO 13790 [96] to calculate corresponding heating and cooling degree days to be used in their energy balance equations that rely only on the g and Uw values of the windows. Other simple rating systems exist in Denmark, Finland, France, Portugal, Slovakia, Spain and Sweden as well (see in [91]), all relying on simple performance indices (Uw, g or SHGC and possible some infiltration rate) and simple balance equations and as a consequence largely ignoring differences in local climate, orientation, shading and other possibly important variables. Most are limited to a single building type.

In their paper Hanam et al. [81] analyzed the limitations of the Canadian ER system by investigating the correlation between the calculated window ratings and the results of dynamic building energy simulation made with Design Builder and EnergyPlus [67] for a large sample of window options and building types. The results were only good when the orientation and window to wall area of the simulated buildings were comparable to the theoretical average building used to derive the ER system. Furthermore, they found that the strictly heat balance based rating gives no indication on how the window will effect the thermal comfort and the risk of overheating.

2.4.2 Intermediate level fenestration heat balance models

The method described in the international standard ISO 18292 [98] is of intermediate complexity as it relies on ISO 13790 [96] for a hourly calculation of the het losses and solar gains using solar heat gain utilization factors to calculate the overall fenestration heat balance. The IFT Rosenheim's online window energy labelling tool [89] uses the ISO 18292 standard with preset window sizes and orientations to compare window products. The Danish Building research Institute's program WinDesign [8] utilizes ISO 13790 to perform simplified hourly dynamic multizone building energy simulations of entire buildings to compare the impact of different window options. It is still based on simple performance indices (Uw and g values) but the hourly nature of the calculation can allow for a much more precise treatment of orientation, external shading and the presence and operation of shading devices.

The models presented by Schulze et al. [150] and Karlsson et al. [103] both fall in the intermediate category. They require at least a limited information of the building and the same basic information of the windows themselves (U_w and g values). The incidence angle dependence of the solar transmission is calculated using empirical formulations. Schulze et al. compared their program to dynamic simulations and found a generally good agreement in the heating energy demand, with the exception of very heavy construction types in combination with large solar gains (the effective thermal mass had to be specified in an inherently approximate way). Like Hanam et al. [81] they found the predicted number of hours with overheating the least reliable.

2.4.3 Dynamic building energy simulations

The main advantage of simple and intermediate calculation tools is their relative ease of use and the simplicity of the necessary input data as compared to more sophisticated numerical simulations. But as demonstrated by several authors this can come at a cost of accuracy. Another approach is to improve the usability of dynamic building simulation engines with the addition of an intuitive GUI and predefined libraries, so more users can take advantage of their advanced modelling capabilities and higher accuracy. Two notable examples are the programs developed by the Windows and Daylighting Group at the Lawrence Berkeley National Laboratory (LBNL) in the US, that are aimed at the design of residential and commercial fenestration respectively: RESFEN by Sullivan et. al [156] and COMFEN by Selkowitz et. al [151]. RESFEN utilizes the DOE-2 simulation [43] engine, while COMFEN is based on EnergyPlus [67] and Radiance [161]. Although the actual simulation engines are capable of very complex calculations the input parameters are still restricted by the GUI to make the programs more usable by non-professionals. RESFEN only uses simple performance indices (U and g values) and it is intentionally limited in its scope to residential use. COMFEN utilizes the whole of the software 'ecosystem' created by the Window and Daylighting Group at the Lawrence Berkeley National Laboratory to facilitate the thermal and optical description and modeling of the fenestration which is the state of the art in any building simulation. But the rest of the parameters, such as building type, schedules, window and shading control algorithms and available HVAC system are restricted to a minimum. Though COMFEN offers modeling of natural ventilation as of now it is limited to buoyancy driven single-sided ventilation through the open windows, while infiltration modelling is absent. A further limitation is that even this ventilation model can't be used together with mechanical cooling. RESFEN uses the Sherman and Grimsrud infiltration model [152] instead.

These simplified interfaces are clearly intended to aide the everyday practice of architects and civil-engineers in the design of contemporary buildings and windows, and they have significant merit in that regard. However, for the central-European building heritage is characterized by very large thermal mass, low air-tightness plus natural ventilation and historic double-skin windows, the reliable modelling of which may not be the strong suite of these tools. The non-simplified use of dynamic building-simulations seems a more favorable way to follow, at least for research purposes. An examples for this approach is found in Nikoofard et al. [134], who used the thermal dynamic building-simulation engine ESP-r [68] to study the effect of window modifications in Canada and the possibilities of solar energy utilization in the cooling season. Mainini et al. [124] used dynamic building energy simulations in EnergyPlus [67] and visual comfort simulations in Radiance to compare different retrofit option for the glazing system in a small Italian office cell with a southern orientation for both Milano and Palermo. They investigated a low-e glazing, a reflective window film and a controlled external shade option. The found that the controlled shading gave comparable results to the low-e glazing even in heating energy demand reduction in the more cooling dominated location of Milano, although it was the least favorable due to its cost. All scenarios performed similarly in terms of thermal comfort too, which they analyzed with the help of the ISO 7730 standard [92].

A further possibility to enhance the utility of dynamic simulations is the utilization of custom code or additional modules for parameter studies, optimization and custom control algorithms. Firlag et al. [72] studied control strategies for dynamic windows using EnergyPlus with the help of the Energy Management System module [48] to model the advanced control algorithms they wanted to investigate. Michele et al. [126] used the softwares TRNSYS [162] and Radiance to create a framework for coupled thermal and daylighting simulations and the possibility to use the data from the daylighting simulation to dynamically control the state of the shading devices. Reinhart et al. [145] developed a custom simulation engine for the thermal and natural lighting design of offices and classrooms using their earlier daylighting models, a coupling to ESP-r for the thermal simulation and occupant behavior models. Petersen et. al [139] created an entirely new code in MATLAB to enable the development of new algorithms aiding the early design decision of external thermal envelopes.

3 Characterizing the heat transfer in box type windows

As it was demonstrated in chapter 2. the most frequently used fenestration heat transfer calculation methods rely on a series of implicit assumptions and simplifications to remain manageable. As also mentioned these rest on the common physical properties of most contemporary window constructions. Most contemporary windows are constructed as a single-skin or single layer framework with fix and/or operable sashes that hold relatively thin (ca. 10 – 40 [mm]) hermetically sealed multipane insulating glass units or opaque insulated panels of similar dimensions. IG units are completely self contained and only interface with the frame and sash elements at a narrow stretch around their perimeter: the edge-of-glass area. The thermal interaction between glazing and frame and the effect of the spacer bars in the IG unit is limited to this area and the processes within the glazing (convection and thermal radiation) itself are well approximated with one-dimensional models.

Historic double-skin box type windows are however very different in their construction. The main glazing cavity of box type windows is not sealed like in an IG unit, and it is formed not by small spacer bars but with the distance between two layers of sashes. The thickness of the cavity is much larger, its height to width ratio much smaller and is flanked by parts of the window frame itself. This puts at least some of the simplifications in contemporary calculation methods in question: the different cavity dimensions result in a type of natural convection significantly different from the one in IG units, one which is not well described by one-dimensional models and effective material properties, and the interaction between the convective and radiative heat transfer in the cavity and conduction in the solid bodies of the frame is made much more pronounced (see also in Bakonyi and Becker [16]).

These differences warrant a detailed investigation of the fenestration heat transfer models' applicability for calculating box type windows. We have to first review the models describing the convective heat transfer in enclosed cavities (a key part of fenestration heat transfer models) and analyze their accuracy for box type windows. Multiphysics models need to be developed and if possible validated to study the heat transfer in box type windows in its entire complexity and to investigate the accuracy of fenestration heat transfer models for this window type.

3.1 Fundamentals

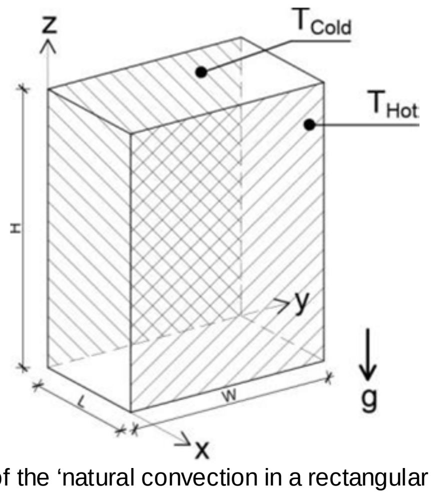

Fig. 3. – Schematic representation of the 'natural convection in a rectangular differentially heated cavity' problem

The starting point for studying the natural convection heat transfer in windows is the simplified case of a gas filled rectangular cavity with two differentially heated (or cooled) surfaces. By creating a temperature difference across these surfaces of the enclosure a natural convection is initiated by the temperature gradient. This convection is a function of many parameters:

- The geometry of the cavity (see Fig. 3) described by the following parameters:
  - L [m] – the thickness of the cavity in the x direction (the horizontal distance of the opposing faces where the temperature difference is applied)
  - W [m] – the width of the cavity in the y direction (the horizontal dimension of the cavity perpendicular to the main temperature gradient)

  - H [m] – the height of the cavity in the z direction
  - φ [°] – the angle of inclination of the cavity (if it is not vertical)
- The thermal boundary conditions: the surface temperature of the two differentially heated surfaces (if they are isothermal) and a description of the other surfaces which can be either adiabatic or have a constant temperature gradient between the two heated surfaces (linear temperature profile). These are simplifying assumptions necessary to devise measurement methods and enable simple analytical solutions and they will later be abandoned. Isothermal heated (or cooled) cavity surfaces are specified by their surface temperatures:
  - T_H [K] – the temperature of the hot side of the cavity
  - T_C [K] – the temperature of the cold side of the cavity
- The physical properties of the gas filling the cavity:
  - μ [kg/ms] – the dynamical viscosity
  - ρ [kg/m^3] – the density
  - λ [W/mK] – the thermal conductivity
  - c_p [J/kgK] – the specific heat (at constant pressure)
  - β [1/K] – the thermal expansion coefficient

Besides the study of the actual temperature, velocity, pressure etc. fields in the fluid the determination of the overall convective heat transfer between the two differentially heated surfaces and the derivation of simple easy-to-use methods for its calculation are the main goals of most of the research done on the problem. This requires the reduction of the number of influencing parameters which is usually achieved with the help of dimensional analysis. The dimensionless groups most commonly used to describe the problem are the dimensionless aspect ratio, the Prandtl, Grashof, Rayleigh and Nusselt numbers. As a further simplification the flow is usually taken to be 2 dimensional which is accurate enough if the width of the cavity is sufficiently larger than its thickness (which is true for most fenestration glazing cavities).

The dimensionless **aspect ratio** is simply defined as the ratio between the total cavity height and the cavity thickness:

$$Ar = \frac{H}{L} \tag{3}$$

where: Ar [-] – the dimensionless aspect ratio
H [m] – the total height of the cavity
L [m] – the thickness of the cavity in the direction of the main temperature difference

The **Prandtl number** is a material property of the fluid (and the fluid's state – e.g. temperature) and it is a measure of the ratio between the viscous or momentum and thermal diffusion rates:

$$\mathrm{Pr} = \frac{\mu c_p}{\lambda} = \frac{\nu}{\alpha} \tag{4}$$

where: Pr [-] – the Prandtl number
μ [Ns/m^2] – the dynamic viscosity
c_p [J/kgK] – the specific heat capacity
λ [W/mK] – the thermal conductivity
ν [m$^{2/}$s] – the kinematic viscosity
α [m^2/s] – the thermal diffusivity

If Pr<<1 the thermal diffusion will tend to dominate and the thermal boundary layer will be much thinner than the momentum boundary layer, and if Pr>>1 the opposite will be true. For most gases the Prandtl number is approximately constant for a wide range of temperatures and pressures and for our purposes (building physics) it can be taken as Pr = 0.71 [-]. This indicates that both thermal diffusion and convection effects will be around the same order of magnitude.

The **Grashof number** is used to describe natural convection and it can be thought of as the ratio of buoyant to viscous forces in a unit volume of the fluid:

$$Gr = \frac{g\Delta\rho V}{\rho\nu^2} = \frac{g\beta(T_1 - T_2)l^3}{\nu^2} \tag{5}$$

where: Gr [-] – the Grashof number
g [m^2/s] – the acceleration of gravitaty
ρ [kg/m^3] – the density
V [m^3] – the volume
v [m^2/s] – the kinematic viscosity
β [1/K] – the thermal expansion coefficient
T [K] – temperature
l [m] – the characteristic length

For the natural convection in a rectangular cavity problem the temperatures are usually taken as the surface temperatures of the differentially heated surfaces and the characteristic length l as the thickness of the cavity: L. If Gr>>1 buoyancy dominates over viscosity.

The **Rayleigh number** is the product of the Prandtl and Grashof numbers and it is widely used in the description of natural convection problems:

$$Ra = Gr * \Pr = \frac{\rho^2 l^3 g c_p \Delta T}{\mu\lambda T_m} \tag{6}$$

where: Ra [-] – the Rayleigh number
Gr [-] – the Grashof number
Pr [-] – the Prandtl number
ρ [kg/m^3] – the density
g [m^2/s] – the acceleration of gravity
c_p [J/kgK] – the specific heat capacity
ΔT [K] – the temperature difference
μ [Ns/m^2] – the dynamic viscosity
λ [W/mK] – the thermal conductivity
T_m [K] – the average temperature of the fluid

The heat transfer is dominated by thermal diffusion under and by convection above a certain critical Rayleigh number. The Rayleigh number is normally used to derive equations that are true for different types of fluids as it is a function of both the balance between buoyant and viscous forces and the fluid material properties.

The **Nusselt number** is defined as the ratio of the convective and conductive heat transfer coefficients across a fluid in natural convection:

$$Nu = \frac{h_{conv}}{h_{cond}} = \frac{h_{conv}}{\frac{1}{R_{cond}}} = \frac{h_{conv}}{\frac{\lambda}{L}} \tag{7}$$

where: Nu [-] – the Nusselt number
h_{conv} [W/m^{2}K] – the convective heat transfer coefficient
h_{cond} [W/m^{2}K] – the conductive heat transfer coefficient
R_{cond} [m^{2}K/W] – the conductive heat transfer resistance
λ [W/mK] – the thermal conductivity
L [m] – the characteristic thickness (the thickness of the cavity)

The conductive heat transfer coefficient is the heat transfer coefficient of an imaginary stagnant body of fluid where heat transport happens only by thermal conduction (thermal diffusion). If Nu≈1 the convective heat transfer is negligible and as far as heat transport is concerned the fluid is stagnant. In the cavity convection problem a ≈1 Nusselt number means a near zero velocity perpendicular to the heated boundaries over much of the cavity. If however Nu>1 the convective heat transfer will become important and in case of Nu>>1 become dominant over thermal diffusion.

Since the cavity thickness is usually known and the thermal conductivity of the fill gas is easy to determine (in the conditions usually encountered in building physics it is a function of the gas temperature only) the Nusselt number is the most convenient way to describe the total convective heat flow across the cavity. The determination of the Nusselt number from the other properties is thus the main task in most thermal calculations of cavity convection and a considerable body of work is devoted to it. This is done either by measurement, CFD simulations or with simple empirical equations previously derived from the last two. The equations are called Nusselt correlations as they are derived from analyzing the relationship between the Nusselt number and the other dimensionless groups mentioned earlier. All fenestration heat transfer calculation methods have a set of Nusselt correlations in their algorithms that were selected from the literature or developed for the explicit purpose of modelling the thin cavities of insulating glass units.

3.2 Heat transfer by natural convection in glazing cavities

3.2.1 Literature review

The natural convection in differentially heated rectangular enclosed cavities is a problem of interest for many scientific and engineering fields and as a result we can find a truly large number of publication devoted to the subject. The ones most important for the calculation of glazing systems will briefly be summarized here.

Batchelor [23] was one of the first researchers to investigate the temperature field in a rectangular enclosure with isothermal differentially heated surfaces. His work focused on laminar flows with relatively low Grashof or Rayleigh numbers. He was the first to identify the so called ‘conduction’ and ‘boundary layer’ flow regimes based on analytical principles. A flow is in the conduction regime when it is under a certain Gr or Ra number and the heat transfer is predominantly via heat conduction (thermal diffusion) in the fluid (see Fig. 4). This regime is characterized by a constant temperature gradient across the cavity between the heated surfaces, a temperature field that satisfies the Laplace equation much like the temperature field one would encounter in a homogeneous solid material after the steady-state is reached. But if the Gr and Ra numbers are increased (e.g. by increasing the temperature difference), the flow will enter the boundary layer regime where the heat transfer is instead due mainly to convection (see Fig. 5). Distinct boundary layers form with high temperature gradients at the two heated surfaces while the core of the fluid between these layers will demonstrate a near zero horizontal temperature gradient. Batchelor [23] predicted that the core will show no vertical temperature gradients either (completely isothermal core). This later turned out to be incorrect.

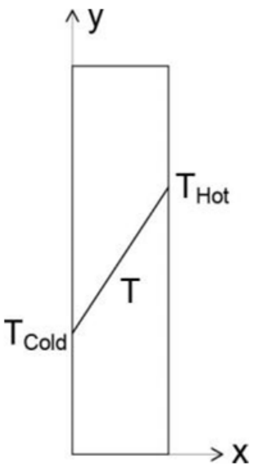

Fig. 4. – Schematic representation of the conduction regime

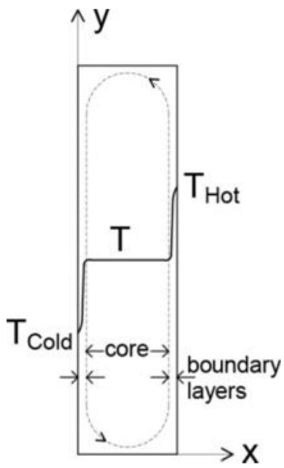

Fig. 5. – Schematic representation of the boundary layer regime

Eckert and Carlson [34] conducted interferometry experiment to investigate the temperature field in differentially heated cavities of different size and aspect ratios at different Grashof numbers. They confirmed the existence of the distinct conduction (Fig. 6) and boundary layer regimes (Fig. 8) reported by Batchelor [23] at low Gr numbers above a certain aspect ratio and at high Gr numbers under a certain aspect ratio respectively. Unlike Batchelor however they also noted the existence of a third flow regime between the last two: the so called 'transition' regime (Fig. 7). In these transitional flows the temperature field does no longer satisfy the Laplace equation: a stronger temperature gradient starts to form near the boundaries but these temperature boundary layers still interact in the core and the fully formed boundary layer regime is not jet reached. Sometimes this kind of flow is also characterized by the emergence of a series of secondary convection cells. Another of their findings was the existence of a strong vertical temperature stratification in the fluid core in the boundary layer regime which goes contrary to Batchelor's isothermal core hypothesis.

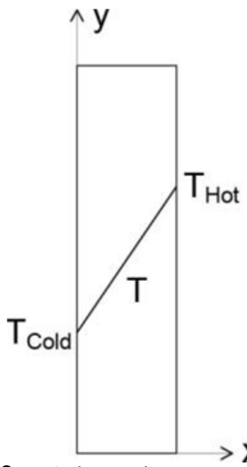

Fig. 6. – Schematic representation of the conduction regime

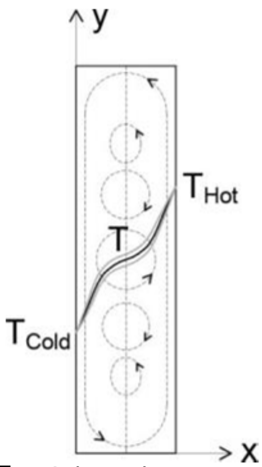

Fig. 7. – Schematic representation of the transition regime with secondary convection cells

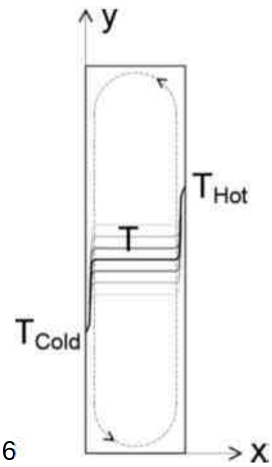

6

Fig. 8. – Schematic representation of the conduction regime, with a vertical temperature gradient in the fluid core

Eckert and Carlson did not perform enough experiments to pin down the exact limits of transition between the different flow regimes very reliably but they did derive two correlations for the Nusselt number in the conduction and the boundary layer regimes respectively. These use the aspect ratio and the Grashof number.

The correlation for the conduction regime:

$$Nu_{cond} = 1 + 0.00166 \cdot \left(Gr_L\right)^{0.9} \cdot Ar \tag{8}$$

where: Nu_{cond} [-] – the Nusselt number for the conduction regime
Gr_L [-] – the Grashof number based on the cavity thickness
Ar [-] – the dimensionless aspect ratio

The correlation for the boundary layer regime:

$$Nu_{BL} = 0.119 \cdot \left(Gr_L\right)^{0.3} \cdot Ar^{-0.1} \tag{9}$$

where: Nu_{cond} [-] – the Nusselt number for the conduction regime
Gr_L [-] – the Grashof number based on the cavity thickness
L [m] – the cavity thickness
H [m] – the cavity height

These correlations have limited applicability since they lack a description of the transition regime. Their correlations are based on data gathered for cavity aspect ratios of Ar=2.5-46.7 [-] and Grashof numbers of Gr=8e4-2e5 [-]. The limits of transition between the different flow regimes they proposed are shown in Fig. 14.

Elder [47] conducted experiments on natural convection for cavities with aspect ratios of Ar=1-60 [-] and Rayleigh numbers of Ra<1e8 [-] with a fluid of Pr=103 [-]. The heated cavity walls were kept isothermal. For Re<1e3 the temperature field closely satisfied the Laplace equation (conduction regime), though even here a single cell convection is still present but with nonzero horizontal velocities only around the top and bottom edges of the cavity (up to a distance of around L) (see Fig. 9). Between Re=1e3 [-] and Re=1e5 [-] the temperature gradients next to the heated wall begin to grow and a vertical temperature stratification starts to form in the core and at around Ra=1e5 [-] a 'cat's eye pattern' of secondary convection cells is starting to form that grow larger in amplitude and begin to interact at around Ra=1e6 [-] (Fig. 10). The boundary layers have a thickness that is ~Ra^1/4. The higher the Rayleigh number gets the thinner the boundary layers become which finally results in the boundary layer regime described earlier (Fig. 11).

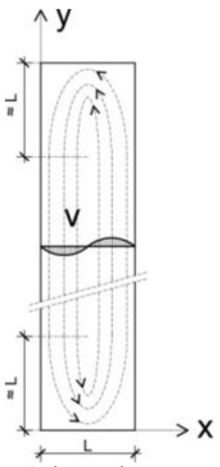

Fig. 9. – Schematic representation of the flow in the conduction regime

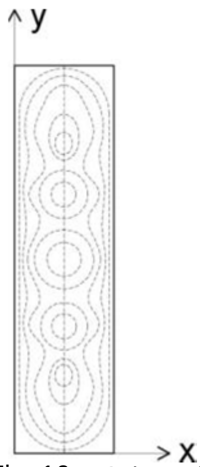

Fig. 10. – Schematic representation of the flow in the transition regime

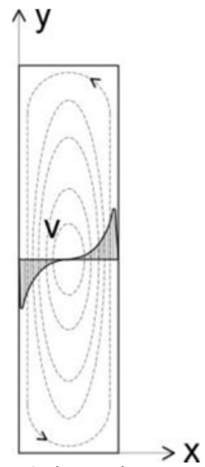

Fig. 11. – Schematic representation of the flow in the boundary layer regime

In his 1967 book Jakob [99] proposed another correlation for the Nusselt number based on earlier experimental datasets. The correlation is derived for cavities with Ar=3.12-42.2 [-] and Gr=2e4-2e5 [-]. The correlation takes the following form:

$$Nu = 0.18 \cdot \left(Gr_L\right)^{0.25} \cdot Ar^{-0.111} \tag{10}$$

The Nusselt number is thus found to be directly proportional to the temperature gradient and inversely proportional to the aspect ratio, albeit only weakly. This form of correlation - Nu = C * Gr^a * Ar^b - is found in the works of many other authors as well: Newel and Schmidt [133], Yin et al. [35], Eckert and Carlson [34] and Yang [174].

Newell and Schmidt [133] used a Finite Difference Method based CFD code to study the laminar convective heat transfer in rectangular cavities with Ar=2.5-20 [-] and Gr=4e3-1.4e5 [-]. Their Nu number results gave the following correlation with the Ar and Gr numbers:

$$Nu = 0.115 \cdot Gr^{0.315} \cdot Ar^{-0.265} \tag{11}$$

Hollands et al. [84] in their 1976 article studied the free convection in inclined rectangular cavities with high aspect ratios of Ar>20 [-] and Rayleigh numbers of Ra<1e5 [-] and inclinations of 0°≤φ<70° with upward heat transport (heated from below, cooled form above). They proposed a new correlation for the Nusselt number is today incorporated into the widely used international and harmonized European standard ISO 15099 [97]:

$$Nu = 1 + 1.44 \cdot \left[1 - \frac{1708}{Ra \cdot \cos(\varphi)}\right]^{\bullet} \cdot \left[1 - \frac{\left(1708 \sin^2(1.8 \cdot \varphi)\right)}{Ra \cdot \cos(\varphi)}\right] + \left[\left[\frac{Ra \cdot \cos(\varphi)}{5830}\right]^{1/3} - 1\right]^{\bullet} \tag{12}$$

where: $[x]^{\bullet} = \left(x + |x|\right)/2$

Nu [-] – the Nusselt number
Ra [-] – the Rayleigh number
φ [°] – the inclination of the cavity (from horizontal)

Yin et al. [35] conducted natural convection experiments for air filled cavities with aspect ratios of Ar=4.9-78.7 [-] over a wide range of Grashof numbers: Gr=1.5e3-7e6 [-]. They measured temperature profiles and overall heat transfer rates and derived a correlation for the Nusselt number dependent on both the Grashof number and the aspect ratio:

$$Nu = 0.21 \cdot Gr^{269} \cdot Ar^{-0.131} \tag{13}$$

Yin et al. also proposed values for the limits of transition (Gr or Ra numbers) between the conduction, transition and boundary layer regimes as well as between laminar and turbulent flows depending on the cavity aspect ratio (see Fig. 14).

Raithby and Wong [143] performed numerical simulations to come up with a new correlation for the Nusselt number for cavities with Ar=2-80 [-] and Ra=1e3-2e5 [-]:

$$Nu = \left(1 + \left(\frac{0.344 \cdot Ra'^{0.25}}{1 + \frac{112}{Ra'^{0.87}}} \right)^2 \right)^{0.5} \tag{14}$$

Where Ra' is given by the following expressions depending whether the side walls of the cavity were modelled with a linear temperature profiles or as adiabatic:

$$Ra' = \left(1 - \frac{1.02}{Ar^{0.44}} \right) \cdot \frac{Ra}{Ar} \quad \text{for a linear temperature profile} \tag{15}$$

$$Ra' = \left(0.89 - \frac{0.73}{Ar} \right) \cdot \frac{Ra}{Ar} \quad \text{for adiabatic side walls} \tag{16}$$

ElSherbiny et al. conducted one of the most comprehensive and most cited measurement campaigns in the literature about the natural convection in rectangular cavities. In a first publication [50] they investigated the effect the treatment of the side wall boundary conditions have on measurement results. Most convective heat transfer measurements are done by creating a linear temperature profile at the side walls of the cavity. While this is a good fit for flows in the conduction regime where the temperature gradient in the fluid is itself linear which results in basically no sideways heat flux, it complicates matters when a boundary layer regime flow is investigated. Here, especially at the top and bottom zones of the cavity, the core of the fluid is close to either the cold or the hot boundary temperature while the solid wall of the cavity tries to enforce a linear temperature profile which will lead to nonzero sideways heat flux.

In their second paper [51] they present an extensive set of measurement data of Nusselt numbers for air filled cavities with aspect ratios between 5 and 110 and Rayleigh numbers of Ra=1e2-2e7 [-]. Besides publishing the raw data they propose a whole set of correlations for the Nu number: a series of 6 equations valid only for distinct aspect ratios but with a better fit and two more complex correlation functions that incorporate the whole range of the measurements called design correlations for vertical and for inclined cavities of arbitrary aspect ratios and Rayleigh numbers. The measurements were done with isotherm heated surfaces and linear temperature profiles at the side walls.

The 6 equations for the Nusselt number in cavities for distinct aspect ratios:

$$Nu = \left\{ \left[1 + \left(\frac{0.193 Ra^{0.25}}{1 + \left(1800 / Ra\right)^{1.289}} \right)^{3} \right]^{1/3}, 0.0605 * Ra^{1/3} \right\}_{\max} \qquad \text{for Ar=5 [-], Ra<1e8 [-]} \tag{17}$$

$$Nu = \left\{ \left[1 + \left(0.125 Ra^{0.28} \right)^{9} \right]^{1/9}, 0.061 * Ra^{1/3} \right\}_{\max} \qquad \text{for Ar=10 [-], Ra<9.7e6 [-]} \tag{18}$$

$$Nu = \left[1 + \left(0.064 Ra^{1/3} \right)^{6.5} \right]^{1/6.5} \qquad \text{for Ar=20 [-], Ra<2e6 [-]} \tag{19}$$

$$Nu = \left[1 + \left(0.0303 Ra^{0.402} \right)^{11} \right]^{1/11} \qquad \text{for Ar=40 [-], Ra<2e5 [-]} \tag{20}$$

$$Nu = \left[1 + \left(0.0227 Ra^{0.438} \right)^{18} \right]^{1/18} \qquad \text{for Ar=80 [-], Ra<3e4 [-]} \tag{21}$$

$$Nu = \left[1 + \left(0.0607 Ra^{1/3} \right)^{18} \right]^{1/18} \qquad \text{for Ar=100 [-], Ra<1.2e4 [-]} \tag{22}$$

These equations are regarded by man authors as the most accurate till date. The general purpose multi aspect ratio correlations they propose finds the actual Nusselt number as the maximum of three functions:

$$Nu = Max \begin{bmatrix} Nu_1 = 0.0605 Ra^{1/3} \\ Nu_2 = \left[1 + \left(\dfrac{0.104 Ra^{0.293}}{1 + \left(\dfrac{6310}{Ra} \right)^{1.36}} \right)^{3} \right]^{1/3} \\ Nu_3 = 0.242 \left(\dfrac{Ra}{Ar} \right)^{0.272} \end{bmatrix} \tag{23}$$

Nu_1 usually describes the flow in case of large Ra numbers (boundary layer regime), Nu_2 in the conduction regime and Nu_3 in the transition regime.

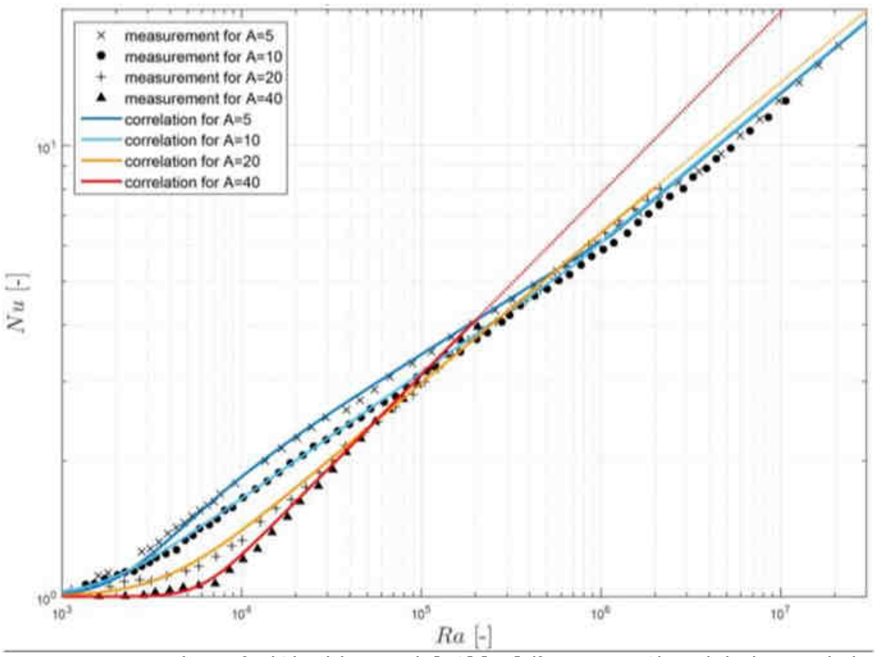

Fig. 12. – The measurement data of ElSherbiny et al. [50] [51] (for Ar=5-40) and their correlations for distinct aspect ratios (the dashed end of the lines represent the correlations extrapolated outside their reported range of validity)

For inclined cavities – with inclinations between 60° and 90° – they propose the following method: there is a correlation for when the inclination is equal to 60° while values for other inclination are found with linear interpolation between the 60° and 90° values. The correlation for 60° is:

$$Nu_1 = \left[1 + \left[\frac{0.0936 \cdot Ra^{0.314}}{1+G}\right]^7\right]^{1/7} \tag{24}$$

$$G = \frac{0.5}{\left[1 + \left[\frac{Ra}{3160}\right]^{20.6}\right]^{0.1}} \tag{25}$$

$$Nu_2 = \left[0.104 + \frac{0.175}{Ar}\right] \cdot Ra^{0.283} \tag{26}$$

$$Nu = Max\left(Nu_1, Nu_2\right) \tag{27}$$

Korpela and Lee [111] studied the multicellular convection in the transition regime with numerical simulations to find the critical Gr numbers where this kind of flow pattern is encountered. They investigated aspect ratios of 10-40 [-] and a wide range of Grashof numbers and developed a simple equation for the aspect ratio dependent limit:

$$Gr_c = \frac{1 + \frac{5}{Ar}}{1.25 \cdot 10^{-4}} \tag{28}$$

The limit is visualized is Fig. 14. Under an aspect ratio of Ar=12 [-] secondary flow was not detected. Their results compared well with measurements done with smoke aided flow visualization and interferometry.

Shewen et al. [153] have developed a new method for the simultaneous heating or cooling of and heat flux measurement on cavity walls in experimental apparatus aimed at the study of natural convection in rectangular cavities based on the Peltier effect. Relying on this work they present their own measurements and a correlation for the Nusselt number for cavities with aspect ratios of 40 or larger and Rayleigh numbers less than 1e6 in another article [154]. The aspect ratio and Rayleigh number range is clearly aimed at insulating glass units.

$$Nu = \left[1 + \left(\frac{0.0665 \cdot Ra^{1/3}}{1 + \left(\frac{9000}{Ra} \right)^{1/4}} \right)^2 \right]^{1/2} \tag{29}$$

Wright and Sullivan [169] present an exhaustive literature review of works concerning the modeling of the natural ventilation in rectangular cavities in their effort to find a suitable model for predicting the lowest internal surface temperature at the bottom edge of insulating glass units. IG units have typical cavity aspect ratios of around 70 or higher but relatively low typical Ra numbers. A properly sized IG unit is usually in the conduction regime where the flow is very weak and strictly vertical throughout most of the glazing. However, even the weak convection cell of a conduction regime flow must close and loop around at the bottom and top edges. Here the normally linear temperature profile get distorted: the bottom edge gets cooler and the top edge warmer at the interior side due to convective cooling or heating. This is the reason why the minimum surface temperature prediction of most thermal bridge simulation programs that only solve the Fourier equation are unreliable in these regions.

In another article Wright [170] analyses the Ra-Nu data and correlations of ElSherbiny et al. [51] [50] and Shewen et al. [153] [154] for the Ar and Ra number region most interesting for the thermal calculation of insulating glass units: Ar>40 [-] and Ra<1e6 [-]. Every correlation starts with the conduction regime at the smallest Ra numbers where Nu=1 [-] and ends at the very large Ra numbers of the fully developed turbulent boundary layer flows where the slope of the Ra-Nu function is found to be around 1/3 on a logarithmic plot by all authors. The transition from the conduction to the transition and from the transition to the fully formed turbulent boundary flow regimes is showed to be a function of Ar. Taller cavities leave the conduction regime earlier and can become turbulent at smaller Ra values than cavities with a smaller aspect ratio. The transitional Nu numbers at low Ar values are highly dependent on the A value itself and are represented by a bend in the Ra-Nu functions between the conduction and boundary layer regimes. At high values of Ar its effect becomes smaller and impossible to reliably quantify due to the unpredictability of the secondary flows in the transition regimes. Or at least this was the case in ElSherbiny's [51] dataset Wright used. They conclude that an A value independent correlation is asked for.

Wright selects the measurements of Sheven for Ar=60, 80 and 110 as well as ElSherbiny's data to derive his own correlations that are tailored to the zone of insulating glazing units – Ar>40 [-] and Ra<1e5 [-]. The correlation is derived to minimize the errors in the zone where the unresolved A value dependence creates disturbances in the data. Ra values between 1e5 and 1e6 were added to the dataset to account for krypton gas fills and the larger pane spacing of storm windows. The new set of correlations is:

$$Nu = Max \left[\begin{array}{l} Nu_1 = \left(\begin{array}{l} 0.0673838 \cdot Ra^{1/3} \ \text{ for } \ \mathrm{Ra} > 5*10^4 \\ 0.028154 \cdot Ra^{0.41399} \ \text{ for } 10^4 < Ra \leq 5*10^4 \\ 1 + 1.75967 \cdot 10^{-10} \cdot Ra^{2.2984755} \ \text{ for } \mathrm{Ra} \leq 10^4 \end{array} \right) \\ Nu_2 = 0.242 \left(\frac{Ra}{Ar} \right)^{0.272} \end{array} \right] \tag{30}$$

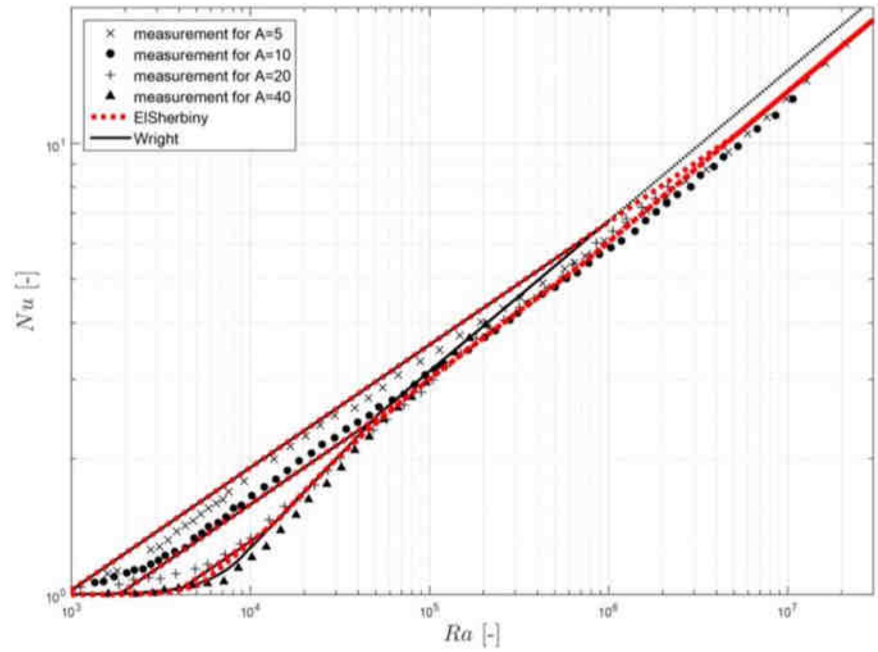

Fig. 13. – The measurement data of ElSherbiny et al. [51] (for Ar=5-40) and their and Wright's [170] general correlations (the dashed end of the lines represent the correlations extrapolated outside their reported range of validity)

Although the data used for the derivation stopped at Ra=1e6 [-] Wright claims that there is no theoretical limit to the validity of the correlation in the even larger Ra numbers of the boundary layer regime. The 1/3 slope of the Ra-Nu function in this region and the fact that Ra is proportional to the third power of the cavity thickness means that the convective heat transfer coefficient in very large cavities will be basically independent of the cavity thickness. This shows that there is a theoretical maximum convective heat transfer resistance one can achieve with a single air gap.

In these equation the term Nu_2 does show a dependence on Ar, but it is only ever effective for Ar<25 – outside the official validity range of the correlations.

The correlations presented by Wright are currently an integral part of the harmonized European and international standard EN ISO 15099 [97] for the calculation of center of glazing heat transfer indices of IG units and the widely used glazing thermal calculation program LBN WINDOW [119], however, the limitations in Ar and Ra values originally reported by Wright are not mentioned in either one. For cavities with smaller Ar values, where the Ar value dependence of the Nusselt number is more important Wright suggests using the original 6 correlations of ElSherbiny [51] instead.

In another article Wright [171] introduces a model for the calculation of minimum surface temperatures of windows that instead of a purely conduction calculation relies on a one-way coupling between a CFD simulation for the velocity field in glazing cavity and the thermal conduction calculation in the solid parts (frame, glazing, etc.). A precalculated velocity field in the glazing cavity is used to define the convective heat transfer in the thermal simulation of the glazing-spacer-frame assembly. The program is able to handle both simple conduction regime and transition regime flows but it was not intended for the boundary layer regime.

Zhao et al. [177] set out to improve the correlation of Wright and to resolve the Ar value dependence of the Nussel numbers for cavities with an aspect ratio of 5-110 [-] and a Rayleigh number of up to 2e4 [-]. In their survey of the literature and the published data they have found that Nu is always a function of Ar if Ar<40 [-] and even between Ar=40-80 [-] if Ra>5950 [-] which is shown in the data of Korpella et. al. [111], ElSherbiny et al. [51] and Yin et al. [35] alike. Theoretically for the same Ra number the Nu number should decrease with larger aspect ratios, as a large part of the convective heat transfer happens at the top and bottom edges of the cavity where the flow loops around the relative effect of which is decreased when the total height of the cavity is increased. ElSherbiny's data is found to show unphysical tendencies in this regard. Also in ElSherbiny's measurement for Ar=40-110 [-] the transition point between the conduction and transition regimes is shown to deviate significantly from what it expected form the rest of the literature. Since the correlations of Wright [170] are partly based on this dataset they warn that they could require some revision.

Instead of measurement data Zhao et al. used CFD simulation results to derive their new correlation since unlike measurements CFD simulations can produce reproducible Ar value dependent Nusselt values in every flow regime. Their new correlation is:

$$Nu_1 = \left[1 + \left(\frac{0.788335 \cdot \left(\left(1.42227 - \frac{1.41845}{Ar} \right) \frac{Ra}{Ar} \right)^{0.881073}}{139.677 + \left(\left(1.42227 - \frac{1.41845}{Ar} \right) \frac{Ra}{Ar} \right)^{0.724505}} \right)^2 \right]^{0.5} \quad \text{for } 5 \le Ar \le 30 \qquad (31)$$

$$Nu_2 = \left(1 + 0.00044265 \cdot \left(\frac{Ra}{Ar} \right)^{1.36869} \right)^{0.326071} \quad \text{for } 30 < Ar \le 110 \qquad (32)$$

The new equation compares well with the data of ElSherbiny for A=5-20 [-] but deviates for A=40-110 [-] for the reason discussed earlier.

Zhao, Goss, Curcija and Power [178] also studied the limits for multicellular patterns in the natural convection in rectangular cavities. Unlike Korpela and Lee [111] they reported both lower and upper limits in Ra number for cavities with aspect ratios between 10.7 and 80 [-]. Their calculations showed an absolute lower limit of Ar=10.7 [-] under which no multicellular flow occurred. In cavities with Ar=10.7-30 [-] the multicellular convection died before reaching the turbulence regime. Their Ra limits are shown in Fig. 14.

In his PhD thesis Power [140] performed CFD simulations with the help of the Finite Element Method to study the transition between laminar and turbulent flow in the natural convection in rectangular differentially heated cavities. He used a transient solver to look for fluctuations in the solution that may indicate the onset of turbulence. He devised a power-law correlation between the Ra and Ar numbers for the transition limit that is shown in Fig. 14.

Power also proposed a new Nusselt number correlation in and around the laminar-turbulent transition regime he investigated: Ar=5, 10, 20, 30, 40, 50, 60, 80 [-] and Ra=1e4-5.25e5 [-]. His correlation is:

$$Nu = 0.1098 \cdot \left(Ra^{1/2} \cdot Ar^{-1/6} \right)^{0.6113} \qquad (33)$$

The range of the correlation's validity is:

3.5e4<Ra<5.25e5	for Ar=20 [-]
3e4<Ra<4.06e5	for Ar=30 [-]
1e4<Ra<1.7e5	for Ar=40 [-]
1e4<Ra<1e5	for Ar=50 [-]
2e4<Ra<4.4e4	for Ar=60 [-]

Yang's dissertation [174] studied several aspect of the natural convection in differentially heated rectangular cavities: the inclination angle dependence of the heat transfer, the modelling of turbulence in the flow, the limits of transition between laminar and turbulent flow regimes. A new correlation for the Nusselt number is also presented. 2D CFD simulations of inclined cavities failed to produce any results that compared favorably with existing measurement data in the literature indicating that this type of flow is strongly 3D in nature.

Yang used a k-ω turbulence model for his simulations and relied on the comparison of simulation with and without the turbulence model to find the laminar-turbulent transition points. According to his findings the transition occurs at Ra=1e9*Ar^-3 if A<33 [-] and at Ra 360.418*Ar^-0.7573 if 33<Ar<74.

This limit is in relatively good agreement with the results of both Power [140] and Batchelor [23] as seen in Fig. 14.

The new correlation for the Nusselt number is derived for aspect ratios of A=20-100 [-] and Rayleigh numbers of Ra=2e4-2e5 [-]:

$$Nu = 0.0979573 \cdot Ra^{0.310338} \cdot Ar^{-0.0860783} \tag{34}$$

Xaman et al. [172] performed CFD simulation with the Finite Volume Method with either a laminar or four different k-ε turbulence models for natural convection in cavities of aspect ratios of Ar=20, 40 and 50 [-] and Rayleigh numbers of Ra=1e3-1e6 [-] for the laminar and Ra=1e4-1e8 [-] for the turbulent simulations. From the four investigated turbulence models they found the one of Ince and Launder [90] to agree the best with measurement data taken from the literature. They used this model to derive two set of correlations of their own for the Nusselt number based on either laminar or turbulent calculations and for Ar=20,40 and 80 [-].

The laminar correlations (for 1e3≤Ra≤1e6) are:

$$Nu = 0.1731 \cdot Ra^{0.2617} \; for \; Ar = 20 \tag{35}$$

$$Nu = 0.1865 \cdot Ra^{0.245} \; for \; Ar = 40 \tag{36}$$

$$Nu = 0.1897 \cdot Ra^{0.2398} \; for \; Ar = 80 \tag{37}$$

The turbulent correlations (for 1e4≤Ra≤1e8) are:

$$Nu = 0.0857 \cdot Ra^{0.3033} \; for \; Ar = 20 \tag{38}$$

$$Nu = 0.0635 \cdot Ra^{0.323} \; for \; Ar = 40 \tag{39}$$

$$Nu = 0.054 \cdot Ra^{0.3335} \; for \; Ar = 80 \tag{40}$$

By comparing their results with the correlations of Yin et al. [35], ElSherbiny [51], Wright [170], Zhao et al. [177] and EN 673 [53] they found that their laminar result agreed best with the data of Yin et al. and their turbulent results with most all except for EN 673. It must be noted however that their laminar calculation reached well into the fully turbulent regimes for Ar=40 and 80, and none of the data they used for comparison reached as far as theirs in the turbulent regime.
The European standard EN 673 [53] for the calculation of the thermal transmittance of glazing systems presents a single set of three correlations for the calculation of the Nu number dependent only on the Gr and Pr numbers (i.e. the Ra number) and the inclination of the cavity:

$$Nu = 0.035 \cdot (Gr \cdot \mathrm{Pr})^{0.38} \; for \; \varphi = 90° \tag{41}$$

$$Nu = 0.1 \cdot (Gr \cdot \mathrm{Pr})^{0.31} \; for \; \varphi = 45° \tag{42}$$

$$Nu = 0.16 \cdot (Gr \cdot \mathrm{Pr})^{0.28} \; for \; \varphi = 0° \tag{43}$$

For other inclinations the Nu number is to be determined by linear interpolation. There aspect ratio dependence is completely neglected.

The EN ISO 15099 [97] standard is much more comprehensive than EN 673 [53] as it incorporates both center of glazing thermal and optical calculations and multi-dimensional calculations of hat transmission through glazing-spacer-frame assemblies as well as the effect of the addition of shading devices. The set of correlations found in the standard is collection from the literature introduced above:

The correlation for vertical (φ=90°) cavities:

$$Nu = Max\left[\begin{array}{l} Nu_1 = \begin{pmatrix} 0.0673838 \cdot Ra^{1/3} \text{ for } \mathrm{Ra}>5*10^4 \\ 0.028154 \cdot Ra^{0.41399} \text{ for } 10^4 < Ra \leq 5*10^4 \\ 1+1.75967 \cdot 10^{-10} \cdot Ra^{2.2984755} \text{ for } \mathrm{Ra} \leq 10^4 \end{pmatrix} \\ Nu_2 = 0.242\left(\dfrac{Ra}{Ar}\right)^{0.272} \end{array}\right] \tag{44}$$

For inclinations between 60° and vertical (60°<φ<90°) the Nusselt number is to be determined by linear interpolation between the Nu_{90} and Nu_{60} values. This is reported to be valid by the standard for cavities with 1e2<Ra<2e7 and 5<Ar<100.

the correlation for cavities inclined at φ =60°:

$$Nu_1 = \left[1+\left[\frac{0.0936 \cdot Ra^{0.314}}{1+G}\right]^7\right]^{1/7} \tag{45}$$

$$G = \frac{0.5}{\left[1+\left[\dfrac{Ra}{3160}\right]^{20.6}\right]^{0.1}} \tag{46}$$

$$Nu_2 = \left[0.104+\frac{0.175}{Ar}\right] \cdot Ra^{0.283} \tag{47}$$

$$Nu = Max\left(Nu_1, Nu_2\right) \tag{48}$$

The correlation for cavities inclined at 0≤φ<60° (valid for Ra<1e5 [-] and Ar>20 [-]):

$$Nu = 1+1.44 \cdot \left[1-\frac{1708}{Ra \cdot \cos(\varphi)}\right]^{\bullet} \cdot \left[1-\frac{\left(1708 \sin^2(1.8 \cdot \varphi)\right)}{Ra \cdot \cos(\varphi)}\right]+\left[\left[\frac{Ra \cdot \cos(\varphi)}{5830}\right]^{1/3}-1\right]^{\bullet} \tag{49}$$

where the operator: $[x]^{\bullet} = \left(x+|x|\right)/2$

The correlation for φ=90° is based on the work of Wright [170], the ones for φ=60° and the method for interpolation for 60°<φ<90° on ElSherbiny et al. [51] and the correlation for 0≤φ<60° on Hollands et al. [84]. The correlation for φ=90° is given without any limits on the Ar and Ra numbers, which is questionable as it was derived for a much more limited range of measurement values as we have seen earlier.

3.2.2 Flow regimes of IG units and box type windows

Fig. 14 shows the Ra and A limits of the different flow regimes as described by the various authors in the literature review. Though the various sources don't agree with each other completely do to differences in methodology, possibly measurement and calculation accuracy issues and the different area they investigated, the approximate limits for the main flow types are clear.

By performing a simple Monte Carlo simulation on the expected range of the relevant geometrical and thermal parameters (cavity height, cavity thickness and temperature difference) we can determine the Ar and Ra number range we can expect to encounter in the cavities of IG units (H=0.4-3.5 [m], L=0.04-0.025 [m], dT=1-30 [K]) and box type windows (H=1-3.5 [m], L=0.1-0.2 [m], dT=1-30 [K]) respectively. The results are shown with grey and red dots on the chart.

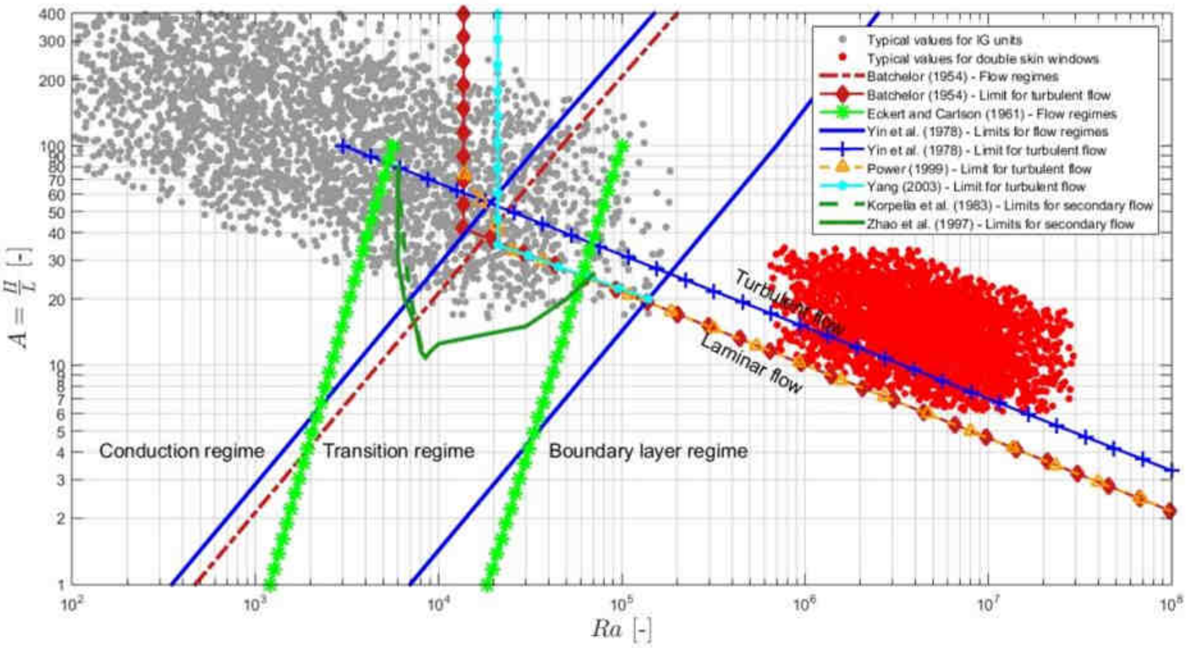

Fig. 14. – The different flow regimes reported in the literature dependent on the Ra and A numbers and the typical A-Ra number pairs for IG units and boy type windows

Insulating Glass units have typical aspect ratios of 30-40 [-] and more and their thin cavities limits the Ra number to relatively low values (<10e5 [-]) for most cases (as the Ra number is proportional to the third power of cavity thickness). As a result most IG units are in the laminar conduction regime, only for small aspect ratios and very large Ra numbers (relatively large cavity thickness and large temperature difference) do they reach into the transition regime. An example for such an extreme case would be a very small IG unit with above standard cavity width. Both Batchelor [23] and Yang [174] reported a bottom Ra number limit for the onset of turbulence (Unlike Yin et al. [35]). This limit is quite high so turbulence is also rarely encountered. The creation of secondary convection cells however can occur at slightly smaller Rayleigh numbers.

The large cavities of box type windows occupy a different position on the chart. The aspect ratio ranges from 6 to around 33 [-] and the Rayleigh number from 6e5 to 3e7 [-]. This puts these cavities clearly in the turbulent boundary layer flow regime (except for the smallest of temperature differences which are right at the edge of turbulence). They are well above the upper limit for secondary flows but according the to Batchelor [23] and Eckert and Carlson [34] a pronounced vertical temperature stratification is expected instead which is a characteristic of boundary layer regime flows.

3.2.3 Critical analysis of Nu correlations for the case of box type windows

The correlations found in the literature to calculate the Nu number are summed up in Table with the Ar, Pr, Gr or Ra number ranges they were based on. These ranges are often neglected, but are important as one should only use equations which were derived and validated for the flow regime under investigation. The range of the most important studies is also visualized in Fig. 15.

source	method	Ar	Pr	Gr	Ra	correlation
Eckert and Carlson [34]	meas.	2.5 - 46.7	0.71	8e4 - 2e5		Nu=1+0.00166*Gr^0.9*Ar (cod. r.) Nu=0.119*Gr^0.3*Ar^-0.1 (BL. r.)
Jakob [99]	meas.	3.12 - 42.2	0.71	2e4 - 2e5		Nu=0.18*Gr^0.25*Ar^-0.111 (2e4<Gr<2e5)
Newell and Schmidt [133]	CFD	2.5 - 20	0.71	4e3 - 1.4e5		Nu=0.115*Gr^0.315*Ar^-0.265
Yin et al. [35]	meas.	4.9 - 78.7	0.71	1.5e3 - 7e6		Nu=0.21*Gr^0.269*Ar^(-0.131)
Raithby and Wong [143]	CFD	2 - 80			1e3 - 1e5	Nu=(1+((0.344Ra*^0.25)/(1+112/Ra*^0.87))^2)^0.5 where: Ra*=(0.89-0.73/A)*Ra/Ar for adiabatic side walls Ra*=(1-1.02/A^0.44)*Ra/Ar for LTP side walls
El Sherbiny [51]	meas.	5 - 110			1e2 - 2e7	Nu(Ar=5)=max((1+(0.193Ra^0.25/(1+(1800/Ra)^1.289))^3)^1./3; 0.0605*Ra^1/3) Nu(Ar=10)=max((1+(0.125Ra^0.28)^9)^1/9 ; 0.061Ra^1/3) Nu(Ar=20)=(1+(0.064Ra^1/3)^6.5)^1/6.5 Nu(Ar=40)=(1+(0.0303Ra^0.402)^11)^1/11 Nu(Ar=80)=(1+(0.0227Ra^0.438)^18)^1/18 Nu(Ar=100)=(1+(0.0607Ra^1/3)^18)^18 Nu1=0.0605*Ra^1/3 Nu2=(1+(0.104Ra^0.293/(1+(6310/Ra)^1.36))^3)^1/3 Nu3=0.242*(Ra/Ar)^0.272 Nu=max(Nu1,Nu2,Nu3)
Wright [170] ISO 15099 [98]		>40			<1e5 (1e6)	Nu1=0.0673838*Ra^1/3 (Ra>5e4) Nu1=0.028154*Ra^0.4134 (1e4<Ra<5e4) Nu1=1+1.75967*10^-10*Ra^2.2984755 (Ra<1e4) Nu2=0.242*(Ra/Ar)^0.272 Nu=max(Nu1,Nu2)
Shewen et al. [154]	meas.	>40			<1e6	Nu=(1+(0.0665Ra^1/3/(1+(9000/Ra)^1/7))^2)^1/2
Zhao [177]	CFD	5-110			<2e4	Nu1=(1+((0.788335*B^0.881073)/(139.677+B^0.724505))^2)^0.5 B=(1.42227-1.41845/Ar)*Ra/Ar (Ar=5-30) Nu2=(1+0.00044265*(Ra/Ar)^1.36869)^0.326071 (Ar=30-110)
Power [140]	CFD	20-60			~A	Nu=0.1098*(Ra^1/2*Ar^-1/6)^0.6113 (Ar=20 3.5e4<Ra<5.25e5) (Ar=30 3e4<Ra<4.06e5) (Ar=40 1e4<Ra<1.7e5) (Ar=50 1e4<Ra<1e5) (Ar=60 2e4<Ra<4.4e4)
Yang [174]	CFD	20-100			2e4- 2e5	Nu=(0.0979573*Ra^0.310338)/(Ar^0.0860783)
Xaman et al. [172]	CFD	20,40, 80			1e3- 1e8	laminar (Ra=1e3-1e6): Nu=0.1731Ra^0.2617 (Ar=20) Nu=0.1865Ra^0.245 (Ar=40) Nu=0.1897Ra^0.2398 (Ar=80) turbulent (Ra=1e4-1e8): Nu=0.0857Ra^0.3033 (Ar=20) Nu=0.0635Ra^0.323 (Ar=40) Nu=0.054Ra^0.3333 (Ar=80)
EN 673 [53]	-					Nu=0.035*(Gr*Pr)^0.38 (φ=90° or vertical or vertical) Nu=0.1*(Gr*Pr)^0.31 (φ=45°) Nu=0.16*(Gr*Pr)^0.28 (φ=0°or horizontal)

Table 2. – summary of correlations for the Nu number from the literature with their ranges of validity

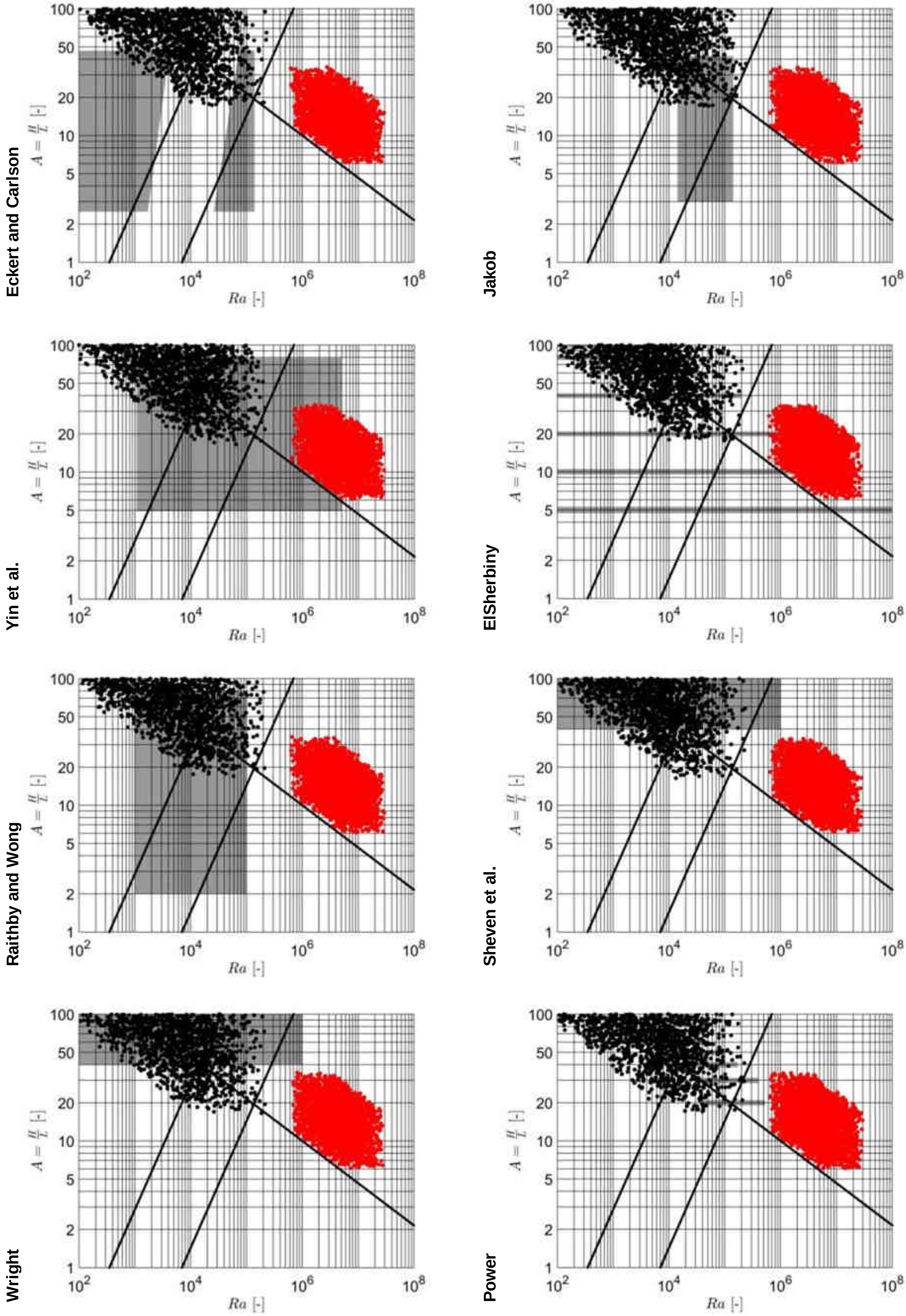
Eckert and Carlson
Jakob
Yin et al.
ElSherbiny
Raithby and Wong
Sheven et al.
Wright
Power
$A = \frac{H}{L}$ [-]
Ra [-]
100
50
20
10
5
2
1
10^2
10^4
10^6
10^8

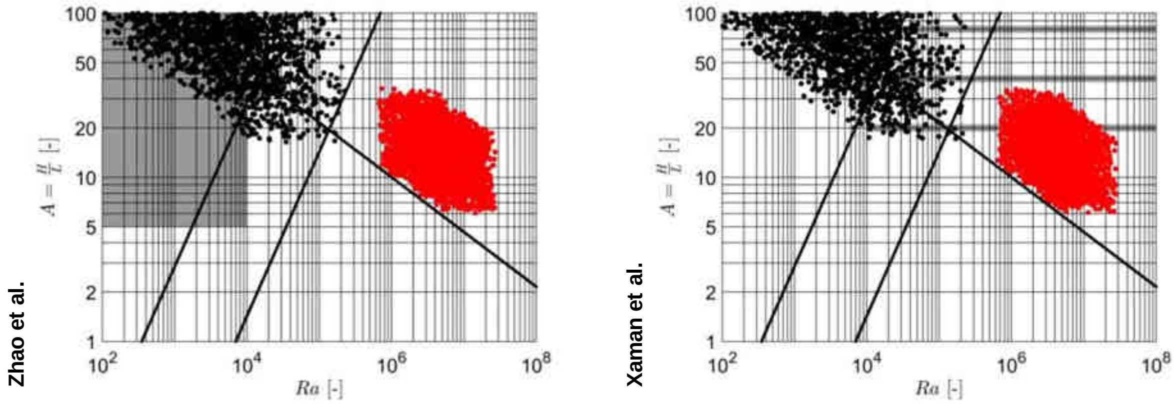

Fig. 15. – A comparison of the range of validity for various Nu correlations as published by their authors

As mentioned earlier the correlation of Wright [170] in the widely used ISO 15099 [97] standard are based on data that does not extend into the range of box type windows. His main source ElSherbiny did make measurements for Ar = 10 and 20 [-] that at least partially extended into the concerned zone, so did Yin et al [35]. We also have the turbulent CFD results of Xaman et al. [172]. Most other authors concentrated their study on the flow regimes shown to be relevant for IG unity only.

We can compare the Nu number prediction of the various correlations for a given aspect ratio of Ar=20 [-] by plotting them against one another in Fig. 16 and by comparing their %Error to the most widely used correlation of Wright (Nu / Nu_{Wright}) in Fig. 17. The aspect ratio Ar=20 [-] is chosen as a characteristic value for many box type windows which is still at least in the vicinity of some IG units. All correlations start from Nu=1 for the smallest Ra numbers as to be expected from theory and they only start trending upwards between Ra=1e3 and 1e4 [-] where the convective heat transfer begins to express itself. For calculating IG units this Ra region is the most important for the optimal sizing of the cavity thickness. A suboptimal thickness limits the useful convective heat transfer resistance of the cavity, while an above optimal thickness will result in an increased Nusselt number which also limits the thermal resistance.

The different correlations give significantly different results for bot intermediate (up to 10% difference for Ra=1e3-2e4) and large Ra number flows (>20% difference for Ra>1e5). The EN 673 [53] and Yin et al [35] correlations give the most outlying results. For box type windows the EN 673 correlation gives the largest Nu value followed by Wright while all other sources report values that are smaller. ElSherbiny's [51] correlation for Ar=20 [-] is 10% while Xaman et al.'s [172] turbulent correlation up to 20% lower than Wright. Most of the other equations are not valid for such high Ra numbers and the EN 673 equation has no specified range of validity. Its lack of Ar dependence is another reason to mistrust it for cavities with Ar<40.

ElSherbiny's data and independent correlations for Ar=5, 10 and 20 would be a good candidate to base our calculation for box type windows on, but as reported by Zhao [177] they show an unphysical tendency for large Ra numbers. As described earlier the Nu number should decrease with increasing aspect ratio for any given Ra number as the top and bottom corners of the cavity (where the convection cell loops around) get further apart. The data of ElSherbiny shows the opposite trend indicating a possible measurement error. The turbulent CFD simulation of Xaman et al. gives Nu numbers some 20% smaller than Wright but further study is needed to corroborate their findings.

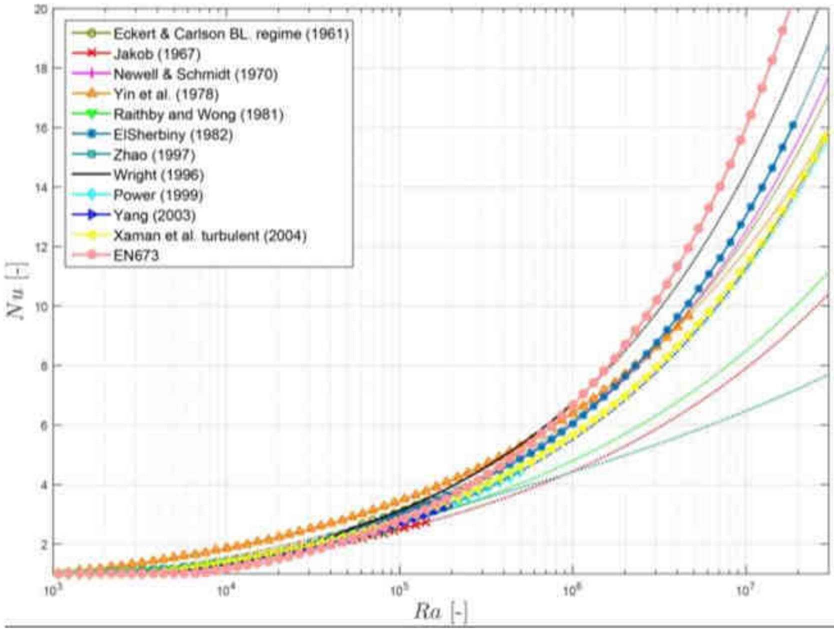

Fig. 16. – A comparison of the different Nu correlations for Ar=20 [-]

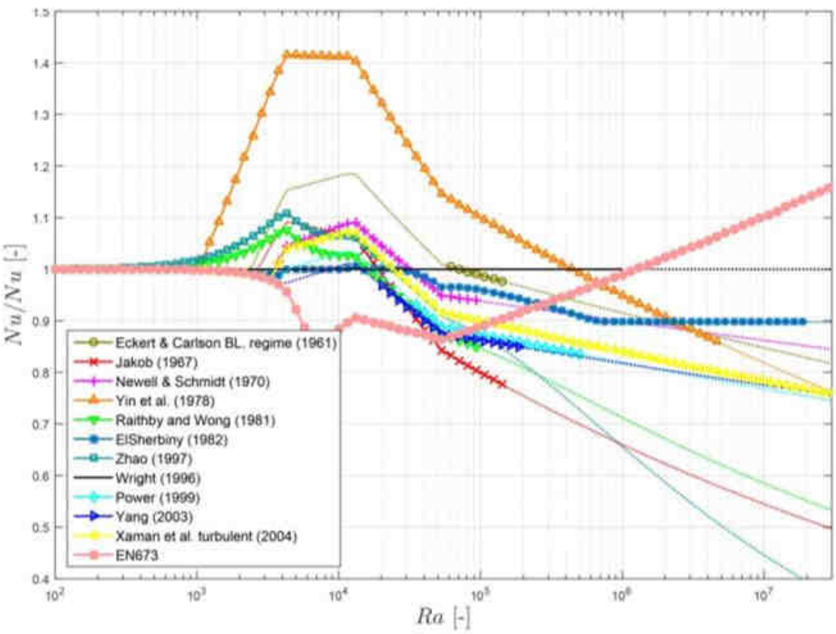

Fig. 17. – A comparison of the different Nu correlations for Ar=20 [-] to the correlation of Wright / ISO15099

The different cavity dimensions of Box type windows were shown to result in a type of natural convection very different from the one encountered in the much thinner cavities of insulating glass units. The literature review of publications on flow characterization and convective heat transfer calculations that serve as a basis for most contemporary fenestration heat transfer calculation tools reveals their understandable bias towards the geometry and Rayleigh number range of IG units. A flow regime with very different characteristics. As a consequence the analysis of published Nusselt number correlations shows few equations that are useful for box type windows and a very large discrepancies in their predictions. The correlations in the most commonly used standards EN 673 and ISO 15099 both seem inadequate due to their neglect of the cavity aspect ratio as an influencing parameter, the fact that box type windows lie outside their published area of validity and their disagreement with more recent results. Based on the available literature alone no definitive statement can be made on which correlation is the best suited for box type windows. Further study is needed focusing directly on the flow regime of such windows to generate a new dedicated correlation and to investigate the other effects the difference of box type windows' might have on the accuracy of fenestration thermal calculation tools.

3.3 CFD model

3.3.1 Literature review

In the literature, besides a few analytical papers, we find studies based mainly on either laboratory measurements or Computational Fluid Dynamics simulations. A good review of some of the available convective heat transfer measurement data is found in Ganguli et al. [74]. Good measurement setups are very difficult to construct as the heat flux, temperature differences and velocities to be recorded are all quite small and the required boundary conditions can be hard to achieve in a way that they don't interfere with the measurement accuracy, especially in the case of the convective heat flow. Ecker and Carlson [34] used interferometry to measure the temperature field in cavities but didn't reach Rayleigh numbers high enough to be useful for box windows. The measurements of Yin et al. [35] focused on the aspect ratio range of $4.9<Ar<78.7$ [-] and Rayleigh numbers of $1e4<Ra<7e6$ [-] which extends well into the range of interest for our current study but as Ganguli et al. [74] noted the concentration of heat transfer to the top and bottom edges of the cavity for low aspect ratios raises questions regarding the accuracy of the heat flux measurement methods they used. ElSherbiny et al. [50] [51] conducted one of the most comprehensive and most cited measurement campaigns in the literature about the natural convection in rectangular cavities. They investigated the effect the treatment of the side wall boundary conditions have on measurement results. They used a high conductivity material to form the side walls of their measurement setup resulting in a near linear temperature profile which is a standard practice for most such measurements. While this is a good fit for flows in the conduction regime where the temperature gradient in the fluid is itself linear which results in basically no sideways heat flux, it complicates matters when a boundary layer regime flow is investigated. Here, especially at the top and bottom zones of the cavity, the core of the fluid is close to either the cold or the hot boundary temperature while the solid wall of the cavity tries to enforce a linear temperature profile. This leads to nonzero sideways heat flux possibly causing difficulties when using the data for validation. Zhao [177] noted about ElSherbiny's data that it shows an unphysical tendency for large Ra and small A numbers. According to theory the overall heat transfer coefficient should decrease with increasing aspect ratio for any given Ra number as the top and bottom corners of the cavity, where the convection cell loops around and the heat transfer is more intense, get further apart and their effect gets proportionally smaller in the overall heat transfer. The data of ElSherbiny shows the opposite trend indicating a possible measurement error for highly stratified low aspect ratio flows. Sheven et al. [153] developed a new method for the simultaneous heating or cooling of, and heat flux measurement on cavity walls in experimental apparatus aimed at the study of natural convection in rectangular cavities based on the Peltier effect. Unfortunately their study concentrated on cavities with aspect ratios of 40 [-] or larger and Rayleigh numbers less than 1e6 [-]. At the moment there is no dataset in the literature which covers the entire aspect ratio and Rayleigh number range of flows in box type windows with sufficient resolution and is pronounced reliable by most of the sources to serve as a basis for a new correlation. We have to turn to CFD simulations instead.

With advancements in numerical methods and computational resources most newer studies rely heavily on CFD. While earlier works were limited to laminar flows such as the work of Newell and Schmidt [133] Raithby and Wong [143] Korpella and Lee [111], Wright and Sullivan [169] and Zhao [177], the type of natural convection in the cavities of box type windows is in the fully turbulent boundary layer regime. The choice of turbulence model is thus a key issue and the results have to be thoroughly validated. From the main approaches to turbulence modelling: RANS (Reynolds Averaged Navier-Stokes), LES (Large Eddy Simulation) and DNS (Direct Numerical Simulation) methods RANS models will be investigated here as a great number of individual simulations will be required to adequately resolve the flow regime of box type windows and later to model entire complex window assemblies at an acceptable computational cost.

There are few datasets available in the literature that are intended to aide the validation of turbulence models for natural convection problems in enclosed rectangular cavities. The study best suited for box type windows is that of Betts and Bokhari [26], made available for researchers through the ERCOFTAC website [69]. Betts and Bokhari conducted their measurements by modifying an earlier apparatus of Betts and Dafa'Alla [25]. The test rig enclosed an air filled cavity with 2.18 [m] height, 0,076 [m] thickness and 0.52 [m] length. The temperature difference was applied by the 2.18x0.52 [m] vertical walls that were constructed from polished aluminum with water jackets for cooling or heating, a supporting wooden frame and thermal insulation towards the outside. The aim of the design was to create truly isothermal conditions on the cold and warm sides. This was achieved, among other things, by slightly extending these walls beyond the cavity in the vertical direction. The side walls were created from a rubber material with a thermal conductivity near the effective conductance of the cavity (λ=0.155 [W/mK]). A series of thermocouples were embedded in these rubber walls. They measured a near linear temperature profile in the side walls between the hot and cold aluminum walls without the excessive heat flows of much better conducting walls that were used in many earlier measurements. The flow cavity had an aspect ratio of Ar=28.68 [-] and measurements were conducted at Rayleigh numbers of Ra=0.86e6 and 1.43e6 [-] by varying the temperature difference (ΔT=19.6 and 39.9 [°C]). Although the aspect ratio is at the higher, and the Rayleigh number (for the bigger temperature difference) at the lower end of the range found in box type windows, the results show a very similar turbulent boundary layer flow. Betts and Bokhari reported both the time averaged mean and the root mean square of the temperature and both the horizontal and vertical velocities throughout the cavity along predetermined horizontal and vertical sections (see Fig. 18). The temperature measurements were done with a 75 [μm] diameter K type traversing thermocouple with a response time of 0.07 [s], a position accuracy less than the thermocouple diameter, and a digital accuracy of 0.1 [°C]. Laser Doppler anemometry (LDA) was used for the velocity measurements. Due to the construction of their setup and the nature of the stratified boundary layer flows the convective heat transfer could not be measured directly. Instead they only reported local heat flux densities calculated based on the measured wall-normal temperature gradients in the laminar sublayer at discrete points: $q_{local}=\lambda_{air}*\partial T/\partial n$. An average Nusselt number is also given calculated from the local heat flux densities.

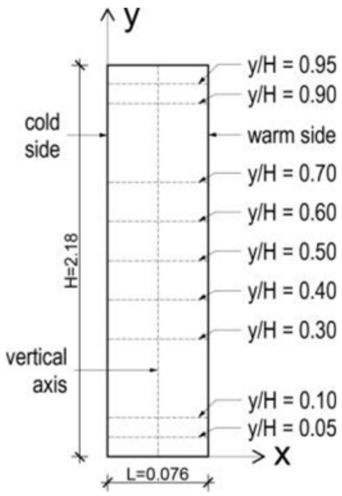

Fig. 18. – A schematic representation of the ‘natural convection in a rectangular differentially heated cavity’ problem

Betts and Bokhari [26] reported an effectively 2D temperature field for 90% of the cavity width. The velocity filed could only be measured for the middle 50% of the cavity where it was also found to be near perfectly 2D. Both velocity and temperature profiles were antimetric. In the core the velocity is near zero but the velocity fluctuations are the strongest (70% of the mean velocity near the walls) due to the interaction of the rising and sinking boundary layers. Peak velocities were found along the bottom of the hot (y/H=0.1 [-]) and the top of the cold (y/H=0.9 [-]) walls in the rising and sinking boundary layers. The temperature field also showed strong boundary layers next to the two vertical walls, with near zero horizontal gradient in the core. The top and bottom ends of the cavity showed strong vertical temperature stratification while the middle portion of the cavity did not.

The data of Betts and Bokhari was since used by many researchers for testing turbulence models. Hsieh and Lien [87] studied low-Re k-ε models for weakly turbulent flows with an unsteady RANS solver. Unlike some other flows the turbulent boundary layer flow in the benchmark of Betts and Bokhari proved sufficiently turbulent to allow for a steady-state solution without the extra computational strain of a transient simulation. They conducted a mesh refinement study but found little difference between their 50x100, 75x150 and 100x200 non-uniform rectangular grids, except in the laminar-turbulent transition point in the boundary layers. Finer resolutions in the longitudinal (vertical) direction gave slightly smaller Nusselt numbers. They also investigated the effect of different treatments of the buoyancy source in the turbulent kinetic energy equation, including the case of a zero buoyancy source, and found little to no difference indicating that the term is negligible. Although the temperature and velocity results were good the Lien and Leschziner k-ε model [121] underpredicted the average Nu number by 20% compared to Betts and Bokhari (see Table 3).

Zhang et al. [175] [176] tested the zero equation models of Chen and Xu [36], the RNG k-ε model of Yakhot and Ország [173], the low-Re k-ε model of Launder and Sharma [118], the SST k-ω model of Menter [128], the modified v2f model of Davidson et al. [39], the Reynolds Stress Model of Gibson and Launder [76] as well as Detached Eddy (DES) and Large Eddy Simulations (LES), among other benchmarks, for the turbulent natural cavity-convection problem. They used a non-uniform rectangular mesh with y+<=0.3 for RANS and 0.1 for DES and LES models. The grid dependence study found no need for further refinement. The zero equation and DES models both performed badly and predicted erroneous velocity fields, while the low-Re k-ε model had trouble predicting the temperature filed at the top and bottom ends of the cavity. The RNG SST and RSM models all gave comparably good results and the v2f model of Davidson achieved the best fit with the measurements. Aksouh et al. [3] compared simulations with the RNG k-ε and SST k-ω models with the data of Betts and Bokhari on 2 and 3 dimensional non-uniform rectangular grids and found the SST model to give superior results for heat transfer and the difference between 2 and 3D calculations negligible. Their calculated average Nusselt number was within 10% of the one reported by Betts and Bokhari (although this is not bourn out by the figure they published for the local Nusselt numbers distribution). In a later article Aksouh et al. [4] revised their results slightly by stating that 3 dimensional effect might after all be important for the flow at least at the very bottom and top ends of the cavity. They also proposed a correlation for the Nusselt number, but only as a function of Rayleigh number and for the singular aspect ratio of the investigated A=28.68 [-]. Keyn and Agarwal [104] performed a similar study comparing the realizable k-ε and k-ω SST models, with results also favoring the latter. Ammour et al. [7] run unsteady simulations with the standard k-ε, k-ω SST, v2f, φ-f and a RSM RANS turbulence models for the lower Ra number case of Betts and Bokhari. They achieved good results with low-Re models and also found the v2f to give the best results, though at the cost of occasional numerical instabilities. Another study of some 20 eddy-viscosity turbulence models based on Betts and Bokhari is found in El Moutaouakil et al. [49]. Regarding both accuracy and total computational time they found the v2f, k-ω SST and the φ-f models as the best choice. The average Nusselt number they calculated with these models fell within 10% of the one predicted by Betts and Bokhari.

A number of other publication could also be cited using the data of Betts and Bokhari, but unlike the ones reviewed here most other works are limited to studying the difference between the calculated and measured temperature and velocity fields and don't give an analysis of the convective heat transfer. The calculated Nusselt numbers found in the literature are summed up in Table 3. Unfortunately though many sources found a good qualitative agreement between the overall calculated and measured temperature and velocity fields the Nusselt number predictions show larger discrepancies.

					Ra=0.86e6 [-] (Nu_{BB}=5.85 [-])		Ra=1.43e6 [-] (Nu_{BB}=7.57 [-])	
source	software	mat. prop.	buoyancy	turb. model	Nu	%Err	Nu	%Err
Hsieh and Lien [87]	?		boussinesq	low-Re k-ε LL 0	-	-	5.99	-20.87%
Aksouh et al. [3]	?		boussinesq	k-ω SST	5.51	-5.8%	6.96	-8.06%
Ammour et al. [7]	Code-Saturn	const.	boussinesq	k-ω SST	5.266	-10%	-	-
El Moutaouakil et al. [49]	custom code	const.	boussinesq	k-ω SST	5.53	-5.47%	6.687	-11.66%

Table 3. – Comparison of calculated Nu numbers compared to the measurements of Betts and Bokhari

3.3.2 Governing equation

Based on the literature review a two dimensional steady state model was built with the turbulence modelling based on the Reynolds Averaged Navier-Stokes equations. The program ANSYS FLUENT release 13.0 [6] was used for all of the CFD simulations. For the buoyancy forces both the Boussinesq approximation and the incompressible ideal gas formulation was tested, with little-to-no difference between the results. In the end the ideal gas model was used. The continuity equation (in Cartesian tensor notation) can thus be expressed as:

$$\frac{\partial}{\partial x_i}\left(\rho \overline{u_i}\right) = 0 \tag{50}$$

where: ρ [kg/m^3] – the density

$\overline{u_i}$ [m] – the i[th] component of the mean velocity vector

Which is solved with the help of the ideal gas law:

$$\rho = \frac{P_{op}}{\frac{R_{univ}}{M_w}T} \tag{51}$$

where: ρ [kg/m^3] – the density
Pop [Pa] – the operative pressure (101325 [Pa])
R_{univ} [J/molK] – the universal gas constant
Mw [kg/mol] – the molecular mass of the fluid (air)
T [K] – the temperature

The momentum equation is:

$$\frac{\partial\left(\rho\overline{u_i}\,\overline{u_j}\right)}{\partial x_j} = -\frac{\partial\overline{P}}{\partial x_j} + \frac{\partial}{\partial x_j}\left(\mu\frac{\partial\overline{u_i}}{\partial x_j} - \rho\overline{u_i'u_j'}\right) - \rho g \tag{52}$$

where: ρ [kg/m^3] – the density
$\overline{u_j}$ [m/s] – the j[th] component of the mean velocity vector
$\overline{P}$ [Pa] – the mean pressure
μ [Ns/m^2] – the dynamic viscosity
u_j' [m/s] – the j[th] component of the fluctuating velocity
g [m/s^2] – the gravitational acceleration

The Reynolds stresses are calculated by one of the following turbulence models:

- the k-ω SST model of Menter [128]
- the RNG k-ε model
- the realizable k-ε model
- the low-Re k-ε model of Abid [2]
- the low-Re k-ε model of Lam-Bremhost [116]
- the low-Re k-ε model of Launder and Sharma [118]
- the v2f model of Durbin [44]

The energy equation takes the following form:

$$\frac{\partial\left(\rho c_p\overline{u_i}T\right)}{\partial x_i} = \frac{\partial}{\partial x_i}\left(\lambda\frac{\partial T}{\partial x_i} + \frac{\eta_t}{\sigma_T}\frac{\partial T}{\partial x_i}\right) \tag{53}$$

The turbulent heat flux in the energy equation is calculated based on the simple gradient diffusion hypothesis with a constant turbulent Prandtl number of σ_T = 0.85 [-].

The pressure-velocity coupling was based on the SIMPLE algorithm with the PRESTO! scheme for the discretization of pressure, and the QUICK scheme for the momentum, velocity, turbulence and energy equations. The properties of the air filling the cavity were calculated as temperature dependent (see Table 4).

property	symbol	value
density	ρ	incompressible ideal gas
specific heat capacity	c_p	1005 [J/kgK] constant
thermal conductivity	λ	piecewise linear interpolation: $\lambda_{T=288.75\,[K]}$ = 0.0253 [W/mK] $\lambda_{T=308.30\,[K]}$ = 0.0268 [W/mK] $\lambda_{T=327.85\,[K]}$ = 0.0283 [W/mK]
dynamic viscosity	μ	acc. the Sutherland formula
molecular mass	M_w	28.97 [g/mol]

Table 4. – material properties

The geometry was defined to match the cavity of the experimental apparatus of Betts and Bokhari, and the boundary conditions were chosen to correspond to the higher Rayleigh number of their measurements (see Fig. 19). The vertical walls were isothermal, with T_{cold}=288.75 [K] and T_{hot}=327.85 [K]. This gives a Rayleigh number based on cavity thickness and $T_m=(T_{hot}+T_{cold})/2$=308.3 [K] of Ra=1.43e6 [-]. The top and bottom walls were defined as either adiabatic (a simplification found in many of the publications) or with a temperature profile taken from the perimeter-thermocouple measurements of Betts and Bokhari [26].

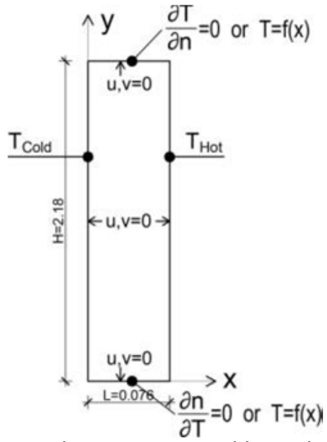

Fig. 19. – The cavity geometry and boundary conditions

A mesh refinement study was made and based on the literature research the effect of both the near wall and the longitudinal (vertical) mesh resolution was investigated. The effect of near wall resolution was <1% between y+=1 and y+=0.035. The longitudinal mesh resolution was also increased. In the end non-uniform rectangular mesh with a constant dy=10 [mm] vertical resolution for 90% of the cavity height was adapted with the same boundary layer refinement for the vertical and top/bottom horizontal surfaces.

3.3.3 Turbulence model validation

The calculation results for all the turbulence models investigated are presented in Fig. 20, Fig. 21, Fig. and Fig. 23. for the temperature and in Fig. 24 and Fig. 25 for the vertical velocity fields. Further results are shown in Appendix B.2.

The low-Re k-ε models give the worst results for both the temperature and velocity fields. They predict excessive vertical temperature stratification at the bottom (y/H<0.3) and top (y/H>0.7) portions and near zero in the middle (0.3<y/H<0.7) of the cavity. They also underpredict the maximum vertical velocities in the boundary layers and with the exception of the Launder-Sharma [118] model can't reproduce the shape of the velocity distribution in the middle of the cavity. The RNG and realizable k-ε models give nearly identical results for both temperature and velocity. Their prediction of the temperature distribution is quite good, especially for the vertical temperature profile across the middle of the cavity, however they overpredict the maximum velocities and fail to reproduce the correct shape of the velocity profile, much like the low-Re k-ε models.

The best result are obtained with the k-ω SST and v2f models, though the v2f model severely overpredicts the temperature stratification in the middle of the cavity. The maximum flow velocities are best predicted by the k-ω SST model and both the v2f and SST models produce a reasonable match for the shape of the velocity profile in the middle of the cavity: antimetric, peak velocity ca. 6-7 [mm] from the walls and a near linear distribution of vertical velocities in between.

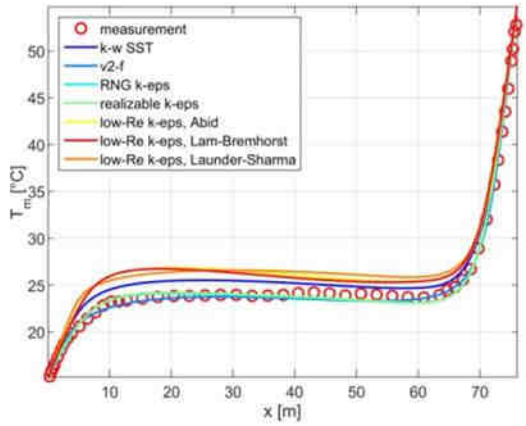

Fig. 20. – horizontal T_m profile at y/H=0.05 [-]

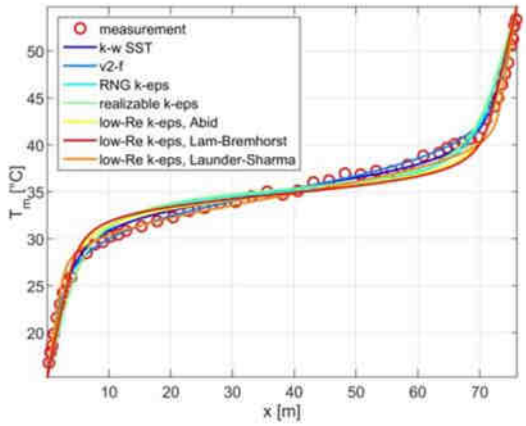

Fig. 21. – horizontal T_m profile at y/H=0.50 [-]

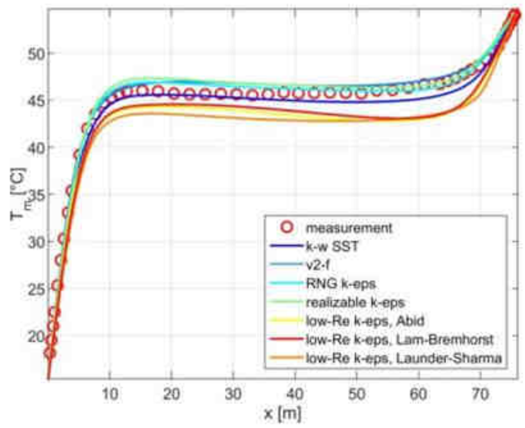

Fig. 22. – horizontal T_m profile at y/H=0.95 [-]

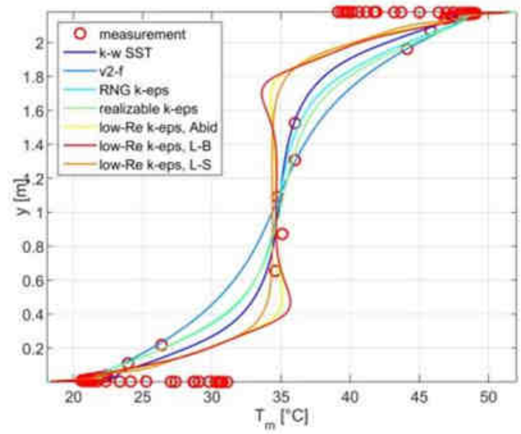

Fig. 23. – vertical T_m profile

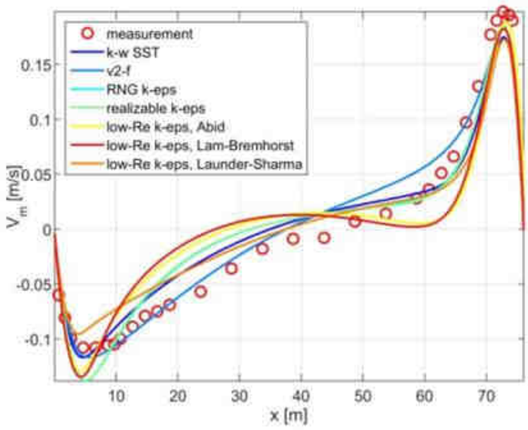

Fig. 24. – horizontal v_m profile at y/H=0.05 [-]

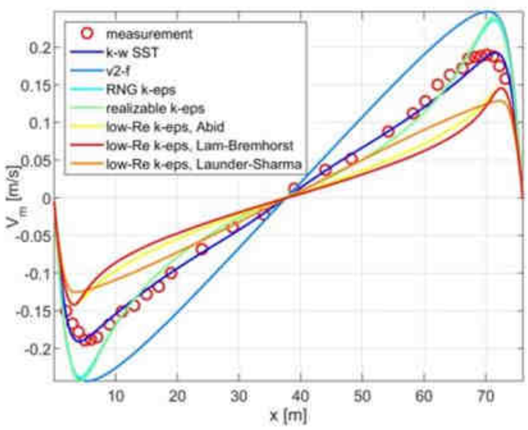

Fig. 25. – horizontal v_m profile at y/H=0.50 [-]

In the laminar sublayer immediately adjacent to the cavity walls heat is only transported in the horizontal direction by thermal diffusion in the fluid (since the wall normal velocity is zero). The local Nusselt number is thus calculated as the ratio between the local surface-normal temperature gradient and a temperature gradient satisfying the Laplace equation (heat flux only by thermal diffusion, i.e. heat conduction in an imaginary stagnant fluid):

$$Nu_{local} = L\frac{\partial T}{\partial x} / \Delta T \tag{54}$$

where: Nu_{local} [-] – the local Nusselt number
L [m] – the total thickness of the cavity
T [K] – the temperature

ΔT [m] – the total temperature difference between the hot and cold sides

The average Nusselt number is calculated by taking the surface integral of the local Nusselt number and dividing it by the total cavity height:

$$Nu = \frac{1}{H}\int_0^H Nu_{local}\,dy \tag{55}$$

where: Nu [-] – the Nusselt number
Nu_{local} [-] – the local Nusselt number
H [m] – the total height of the cavity

The distributions of the local Nusselt number along the cooled vertical wall of the cavity found in the literature are shown in Fig. 26, the calculated distributions in Fig. 27. The measured local and average Nusselt values reported by Betts and Bokhari [26] are shown in both graphs. The best match of the measurements is clearly found in El Moutaouakil et al. [49] with all of their turbulence models shown in Fig. 26 producing a $Nu_{average}$ number within 10% of the measurement. Aksouh et al. [3] published similarly good results but the graph showing the local Nusselt number distribution in their paper is faulty and can't be shown here. The low-Re k-ε model of Hsieh and Lien gives significantly lower values for the convective heat transfer. The picture is different in the calculations of this current study. All models were found to give a low Nu number compared to Betts and Bokhari (see Table 5), except for the Launder-Sharma low-Re k-ε model, which however produced irreal temperature and velocity fields as shown earlier. The lowest number is produced by the RNG and realizable k-ε models. The best match for the average Nusselt number is given by the v2f model, but the shape of the local Nusselt number profile is clearly showing the effect of the model's faulty overprediction of vertical temperature stratification. For the k-ω SST model the shape of the local Nusselt number's distribution along the cavity wall is consistent with the data but the calculated average Nusselt number is 19.1% lower than measured.

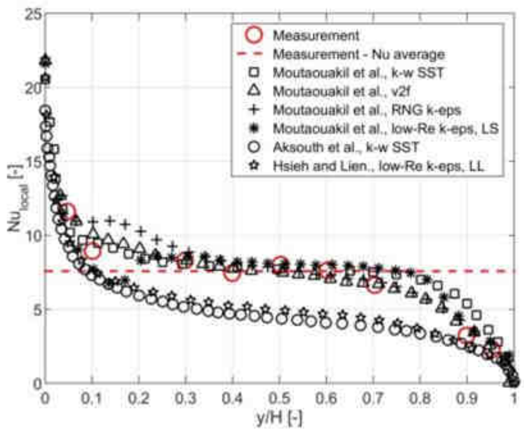

Fig. 26. – local Nusselt number (cold side) - in literature

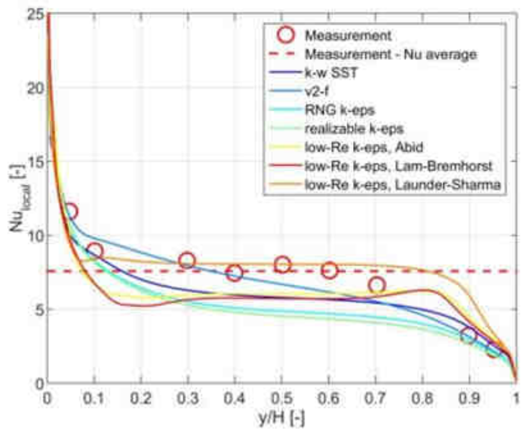

Fig. 27. – local Nusselt number (cold side) - calculated

turb. model	Nu	%Error comp. to Betts and Bokhari (Nu=7.57)
k-ω SST	6.1192	-19.16%
v2f	6.8036	-17.66%
RNG k-ε	5.4335	-28.22%
realizable k-ε	5.1666	-31.76%
low-re k-ε, A	6.2361	-17.16%
low-re k-ε, L-B	5.9629	-21.23%
low-re k-ε, L-S	7.8005	+3.05%

Table 5 – The calculated average Nusselt numbers

The reason for the discrepant Nusselt number results despite the very similar calculated temperature fields is to be found in the wall adjacent temperature boundary layer. The first 7 [mm] of the calculated temperature field at y/H=0.5 [-] along the cold wall, as well as the calculated wall-normal temperature gradients at the same place are found in Fig. 12. and 13. In the first ca. 2-3 [mm] the measured and calculated temperature profiles are near linear indicating that we are in the viscous sublayer. While the temperature fields are very similar, according to Eq. (54) the heat flux is proportional to the temperature gradient. The calculated temperature gradients next to the wall, and the thickness' of the laminar sublayer are very different depending on the turbulence model. In Betts and Bokhari [26] the Nusselt number was also calculated from the wall adjacent temperature gradient, and the average ∂T/∂n was reported as 3900 [K/m]. There were ca. 11 temperature measurement points in the first 7 [mm] of the boundary layer. The exact value of the temperature gradient is hard to determine from the data they published. For their study Betts and Bokhari used a fourth order polynomial fitted to the temperature measurement points, and the gradient was determined from this with a claimed accuracy of +-5%.

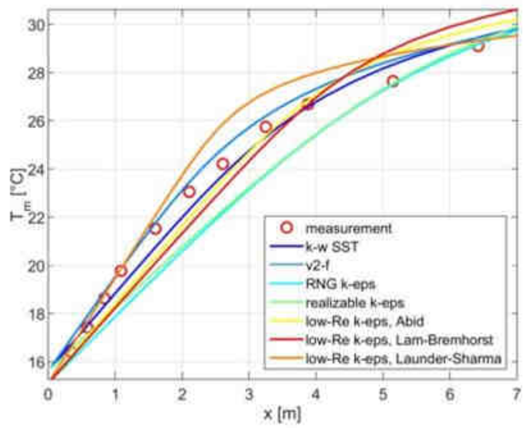

Fig. 28. – temperature field normal to the cold wall at y/H=0.5 [-]

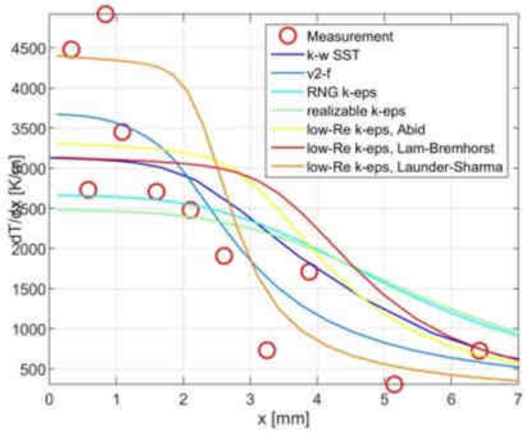

Fig. 29. – temperature gradient normal to the cold wall at y/H=0.5 [-]

It is not clear why the calculations of El Moutaouakil et al. [49] and Ammour et al. [7] produced significantly higher Nu numbers with the k-ω SST model than the current study. The use of the k-ω SST model in FLUENT with and incompressible ideal gas treatment of buoyancy and temperature dependent material properties is generally known to give good results for convective heat transfer. El Moutaouakil used a proprietary code and Ammour et al. a different CFD software (Code-Saturn) but neither paper mentioned any modifications to the governing equations or the turbulence model constants. Mesh refinement studies for the problem all show very little effect for y+ below 1, so it is doubtful that the different computational meshes could be the culprit. The material properties and turbulent Prandtl numbers, which could possibly account for the different result, are not published in either one of the papers cited in Table 3. The calculated wall-normal temperature gradients are likewise unreported.

As Betts and Bokhari's setup could not measure the heat flux densities directly (e.g. by thermopiles or by metering the heating and cooling loads) and used temperature measurements instead there is still sufficient uncertainty to conclude which model is the most accurate. Further study is needed to resolve the differences between the measurements, the published results and the CFD simulations. For the time being we will keep using the k-ω SST model as it performed the best for both temperature and velocity fields. A study of a wider range of flows must be performed to enable a comparison with the rest of the literature reviewed in part 1 of this article.

3.4 Parameters study – simple cavity

To cover the range of flows encountered in the cavities of box type windows a parameter study with 10 times 10 simulations was set up as shown in Fig. 30. The cavity aspect ratio was varied from 7 to 35 [-], and for each aspect ratio the Rayleigh number based on cavity thickness was varied logarithmically spaced between a lowest and a highest value acc. to Table 6. The prescribed cavity surface temperatures were calculated to give the specified Ra number with the cavity thickness and a mean temperature of 283.15 [K]. The boundary conditions were set acc. to Fig. 19, with isothermal vertical walls and adiabatic top and bottom walls.

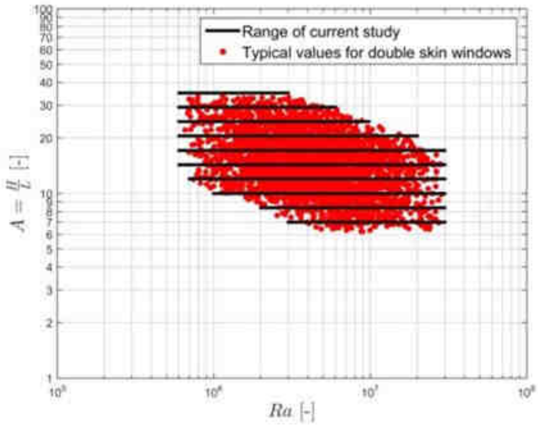

Fig. 30. – The typical flow regime in cavities of box type windows (indicated with pairs of Ra and Ar numbers) and the range of the current study

	Ar [-]									
	7	8.37	10	12	14.3	17.1	20	24.5	29.3	35
Ra_{low} [-]	3e6	2e6	1e6	7e5	6e5	6e5	6e5	6e5	6e5	6e5
Ra_{high} [-]	3e7	2e7	3e7	3e7	3e7	3e7	2e7	1e7	5e6	3e6

Table 6 – The A and Ra number range of the parameter study

Fig. 31. shows the distribution of the dimensionless temperature in the cavities of different aspect ratios and Ra numbers along horizontal sections at heights of y/H=0.1, 0.5 and 0.9 [-]. Fig. 32. displays the temperature profile through the vertical axis of the cavity. The dimensionless temperature is defined as $f=T-T_{cold}/(T_{hot}-T_{cold})$ [-]. The temperature field is similar in all cases, but there is a strong dependence on the aspect ratio. In cavities with small aspect ratios the vertical temperature stratification is almost perfectly linear. As Ar increases the stratification gets stronger in the top and bottom portions and weaker in the middle 2/3 of the cavity, as was the case in the cavity of Betts and Bokhari (Ar_{BB}=28.68 [-]). On the horizontal temperature profiles the temperature boundary layers are always visible but the temperature filed in the core (between the boundary layers) changes considerably with aspect ratio. For small Ar's there is a near zero horizontal temperature gradient between the boundary layers while in more slender cavities a distinct linear temperature is observed with ca. one-fifth of the total temperature difference. The Rayleigh number has a noticeably smaller effect on the temperature field then the aspect ratio. The vertical temperature stratification is almost independent of the Ra number except for the very ends of the cavity. For lower Ra number the thickness of the boundary layers is somewhat bigger and consequently the gradient of the dimensionless temperature in the boundary layer is slightly reduced.

The temperature in the core of the cavity outside the boundary layers is well described by the vertical temperature profile in the axis of the cavity. The temperature at the top and at the bottom of the cavity is at f=0.9 and 0.1 [-] irrespective of the Ra or Ar number and 0.5 [-] at the middle due to the symmetric nature of the flow. As the temperature stratification is often a key question in the hygrothermal behavior of box type windows it is useful to predict this temperature. The following polynomial was created with the help of the nonlinear least squares fit function lsqnonlin of MATLAB to give the dimensionless temperature of the core depending on the dimensionless height and aspect ratio:

$$\begin{aligned} f &= 0.5+0.8963\cdot b+0.0159\cdot b^2-1.5771\cdot b^3-0.0341\cdot b^4+5.2452\cdot b^5 \ldots \\ &-0.0238\cdot Ar\cdot b-0.0010\cdot Ar\cdot b^2+0.1176\cdot Ar\cdot b^3+0.0025\cdot Ar\cdot b^4-0.1282\cdot Ar\cdot b^5 \end{aligned} \quad (56)$$

$$b=\left(\frac{y}{H}-0.5\right) \quad (57)$$

where:
- f [-] – the dimensionless temperature of the core
- Ar [-] – the dimensionless aspect ratio (Ar=H/L)
- y [m] – the height
- H [m] – the total height of the cavity

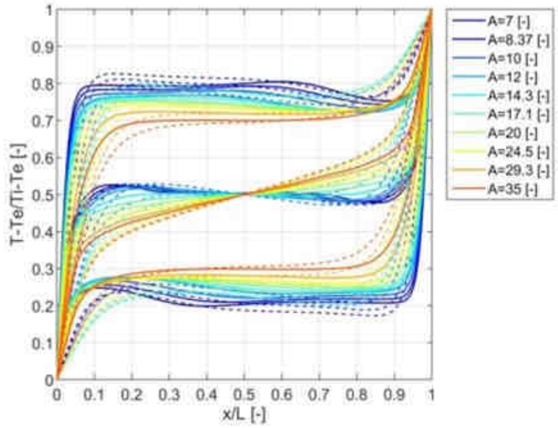

Fig. 31. – Horizontal temperature profiles at y/H=0.1,0.5 and 0.9, for high Ra (solid) and low Ra (dashed) simulations

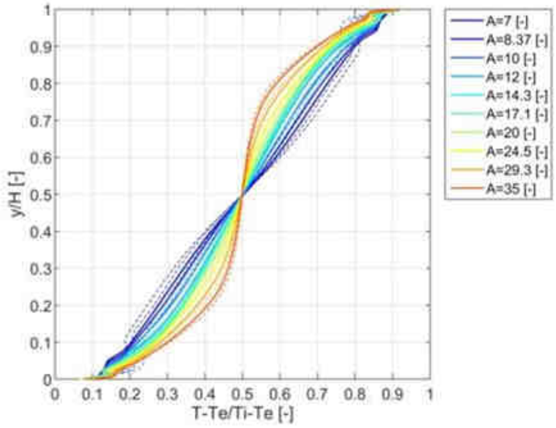

Fig. 32. – Vertical temperature profile in the cavity axis for high Ra (solid) and low Ra (dashed) simulations

The overall shape of the velocity field (vertical velocity) is also strongly dependent on the aspect ratio, as can be seen on Fig. 33. The velocity field is always antimetric with peak values in the boundary layer, but for small aspect ratios the velocity in the core of the cavity is zero while for larger aspect ratios there is a near linear distribution of velocities between the two peaks. The maximum vertical velocity for the largest Ra number is between 0.2 and 0.3 [m/s] depending on the aspect ratio. For small Ra numbers the peak velocities decrease, as expected, but the shape of the velocity profile is not changed. As with the temperature velocity profiles similar to the one found in Betts and Bokhari [26] are found in the large aspect ratio cavities.

The relative distribution of the surface heat flux along the cold vertical walls of the cavities is shown in Fig. 34. The calculated heat flux densities were "normalized" to give an integrated value of 1 to give a picture of their relative distribution. The convective heat transfer is always strongest at the top edge of the cold wall (and the bottom edge of the warm wall) where the flow inside the cavity loops around. Cavities with a small aspect ratio have a near linearly increasing heat flux density profile from the bottom to the top of the wall, while in more slender cavities there is a middle near constant section where the vertical temperature gradient in the core was shown to be the smallest.

Though all the investigated cavities are in the turbulent boundary layer flow regime the range of cavity aspect ratios Ar=7-35 [-] represents a transition zone between close-to-rectangular and tall and slender cavities, with different patterns in the temperature stratification and velocity field. In small aspect ratio cavities the boundary layers resemble those in a square cavity with a horizontally isotherm and vertically stratified core. For larger aspect ratios the boundary layers begin to interact more and more strongly creating better mixing and less stratification in the core.

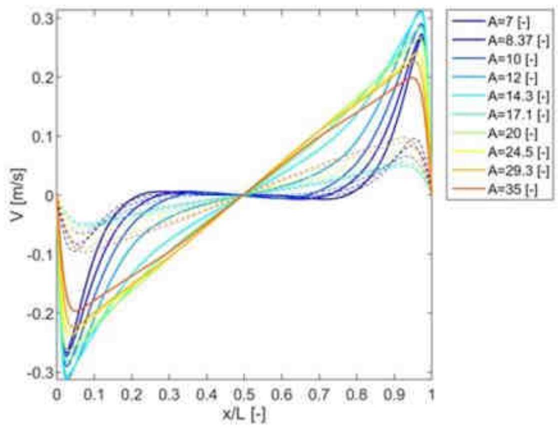

Fig. 33. – Vertical flow velocity along the horizontal section at y/H=0.5 for high Ra (solid) and low Ra (dashed) simulations

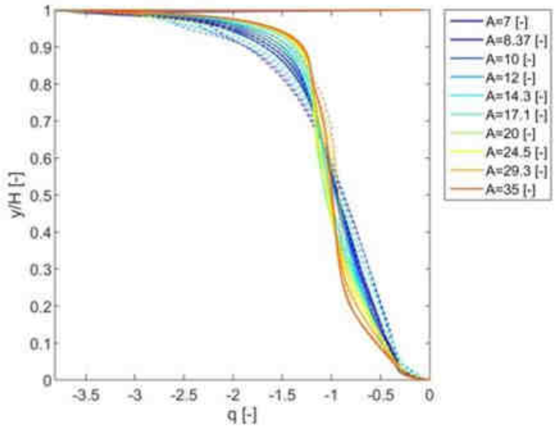

Fig. 34. – Relative distribution of heat flux density along the height of the cold cavity wall

The average Nusselt numbers calculated are shown in Fig. 35. The Nusselt number is a function of both Ra and Ar, with bigger aspect ratios producing smaller Nusselt number for any given Ra, as it is expected based on the theory. The effect of Ar can reach 10-15%. Based on these results the following new correlation is proposed for calculating the Nusselt number in the cavities of box type windows:

$$Nu = \max \begin{cases} Nu_1 = 0.0776 Ra^{0.3041} \\ Nu_2 = 0.0193\left(1 + Ra^{0.0897} Ar^{-0.0382}\right)^{3.9826} \end{cases} \tag{58}$$

The correlation (see Fig. 36.) is only intended for box type windows, with the Ar and Ra range of validity clearly set by Table 4. Nu1 gives the minimum Nusselt number and it is effective for higher aspect ratios and larger Ra numbers. For a given A Nu2 gives Nu=f(Ra) functions with a smaller slope on the double logarithmic graph than Nu1 that intersect with the latter at larger and larger Ra numbers for lower and lower aspect ratios. This indicates that the aspect ratio becomes more important for smaller Rayleigh numbers. As Ra is increased the convective heat transfer becomes more and more aspect ratio independent.

The comparison of the new correlation for Ar=20 [-] with others found in the literature is shown in Fig. . The predicted convective heat transfer is clearly smaller than the standards EN 6730 and ISO 15099 [97] (and Wright [170] on which it is based). The nearest match is with the turbulent correlations of Xaman et al. [172].

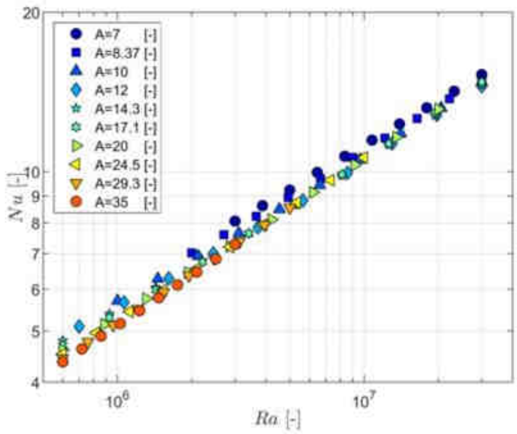

Fig. 35. – calculated Nusselt numbers

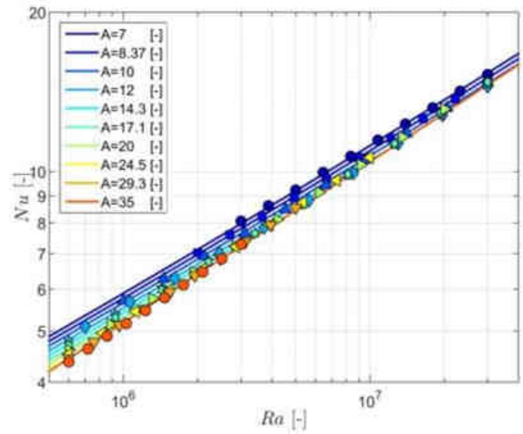

Fig. 36. – the new Nusselt number correlation

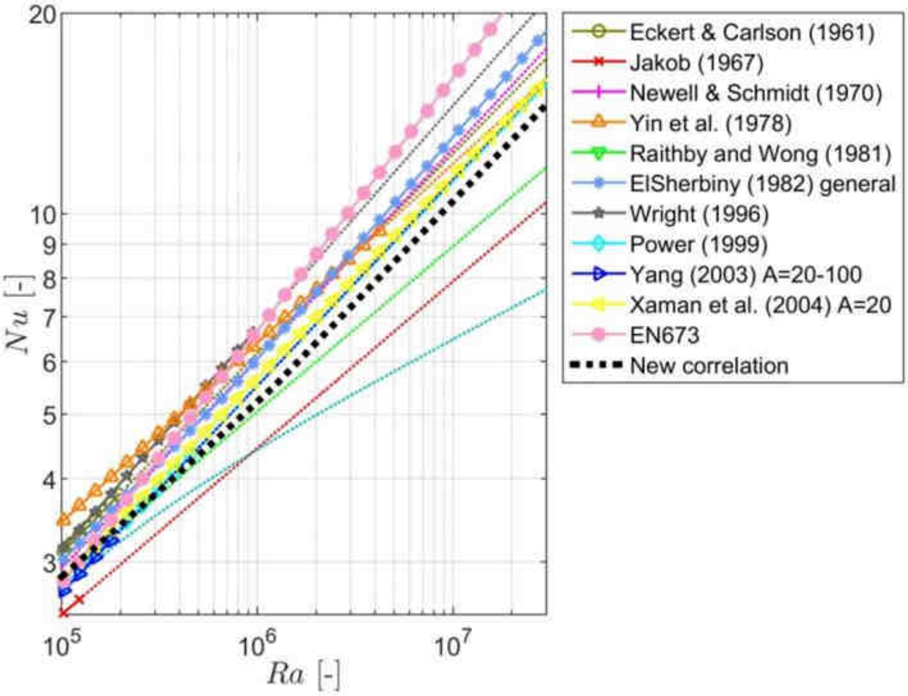

Fig. 37. – Comparison of the new correlation for the Nusselt number with the ones found in the literature, for Ar=20 [-]

3.5 Parameter study – simple glazing system

A second parameter study was conducted by modeling the entire simplified representation of the glazing system of box type windows (see Fig. 38). A basic case is a glazing system with a cavity enclosed by two panes of float glass, t_{gl}=0.003 [m] thick, on either side. So besides the fluid domain of the cavity the internal and external solid glazing layers were also added to the model. The aim of this study was to investigate the possible difference in the velocity and temperature field when the boundaries of the cavity are defined, instead of unrealistic isothermal walls, with much more realistic glazed surfaces, whose surface temperature is itself a function of the heat transfer processes in the cavity. Furthermore, in many cases the most important factor in analyzing a box type window is the lowest surface temperature in the cavity, since that is the point where moist air, filtrating into the window from inside the building, can begin to condense.

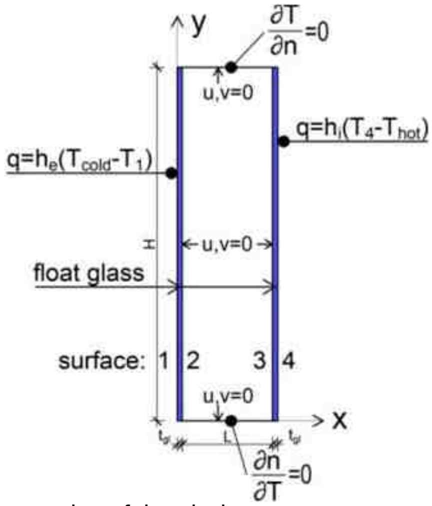

Fig. 38. – Schematic representation of the glazing system geometry and boundary conditions

The properties of the glazing material were: ρ_{gl}=2400 [kg/m^3], $c_{p,gl}$=850 [J/kgK] and λ_{gl}=1 [W/mK]. As in box type windows the cavity is formed by the frame itself no spacers were added for this study. The top and bottom edges were kept as adiabatic, while the cold and hot side boundary conditions were changed from first-type isothermal to a third type boundary with heat transfer coefficients representative for a winter condition: he=24 [W/m^{2}K] and hi=8 [W/m^{2}K]. The glazing surfaces are numbered 1 through 4 from the cold to the hot side of the entire glazing system. The internal dimensions of the cavity were defined the same ways as before, while the T_{cold} and T_{hot} temperatures were computed to give the same Rayleigh numbers in the cavity as in Table 4, but calculated based on the average temperatures of the cavity adjacent glazing surfaces – surfaces 2 and 3 instead. This was achieved by running 1dimensional calculations of the glazing system based on the ISO 15099 standard [97] to find the right temperatures.

Due to the addition of the glazing surfaces an infrared radiation model had to be add to get realistic surface temperatures. the longwave infrared radiation was taken as grey and diffuse, with no interaction with the air in the cavity. The surface-to-surface view factor radiation model of FLUENT was used for the task with a glazing surface longwave infrared emissivity of ε_{gl}=0.84 [-]. Radiative heat transfer was only modelled in the cavity. On the external surfaces of the glazing layer the heat transfer coefficients accounted for both convection and radiation.

The vertical temperature profiles on the number 2 and 3 surfaces as well on the vertical axes of the cavity are shown in Fig. 39 The dimensionless temperature is calculated as $f=T-T_2/(T_3-T_2)$ [-], where T_2 and T_3 are the average surface temperatures of the cavity adjacent glazing surface 2 and 3. As seen on Fig. 39. the temperature stratification of the core is virtually unchanged, while an additional stratification is now visible on the glazing surfaces. The temperature of surface 2 ranges from -0.1 to 0.1 [-], i.e. it can reach a 10% lower or higher temperature between T_{cold} and T_{hot} as the surface average T_1. On the warm side of the cavity the stratification is larger: between 0.85 and 1.2 [-]. It is obvious that due to the stratified turbulent boundary layer flow in such windows the critical surface temperatures can’t be determined by one dimensional glazing heat transfer simulations only.

The amplitude of the surface temperature stratification is clearly a function of the heat transfer coefficient. A larger heat transfer coefficient (smaller heat transfer resistance) limits the stratification compared to a smaller one. The effect of the surface emissivity was not investigated at this point, but it is reasonable to assume that a low emissivity coating on one side of the cavity and the resulting drop in radiative heat transfer would increase the surface temperature stratification.

As in the simple cavity the Rayleigh number has only a limited effect on the temperature field, while the cavity aspect ratio is influential in determining not just the core temperature stratification but the surface temperature stratification as well. Lower aspect ratio cavities have a near linear temperature profile between the coldest and hottest surface temperatures, while slender cavities are characterized by a distinct S shape in the profile. The absolute minimum and maximum temperatures are Ar independent but show a larger variance for the very low Ra numbers. Fortunately surface temperatures are only crucial when the external temperature is low and the total temperature difference and the cavity Ra number are high.

As expected the convective heat transfer in the cavity (subtracting the radiative heat transfer from the total heat transfer) was unchanged when compared to the simplified cavity modelled without the glazing system (for the same Ar and cavity Ra number).

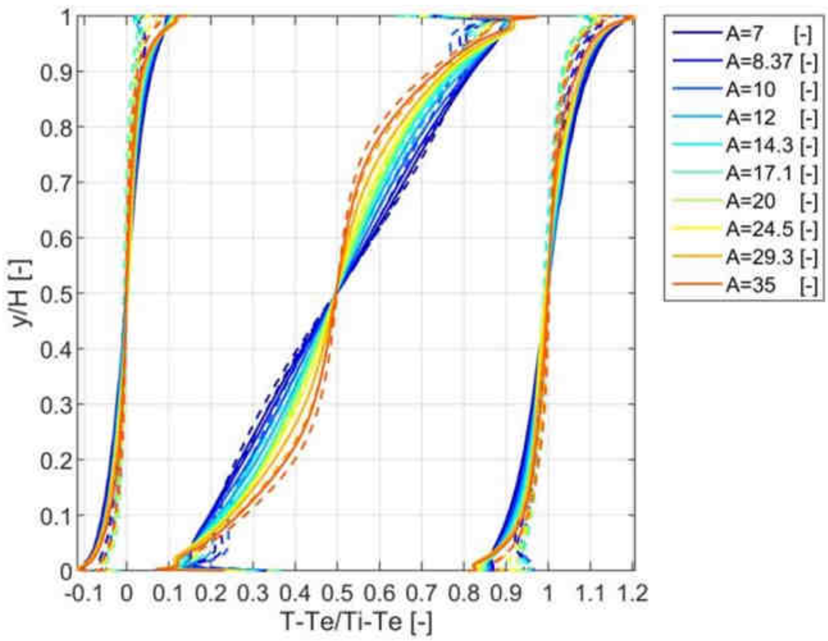

Fig. 39. – Vertical temperature profile in the cavity and on the cavity walls (glazing surfaces)

Two dimensional steady computational fluid dynamics simulations models were built to study the convective heat transfer in and the temperature and velocity fields of the cavities of box type windows. Although the precise convective heat transfer predictions of the model could not be entirely validated the k-ω SST turbulence model of Menter [128] was found to give good results for the overall temperature and velocity field when compared the benchmark measurements of Betts and Bokhari [26].

A parameter study of 100 data points over the entire cavity aspect ratio and Rayleigh number range of box type window cavities gave new insights into the types of natural convection found in these constructions. Although the flow is always in the turbulent boundary layer regime large differences exist in the temperature field, cavity stratifications as well as velocity fields of small and large aspect ratio cavities. Small aspect ratios are characterized by distinct boundary layers, a near zero mean velocity core and a linear vertical temperature stratification, while more slender cavities have strongly interacting boundary layers and as a result limited stratification. The cavities of box type windows thus lie midway between the much more slender insulating glass units of contemporary windows and the near square cavities not studied by many authors focusing researching glazing heat transfer.

As the convective heat transfer and the Nusselt number in the cavity was found to be a function of both Rayleigh number and aspect ratio a new correlation is proposed to capture this dependence. This new equation is intended to be used only for the cavities of box type windows and it predicts a smaller convective heat transfer than the ones used in the two glazing heat transfer calculation standards most used today (EN673 [53] and ISO 15099 [97]).

With another parameter study of a complete, albeit simplified, glazing system it was demonstrated that the vertical temperature stratification in the core of the cavity causes a significant temperature stratification in the glazing surface temperatures as well. This has to be incorporated into calculation aimed at studying the condensation resistance of box type windows. The results of this article could prove useful to predicting the lowest glazing surface temperatures, although further study is still needed to investigate the effects of more of the influencing parameters (glazing surface emissivity, internal and external heat transfer coefficients, etc.).

3.6 Whole window heat transfer modeling

The literature contains data from several hot-box measurements of U values for box type windows (e.g. [85] and [165]) but the detailed geometry of the tested windows, boundary conditions etc. is usually missing in these publications, therefore they can’t be used for the validation of fenestration heat transfer models. The study conducted by Homb and Uvslok [86] is perhaps the only one that presents a validation with a comparison between hot-box measurements and standard calculations performed on single- and double-skin traditional northern-European windows, the latter of which are similar to Central-European box type windows. They reported a remarkably good agreement between calculation with the CEN method and measurement. Unfortunately, even this publication isn't quite detailed enough to recreate their results. We have to rely on simulations.

Based on the turbulence model and settings found to best suite the benchmark of Betts and Bokhari [26] and tested on rectangular cavities we can now move on to modeling the conjugate heat transfer in the real life complex geometries of double-skin box type windows. However, all previous validation and verification of the CFD models were performed for simple rectangular cavities. Comparison with measurements done on actual windows is needed to increase the confidence in the simulations. In-situ monitoring measurements of box windows in actual operating buildings are not ideal to supply such data due to the fact that boundary conditions can't be controlled or measured with a high enough accuracy and are inherently instationary. Laboratory measurements of the temperature fields are needed.

3.6.1 Measurements

In the spring of 2015 we conducted a measurements campaign on double-skin box type windows to study their temperature field and to create a dataset for the validation of CFD models. The measurements were conducted with the financial support of the Budapest University of Technology and Economics Faculty of Architecture as a part of the ODOO+ project[7] and with the material support of the Hofstädter Kft.[8], a Hungarian window manufacturing corporation. The work took place in the Budapest laboratory of the ÉMI Minőségellenőrző Innovációs Nonprofit Kft.[9]. Unfortunately there was no test apparatus available in the country that could be used to install full-size box windows in, so an improvised rig had to be created for the task.

Fig. 40. – The hot box in operation

Fig. 41. – test window No. 2b installed in the surround panel

The aim was to create a calibrated hot box, as described in the standards EN ISO 8990 [60] and EN ISO 12567 [63], with an opening at least 1.35 by 1.93 [m] big to fit the selected test windows described below. Such a device consists of two (a cold and a hot) thermally insulated temperature controlled chambers on either side of a well insulated panel (surround panel) housing the test specimens in an opening between the two environments. Both chambers have to be controlled to a very small temporal and spatial temperature variance so a near stationary state can be reached during the test. A temperature difference of 20 ± 2 [K] with a 10 [°C] mean temperature is customary for testing building products as a good approximation of winter conditions. The most crucial part of a hot box is the

[7] ODOO+: a "SolarDecathlon versenyen eredményes BME ODOOprojekt további hasznosításának vizsgálata " c. projekt, illetve az azt támogató „Új Széchenyi Terv ED_13-1-2013-0005 programja" keretében

[8] Hofstädter Kft. window manufacturer corporation, Budapest, Teve utca 7-11

[9] ÉMI Minőségellenőrző Innovációs Nonprofit Kft, Building Constructions laboratory, Budapest, Diószegi út 37

heating and cooling system for which we had very limited resources. We decided to utilize the temperature control subsystem of the EMI's Holten Typ Rosenheim window air permeability, watertightness and wind load resistance test rig which is normally used to perform testing according the EN 1026 [54], EN 1027 [55] and EN 12211 [58] standards respectively. The rig has a strong metal frame with and adjustable aperture chamber, a pressurization and airflow measuring system with a strong centrifugal fan and a 2.09 [kW] cooling unit to test windows with temperature sensitive materials in winter conditions.

The cold chamber of the hot box was constructed to fit inside the aperture of the window test rig as a thermally insulated removable inlay with cooling provided by the rig's air handling system. The walls of the inlay are made out of XPS foam 5 [cm] thick at the back side, as the space was limited inside the test rig, and 20 [cm] on the lateral sides. The external dimension of the cold chamber are 2.18 by 2.8 by 0.4 [m] and the internal dimensions 1.76 by 2.36 by 0.35 [m]. The air enters through a distributer box at the top of the chamber and is collected by a similar chamber at the bottom. A black painted OSB baffle provides shielding between the test specimen and the air intake and outlet, as well as a possibility the surface temperatures the test specimen is in radiative heat exchange with. The spacing of the surround panel (the panel housing the test specimen and separating the two chambers) and the baffle is 10 [cm] and the baffle extends at least 10 [cm] beyond the test aperture in every direction. Two 10 [cm] high slits at the top and bottom allow for air circulation around the baffle. The exhaust air of the cooling was recirculated into the air handling system with a flexible plastic pipe. Three linear squirrel cage fans under the baffle provide good air mixing between the two sides of the baffle, avoid temperature stratification and ensure a sufficiently high flow velocity to create a convective heat transfer coefficient representative of the outside environment (the flow velocity was ca. 3.3 [m/s]). The flow direction next to the test specimen was upward, matching the direction of natural convection next to the exterior of a construction heated from the other side.

The surround panel has a loadbearing frame of 5 by 5 [cm] pine battens, a 20 [cm] thick XPS foam insulation and a 12 [mm] thick OSB planking on either side. The joints on the panel surface are sealed with duct tape. The entire panel is 2.83 by 2.89 by 0.244 [m] as it has to extend beyond the external dimensions of the cold and hot chambers and the air ducts and be fixed to the metal frame of the window test rig. The panel has a 6 by 6 [cm] solid wood rim which is pressed into the rubberized foam seal on the window test rig by a system of adjustable position metal bolts. The surround panel's internal aperture is 1.35 by 1.93 [m] and is lined with a 3 cm thick purenit block at its perimeter to provide a solid, but relatively thermal bridge free surface to fix the test specimen to. The windows were installed into the surround panel and outfitted with sensors at a separate stand and the whole assembly was moved in place with the help of a crane. The aperture size was designed to encase all test windows with a 1 [cm] clearing. During installation of the test windows of various sizes the excess space in the opening was filled in with XPS foam. The space crated by the frame of the windows was filled in with glass wool insulation and an airtight seal was created between frame and surround panel with adhesive tape.

The warm side chamber is a 2.18 by 2.76 by 0.7 [m] XPS foam 5 sided box with 1.75 by 2.33 by 0.485 [m] internal dimensions, an inner OSB lining and a black painted OSB baffle similar to the one in the cold side chamber. The thermal insulation of the walls is 20 [cm] thick with two layers of 10 [cm] XPS blocks in an offset pattern. The heating was provided by electric heating cables stretched into the air stream behind the baffle. The baffle is fixed 20 [cm] from the surround panel face and it extends at least 10 [cm] beyond the test aperture on all sides with 10 [cm] gaps at the top and bottom to allow air circulation. Two small squirrel cage fans provide necessary air circulation to prevent temperature stratification. The flow direction was downward at the face of the test specimen to match the direction of natural convection for a construction cooled from the other side. The entire warm side chamber was put on wheels to make it easier to move. For the measurements it was moved next to the surround panel enclosing the test specimen and an airtight seal was created by expanding foam strips fixed to the contact surface on the surround panel when the chamber was pressed on the surround panel with ratchet straps. The seal was checked with a handheld thermo-anemometer at the beginning of each measurement.

The air handling and cooling unit had its own PID controller while the heating in the warm chamber was controlled with the help of a P100 sensor placed into the airstream and a IAS Ecotherm-UNI digital temperature controller. For the temperature measurement we had a National Instruments data logger with altogether 60 thermocouple channels with zero point compensation and T-type (copper/constantan) thermocouples at our disposal. 9-9 sensors were placed in a 3 by 3 grid pattern on the cold and warm side baffles to record the mean radiative temperature facing the test specimen. 5 sensors were placed in the middle of the air stream in the cold and 3 in the warm chamber between test specimen and baffle panels at three different heights to measure the air temperature and check for temperature stratification. Two sensors were placed on either side of the surround panel and two or three outside the hot box to record the temperature in the laboratory. 29 sensors were left to be placed on the test windows themselves. The limited number of thermocouples did not allow for a proper instrumentation of the hot box walls and the surround panel so the setup could not fully comply with the requirements of the EN ISO 8990 [60] standard. As the heat flux density through the glazing system is a function of the exact position heat flow sensors were not used except for the early calibration measurements of the hot box.

Three windows, two original and one newly constructed, in altogether 5 configurations were prepared for testing to cover a wide range of constructional variants. Photo documentation and plans of the test windows are found in Appendix A while a short description is given here in Table 7.

test specimen	size [m]	short description
No. 1	1.11/1.9	Early 20th century inward opening box type window with two times 4 sashes in a cross pattern with horizontal and a single (upper external) mullion, no refurbishment, 3 [mm] thick uncoated glass
No. 2	1.325/1.54	Ca. mid. 20th century inward opening box type window with two times two sashes, without mullions, no refurbishment, 3 [mm] thick uncoated glass
No. 2b	1.325/1.54	Window refurbishment option demonstrated with the modification of window No. 2: the internal sashes are removed and replaced with a completely new internal window skin out of ISO 68 glulam profiles with 4-16-4 argon filled soft coated low-e IG units, modern hardware and rubber gasket seal.
No. 2c	1.325/1.54	Window refurbishment option demonstrated with the modification of window No. 2: both internal and external sashes removed and replaced with a completely new single skin window installed in the original frame at the external side. The new construction is a ISO 78 glulam system with a 4-12-4-12-4 argon gas filled soft coated low-e triple IG unit, modern hardware and rubber gasket seal.
No. 3a	1.124/1.91	Newly constructed inward opening box type window with geometry modelled after window No. 1. 40 [mm] external and ISO 68 internal glulam frame and sash with modern hardware and internal rubber gasket seal. Glazing system: thin IG unit in the external sash (4-6-4) and single clear 4 [mm] uncoated float glass in the internal sash.
No. 3b	1.124/1.91	The same window as No. 3a but with a different glazing system: single clear 4 [mm] float glass in the external and 4-16-4 argon filled soft coated low-e IG units in the internal sash.

Table 7 – Short description of the test windows.

As already mentioned the main goal of the measurements was to capture the characteristic stratified temperature field in the double skin windows and to establish a dataset for the validation of CFD simulations. As (according to the literature) the flow field is nearly 2D for the middle of the cavity (between the jambs, mullions, etc.) a characteristic vertical cross section was selected for each specimen at the centerline of the right hand side sash. Most sensors were placed in these characteristic sections at different heights on the external and internal glazing surfaces, in the middle of the cavity (suspended by wire) and at additional points of interest e.g. glazing perimeters, etc.). Additional sensors were placed in the symmetry plane of the windows and on the surface of the lateral walls of the cavity. The sampling frequency was 1 [1/s] and the one minute running average was saved. Plans of sensor placement on the test windows as well as graphs showing the raw data are found in Appendix A.

Each measurement was conducted during a single day (after several days of preparations). The hot chamber reached operating conditions after only about 1.5 hour while the chill down of the cold chamber took around 3 to 4 hours with an additional 1 to 2 hours for temperature stabilization. This left an additional 2-3 hours of near stationary operation. The hot box's operation was maintained within the design limits: vertical temperature stratification under 2 [K/m], mean operating temperature between 10 and 20 [°C], total temperature difference greater than 20 [K]. The cooling system wasn't strong enough to reach a near zero temperature in time so the measurements were done at a higher mean temperature than 10 [°C].

The heating and mixing fan power was continuously metered with a precision analog power meter and an attempt was made to calibrate the hot box according to the method described in ISO 8990 [60] to enable the direct measurement of the overall thermal transmittance U_w of the test windows. A series of calibration measurements were performed with the help of calibration panels but the effort was ultimately unsuccessful due to the very limited time allotted to us for each measurement (the facility could not be used outside working hours) and the limited number of all possible measurement days. The hot box construction was relatively low thermal mass but the stationary state could not be maintained long enough to reduce measurement errors to an acceptable level and there was no possibility for calibrating the temperature difference dependent heat losses of the metered chamber. The speed of the circulation fans in the chambers could not be controlled and the measured surface heat transfer coefficients: h_e = 38 [W/m^{2}K] and h_i = 8.9 [W/m^{2}K] could not be fine tuned to give the required average total heat transfer resistance of $R_{s,tot}$ = 0.17 [m^{2}K/W]. This still can't be summarized as a failure as the even lower mass of the test windows made it possible to keep them under steady-state conditions. The measured temperature fields alone constitute a very valuable dataset for the study of traditional box type windows, one which is unavailable from other sources. The main structural components were put into storage and could be used again in the future under more optimal circumstances.

3.6.2 Measurement results compared to 2D CFD simulations

The CFD simulations were performed in FLUENT using the best settings found earlier: 2D stationary double precision calculation with temperature dependent thermophysical properties for the fluid (air), constant properties for the solid materials, incompressible ideal gas model for the buoyancy forces, the SIMPLE (Semi-Implicit Model for Pressure-Linked Equations) pressure based solver, the PRESTO! scheme for pressure interpolation, the QUICK scheme for the momentum, turbulence and energy equations and the k-w SST turbulence model of Menter [128] for closure of the RANS equations. The turbulent Prandtl number for the energy equation was 0.85 [-] and the longwave radiation was modeled with the help of the surface-to-surface radiation model with view-factors calculated using ray-tracing. The flow in IG units (for the windows with IG units) was modelled as a laminar zone. The material properties of the solid components are summed up in Table 8. Detailed descriptions of the computational mesh, boundary conditions and plots of the results are found in Appendix B.4.

material	thermal conductivity [W/mK]	emissivity [-]
aluminum (painted)	160	0.9
EPDM	0.25	0.9
frame cavity[10]	0.09 (effective value)	-
glass	1.00	0.837 (uncoated) 0.18 (hard coated low-e) 0.037 (soft coated)
insulation (glass wool)	0.04	0.9
IG sealant	0.4	0.9
PUR foam	0.025	0.9
purenit	0.086	0.9
putty (linseed oil based)	0.6	0.9
PVC	0.17	0.9
silicone	0.5	0.9
spacer[11]	0.71 (effective value for aluminum spacer)	0.9
wood / OSB	0.13	0.9

Table 8 – Material properties used in the simulations

The first to be modelled was test window No. 1. Besides the window itself the XPS foam insulation underneath and above the frame (put there to fill the aperture of the surround panel), as well as part of the surround panel between the cold and hot chambers was also modelled. The first simulation used boundary conditions specified with the ambient temperatures and measured surface heat transfer coefficients: h_e = 38 [W/m^{2}K] and h_i = 8.9 [W/m^{2}K]. These were determined from the initial calibration

[10] The internal cavities in the window frame (the small operating joints between frame and sash) were not modelled as independent flow domains as they have very little influence on the thermal properties of box type windows. The cavities were instead treated with an effective thermal conductivity calculated based the model described in ISO 15099 [97] with the program LBNL THERM [119]

[11] The IG spacers were not modelled with their exact geometry, as that would have complicated the meshing process, instead the effective thermal conductivity model of Van den Bergh et al. [164].

measurements in the hot box with the help of calibration panels, a heat flux meter, surface, air and baffle surface temperature measurements. A comparison of measured temperatures and calculated temperatures are found in Fig. 42. The calculated temperature (in green) is shown on the x axis, while the height is indicated on the y axis. The temperature is plotted for all surfaces (hot side, cold side, inside the cavity). Measurements are shown as single data points. The agreement between measurement and simulation is not very good: the CFD model underpredicts temperature stratification for both the internal (right) and external (left) surfaces by more than 2 [K]. The temperature difference between the two glazing surfaces was also too large. This was unexpected as comparison with the benchmark of Betts and Bokhari [26] showed remarkably good results for the temperature field. This hinted at the boundary conditions as a possible source of the large error.

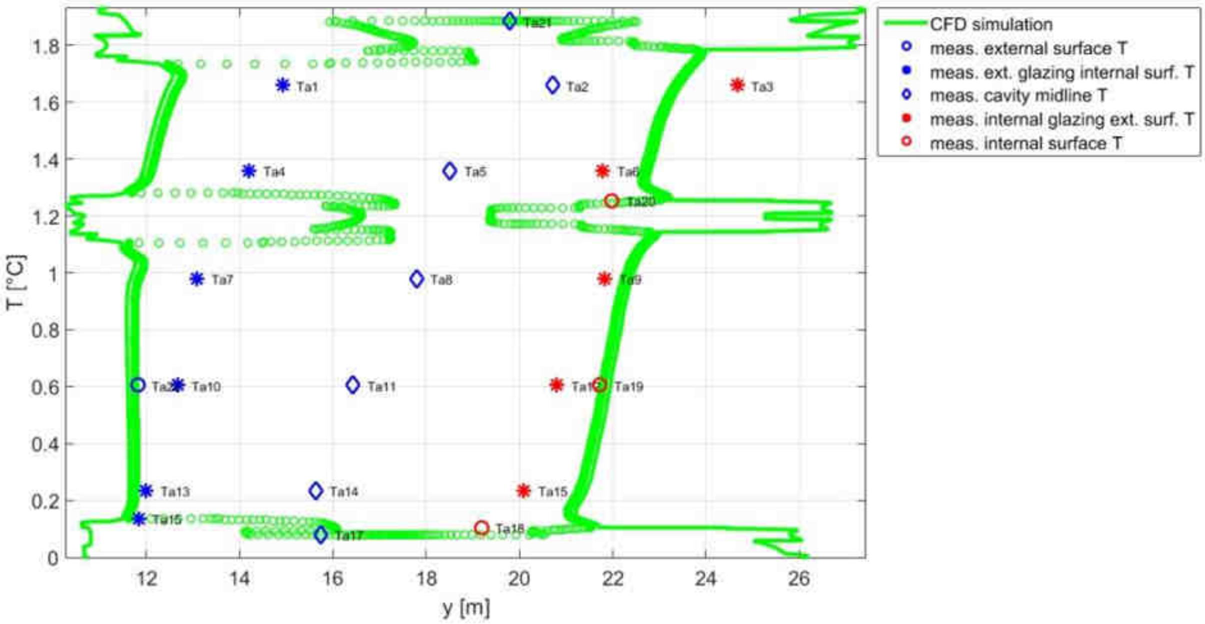

Fig. 42. – test window No. 1 – comparison of measurement and simulation (only the window modelled), $T_{e,air}$ = 10.75 [°C], $T_{i,air}$ = 27.97 [°C]

For the subsequent simulation the space between the test specimen / surround panel and the cold and hot side baffles were also added to the simulation (see Fig. 43). The baffle surface temperatures (as a function of height) were set as first type temperature boundary conditions to be included in the surface-to-surface radiation calculation. For the convective heat transfer the air circulated in the channels was modelled with flow domains. The inlet at the cold side (bottom of the channel) was defined as a velocity inlet with the measured flow speed of the circulation fans (3.3 [m/s]), a turbulence intensity of 10% (as it is close to the exhaust of the circulation fans) and a turbulent length scale of 0.007 [m]. The outlets were pressure outlets wit a zero gauge pressure. The inlet of the warm side air channel is at the top with a 0.15 [m/s] inflow velocity, 5% turbulent intensity and the same length scale. The outlet of the warm air channel is also of a pressure outlet type with zero gauge pressure. By defining the boundary conditions this way both the internal and external convective and radiative heat transfer could be calculated more precisely.

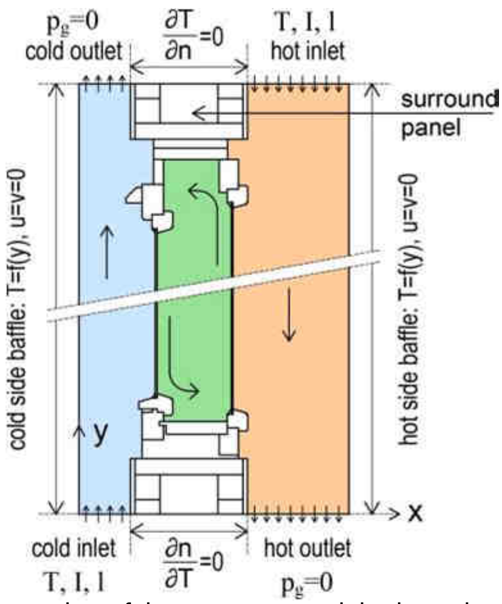

Fig. 43. – schematic representation of the geometry and the boundary conditions for the 2D CFD simulations: test windows, surround panel, hot and cold air channels and baffles

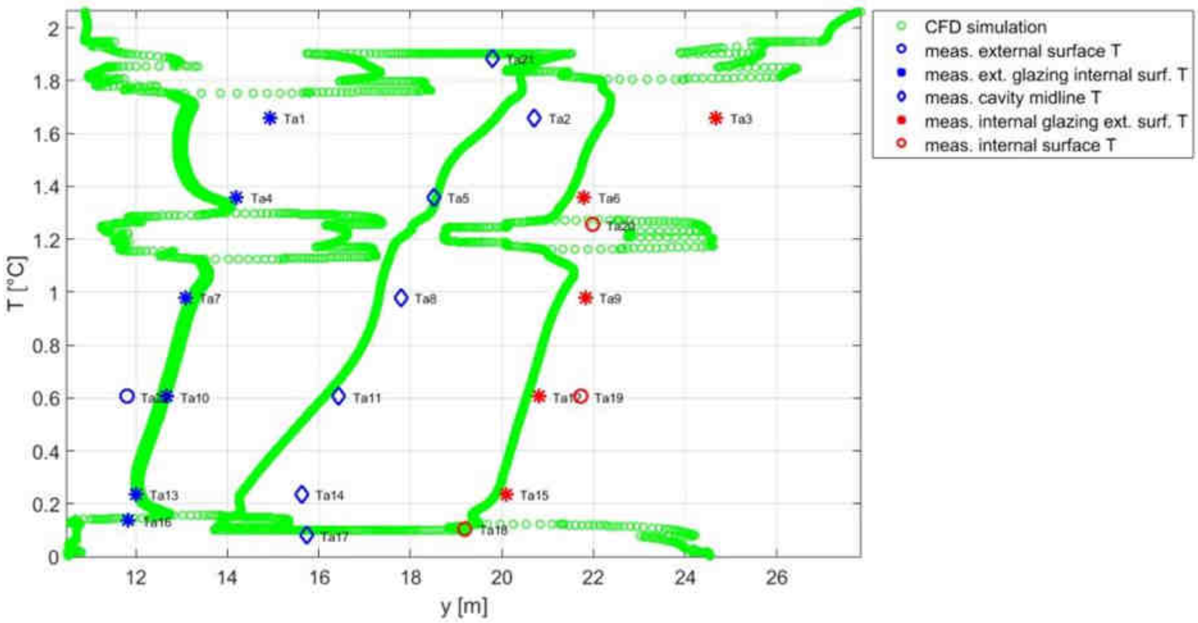

Fig. 44. – test window No. 1 – comparison of measurement and simulation (internal and external environment added to the model), $T_{e,air}$ = 10.75 [°C], $T_{i,air}$ = 27.97 [°C]

The more realistic boundary condition definitions improved the results considerably, as can be seen on Fig. 44. The measured temperature stratification in the core of the cavity is also indicated here by the green data points in the middle. The vertical aspect ratio of the window cavity was Ar=11.72 [-] which is near the lower end of the range expected in box type windows. Correspondingly the calculated vertical temperature stratification in the core is near linear with height (as predicted by the parameter study earlier) is matched well by the measurements. The glazing surface temperatures are also well captured by the CFD, except for the top sashes where a sudden temperature drop is visible simulation. The upward flow in the external air channel is suddenly accelerated by the protrusion of the fix horizontal transom of the window and a separation bubble is formed next to the glazing behind the protrusion. The shear layer between the low and high velocity fluid regions increases turbulence considerably resulting in much more intensive convective heat transfer on the surface. This was not encountered in the measurements. Further improvements to the simulation could be made by modelling the entire 3D geometry of the test windows and the whole of the hot box chambers, but due to the very high computational load this was outside the possibilities of this work.

The average temperatures at either side of the glazing cavity are hard to pinpoint exactly due to the stratified nature of the flow, the complexity of the geometry and the small number of temperature measurement points. However, if we use linear least squares fits on the glazing surface temperatures and evaluate the result at the mid cavity height we get 13.69 [°C] on the cold and 22.2514 [°C] on the warm side as approximate average surface temperatures, and a Rayleigh number of Ra = 2.7871e6 [-]. The lowest measured surface temperature inside the glazing system is at Ta16 = 11.8441 [°C] which gives a dimensionless temperature based on the mean hot and cold surface temperatures ($f=T_s-T_{cold}/(T_{hot}-T_{cold})$ of $f_{a16}=-0.22$ [-], i.e. 22% of the total cavity temperature difference lower than the cold side mean temperature. This is even lower than was predicted by a simple rectangular glazing cavity (although the boundary conditions were different for those calculations). The dimensionless temperature in the core of the cavity varies between 0.15 and 0.82, which is close to the earlier predictions.

The geometry of the window's cavity is much more complex than the simple rectangles studied earlier. The calculated velocity magnitude plot seen in Fig. 47 shows the distinct boundary layer flows at the cold and warm sides and that they loop around the horizontal transoms and sashes at the middle of the window. At the very top and bottom of the cavity however the flow separates from the surface and small counter rotating cells can be observed.

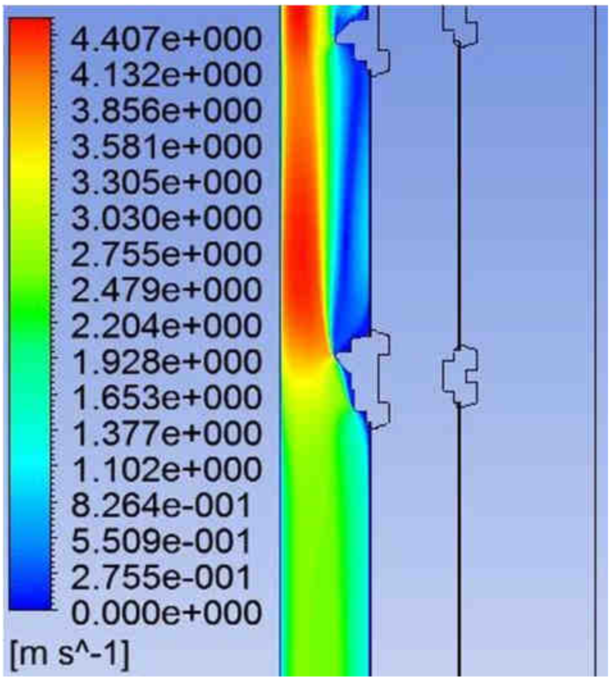

Fig. 45. – the accelerated flow in the cold air channel around the horizontal mullion of the window frame

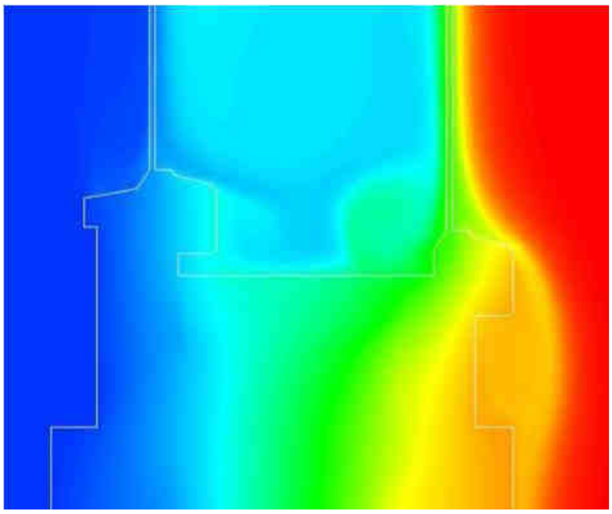

Fig. 46. – Temperature field at the bottom of the cavity

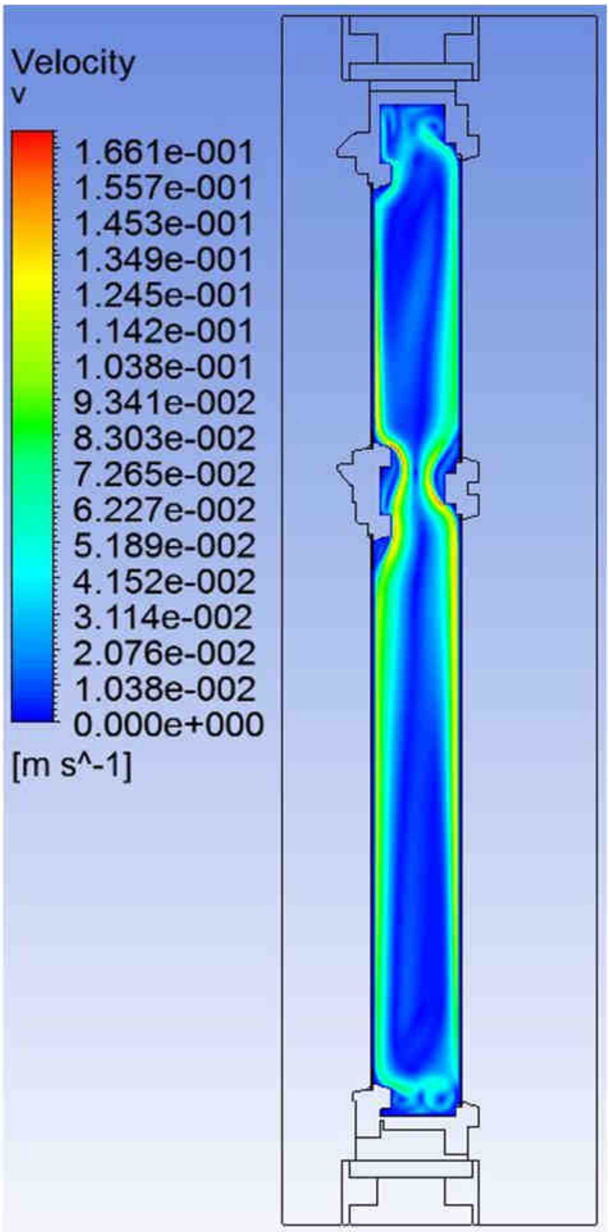

Fig. 47. – Velocity magnitude in the cavity of test

in test window No. 1 window No. 1

The comparison of measurement and simulation for test window No. 2 is shown in Fig. 48. The results is even better than for window No 1, possibly due to the simpler geometry. The vertical cavity aspect ratio was Ar = 12.26 [-], once again around the lower end for box type windows. The temperature stratification in the core is nearly linear, without the disturbances caused by fix transom as in window 1. The highest internal surface temperatures show the largest deviation while the lowest temperatures are well predicted.

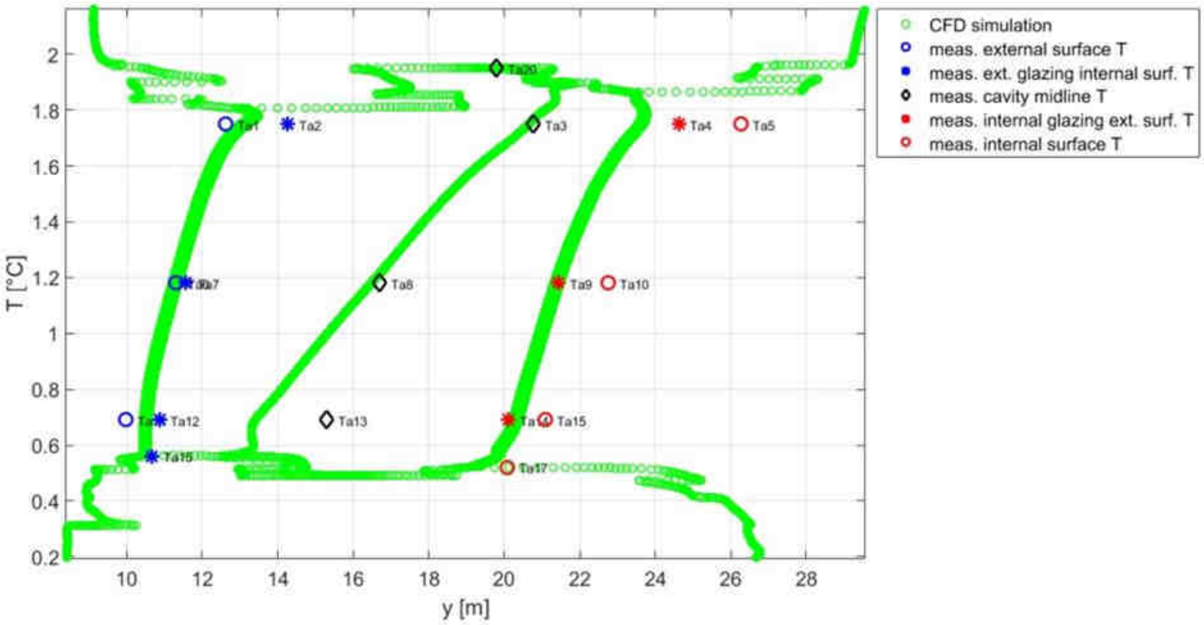

Fig. 48. – test window No. 2 – comparison of measurement and simulation (internal and external environment added to the model), $T_{e,air}$ = 8.4 [°C], $T_{i,air}$ = 30.56 [°C]

In test window No. 2b the internal skin is replaced by a new ISO 68 glulam construction with a standard two layer low-e IG unit. As a result most of the thermal resistance is provided by the IG unit and the temperature difference in the main cavity is reduced and the mean temperature is closer to the external (cold) air temperature. As demonstrated for simple rectangular cavities in the parameter studies however, the flow regime in the main cavity is the same for even smaller Ra numbers. This is borne out by this simulation as well as we get the same temperature stratification profile as earlier.

The IG unit's surface temperature is much more uniform in the vertical direction as it is in the conduction regime with a vertical aspect ratio of Ar=82.74 [-] and a much smaller Ra number due to the 16 [mm] thin cavity. The small temperature stratification effect on the IG unit surface is an artifact of the large cavity. At the top and bottom of the IG unit the effect of the edge spacer is clearly visible as its high thermal conductivity brings the external and internal temperatures closer to each other.

On window No. 3a a thin double pane air filled IG unit of 4-6-4 [mm] is placed at the cold side while the internal glazing is the traditional clear single pane float glass. This setup can be beneficial as even such a relatively thin and low thermal resistance glazing can significantly increase the lowest surface temperature in the cavity, a critical property of the window when it comes to the danger of interpane condensation (due to air exfiltration from the warm and humid internal environment). The comparison between simulation and measurement is shown in Fig. 50.

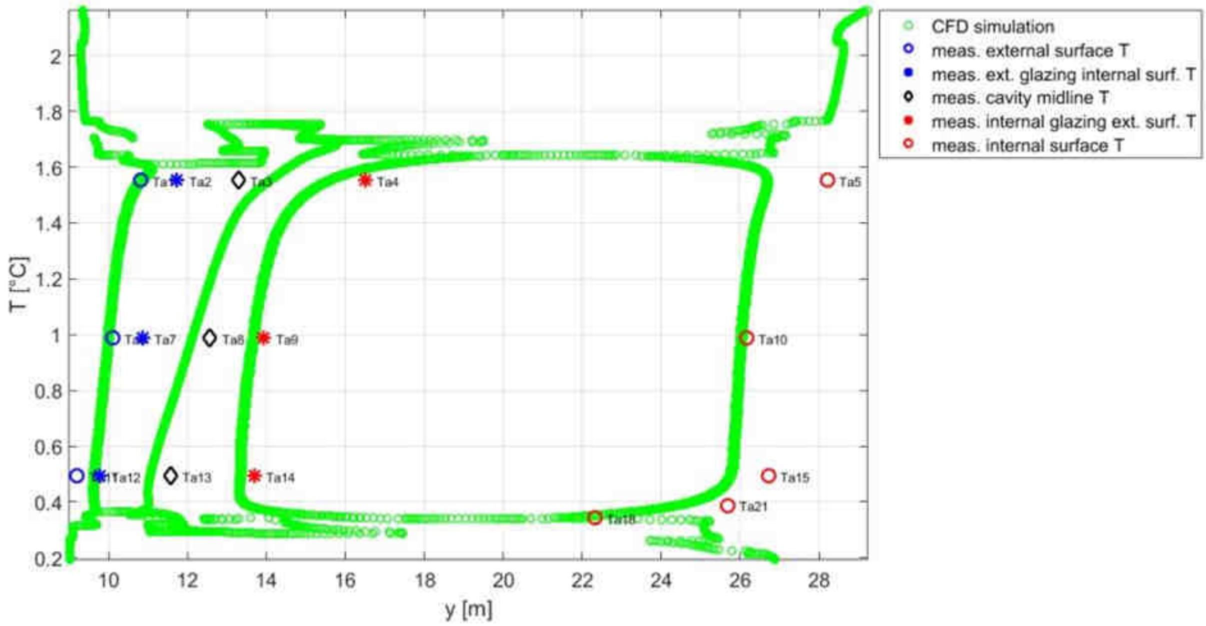

Fig. 49. – test window No. 2b – comparison of measurement and simulation (internal and external environment added to the model), $T_{e,air} = 9.1$ [°C], $T_{i,air} = 29.36$ [°C]

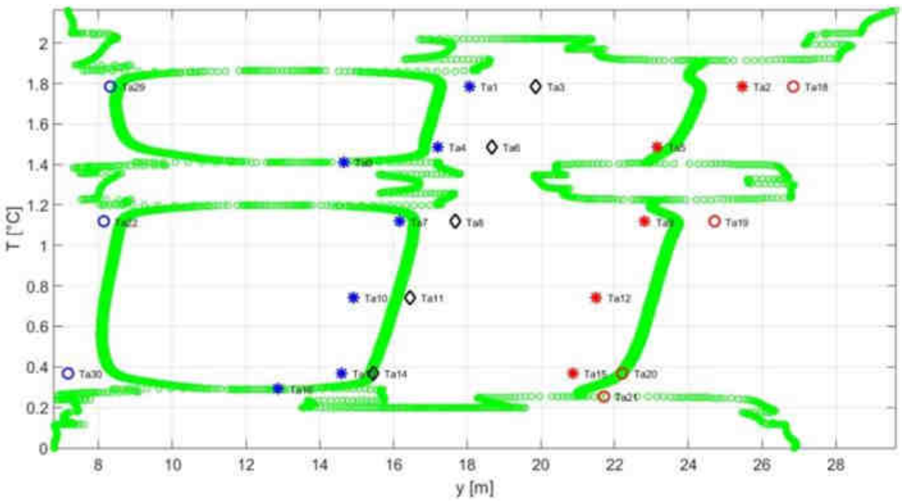

Fig. 50. – test window No. 3a – comparison of measurement and simulation (internal and external environment added to the model), $T_{e,air} = 6.79$ [°C], $T_{i,air} = 29.8$ [°C]

3.6.3 Three dimensional simulations

Two dimensional simulations are sufficient for comparing CFD models and measurements as the flow is near two two-dimensional for most of the width of box windows. However to study the overall heat transmittance of windows three-dimensional simulations are needed. A 3D CFD/Multiphysics simulation gives the U_w value by simply dividing the integrated heat flow through the model by its surface area and the total temperature difference. This can then be compared to U_w values calculated based on the simplified thermal models described in section 2. Based on the difference we can assess the accuracy of the simplified models for the case of traditional double-skin box type windows. From the two main fenestration heat transfer calculation methods CEN and NFRC/ISO the latter is selected for the comparison as its method of calculating the overall window thermal transmittance U_w is better suited for box type windows.[12] The CEN and NFRC/ISO methods give very similar results if we change

[12] The surface weighted method of NFRC/ISO for calculating U_w is easier to interpret for box type windows as it does not require the simulation of a polyurethane foam panel in place of the glazing system for calculating the U_f frame heat transfer coefficient like in the CEN method. The insertion of such a panel into the frame thermal model is very physically unrealistic for box type windows as their glazing system is created by and interwoven with the frame. For further reference see Bakonyi and Becker [13]

their boundary conditions to match therefore it would be unnecessary to check both. The thermal calculation were performed with correlations for calculating the Nusselt number in the main cavity according the ISO 15099 [97] and according the new proposed correlation – Equation (58) – introduced earlier.

3D CFD simulations are inherently computationally intensive. As demonstrated earlier a very fine mesh resolution is needed to resolve the thermal and velocity boundary layers next to the cavity surfaces to calculate convective heat transfer. The mesh sensitivity study conducted for the benchmark of Betts and Bokhari [26] indicated that a mesh with a first element thickness of 4.5e-4 [m] is sufficient to get a mesh independent result, which was shown to yield y+ values of <1 [-] by the rectangular cavity parameter study. Values of y+<1 are recommended in the literature and the FLUENT manual [6] too for convective heat transfer modeling with k-w SST turbulence models. Thus a first element thickness of 4.5e-4 [m] was taken as the starting basis for the 3D mesh generation that necessitates many million elements to mesh the entire geometry.

To reduce the computational load advantage is taken of the typical axis symmetry of windows. The flow domain is reduced to 50% of the original with the help of symmetry boundary conditions. Even so, the geometry of real life box type windows is quite complex, so instead of modelling all the test windows used in the measurement series introduced earlier a “generic” simplified window geometry was created. This generic window has only one sash (in each layer) and has the same basic profile on all sided (sill, jamb, head) to simplify meshing. This is off course unrealistic, but box type windows come in many shapes and sizes, and the completely faithful representation of a specific real life windows is not the main goal. The aim is to study the difference between CFD simulation results and the results of the simple fenestration heat transfer calculations performed with the help of the program LBNL THERM.

name	short description
generic 3D window	1.2/1.5 [m] generic double-skin box type window with only one sash in every layer glazing system: 3-137-3 with uncoated float glass and air filled cavity, cavity aspect ratio Ar=10.16 [-]
generic 3D window + external hardcoated low-e	the same as before, but with an alternate glazing system: 3*-137-3 with external hardcoated low-e glass ($\varepsilon_{coationg}$ = 0.18 [-])
generic 3D window + internal hardcoated low-e	the same as before, but with an alternate glazing system: 3-137-*3 with internal hardcoated low-e glass ($\varepsilon_{coationg}$ = 0.18 [-])
generic 3D window + internal thin IG unit	the same as before, but with an alternate glazing system: 3-137-3-6-*3 with a thin krypton filled IG unit (3-6-*3) with soft coated low-e glass ($\varepsilon_{coationg}$ = 0.037 [-]) in the internal sash and uncoated float glass in the external sash
generic 3D window + internal thin IG unit + external hardcoated low-e	the same as before, but with an alternate glazing system: 3*-137-3-6-*3 with a thin krypton filled IG unit (3-6-*3) with soft coated low-e glass ($\varepsilon_{coationg}$ = 0.037 [-]) in the internal sash and a hardcoated low-e glass in the external sash ($\varepsilon_{coationg}$ = 0.18 [-])
generic 3D window + internal thin IG unit + external hardcoated low-e	the same as before, but with an alternate glazing system: 3-6-*3-128-*3 with a thin krypton filled IG unit (3-6-*3) with soft coated low-e glass ($\varepsilon_{coationg}$ = 0.037 [-]) in the external sash and a hardcoated low-e glass in the internal sash ($\varepsilon_{coationg}$ = 0.18 [-])
generic 3D window + external thin IG unit	the same as before, but with an alternate glazing system: 3-6-*3-128-3 with a thin krypton filled IG unit (3-6-*3) with soft coated low-e glass ($\varepsilon_{coationg}$ = 0.037 [-]) in the external sash and uncoated float glass in the internal sash
test window No. 2	1.325/1.54 [m] double-skin box type window with double inward opening sashes in both layers (without mullions or transoms), glazing system: 3-119-3 with uncoated float glass and air filled caity, cavity aspect ratio Ar=12.26 [-]

Table 9 – Short description of the windows for 2D/3D thermal modeling

A representation of the generic window model is shown in Fig. 51. The window is calculated in several version: original state with clear float glass, refurbishment with hard coated low-e glass in either the external or the internal sash (coating facing the cavity) and thin insulating glass (3-6-3 [mm] krypton filled with soft low-e coating) in either the external sash. For a short description see Table 9 and a more detailed summary Appendix B.5. The dimension of the frame/sash profile for the different variants are shown in Fig. 52 to Fig. 57. The windows were modelled with thermal insulation in the external corners of the cavity to get the same internal and external dimensions. Besides the generic geometry one of the test windows, window No. 2, was also modelled in 3D to investigate the effect of more complicated geometries as well.

Detailed description of the geometry, mesh generation, mesh element counts etc., as well as a detailed graphical representation of all the CFD and thermal simulation results are also found in Appendix B.5. The 3D CFD simulation used the same settings as the 2D, with the exception of the discretization scheme for momentum, turbulence and energy which was switched to the MUSCL scheme due to its better accuracy for unstructured meshes[13]. The material properties were the same as in Table 8. The boundary conditions were not set according to the NFRC/ISO standard[14] but simplified to eliminate them as a potential source of error between the thermal and CFD calculations. The internal boundary condition was a simple constant h_i=8 [W/m^{2}K] combined surface heat transfer coefficient and a T_i=20 [°C] ambient temperature, while the external boundary was h_e=24 [W/m^{2}K] and T_e=0 [°C]. Lateral walls were defined as adiabatic.

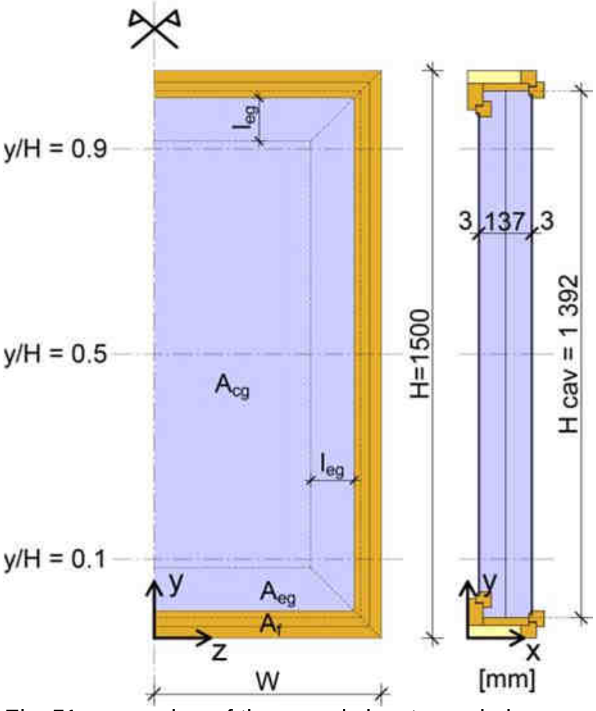

Fig. 51. – overview of the generic box type window geometry

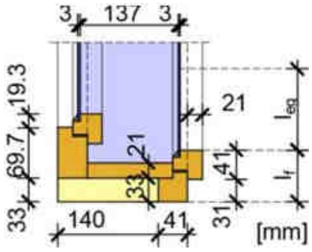

Fig. 52. – single pane 3 [mm] glass in each sash

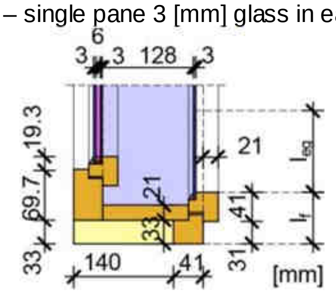

Fig. 53. – 3-6-3 [mm] thin insulating glass in external sash

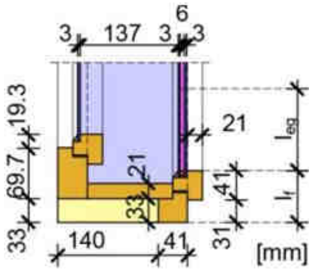

Fig. 54. – 3-6-3 [mm] thin insulating glass in internal sash

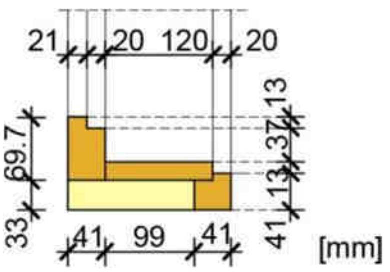

Fig. 55. – geometry of the frame

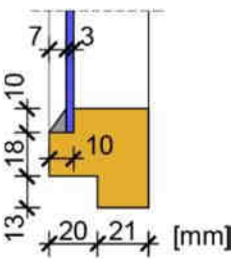

Fig. 56. – geometry of the sash with single pane 3 [mm] glass

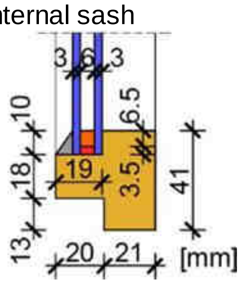

Fig. 57. – geometry of the sash with 3-6-3 [mm] thin insulating glass

[13] Structured mesh was used with as much of the geometry as possible, but the corner regions could only be meshed by an unstructured free tetrahedral mesh.

[14] The NFRC/ISO standards have a temperature difference dependent internal convection coefficient and a view factor based radiative heat transfer coefficient for the internal surfaces.

Visualization for the results of the 3D generic box window simulation are shown in Fig. 51 to Fig. 65. Horizontal temperature and velocity field plots are presented at three heights in the main cavity at y/H=0.1, 0.5 and 0.9 where y is the height above the cavity floor and H the total height of the cavity.

Streamline, velocity magnitude as well as temperature field plots show that the heat transfer is indeed nearly 2D for the middle portion (horizontally) of the window. Like for some of the 2D simulations the cold air descending in the boundary layer at the external side of the cavity impinges on the bottom horizontal profile of the external sash and separates, hitting the internal glazing surface at the warm side of the cavity (see Fig. 59). Counter rotating convection cells are formed underneath with smaller velocity magnitudes. These cells are stretched in the horizontal direction and reach until the lateral walls of the cavity where they feed the ascending flow next to the relatively warm wall of the jamb. The big cell at the bottom is powered not by natural convection, as it is rotating in the wring direction (ascending on the cold side, descending on the warm side), but by the flow in the main convection cell above. Altogether the ascending warm boundary layer flow is somewhat longer in the horizontal direction as the internal glazing is bigger than the external and the flow wraps on to the lateral cavity wall as well. As mass balance has to be preserved this is compensated by somewhat bigger velocities in the descending external boundary layer. The maximum flow velocities are found in the vertical corners of the glazing and the sash profile as the fluid is cooled/heated from two directions in these positions. The convection is thus three-dimensional and dependent on the actual geometry of the window (size and sash of the sash profiles could effect boundary layer separation, difference between internal and external geometries create separate convection cells).

Despite the complex flow field the temperature stratification is not different from the one seen in the two dimensional and two-dimensional rectangular geometry simulations. The effect of the three dimensional effects is localized except for the lateral wall of the jamb where a boundary layer is present that could not be predicted by two dimensional simulations. The core of the flow outside the ca. 1 [cm] thick thermal boundary layers is almost isotherm horizontally while the temperature field in the jamb is close to linear between the cold and hot side, which results in sideways heat flux. This heat flux is a function of height in the cavity due to the temperature stratification.

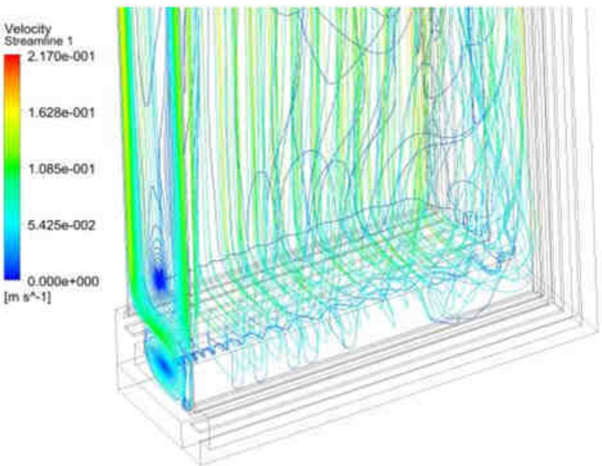

Fig. 58. – generic 3D window, streamlines at the bottom of the cavity (3D view)

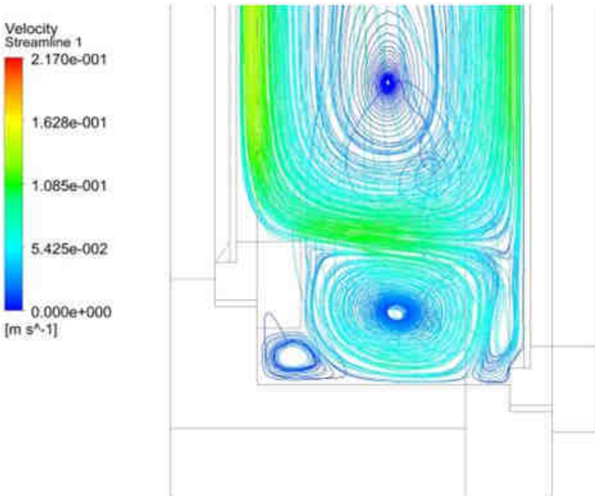

Fig. 59. – generic 3D window, streamlines at the bottom of the cavity (2D view)

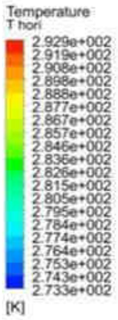

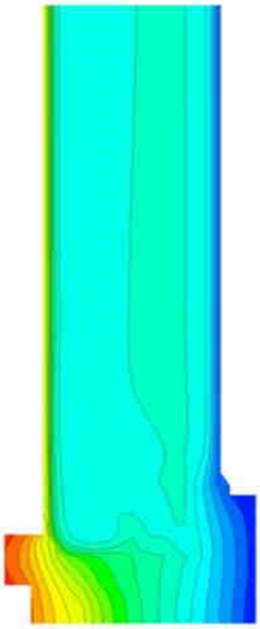

Fig. 60. – generic 3D window, T at y/H=0.1 [-] (horizontal section)

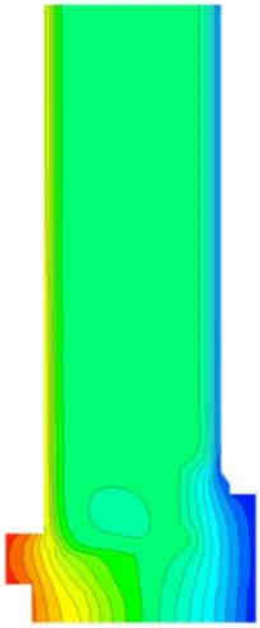

Fig. 61. – generic 3D window, T at y/H=0.5 [-] (horizontal section)

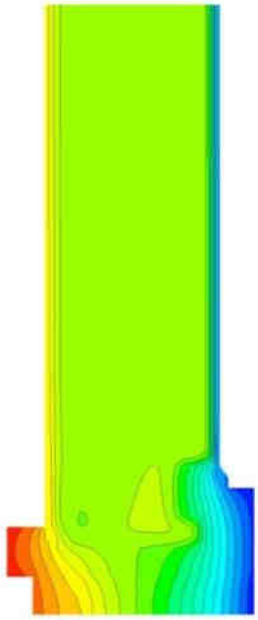

Fig. 62. – generic 3D window, T at y/H=0.9 [-] (horizontal section)

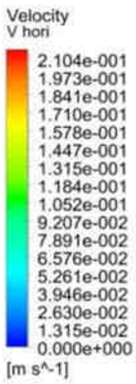

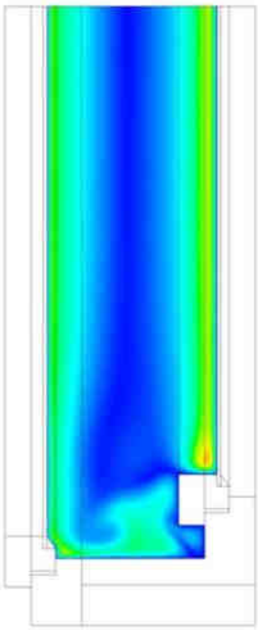

Fig. 63. – generic 3D window, T at y/H=0.1 [-] (horizontal section)

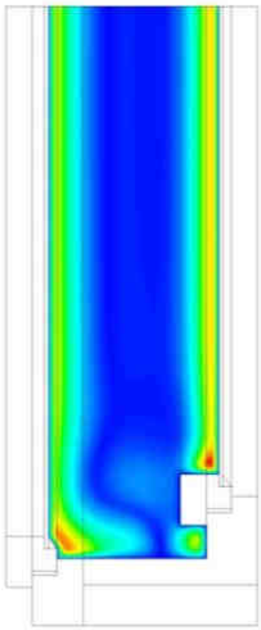

Fig. 64. – generic 3D window, T at y/H=0.5 [-] (horizontal section)

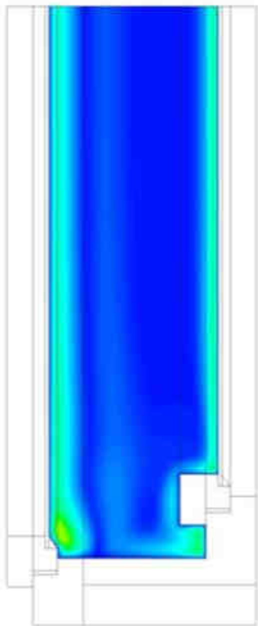

Fig. 65. – generic 3D window, T at y/H=0.9 [-] (horizontal section)

Detailed result for the other cases of the generic 3D box type window (found in the appendix) are similar. The use of hardcoated low-e glass decreases radiative heat transfer in the cavity and as a result increases the temperature difference leading to somewhat bigger flow velocities and larger convective heat transfer. The internal and external thin insulating glass units decrease the temperature difference and reduce convective heat transfer.

3.6.4 Comparison of 3D CFD and standard calculations

The standard fenestration heat transfer calculation according the NFRC/ISO method were performed with the help of EPICAC ISO[15] for the glazing system calculations and the program THERM [119] for the two-dimensional component level thermal calculations. The NFRC/ISO method uses Equation (2) for calculating the window thermal transmission coefficient U_w. The calculation were performed with an edge-of-glazing area width of 63.5 [mm] (2 [inch], see Fig. 51) given in NFRC 100-2010 [135] and 100, 150, 200 and 250 [mm] as well. With the 3D models and meshes of all the investigated windows at hand the thermal calculation were conducted in full 3D as well by replacing the air cavity in the CFD models with the equivalent thermal conductivity material of the simplified method. A 3D calculation negates the need for individual 2D component simulations and the use of the area weighted approximation of equation (2) to calculate $U_{w.}$ We can thus analyze the error between the 2 and 3D thermal simulations.

The calculated Uw values for the NFRC/ISO method for all the investigated windows, with and without replacing the convective heat transfer correlation for the cavity, and for different values of l_{eg} [m], are found in Table 10. A graph visualizing the percentage error between 2 and 3D thermal models for different l_{eg} values is shown in Fig. 66. For the wide construction of box type windows the 63.5 [mm] wide edge-of-glass area is clearly insufficient to capture the multi-dimensional heat flow in the component simulations. An l_{eg} of 200 [mm] seems to give a reasonable requirement to achieve an approximatively l_{eg} independent solution without extending the edge-of-glass area to the point where in may "touch" the opposite side in case of smaller glazing surfaces. The importance of l^{eg} is larger when IG units are used and smaller for uninsulated or hardcoated low-e glass insulated cavities. There errors between the 2D approximation and 3D calculation are significant even for the increased l_{eg} values and can reach values upwards of 6%. The generic 3D window geometry shows somewhat smaller errors (with a large enough leg) while the complex shape of window No. 2 leads to poorer results.

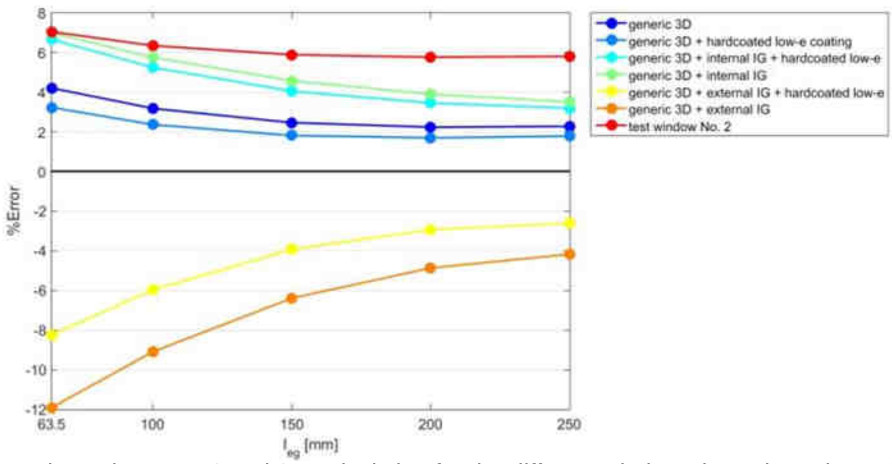

Fig. 66. – %Error in Uw between 2 and 3D calculation for the different windows investigated as a function of l_{eg}

window	model	l_{eg} [mm]					
		63.5	100	150	200	250	3D
generic 3D	NFRC/ISO	2.346 +4.2%	2.323 +3.18%	2.307 +2.46%	2.302 +2.23%	2.303 +2.27%	2.252 0%
	new corr.	2.245 +4.01%	2.223 +2.99%	2.209 +2.37%	2.203 +2.08%	2.204 +2.12%	2.158 0%
+ internal thin IG unit	NFRC/ISO	1.169 +6.99%	1.156 +5.75%	1.143 +4.57%	1.135 +3.89%	1.131 +3.51%	1.093 0%
	new corr.	1.151 +6.98%	1.137 +5.73%	1.124 +4.54%	1.117 +3.86%	1.113 +3.48%	1.076 0%

[15] EPICAC ISO is a one-dimensional glazing system simulation program created by the author in MATLAB for solar-optical and heat transfer simulations according to the ISO 15099 standard [97] or similar algorithms. The program is cross-validated to the LBNL WINDOW [120] and gives identical results for the same inputs and algorithms. The use of an open source research program instead of the standard software allows for replacing and testing for parts of the algorithm, e.g. the correlation used the calculate the convective heat transfer in the cavities, and extract intermediate calculation results, such as Ra and Nu numbers, that are not available in the standard program.

+ external thin IG unit	NFRC/ISO	1.023 -11.93%	1.056 -9.11%	1.088 -6.41%	1.105 -4.88%	1.113 -4.19%	1.162 0%
	new corr.	1.014 -11.67%	1.046 -8.87%	1.077 -6.21%	1.094 -4.72%	1.101 -4.05%	1.148 0%
test window No2	NFRC/ISO	2.271 +7.04%	2.256 +6.34%	2.246 +5.88%	2.244 +5.76%	2.245 +5.80%	2.122 0%
	new corr.	2.190 +6.92%	2.176 +6.27%	2.167 +5.82%	2.165 +5.71%	2.166 +5.75%	2.048 0%

Table 10 – Uw values for the NFRC/ISO method for all the investigated windows, with the standard and the proposed convective heat transfer correlation, forr different values of l_{eg} [m] and compared to the 3D heat transfer results

Comparison between the simulated internal surface temperatures of the standard method's 2D component level thermal simulations and the 3D CFD/Multiphysics simulations for the simple generic 3D box type window geometry are shown in Fig. 67 and Fig. 68. The heat conduction simulation is off course unable to predict the temperature stratification and yields completely unrealistic internal glazing temperatures over much of the surface. The CFD gives lower minimum temperatures which are important for condensation resistance calculations. The NFCR/ISO model modified with the proposed new convective heat transfer coefficient correlations gives somewhat higher surface temperatures that are closer to the mean of the CFD simulation, but the differences are small. The prediction of frame surface temperatures are relatively close to each other but the effect of temperature stratification is noticeable even here.

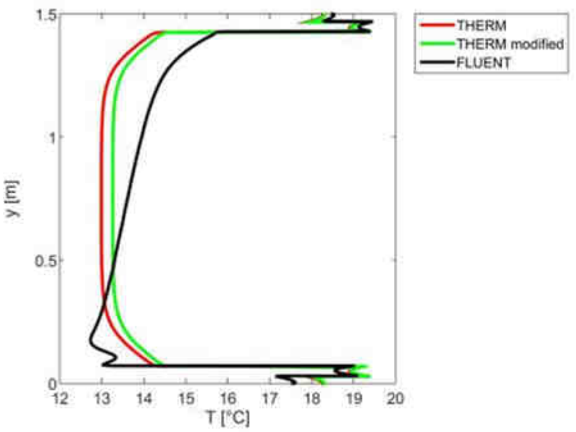

Fig. 67. – comparison of the internal surface temperature at symmetry plane of the generic 3D window case

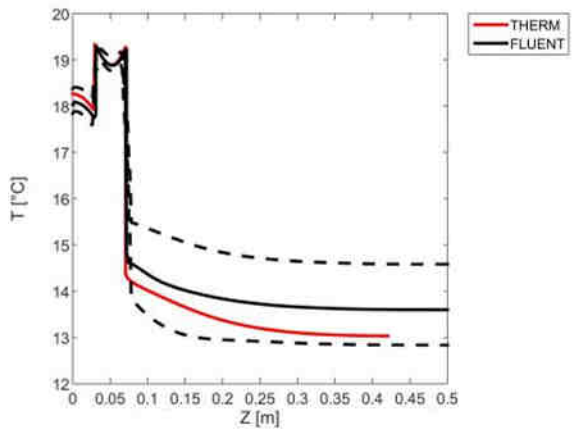

Fig. 68. – comparison of the internal surface temperature at horizontal sections through the generic 3D window. The CFD results are shown at y/H=0.5 (solid line) and 0.1, 0.9 [-] (dashed lines)

	NFRC/ISO			NFRC/ISO + new correlation			CFD
window	Ug [W/m²K]	Uw [W/m²K]	Uw,3D [W/m²K]	Ug [W/m²K]	Uw [W/m²K]	Uw,3D [W/m²K]	Uw [W/m²K]
generic 3D	2.805	2.30 108.49%	2.25 106.13%	2.697	2.203 103.9%	2.158 101.79%	2.12 100%
+ external hardcoated low-e	1.917	1.594 104.18%	1.567 102.42%	1.708	1.432 93.6%	1.41 92.16%	1.53 100%
+ internal hardcoated low-e	1.917	1.594 105.15%	1.567 103.36%	1.708	1.432 94.46%	1.41 93.01%	1.516 100%
+ internal thin IG unit	1.027	1.136 105.28%	1.093 101.3%	1.015	1.117 103.52%	1.076 99.72%	1.079 100%
+ internal thin IG unit + external hardcoated low-e	0.854	0.899 99.23%	0.869 98.9%	0.814	0.850 93.8%	0.823 90.84%	0.906 100%
+ external thin IG unit	1.034	1.105 99.1%	1.162 104.2%	1.025	1.094 98.12%	1.148 102.96%	1.115 100%
+ external thin IG unit + internal hardcoated low-e	0.848	0.885 96.09%	0.912 99%	0.812	0.845 91.75%	0.887 96.3%	0.921 100%
test window 2	2.805	2.244 107.16%	2.122 101.34%	2.698	2.165 103.39%	2.048 97.8%	2.094 100%

Table 11 – comparison of the 2/3 D thermal and 3D CFD calculation for the overall thermal transmittance

Table 11 shows the Uw total heat transmission coefficients calculated with NFRC/ISO, the modified NFRC/ISO and with the 3D CFD simulations. For the NFRC/ISO calculation both the 3D and the standard 2D calculation is shown with an l_{eg} value of 200 [mm]. The results show a very mixed picture. We can summarize the findings with the following points:

- The simplified thermal simulation lie within 10% of the CFD results.
- The 3D thermal simulations are generally closer to the CFD results as the 2D calculations
- The standard NFRC/ISO method tends to overpredict heat transfer for
- The NFRC/ISO method with the modified convective heat transfer correlation tends to underpredict heat transfer when the glazing system is modified, while for the original state (only float glass) it gives the best results
- The fact that improving the convective heat transfer correlation to match the results of the same CFD model in 2D for some cases reduces the accuracy compared to the 3D CFD simulation indicates that there are more sources of inaccuracy that might cancel out or strengthen each other depending on the situation
- The small difference in heat transfer between placing hardcoated glazing in the internal vs. the external sashes is predicted only by the 3D simulation indicating that the multidimensional radiative effect in the cavity have a noticeable effect on the results

3.7 Evaluation of current fenestration heat transfer calculation methods

The standardizes fenestration heat transfer models introduced in chapter 2 use a series of simplified assumptions to keep the calculation manageable which were shown to rely on the physical characteristics of the convective heat transfer inside the internal cavities of thin and high vertical aspect ratio insulating glass units. It was also shown that many of these assumption are no longer valid for double-skin box type windows due to their larger, frame-enclosed and small aspect ratio cavities. Based on the investigations in this chapter: a thorough review of the literature that forms the basis of the calculation methods, a validated CFD simulation study of the convective heat transfer in cavities representative of box type windows and the validated simulation of the multi-dimensional conjugate heat transfer in the complex geometries of box type windows; we can conclude that:

- the unmodified use of the NFRC/ISO fenestration heat transfer model overpredict the center-of-glazing heat transfer by over-estimating the convective heat transfer in the cavities,
- gives component heat transfer and temperature distribution results that are unphysical and unsuitable for predicting condensation resistance as they over-predict minimum surface temperatures, but
- can deliver U_w overall window thermal transmittance results of within. ± 10% accuracy, if the center-of-glazing area in the calculation is increased to at least 200 [mm] from the internal glazing edge.
- The use of a proposed new correlation for calculating convective heat transfer in the cavities of box type windows can increase the accuracy of center-of-glazing calculations, and increase the accuracy of the Uw value prediction for uninsulated box type windows.
- For higher accuracy of U_w it is recommended to use 3D thermal models, if at all possible, and CFD simulations to predict realistic temperature fields and surface temperatures.

Additionally a new method is proposed for the approximation of the overall temperature stratification in the cavity and lowest glazing surface temperatures based on the cavity aspect ratio that can be used together with a one-dimensional gazing heat balance calculation.

These results fall in line with the findings of Gustavsen [79] as he investigated the standard fenestration heat transfer models with regards to their ability to predict heat transfer in windows frames with large internal cavities. Simplified models are tuned to give approximate results that can be perfectly acceptable for most users and purposes, but if results of local heat transfer or accurate surface temperatures are needed the oversimplification of complex multi-dimensional heat transfer processes is no longer viable.

4 Interaction between fenestration and masonry heat transfer

Wherever constructions of different types interface the physical processes at their connecting edge will be a function of both of their characteristics. Historically double-skin box type windows developed together with the other constructions of the external thermal envelope, most importantly the external masonry. The importance of box type windows' constructional thickness and the design of their window-to-wall interface for the prevention of moisture damages and mould growth in uninsulated, thick but good conductance masonries was the subject of many publications, e.g. Bakonyi and Becker [12], Holste at al. [85], Heimatschutz Basel [141], to name just a few. Like the question of such possible moisture problems the influence different window options have in the overall heat losses of the external envelope is however often overlooked by practitioners, and completely neglected by most simplified building energy calculations. This can lead to large calculation errors when comparing window options with significantly different window-to-wall interfaces if the change in the windows installation thermal bridge is not considered (see in Bakonyi and Becker [13]. To find the correct approach to such calculations we have to review the methodology of thermal bridge calculations and investigate a large sample of different constructional variants.

4.1 The treatment of thermal bridges in building heat loss calculations

The precise calculation of the thermal transmittance of the external building fabric is a key issue of all building energy computations. One of the main difficulties lies in the treatment of thermal bridges in opaque constructions. A thermal bridge is defined as a part of the external thermal envelope where heat fluxes become multi-dimensional, as opposed to a theoretical infinite planar assembly where heat fluxes are strictly parallel. There are two distinct groups of thermal bridges to differentiate:

1) repeating thermal bridges, under which we understand inhomogeneities in the external constructions demonstrating a recurring pattern within a single planar construction (e.g. wooden studs in lightweight walls or wall-ties in cavity walls), and
2) non-repeating thermal bridges, which occur at the large scale details and junctures of different constructions (e.g. wall corners, slab to wall connections, the connection of partition walls to exterior walls, etc.), where the interior and exterior surface dimensions are not equal or where materials with different thermal conductivities are present.

According to current regulations heat losses resulting from repeating thermal bridges must be incorporated into either the thermal conductivity of the materials (e.g. the thermal conductivity of a masonry must represent the joint characteristics of both brick and mortar), or into the U-value of the individual construction (e.g. the correction for mechanical fasteners in ETICS - see EN-ISO-6946 [59]). Repeating thermal bridges, as they do not relate to windows, are not a subject of this study.

The detailed calculation of non-repeating thermal bridges (henceforth just thermal bridges) is described in the standards EN ISO 10211 [61], for calculating their thermal transmittance, and in EN ISO 13789 [64], for calculating the transmission heat losses of entire buildings of building parts. For detailed a calculation one must make a 2 (or 3) dimensional thermal model of the details in question (some numerical solution of the stationary heat transfer equation over the domain) according to the specific thermal boundary conditions described in the standard ISO 10211 [61] (temperatures and surface heat transfer coefficients). A good summary of the different numerical calculation approaches to thermal bridge simulations is found in [130]. A thermal bridge simulation yields the heat flux densities over the surface of the construction from which we can derive the thermal transmittance of the thermal bridge the following way (as illustrated with a simple 2D case seen in Fig. 69.).

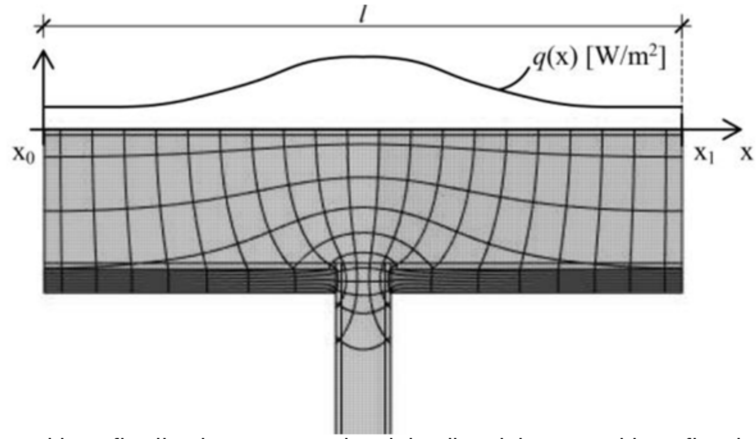

Fig. 69. – Isotherm and heat flux line in a constructional detail and the normal heat flux density on the surface

By integrating the surface normal component of the heat flux density over l we get the total heat flux for unit length through the entire detail:

$$Q_l = \int_{x0}^{x1} q\left(x\right)dx \tag{59}$$

where Q_l [W/m] is the total heat flux for a unit length, and q_n [W/m2] the surface normal component of the heat flux density. If we divide this value with the temperature difference we get the so called 2D thermal coupling coefficient which gives the heat flux through 1[m] of the detail for a temperature difference of 1[K]:

$$L_{2D} = \frac{Q_l}{\Delta T} \tag{60}$$

where L_{2D} [W/mK] is the 2D thermal coupling coefficient, Q_l [W/m] the total heat flux for a unit length and ΔT [K] the temperature difference. The L_{2D} value represents the heat losses of the detail with complete accuracy, so an ideal calculation method would be to compute the heat losses of the whole building in a similar manner. However to model an entire building thusly is not yet practical even with today's computer capacities, therefore we have to calculate individual thermal bridges separately, and then divide the calculated heat fluxes into one-dimensional (U-value) and multi-dimensional (ψ-value) parts that can later be used in the whole building's heat loss calculation:

$$L_{2D} = \Psi + \sum\nolimits_{i=1}^{n} l_i U_i \qquad \text{or} \qquad \Psi = L_{2D} - \sum\nolimits_{i=1}^{n} l_i U_i \tag{61}$$

where ψ [W/mK] is the linear thermal transmittance, L_{2D} [W/mK] the 2D thermal coupling coefficient, l_i [m] the length of surface i, and U_i [W/m^{2}K] the thermal transmittance of surface i.

So as we can see the total heat transmittance of a detail is the sum of the one-dimensional heat losses (in our example the heat loss through the planar wall given by its U-value and surface area) and the multi-dimensional heat losses given by the so called linear thermal transmittance value. In other words the linear thermal transmittance value is the difference between a strictly one-dimensional heat loss calculation and an exact calculation that accurately models the multi-dimensional heat transfer effects. In a way it is the calculation error of the one dimensional models. Keeping this in mind it is clear that there are no 'thermal-bridge free" constructions or designs in this sense, because this calculation error is never exactly zero. A further observation to make is that the exact value of the linear thermal transmittance is dependent on the coordinate system we use for our calculations. If one uses the internal surface dimensions of a building (surface areas as measured in the interior) to calculate the heat losses the ψ_i (interior) value of the thermal transmittance must be used in order reproduce the exact value according to Eq. (61), whereas by using the external dimensions the ψ_e (exterior) value is needed. For every detail where the internal and external dimensions are not identical we can calculate two values for ψ, and in some extreme cases the external value may even be negative, as demonstrated in Fig. 70. This does not mean that the detail has heat gains, but simply indicates that by using only the one-dimensional U-value and the external surface area of the building the heat losses were overestimated.

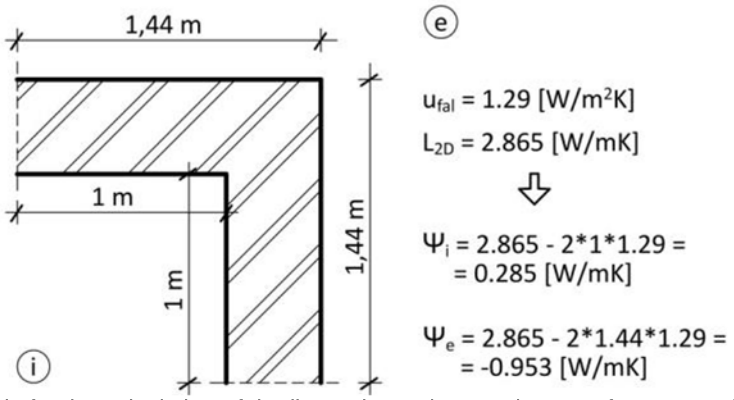

Fig. 70. – An example for the calculation of the linear thermal transmittance of an external wall corner based on external and internal dimensions

In the Hungarian building energy certificate calculations according the effective Government Regulation [1] the multi-dimensional heat loss effects of the thermal bridges must be incorporated into the specific net heating energy demand of the building. This can be done with a detailed or a simplified calculation. According to the detailed calculation:

$$q = \frac{1}{V}\left(\sum_{i=1}^{n} A_i U_i + \sum_{j=1}^{m} l_j \Psi_j - \frac{Q_{sd} + Q_{sid}}{72} \right) \tag{62}$$

where q [W/m^{3}K] is the specific net heating energy demand of the building, V [m^3] is the heated air volume, A_i [m^2] the area of surface i, U_i [W/m^{2}K] the thermal transmittance of surface i, l_j [m] the length of the linear thermal bridge j, ψ_j [W/mK] the linear thermal transmittance of thermal bridge j, Q_{sd} [kWh/a] the direct solar heat gains and Q_{sid} [kWh/a] the indirect solar heat gains.

In Eq. (62) the one- and multi-dimensional heat losses are in separate terms and if data is available for every thermal bridge we can calculate the exact heat transmittance values for the whole building as shown in Eq. (61) and described in more detail in the standard EN ISO 13789 [64]. The question is: does one have the ψ values to substitute into Eq. (62)? While softwares to perform such calculations are now easily available and the necessary computational load is usually minimal for contemporary machines the manual workload to build the models themselves and the level of expertise required is still quite large. As a result precise thermal bridge simulations are still very rarely used by everyday practitioners. To try to address this problem some researchers use different machine learning approaches to try to find approximate relationships between the relevant parameters and the thermal transmittance of characteristic thermal bridge types to eliminate the need for thermal simulations. One such approach using Artificial Neural Networks is found in Orosz and Csanaky [137]. Meanwhile the regulation of most countries permit some kind of simplified treatment of thermal bridges in heat transfer calculations. Usually a certain correction is applied to the calculated one dimensional overall thermal transmittance (U value) to account for multidimensional effects. This correction is prescribed without actually performing thermal bridge simulations or using a detailed thermal bridge atlas. A good summary of such simplified calculation methods in EU countries is given in Citterio et al. [37]. In the context of the Hungarian building energy regulation [1] the following simplified method is used in calculating the total thermal transmittance of the thermal envelope:

$$q = \frac{1}{V}\left(\sum_{i=1}^{n} A_i U_{R,i} + \sum_{j=1}^{m} l_j \Psi_j - \frac{Q_{sd}}{72} \right) \tag{63}$$

where q [W/m^{3}K] is the specific net heating energy demand of the building, V [m^3] the heated volume, A_i [m^2] the (internal!) area of surface i, $U_{R,i}$ [W/m^{2}K] the effective thermal transmittance value of surface i, l_j [m] the length of the plinth detail j (slab-on-grade perimeter) or basement wall, $\psi_{,j}$ [W/mK] the linear thermal transmittance value of the plinth or basement wall detail, and Q_{sd} [kWh/a] the direct solar heat gains.

In Eq. (63) multi-dimensional heat transfer effects are not treated explicitly (except for the heat losses towards the ground – see e.g. in Nagy [131]). In order to avoid the huge calculation errors that this simplification would bring an U_R effective thermal transmittance value is introduced. This contains a prescribed thermal bridge supplement specified in the regulation, and in addition to one-dimensional heat transfer it is supposed to account for the effect of the thermal bridges as well. U_R is calculated as:

$$U_R = (1+\chi)U \tag{64}$$

where U_R [W/m^{2}K] is the effective thermal transmittance value, χ [-] the thermal bridge correction factor, and U [W/m^{2}K] the thermal transmittance value of the planar construction. Eq. (63) and (64) are based on the assumption that the following equality is approximately true:

$$\sum_{i=1}^{n}(1+\chi_i)U_i \cong \sum_{i=1}^{n}U_iA_i + \sum_{j=1}^{m}\Psi_j l_j \tag{65}$$

The χ values to be used on which the accuracy of the simplified method depends are given in the regulation (acc. to II.3.b in [1]) in a tabulated form which is shown here in Table I. To use this method the geometry of the individual surfaces must be calculated with their internal dimensions, than the ratio of the total length of thermal bridges to the wall area (Σl/A) must be determined. For external walls the χ value to be used is only dependent on whether the wall has a continuous thermal insulation layer or not and on the value of Σl/A. The type or thickness of the masonry, the exact position or thickness of the thermal insulation or the thermal quality of the details used is not taken into consideration. This raises questions regarding the method's accuracy. In [158] Talmon and Csoknyai found the simplified calculation very unreliable for the building type of prefabricated "panel" buildings. Simplified calculations in other countries can suffer from the same lack of accuracy as demonstrated in Theodosius and Papadopulos [159] for the Greek energy code and in Berggren and Wall [24] in a more comprehensive study among Norvegian practitioners.

	Σl/A [1/m]		
geometrical limits for choosing the correction factor	< 0.8	0.8 – 1.0	> 1.0
	χ [-]		
external wall with continuous thermal insulation	0.15	0.20	0.30
external wall without continuous thermal insulation	0.25	0.30	0.40

Table 12 – χ values in [1] for external walls and the limits for their selection according to Σl/A

The thermal bridge calculation framework introduced here is intended for relatively simple yearly or monthly building heat loss calculations based on methods using heating degree days. Contemporary trends point towards the ever grooving use of dynamic thermal simulation in building energy design. Unfortunately dynamic building energy simulation programs often neglect thermal bridges altogether. It is hard to incorporate multi dimensional heat flows into a dynamic calculation without having to perform computationally very expensive transient 2 or 3 dimensional thermal simulations. The research to find computationally affordable ways to include the dynamic behavior of multi-dimensional constructions is in its relatively early stages (see e.g. in Quinten et al. [142], Ascione et al. [9] and Brumă et al. [28]). However, such calculations are no the subject of this current study.

4.2 A new method for improving the simplified calculation method

In the years 2011-2012 the Department of Building Construction[16] conducted a government grant aided research into the possibilities of the thermal insulation of historical buildings with protected facades (see e.g. in Kakasy [102] and Kuntner [113]). During the project a comprehensive thermal bridge atlas was created (Bakonyi and Kuntner[17]), a database containing an extensive set of linear thermal transmittance values, and other numerical results like minimum internal surface temperatures according to the standard DIN-4108-2 [6]. Based on the atlas in Bakonyi [15] I published a case study

[16] The participants of the research project were László Kakasy, Dániel Bakonyi, Ferenc Kuntner and Zsuzsanna Fülöp. Faculty of Architecture, Budapest University of Technology and Economics.
The contents of the project was connected to the realization of the goals of the „Minőségorientált, összehangolt oktatási és K+F+I stratégia, valamint működési modell kidolgozása a Műegyetemen" project. The project was founded by the Széchenyi Terv TÁMOP-4.2.1/B-09/1/KMR-2010-0002.
[17] The thermal bridge database has not jet been published

of a 19th century urban apartment building in Budapest where simplified and detailed thermal bridge calculations could be compared. Large discrepancies were found in the results between the two methods. Case studies alone however are not enough to make far reaching conclusions. A more systematic approach is needed.

4.2.1 Methodology

In Bakonyi and Dobszay [17] and [20] we introduced a new method to generate more reliable thermal bridge correction factors for the external walls of buildings (the method is applicable for other parts of the external thermal envelope as well). This new methodology tries to account for as many of the influences on the correct value of the thermal bridge correction factor as possible:

- the geometrical typology of the building: the typical geometry of the façade, the types of thermal bridges present and the relative abundance of these types (e.g. positive corners, presence of balconies, etc.)
- the precise length of these thermal bridges: the variance between individual examples of the same overall building typology (the exact length of the different thermal bridge types)
- the type of the wall: most notably thickness and thermal conductivity (some building typologies can have only one wall type, e.g. certain types of industrially prefabricated buildings)
- the type of the thermal insulation: position (internal/external), thickness and thermal conductivity
- the quality of the constructional details: the continuity of the thermal insulation in window reveals, around connecting constructions, insulation terraces, footings, etc.
- the type and position of the fenestrations, the presence of a shading roller shutter case or other attachments

The method requires the calculation of many possible building facades which is most practically achieved with the parametric generation of virtual buildings as demonstrated by Szalay [157]. The following algorithm is proposed to try to account for all of the parameters mentioned above:

1. For every building typology one must describe the characteristic façade type, determine its **geometrical parameters** (e.g. internal headroom, frequency of connecting internal partition and /or loadbearing walls, typical openings and their distances, etc.) and their expected range (minimum and maximum values and if knowable their statistical distribution)
2. Determine the **constructional variants and parameters** to be investigated for the building typology (e.g. wall type and thickness, type position thickness and conductivity of thermal insulation, etc.) and define their expected range (discrete types or continuous variables with minimum and maximum values and if knowable their statistical distribution)
3. Make a list of the typical (non-repeating) thermal bridges on the façade type in point 1) and perform the necessary thermal simulations to obtain their linear thermal transmittance values for all the possible constructional variants determined in point 2). When applicable perform these simulation for both well and poorly designed details (e.g. continuous or discontinuous thermal insulation in window reveals, etc.).
4. With the data compiled in points 1) 2) and 3) perform a Monte Carlo simulation[18]: generate virtual facades based on all the previously described variables with a sufficiently large sample size and calculate their exact multi-dimensional total heat transfer coefficients. From this data calculate the correct value of the thermal bridge correction factor χ (using equation (65)).
5. Analyze the data to find easy to use relationships between the thermal bridge correction factor χ and the basic parameters of the building typology (e.g. the $\Sigma l/A$ value, the thermal resistance of the insulation, the wall, etc.)
6. Check the accuracy of the result by comparing the values calculated in point 4) and the ones calculated with the method derived in point 5)

The method can compress all the data in a detailed thermal bridge atlas into a few equations and parameters that are much easier to use for everyday practitioners. However, the results are only valid for the specific building typologies, parameters and parameter ranges they were derived for and must be published together with these. The user must be able to make the judgement whether a given

[18] An algorithm based on repeated random sampling of a set of parameters to generate a distribution of numerical outputs with a given model

formula is valid for his or her case. To this end any simplified calculation equations should always be published together with a description of the building and constructional types they were derived for.

4.2.2 Investigated building types and parameter sets

Three building types were selected to serve as a basis for the development and demonstration of the method: 19th century urban apartment buildings, small urban or suburban detached houses based on a Central-European type plan (henceforth 'cube houses') and ca. 1960' type plan urban apartment buildings constructed with prefabricated wall blocks (henceforth 'block houses'). All three types are found in large numbers in Hungary, have well typifyable facades and were built with a limited set of constructional solutions. Only a very brief description of the buildings and their constructional variants are given here and a more detailed summary of the geometrical and constructional parameters used to describe them, as well as the algorithms created for generating the virtual façade geometries for the Monte Carlo simulations are found in Appendix C. A few examples of the calculate virtual façade geometries of the three investigated building types are shown in Fig. 72, Fig. 73 and Fig. 74.

Fig. 71. – The three investigated building types: 19th century apartment building (left), 'cube houses' (middle), 'block houses' (right)

- Multi-story **19th century urban apartment buildings** represent a significant portion of the Hungarian building stock. Underneath the different styles of architectural adornments they are very similar in construction and basic floor plan. Their facades are geometrically very repetitive and we can faithfully represent them with a small, well-chosen representative surface patch (e.g. a façade element belonging to a single small flat). We have to differentiate between the street facing (external) façade and the internal (courtyard) façade with the characteristic cantilever corridors. The external walls are made from solid brick masonry, 1.5, 2 or 2.5 brick thick depending on the storey.

  The investigated constructional variants are:
    - the original uninsulated state,
    - internal insulation with good or bad details, and
    - external insulation where distinction is made between street and courtyard facades (due to the corridor thermal bridge).

  The thermal insulation is taken to be between 2 and 8 [cm] in 2 [cm] increments as a total constructional thickness of more than 10 [cm] (including adhesives, plaster etc.) is rarely possible due to simple geometric limitations.

  The windows are:
    - double-skin box type windows – window type 1
    - contemporary single-skin windows – window type 2

  .
- **'Cube houses'** were built in large numbers is Central- and Eastern-European countries and are based on simple type plans. They are by no means completely uniform, but there is significant commonality between them. The vast majority share a single storey, approximately square floor plan with two external and one internal loadbearing wall and are topped by an unheated and unused attic with a hip roof, usually close to a pyramid shape. The floor level is elevated from

the ground with a large plaster, cast- or quarry-stone covered footing. The bedrooms, living rooms and kitchens have large, horizontally aligned windows, most commonly with two large symmetric windows oriented towards the street. The main entrance door is either connected to a terrace or is in a small lobby protruding from the main body of the building.

Entire virtual facades are generated acc. the algorithm described in Appendix C, and two common construction types are selected for analysis:

- o 38 [cm] thick fired solid clay brick masonry
- o 25 [cm] thick fired aerated clay brick masonry.

The floor is 50 [cm] above ground, uninsulated and has a concrete plinth. The slab be is a prefabricated RC beam construction with prefab. slag filled concrete trays. The reinforced concrete ringbeam is without perimeter thermal insulation. The lintel beams are prefabricated reinforced concrete elements. The walls and the attic slab are either uninsulated, or have an external insulation of 8-20 [cm] in 2 [cm] increments. The thermal conductivity of the insulation is λ=0.04 [W/mK].

Constructional details investigated are either of 'good' (continuous insulation in window rebates, etc.) or 'bad' quality (uninsulated rebates, uninsulated footing, wall and attic insulation not connected at eaves).

The windows are:

- o double-skin box type windows – window type 1
- o contemporary single-skin windows – window type 2
- o double-skin box type windows with inbuilt roller shutters – window type 3
- o contemporary single-skin windows with external roller shutters – window type 4

- **'Block houses'** stem from type plans in the 1960' utilizing a constructional technique that used prefabricated slag-concrete blocks that were either half or full storey high (ca. 279 [cm] slab-to-slab) and 60-90 [cm] long. The blocks were placed next to each other to form the walls with only simple mortar filled joints between them. The buildings were built with a perpendicular shearing wall type loadbearing system and longitudinal prefabricated RC slab panels. Most such type plans had 5 storeys with a flat roof and a long and narrow or tower shaped plan with 3-4 flats per floor clustered around each staircase. Most buildings have loggias that were made with the same kind of prefabricated panels as the internal slabs, without any thermal insulation or thermal brake.

The buildings' façade is quite repetitive, therefore only 3 random façade elements are generated for each virtual building to make up the façade of an imaginary flat. Wall panels are 29 [cm] thick with 2 [cm] plaster on either side. The calculations are made for:

- o the original uninsulated state of the building, or
- o a 8-20 [cm] thick external insulation in 2 [cm] increments.

When applicable the details are calculated as either of 'good' or 'bad' quality according to the continuity of the thermal insulation (in window reveals, on balconies, etc.).

The openings are:

- o double-skinned box type windows – window type 1
- o single skin contemporary constructions (wooden or plastic) – window type 2.

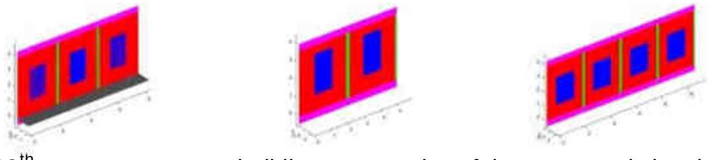

Fig. 72. – 19th century apartment building – examples of the generated virtual facades

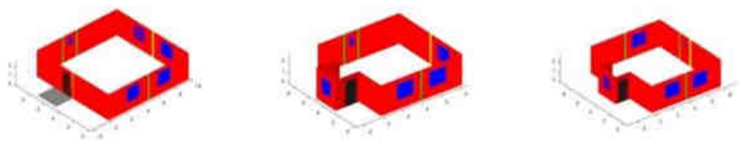

Fig. 73. – ‘cube house’ building type – examples of the generated virtual facades

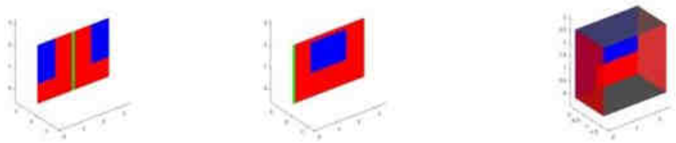

Fig. 74. – ‘block house’ building type – examples of the generated virtual facades

4.2.3 Monte Carlo simulation results

Based on the description of the three building types (parameter set, virtual façade geometry generation algorithm and detailed thermal bridge data summarized in Appendix C) and a thermal bridge database created for each type Monte Carlo simulations were run by generating virtual buildings and then performing the detailed calculation of the total façade thermal transmission coefficient to get a distribution of the proper thermal bridge correction factors reverse calculated from Eq. (65). 100.000 virtual geometries were generated or each building type and constructional variant to guarantee a sufficient coverage of the space of possible variations.

By varying all the constructional (i.e. wall type, insulation type and thickness, etc.) and geometrical parameters (generated virtual façade geometry) of a building type at the same type one can’t distinguish between the influence of individual parameters and can’t derive simplified formulas for the accurate thermal bridge correction factor. The best way to proceed is first to keep all constructional parameters constant, determine the relationship between geometry and thermal bridging for a given construction type and insulation thickness first, than the relationship between insulation thickness and thermal bridging, and then the dependence on the other constructional parameters (wall type, insulation type, window type, etc.). A few examples of the calculated thermal bridge correction factors (χ values) for given sets of constructional variables are plotted against the specific length of thermal bridges (Σl/A) in Fig. 75*,* Fig. 76*,* Fig. 77 *and* Fig. 78. Each figure shows the prescribed thermal bridge correction factors of the current Hungarian simplified calculation method as a reference (three horizontal lines corresponding to the tree levels of correction factors in 7/2006 [1]). The inaccuracy of the simple calculation methods is easy to observe.

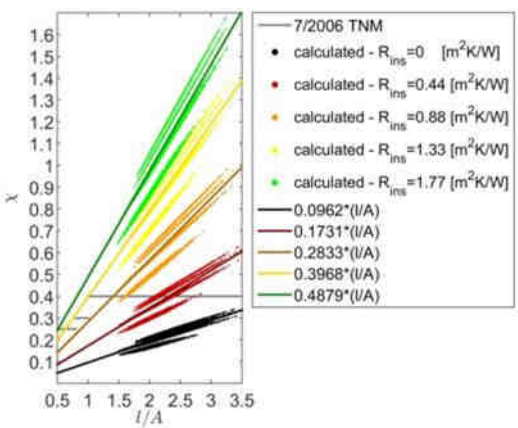

Fig. 75. – 19th century apartment building, 44 [cm] thick solid brick masonry, internal insulation, bad details, various insulation thicknesses

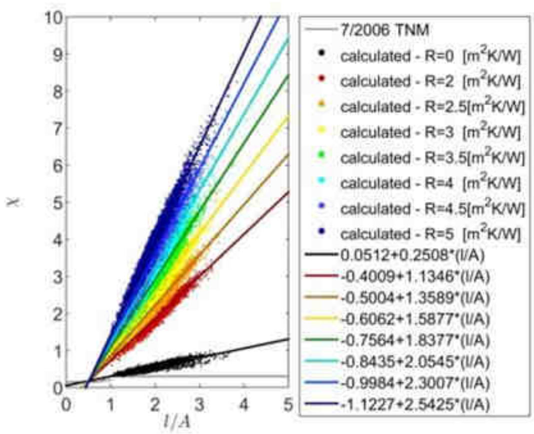

Fig. 76. – ‘Block house’, Window 1, bad details, various insulation thicknesses

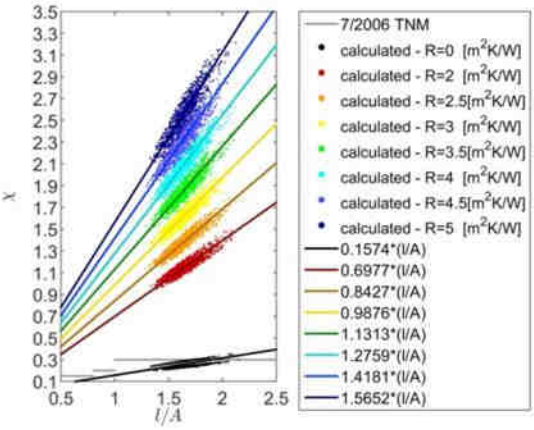

Fig. 77. – ‘Cube house’, solid brick masonry, Window 1, bad details, various insulation thicknesses

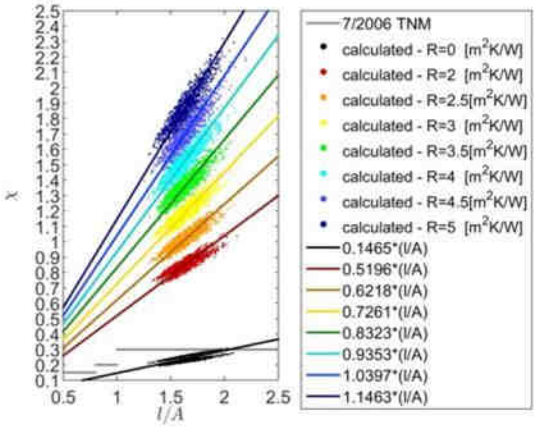

Fig. 78. – ‘Cube house’, aerated clay brick masonry, Window 1, bad details, various insulation thicknesses

For each building type, construction type and thermal insulation thickness (represented by individual colors in the preceding figures) there usually is a good linear correlation between Σl/A and χ. Individual thermal bridges can have very different linear heat transfer coefficients but their relative abundance does not change much between the generated virtual facades for a given building type (for a mix of different building types or buildings that are not typifyable no such clear correlation could be detected). We can easily approximate the results with a collection of lines fitted to the data:

$$\chi = a + s\frac{\sum l}{A} \tag{66}$$

where Χ [-] is the thermal bridge correction factor, a [-] the constant representing the intersection of the line with the y axis, s [m] the constant describing the slope of the line and Σl/A [1/m] the specific length of the thermal bridges on the façade.

For most cases a is around zero and the lines converge in the origin of the Σl/A – χ coordinate system. This is to be expected as an imaginary façade with no thermal bridges (l=0) would have no thermal bridge correction factor either. Slight deviations from this rule can exist, where the geometry and the difference in magnitude between the individual thermal bridges is more complex.

The slope of the line is set by the building type and constructional variant, while the exact value along the line depends on the geometrical variation within the building type. The value of a and s was determined with a least squares fit for every group investigated. The derived dataset of a and s values is summed up in Table 13, Table 14 *and* Table 15 for the three investigated building types and their constructional variants.

				s [m]				
insulation	**details**	**windows**	**R_{wall}**	**R_{ins}=0**	**R_{ins} =0.44**	**R_{ins} =0.88**	**R_{ins} =1.33**	**R_{ins} =1.77**
internal ins.	bad details	window 1	0.608 (44 cm)	0.0962	0.1731	0.2834	0.3973	0.4880
			0.800 (59 cm)	0.1220	0.2078	0.3476	0.4879	0.6092
			0.992 (74 cm)	0.1567	0.2726	0.4294	0.5775	0.7325
		window 2	0.608 (44 cm)	0.1284	0.2817	0.4495	0.6233	0.7653
			0.800 (59 cm)	0.1781	0.3547	0.5445	0.7312	0.9175
			0.992 (74 cm)	0.2326	0.4289	0.6287	0.8242	1.0282
	good details	window 1	0.608 (44 cm)	0.0962	0.0936	0.1633	0.2337	0.2843
			0.800 (59 cm)	0.1220	0.1067	0.1832	0.2777	0.3353
			0.992 (74 cm)	0.1567	0.1444	0.2259	0.3225	0.4166
		window 2	0.608 (44 cm)	0.1284	0.1407	0.2316	0.3325	0.4038
			0.800 (59 cm)	0.1781	0.1803	0.2820	0.4076	0.4976
			0.992 (74 cm)	0.2326	0.2225	0.3356	0.4475	0.5695
				s [m]				
insulation	**details**	**windows**	**R_{wall}**	**R_{ins}=0**	**R_{ins} =0.5**	**R_{ins} =1**	**R_{ins} =1.5**	**R_{ins} =2**
external ins.	ext. façade	window 1	0.608 (44 cm)	0.0963	0.1133	0.1805	0.2506	0.3203
			0.800 (59 cm)	0.1219	0.1250	0.1800	0.2340	0.3082
			0.992 (74 cm)	0.1567	0.1574	0.2092	0.2693	0.3325
		window 2	0.608 (44 cm)	0.1283	0.1048	0.1156	0.1319	0.1504

			0.800 (59 cm)	0.1781	0.1282	0.1307	0.1422	0.1609
			0.992 (74 cm)	0.2325	0.1647	0.1586	0.1664	0.1801
	int. façade	window 1	0.608 (44 cm)	0.0984	0.1603	0.2792	0.4009	0.5200
			0.800 (59 cm)	0.1242	0.1655	0.2673	0.3775	0.4881
			0.992 (74 cm)	0.1592	0.1931	0.2876	0.3912	0.4974
		window 2	0.608 (44 cm)	0.1306	0.1518	0.2143	0.2819	0.3497
			0.800 (59 cm)	0.1803	0.1687	0.2183	0.2767	0.3407
			0.992 (74 cm)	0.2350	0.2004	0.2370	0.2883	0.3444

Table 13 – Summary of s values for the 19th century urban residential building type

masonry	details	win.	s [m]							
			R_{ins}=0	R_{ins}=2	R_{ins}=2.5	R_{ins}=3	R_{ins}=3.5	R_{ins}=4	R_{ins}=4.5	R_{ins}=5
aerated c.b.	good	win. 1	0.1463	0.2185	0.2360	0.2519	0.2696	0.2863	0.3056	0.3224
		win. 2	0.1549	0.2012	0.2138	0.2264	0.2382	0.2507	0.2626	0.2781
		win. 3	0.1363	0.2500	0.2769	0.3026	0.3288	0.3551	0.3819	0.4096
		win. 4	0.1495	0.2313	0.2499	0.2647	0.2727	0.2843	0.2938	0.2821
	bad	win. 1	0.1465	0.5196	0.6218	0.7261	0.8323	0.9353	1.0397	1.1463
		win. 2	0.1571	0.5611	0.6723	0.7855	0.9012	1.0143	1.1240	1.2415
		win. 3	0.1543	0.5620	0.6732	0.7893	0.9047	1.0182	1.1317	1.2468
		win. 4	0.1596	0.6614	0.7777	0.8866	0.9827	1.0673	1.1351	1.1212
solid brick	good	win. 1	0.1545	0.2993	0.3302	0.3596	0.3881	0.4201	0.4493	0.4794
		win. 2	0.1624	0.2670	0.2897	0.3109	0.3311	0.3526	0.3730	0.3945
	bad	win. 1	0.1574	0.6977	0.8427	0.9876	1.1313	1.2759	1.4181	1.5652
		win. 2	0.1641	0.7353	0.8861	1.0386	1.1916	1.3395	1.4919	1.6425

Table 14 – Summary of s values for the 'cube house' building type

details	window	s [m]							
		R_{ins}=0	R_{ins}=2	R_{ins}=2.5	R_{ins}=3	R_{ins}=3.5	R_{ins}=4	R_{ins}=4.5	R_{ins}=5
good	win. 1	s=0.2517 a=0.0450	s=0.4189 a= -0.053	s=0.4874 a=-0.081	s=0.5564 a=-0.107	s=0.6301 a=-0.144	s=0.7070 a=-0.186	s=0.7839 a=-0.228	s=0.8568 a=-0.264
	win. 2	s=0.2823 a=0.032	s=0.3517 a=-0.019	s=0.4389 a=-0.054	s=0.5012 a=-0.082	s=0.5624 a=-0.110	s=0.6284 a=-0.144	s=0.6870 a=-0.168	s=0.7549 a=-0.208
bad	win. 1	s=0.2508 a=0.0512	s=1.1346 a=-0.401	s=1.3589 a=-0.500	s=1.5877 a=-0.606	s=1.8377 a=-0.757	s=2.0545 a=-0.844	s=2.3007 a=-0.998	s=2.5425 a=-1.123
	win. 2	s=0.3021 a=0.0105	s=1.3554 a=-0.567	s=1.6275 a=-0.708	s=1.9088 a=-0.862	s=2.1773 a=-1.000	s=2.4477 a=-1.139	s=2.7376 a=-1.324	s=2.9872 a=-1.437

Table 15 – Summary of a and s values for the 'block house' building type

Such a set of s and a values could already be useful for designers, but it contains too many datapoints to be truly practical as a simplified calculation tool. An even more compact calculation method is reached by finding some relationship between the constructional parameters and the a and s values. The form this relationship can take will wary from building type to building type depending on the number and type of the constructional parameters used to define them.

For the case of the 19th century urban apartment buildings we derived a relationship between the thermal resistance of the insulation, the thermal resistance of the masonry (this building type has different characteristic wall thicknesses) by fitting the following polynomial to the gathered data (see Fig. 79, Fig. 80, Fig. 81 and Fig. 82):

$$
\begin{aligned}
s = {} & p_{00} + p_{10}R_{wall} + p_{01}R_{ins} + p_{20}R_{wall}^{\ 2} + p_{11}R_{wall}R_{ins} \\
& + p_{02}R_{ins}^{\ 2} + p_{21}R_{wall}^{\ 2}R_{ins} + p_{12}R_{wall}R_{ins}^{\ 2} + p_{03}R_{ins}^{\ 3}
\end{aligned} \tag{67}
$$

where s is the slope for Equation (66) (for this building type a = 0), p_{ij} the polynomial coefficients given in Table 16, R_{ins} [m^{2}K/W] the thermal resistance of the thermal insulation and R_{wall} [m^{2}K/W] the thermal resistance for the masonry.

ins.	details	win.	p_{00}	p_{10}	p_{01}	p_{20}	p_{11}	p_{02}	p_{21}	p_{12}	p_{03}
no ins.	-	win. 1	0	0.158	0	0	0	0	0	0	0
		win. 2	0.023	0.1091	0	0.106	0	0	0	0	0
int. ins.	good	win. 1	0.095	-0.262	0.189	0.259	-0.149	0.0098	0.031	0.118	-0.035
		win. 2	0.0656	-0.1046	-0.0924	0.2062	0.4904	0.0992	-0.341	0.0939	-0.0551
	bad	win. 1	0.088	-0.074	0.084	0.148	-0.066	0.153	0.164	0.039	-0.063
		win. 2	0.0334	0.0752	0.0378	0.1295	0.6986	0.0269	-0.3297	0.0258	-0.0173
ext. ins.	ext. f.	win. 1	0.105	-0.116	0.147	0.172	-0.392	0.125	0.182	0.019	-0.034
		win. 2	0.0414	0.0728	0.0453	0.1196	-0.2584	0.0761	0.0238	0.0648	-0.0295

	int. f.	win. 1	0.109	-0.124	0.286	0.177	-0.491	0.136	0.205	0.028	-0.039
		win. 2	0.0478	0.0616	0.1766	0.1268	-0.356	0.0935	0.0464	0.0729	-0.0362

Table 16 – polynomial coefficients in Equation (67) fitted to the data in Table 13 for the 19th century urban residential building type

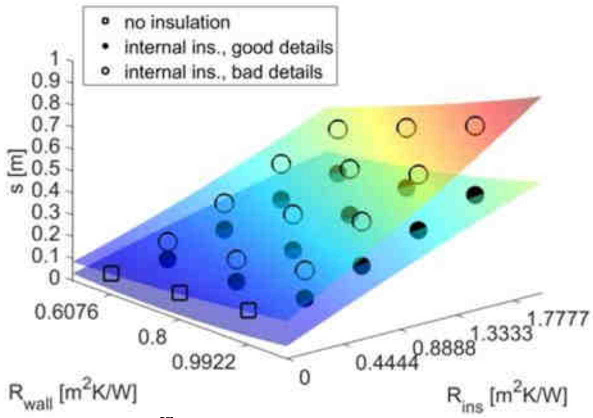

Fig. 79. – 19th century apartment building, internal insulation, window 1, polynomial equations fitted to the calculated data points

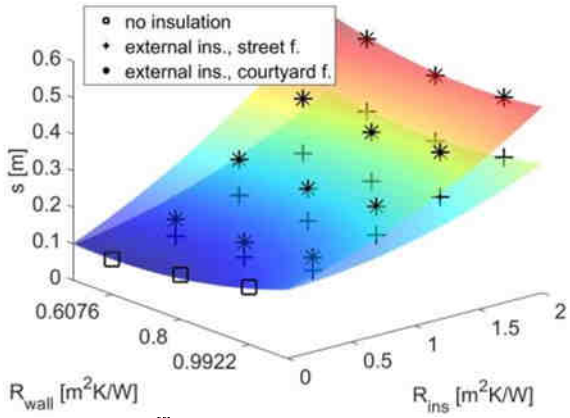

Fig. 80. – 19th century apartment building, external insulation, window 1, polynomial equations fitted to the calculated data points

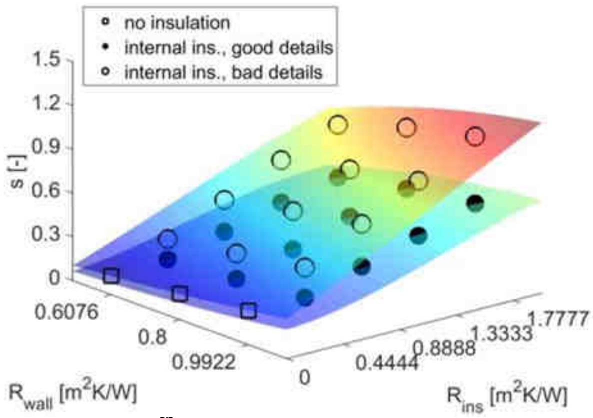

Fig. 81. – 19th century apartment building, internal insulation, window 2, polynomial equations fitted to the calculated data points

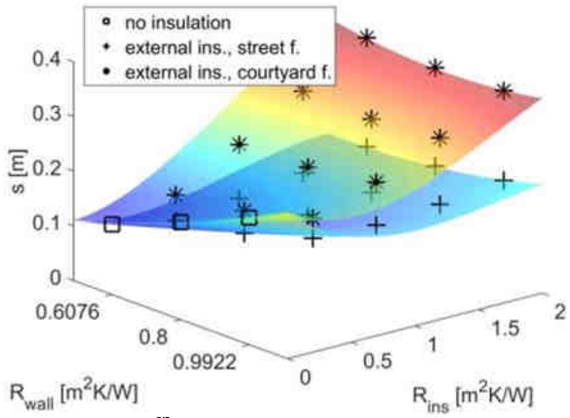

Fig. 82. – 19th century apartment building, external insulation, window 2, polynomial equations fitted to the calculated data points

For the case of the ‘cube houses’ there were two masonry and 2-4 window types investigated. The difference between the two wall types and between the window types would both be hard to express mathematically so we can only establish a relationship between insulation thickness and s value for every wall, window type and detail quality separately. We used a least squares fit with a third order polynomial of the thermal insulation’s resistance (see Fig. 83 and Fig. 84 for the solid and aerated clay brick masonries respectively):

$$s = p_1 R_{ins}{}^3 + p_2 R_{ins}{}^2 + p_3 R_{ins} + p_4 \tag{68}$$

where s is the slope for Equation (66) (for this building type $a = 0$), p_i the polynomial coefficients given is Table 17 and R_{ins} [m^{2}K/W] the thermal resistance of the thermal insulation layer.

masonry	details	window	p_1	p_2	p_3	p_4	R^2
aerated clay brick	good	window 1	0.0002	-0.0018	0.0388	0.1463	0.9999
		window 2	0.0001	-0.0004	0.0239	0.1548	0.9997
		window 3	0.0004	-0.0033	0.0621	0.1363	1.0
		window 4	-0.0011	0.0035	0.0381	0.1496	0.9959
	bad	window 1	-0.0010	0.0111	0.1685	0.1465	1.0
		window 2	-0.0012	0.0129	0.1813	0.1570	1.0
		window 3	-0.0013	0.0138	0.1815	0.1542	1.0
		window 4	-0.0075	0.0351	0.2065	0.1605	0.9991

solid brick	good	window 1	0.0007	-0.0072	0.0838	0.1545	0.9999
		window 2	0.0005	-0.0054	0.0612	0.1623	1.0
	bad	window 1	-0.0009	0.0097	0.2552	0.1573	1.0
		window 2	-0.0010	0.0102	0.2697	0.1640	1.0

Table 17 – polynomial coefficients in Equation (68) fitted to the data in Table 14 for the ‘cube house’ building type

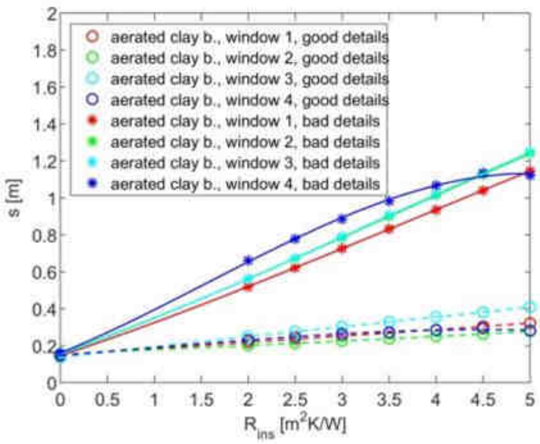

Fig. 83. – ‘cube house’, 25 [cm] aerated clay brick masonry, relationship between R_{ins} and s and the polynomials fitted to the data

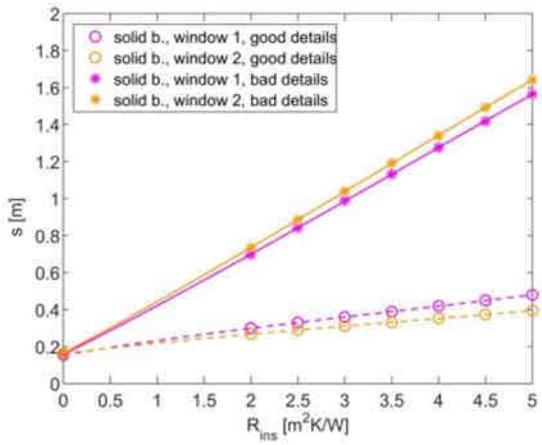

Fig. 84. – ‘cube house’, 38 [cm] thick solid brick masonry, relationship between R_{ins} and s and the polynomials fitted to the data

For the most cases s is a near linear function of R_{ins} when only the thickness of the thermal insulation is varied. For the case of window type 4 in the aerated clay brick masonry the position of the window installation in the wall was also a function of the thermal insulation thickness which resulted in a non-linear relationship and a maximum value for s around R_{ins}=4.5 [m^2K/W] (see Fig. 83). Among all the variants the quality of the constructional details has the largest effect on the thermal bridging. The impact of the masonry type is also significant, as can be seen by comparing Fig. 83 and Fig. 84. Even though both variants have the same overall U value the thicker solid brick wall with the larger thermal conductivity causes more severe thermal bridging. The window type can cause large differences as well. The presence or absence of an inbuilt roller shutter case alone can have a comparable effect in the thermal bridging as the masonry type (see the difference between window type 1 (no shade) and type 3 (inbuilt roller shade) in Fig. 83).

In the case of the ‘block house’ building type a good fit with the simulated data resulted in lines that do not converge perfectly in the origin of the ΣI/A – χ coordinate system (see Fig. 76). The dependence of the a and s values in Equation (66) on the thermal resistance of the thermal insulation was explored by a least squares fit with the following polynomials of the insulation thermal resistance R_{ins} (see Fig. 85):

$$s = p_{1s} {R_{ins}}^2 + p_{2s} R_{ins} + p_{3s} \quad (69)$$

$$a = p_{1a} {R_{ins}}^2 + p_{2a} R_{ins} + p_{3a} \quad (70)$$

where s [m] is the slope and a [-] the intersection for Equation (66), p_{is} and p_{ja} the polynomial coefficients given is Table 18 and Table 19, and R_{ins} [m^2K/W] the thermal resistance of the thermal insulation layer.

details	window	p_1	p_2	p_3	R^2
good	window 1	0.0108	0.0696	0.2482	0.9987
	window 2	0.0137	0.0304	0.2735	0.9880
bad	window 1	0.0056	0.4304	0.2506	0.9999
	window 2	0.0027	0.5264	0.2994	0.9999

Table 18 – polynomial coefficients for s [m] in Equation (69) fitted to the data in Table 15 for the ‘block house’ building type

details	window	p_1	p_2	p_3	R^2
good	window 1	-0.0050	-0.0371	0.0444	0.9990
	window 2	-0.0057	-0.0205	0.0343	0.9956
bad	window 1	-0.0053	-0.2069	0.0483	0.9988
	window 2	-0.0012	-0.2858	0.0107	0.9994

Table 19 – polynomial coefficients for a [m] in Equation (70) fitted to the data in Table 15 for the 'block house' building type

Once again the influence of the details' quality is the most marked, but even the type of window has a smaller but still significant effect.

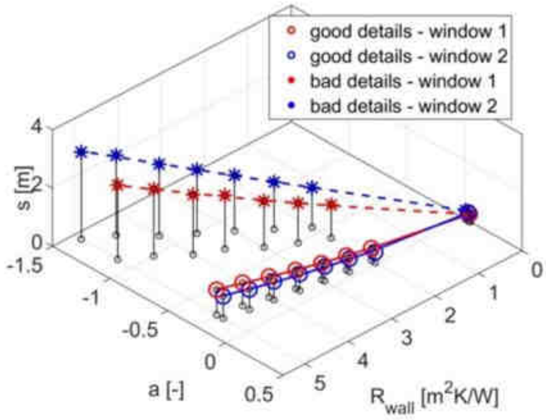

Fig. 85. – 'block building', relationship between R_{wall} and s and a values

4.2.4 Accuracy and impact

The accuracy of the existing and the proposed new calculation method is demonstrated by analyzing the percentage error in the thermal bridge correction factors. The percentage error of the existing Hungarian and the proposed new simplified calculation method is calculated as:

$$\%Error_{7/2006} = \left(\chi - \chi_{7/2006}\right) / \chi \qquad (71)$$
$$\%Error_{new} = \left(\chi - \chi_{new}\right) / \chi$$

where $\%\mathrm{Error}_{7/2006}$ [-] and $\%\mathrm{Error}_{new}$ are the percentage errors of the exiting Hungarian simplified thermal bridge calculation method and the proposed new calculation method respectively, χ [-] the accurate thermal bridge correction factor, $\chi_{7/2006}$ [-] the correction factor of the existing Hungarian and χ_{new} [-] the proposed new simplified calculation method respectively. Examples of the %Error's histogram plots for the tree different building types are found in Fig. 86, Fig. 88 and Fig. 90 (the rest is found in Appendix C) while a tabulated summary of the error's mean and standard deviation is found in Table 20, Table 21 and Table 22 for the three investigated building types.

To assess the impact of the thermal bridge correction's accuracy we can analyze the distribution of calculated thermal bridge corrected wall U values with the existing simplified calculation and the proposed method for different thermal insulation thicknesses and detail qualities. Examples for the tree buildings are found in Fig. 87, Fig. and Fig. 91 (the rest of the data is given in Appendix C).

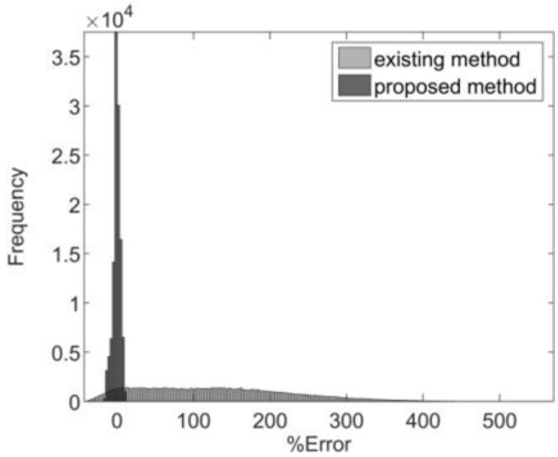

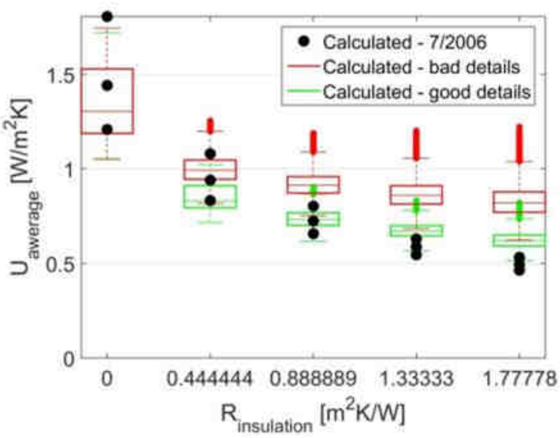

Fig. 86. – 19th century urban apartment building type, internal insulation, bad details, all wall and insulation thicknesses, window 1 – histogram plot of %Error in χ for the existing an proposed methods

Fig. 87. – 19th century urban apartment building, interior insulation, window 1, thermal bridge corrected U values

insulation	details	% Error			
		7/2006		new	
		mean	σ	mean	σ
no ins.	-	-31.4559	17.2865	-0.3434	5.4267
internal ins.	bad details	129.0369	97.6140	-0.4139	4.7950
	good details	27.5788	56.0602	-0.1963	5.3267
external ins.	ext. façade	64.1187	58.1825	-0.1871	3.4646
	int. façade	146.5545	95.9843	0.4449	3.5803

Table 20 – Mean and standard deviation of the percentage error of the current Hungarian and the proposed new simplified calculation method for the 19th century urban apartment building type

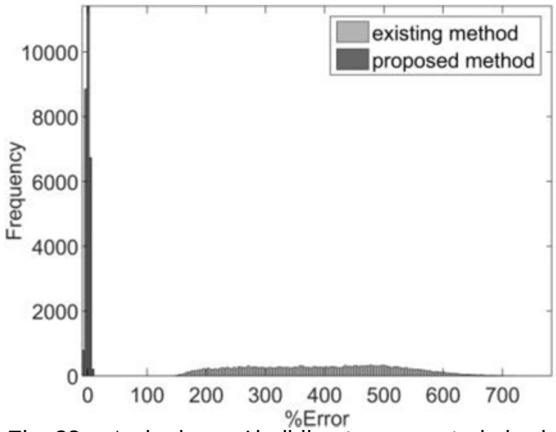

Fig. 88. – 'cube house' building type, aerated clay brick masonry, external insulation, bad details, all insulation thicknesses, window 1 – histogram plot of %Error in χ for the existing an proposed methods

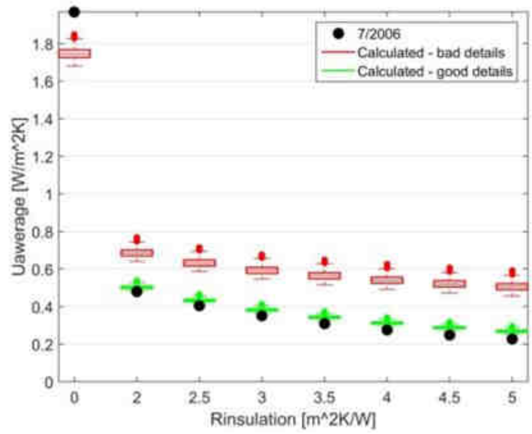

Fig. 89. – 'cube house' building type, aerated clay brick masonry, external insulation, window 1 – thermal bridge corrected U values

masonry	insulation	details	% Error			
			7/2006		new	
			mean	σ	mean	σ
aerated c.b.	no ins.	-	-39.4384	5.8437	0.5623	7.7763
	external ins.	good details	52.3179	29.0526	0.3826	5.5163
		bad details	392.8290	124.1107	0.1818	3.1098
solid brick	no ins.	-	-34.3416	7.0109	0.6895	10.5016
	external ins.	good details	98.9170	36.4795	0.3130	5.0762
		bad details	538.0267	171.5591	0.0958	2.9236

Table 21 – Mean and standard deviation of the percentage error of the current Hungarian and the proposed new simplified calculation method for the 'cube house' building type

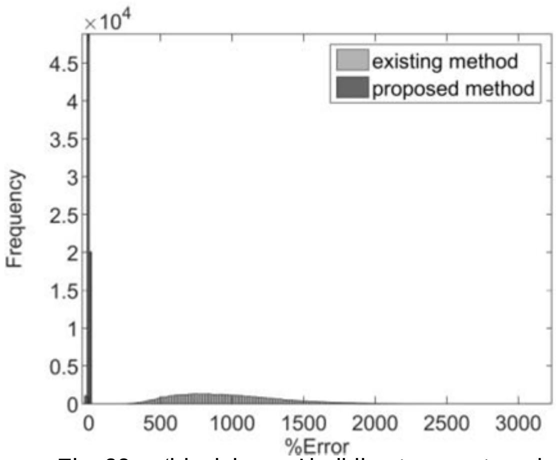

Fig. 90. – 'block house' building type, external insulation, bad details, all insulation thicknesses –

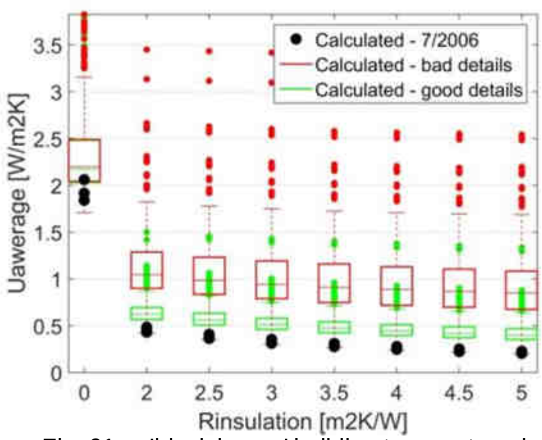

Fig. 91. – 'block house' building type, external insulation, window 1 – thermal bridge corrected U

histogram plot of %Error in χ for the existing an proposed methods (left) and for the proposed method without window installation thermal bridges (right)

values

insulation	details	% Error			
		7/2006		new	
		mean	σ	mean	σ
no ins.	-	45.6936	28.4694	-0.0104	9.4563
external ins.	good details	264.2812	105.3850	0.0128	5.8512
	bad details	970.4797	364.3656	-0.0152	5.3944

Table 22 – Mean and standard deviation of the percentage error of the current Hungarian and the proposed new simplified calculation method (with and without windows) for the ‘block house’ building type

The existing simple calculation methods is found to be very inaccurate for all investigated cases. It overpredicts heat losses for uninsulated buildings. After thermal insulation the opposite is true: heat transfer is under predicted – depending on the detail quality and the resistance of the insulation – by a very large amount. The new method produce errors centered very close around 0 and with much smaller spreads. The errors could be reduced further by using more complex relationships that fit the generated data better, but these would complicate the calculation method. The new method always produces much smaller errors than the existing calculation.

By analyzing the thermal bridge corrected U values of the external walls it is immediately noticeable that the quality of the details and the position of the thermal simulation (internal/external) has a very large impact, a statement which is probably accepted by most designers, jet is not reflected in the current calculation method. The existing method’ results are the most accurate for ‘good quality’ external insulations, but even than tend to underpredict heat loss for larger insulation thicknesses. For all the building types even the good quality thermal insulation scenarios show a significant spread in the U value depending on façade geometry and window type. The spread is even more amplified in case of ‘bad quality’ details. This shows that the precise geometry and constructional solution has to be incorporated into the calculation of the correction factor.

The biggest spread in the U values is seen in the case of the ‘block house’ building type, as this type of building has the biggest differences between the possible virtual façades (i.e. façade with only small windows vs. facades with balconies and large windows / balcony doors) and the ‘strongest’ thermal bridges (e.g. uninsulated reinforced concrete balconies). As a result even the ‘good quality’ variant has average U values far in excess (percentage vise) of the ones calculated by the simple method that does not take such things into consideration. The smallest spread in results is found for the ‘cube house’ building type that has a rather simple geometry and a larger wall area for a unit length of thermal bridge.

4.3 Separating window and masonry calculations

The difficulties with the method are the following:

1. the method is only applicable for buildings that are reasonably well typifyable (the variability between different thermal bridge types and their abundance on the façade is limited),
2. it needs to be derived for different building types individually,
3. a large number of independent parameters for a certain building type requires a large number of thermal bridge simulations to derive the new thermal bridge correction factors (although this work is only needed once),
4. building types with many independent parameters will probably require a more complex system of correction factors (e.g. many such factors) to maintain accuracy,

Points 1) and 2) seem unescapable and therefore indicate a reasonably well defined area area for the use of the method. Given the contemporary trends in architecture and the plethora of new construction materials and solutions it is hard to imagine that any simplified thermal bridge calculation could possibly deliver accurate results to most new designs. Many existing building however can easily be grouped into characteristic building typologies, with similar façade geometries and constructional solutions. For these building the practical usability of the methods seems to rely largely on how much one can reduce the possible number of independent constructional parameters in the description of a building type while still maintaining accuracy.

All investigated building types show that the value of the thermal bridge correction factor is dependent on all the parameters investigated in this study (insulation type and thickness, masonry type and thickness, detail quality, window type, etc.), its not possible to simply eliminate any of them. The question: which parameter can have the most number of unique values and therefore increase the total number of possible cases the most. Mathematically well defined continuous numerical parameters, such as the insulation thickness can take infinitely many values (although thermal insulation is usually only manufactured in certain discrete thicknesses), but we don't have to make calculations for all of them. Relationships such as the one between s, R_{ins} and R_{wall} in Equation (5) for the case of 19th century urban apartment buildings only needed a few values of R_{ins} and R_{wall} to be investigated, and once derived can provide an easy way to interpolate to new values between them.

The real difficulty is with parameters that are mathematically not well defined and don't produce a continuous and smooth distribution of values, such as the window and window installation type. Any relationship for the thermal bridge correction factor is only valid for the fenestration and windows installation type it was derived for and no simple interpolation is possible between different variants (different window and/or window installation types). This is especially problematic as the window and window installation type can show the single greatest variability in the external envelope of many buildings: window frame material, thickness, position in the masonry, shading devices, auxiliary constructions, the thermal insulation of the window reveal, etc. can all have many solutions. The 2-4 window types investigated in this study are but the tip of the iceberg.

4.3.1 The importance of the window-to-wall interface

It is worthwhile to investigate in detail how much window and window installation type influences the thermal bridge corrected U value of the external walls while keeping all other parameters the same.

For the 19th century urban apartment building type a third window options is added to show the importance of including the effects of internal architectural attachments, such as a wooden architrave framing and paneled window reveals (see Fig. 92 for all three window types). The calculated average of the thermal bridge corrected external wall U value is shown in Fig. 93, Fig. 94 and Table 23. In the uninsulated state the average U value is increased ca. 15% with replacing double-skin box type windows with single skin constructions and it is clearly shown that box type windows with internal wooden framing and paneling produces the smallest thermal bridging at the window-to-wall interface. As thermal insulation is added and its thickness is increased the differences between the individual window options grow ever more pronounced. Single skin windows become the most favorable option if a sufficient insulation of the external window reveal is possible ('good quality' variant, at the cost of reduced aperture size, insolation, destruction of architectural character). A box type window with internal attachments can however reduce thermal bridging almost as much without any insulation of the window reveal (window reveal insulation is often not possible with existing windows due to their small frame sizes). For bad quality details (no insulation in the reveal) single skin windows are clearly the worst with the corrected U value increasing by as much as 45% for internal and 20% for externally insulated buildings.

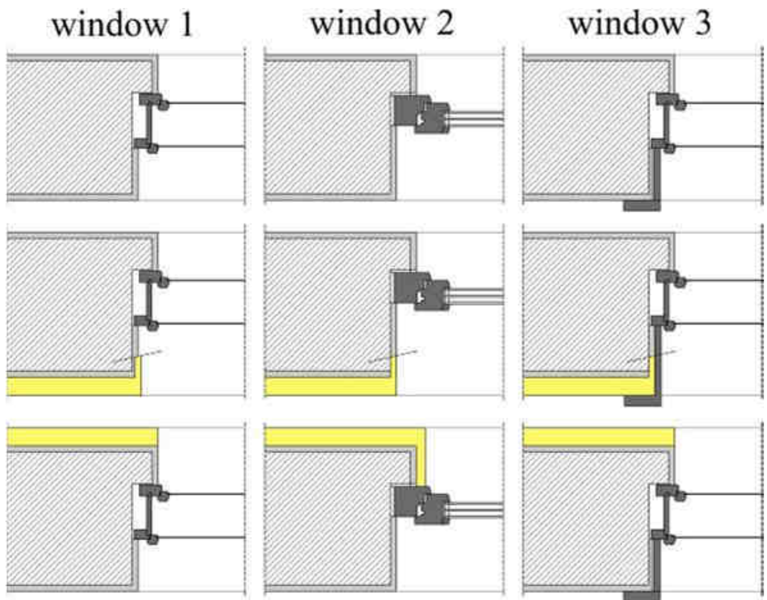

Fig. 92. – 19th century urban apartment building type – the different window options

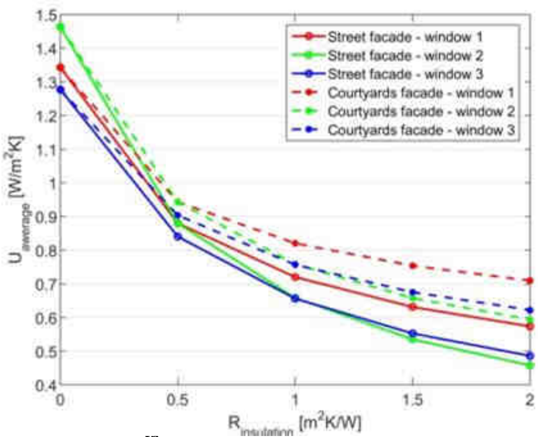

Fig. 93. – 19th century apartment building, external insulation – average of calculated U value for the external wall

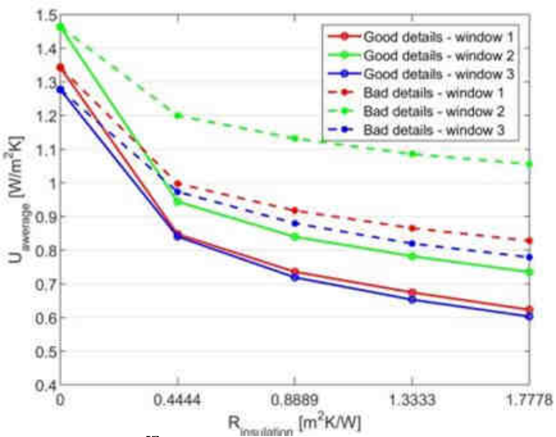

Fig. 94. – 19th century apartment building, internal insulation – average of calculated U value for the external wall

insulation	details	window type	R_{ins} [m²K/W] 0	0.444	0.889	1.333	1.778
internal	good	window 1	1.3428 (0.1718)	0.8475 (0.0661)	0.7358 (0.0458)	0.6745 (0.0386)	0.6229 (0.0419)
		window 2	1.4634 (0.1567)	0.9443 (0.0632)	0.8398 (0.0506)	0.7823 (0.0533)	0.7351 (0.0569)
		window 3	1.2774 (0.1861)	0.8404 (0.0700)	0.7192 (0.0478)	0.6530 (0.0374)	0.6030 (0.0387)
	bad	window 1	1.3428 (0.1718)	0.9978 (0.0694)	0.9176 (0.0628)	0.8655 (0.0714)	0.8279 (0.0801)
		window 2	1.2774 (0.1861)	1.1997 (0.0856)	1.1318 (1.1318)	1.0857 (0.1000)	1.0557 (0.1083)
		window 3	1.2774 (0.1861)	0.9736 (0.0620)	0.8799 (0.0581)	0.8196 (0.0671)	0.7790 (0.0765)

Table 23 – 19th century apartment building type, internal insulation – mean and standard deviation (in brackets) of the external wall U value depending on detail quality, insulation thickness and window type

insulation	façade	window type	R_{ins} [m²K/W] 0	0.5	1.0	1.5	2.0
external	street	window 1	1.3428 (0.1718)	0.8802 (0.0747)	0.7202 (0.0550)	0.6313 (0.0476)	0.5736 (0.0441)
		window 2	1.4634 (0.1567)	0.8799 (0.0656)	0.6582 (0.0404)	0.5352 (0.0290)	0.4576 (0.0232)
		window 3	1.2774	0.8406	0.6563	0.5527	0.4862

			(0.1861)	(0.0866)	(0.0581)	(0.0452)	(0.0385)
	courtyard	window 1	1.3428 (0.1718)	0.9433 (0.0889)	0.8205 (0.0734)	0.7538 (0.0672)	0.7096 (0.0635)
		window 2	1.2774 (0.1861)	0.9431 (0.0797)	0.7586 (0.0588)	0.6578 (0.0485)	0.5936 (0.0428)
		window 3	1.2774 (0.1861)	0.9037 (0.1009)	0.7567 (0.0769)	0.6752 (0.0653)	0.6221 (0.0588)

Table 24 – 19th century apartment building type, external insulation – mean and standard deviation (in brackets) of the external wall U value depending on façade, insulation thickness and window type

For the ‘cube house’ building type the 4 plus 2 investigated window and installation options are the same as before, and are shown here in more detail in Fig. 95 and Fig. 96. The results are in Fig. 98, Fig. 99, Table 25 and Table 26. The differences for uninsulated building are much smaller for ‘cube houses’ due to the much smaller wall thickness and the fact that in small detached houses window installation thermal bridges contribute much less to the overall façade U value as in larger buildings (the specific length of all other details, e.g. wall corners and plinths is much bigger). The difference are somewhat larger for ‘bad quality’ details.

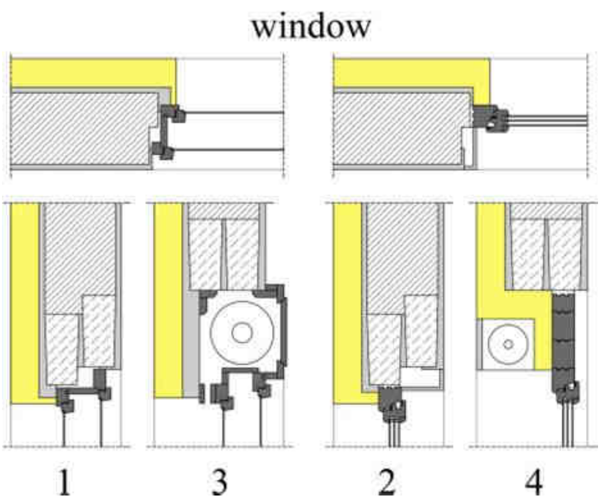

Fig. 95. – ‘cube house’, aerated clay brick masonry – the different window options (‘good quality details’)

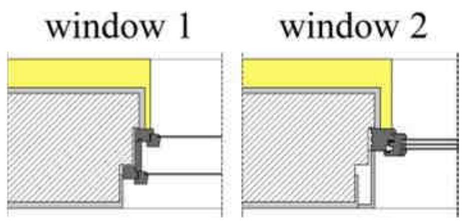

Fig. 96. – ‘cube house’, solid brick masonry – the different window options (‘good quality details’)

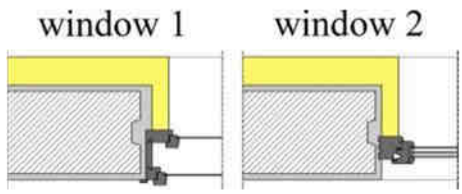

Fig. 97. – ‘block house’ – the different window options (‘good quality details’)

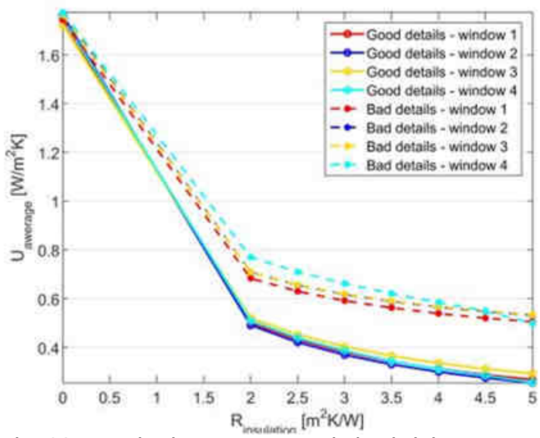

Fig. 98. – ‘cube house’, aerated clay brick masonry – average of calculated U value for the external wall

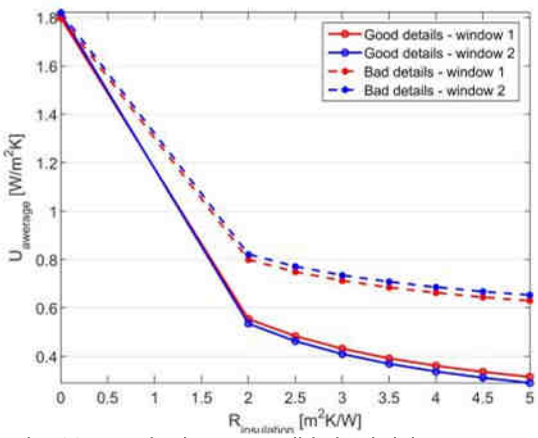

Fig. 99. – ‘cube house’, solid clay brick masonry – average of calculated U value for the external wall

			R_{ins} [m²K/W]							
masonry	**details**	**window**	**0**	**2**	**2.5**	**3**	**3.5**	**4**	**4.5**	**5**
aerated clay brick	good	win. 1	1.7456 (0.0302)	0.5016 (0.0100)	0.4324 (0.0091)	0.3818 (0.0086)	0.3431 (0.0082)	0.3127 (0.0079)	0.2883 (0.0077)	0.2683 (0.0075)
		win. 2	1.7646 (0.0321)	0.4917 (0.0090)	0.4215 (0.0080)	0.3702 (0.0073)	0.3309 (0.0068)	0.3001 (0.0064)	0.2754 (0.0061)	0.2552 (0.0059)

		win. 3	1.7232 (0.0278)	0.5209 (0.0125)	0.4534 (0.0121)	0.4040 (0.0118)	0.3661 (0.0116)	0.3364 (0.0115)	0.3125 (0.0114)	0.2929 (0.0114)
		win. 4	1.7524 (0.0304)	0.5099 (0.0111)	0.4395 (0.0101)	0.3873 (0.0094)	0.3444 (0.0085)	0.3117 (0.0079)	0.2847 (0.0074)	0.2569 (0.0063)
	bad	win. 1	1.7456 (0.0302)	0.6845 (0.0229)	0.6309 (0.0234)	0.5923 (0.0237)	0.5633 (0.0241)	0.5398 (0.0244)	0.5207 (0.0246)	0.5055 (0.0248)
		win. 2	1.7646 (0.0321)	0.7099 (0.0267)	0.6566 (0.0272)	0.6184 (0.0277)	0.5899 (0.0282)	0.5666 (0.0285)	0.5477 (0.0288)	0.5328 (0.0290)
		win. 3	1.7524 (0.0304)	0.7102 (0.0269)	0.6576 (0.0275)	0.6198 (0.0281)	0.5914 (0.0285)	0.5684 (0.0289)	0.5496 (0.0292)	0.5347 (0.0294)
		win. 4	1.7524 (0.0304)	0.7709 (0.0366)	0.7104 (0.0361)	0.6630 (0.0352)	0.6217 (0.0336)	0.5854 (0.0319)	0.5500 (0.0296)	0.4992 (0.0244)

Table 25 – 'cube house', aerated clay brick masonry – mean and standard deviation (in brackets) of the external wall U value depending on detail quality, insulation thickness and window type

			R_{ins} [m^{2}K/W]							
masonry	**details**	**window**	**0**	**2**	**2.5**	**3**	**3.5**	**4**	**4.5**	**5**
solid clay brick	good	win. 1	1.7980 (0.0397)	0.5537 (0.0145)	0.4833 (0.0137)	0.4312 (0.0132)	0.3914 (0.0128)	0.3606 (0.0127)	0.3354 (0.0125)	0.3146 (0.0124)
		win. 2	1.8152 (0.0409)	0.5348 (0.0123)	0.4626 (0.0111)	0.4093 (0.0103)	0.3689 (0.0098)	0.3370 (0.0093)	0.3112 (0.0090)	0.2901 (0.0088)
	bad	win. 1	1.7980 (0.0397)	0.7993 (0.0341)	0.7487 (0.0350)	0.7122 (0.0358)	0.6845 (0.0364)	0.6623 (0.0369)	0.6440 (0.0373)	0.6296 (0.0376)
		win. 2	1.8152 (0.0409)	0.8214 (0.0374)	0.7711 (0.0384)	0.7348 (0.0392)	0.7078 (0.0399)	0.6855 (0.0404)	0.6672 (0.0409)	0.6528 (0.0412)

Table 26 – 'cube house', solid clay brick masonry – mean and standard deviation (in brackets) of the external wall U value depending on detail quality, insulation thickness and window type

Lastly, for the 'block house' building type the two investigated window and installation options are shown in Fig. 97, the results in Fig. 100 and Table 27. The difference between the single- and double-skin window is on the order of 5% for 'good quality' details, but reaches more than 10% for 'bad quality' details. This large building type has a similarly large window perimeter to façade area ratio as the 19th century urban apartment buildings, hence the large influence of windows details. The difference is only not bigger because the other severe thermal bridge types of the building (i.e. reinforced concrete balconies) can 'drown out' the window's effects.

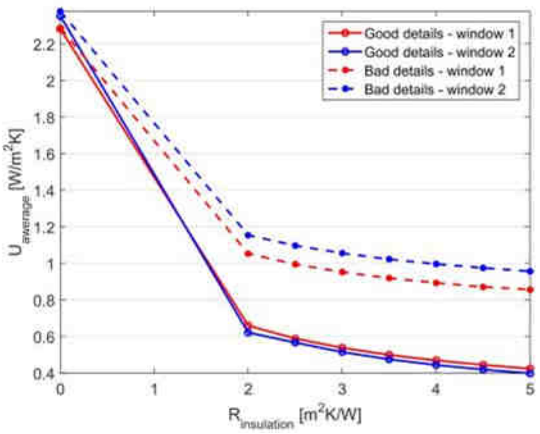

Fig. 100. – 'block house', solid clay brick masonry – average of calculated U value for the external wall

			R_{ins} [m^{2}K/W]							
masonry	**details**	**window**	**0**	**2**	**2.5**	**3**	**3.5**	**4**	**4.5**	**5**
block.	good	win. 1	2.2809 (0.3875)	0.6591 (0.1464)	0.5887 (0.1443)	0.5379 (0.1435)	0.4991 (0.1429)	0.4689 (0.1426)	0.4444 (0.1424)	0.4241 (0.1422)
		win. 2	2.3522 (0.4508)	0.6212 (0.1261)	0.5667 (0.1311)	0.5146 (0.1296)	0.4751 (0.1286)	0.4440 (0.1278)	0.4192 (0.1274)	0.3984 (0.1268)
	bad	win. 1	2.2809 (0.3875)	1.0532 (0.3930)	0.9944 (0.3992)	0.9524 (0.4041)	0.9190 (0.4077)	0.8931 (0.4106)	0.8711 (0.4127)	0.8561 (0.4173)
		win. 2	2.3522 (0.4508)	1.1540 (0.4722)	1.0967 (0.4795)	1.0554 (0.4849)	1.0220 (0.4887)	0.9962 (0.4919)	0.9747 (0.4946)	0.9566 (0.4968)

Table 27 – 'block house' building type – mean and standard deviation (in brackets) of the external wall U value depending on detail quality, insulation thickness and window type

The effect of window and window installation type is thus demonstrated to have a significant on the overall thermal bridge corrected U value of the external wall. Besides the fact that this must be included in every thermal bridge correction factor another point must be made: the difference in heat losses between various window options cant' be accurately calculated by comparing only the windows' U_w thermal transmittance, since the windows effect the heat flow in the wall around them as well. A correct approach of comparing the U values of windows would either have to calculate and compare the thermal bridge corrected heat transfer of the complete façade as well, or much more practically use the $U_{w,inst}$ value of the window for the comparison instead. This is most often used in the design of Passive Houses and is defined as:

$$U_{w,inst} = \frac{A_w U_w + \sum_{i=1}^{n} l_i \Psi_{install,i}}{A_w} \quad (72)$$

where: $U_{w,inst}$ [W/m^{2}K] is the overall thermal transmittance of the window in its installed state, Uw [W/m^{2}K] is the thermal transmittance of the window on its own, A_w [m^2] the surface area of the window, l_i [m] the length of the window-to-wall joint i and $\psi_{inst,i}$ [W/mK] the linear heat transfer coefficient of the window-to-wall joint i. The necessity of calculating the fenestration related heat losses in this way was also demonstrated in Bakonyi and Becker [15].

4.3.2 Modification to the new calculation method

If the window installation thermal bridges have to be calculated to derive the $U_{w,inst}$ value anyway it makes sense to remove them from the wall thermal bridge correction. The simplified calculation of the external building fabric's total heat transmittance would then take the following new form:

$$Q_{trans} = \sum_{i=1}^{n} A_i U_i \left(1 + \chi_{new} \left(\frac{\sum l}{A}, \ldots \right) \right) + \sum_{k=1}^{p} A_{w,k} U_{w,inst,k} + \sum_{j=1}^{m} l_j \Psi_j \quad (73)$$

where: $\dot{Q}_{transm}$ [W/K] is the total thermal transmittance of the external thermal envelope, A_i [m^2] the internal area of the opaque surface i, U_i [W/m^{2}K] the thermal transmittance value of opaque surface i, χ_{new} [-] the new thermal bridge correction factor (neglecting window-to-wall joints and depending on building type, constructional variant and actual geometry), $A_{w,k}$ [m^2] the surface area of window k, $U_{w,inst,k}$ [W/m^{2}K] the installed U value of window k, l_j [m] the length of the plinth detail j (slab-on-grade perimeter) or basement wall, $\psi_{,j}$ [W/mK] the linear thermal transmittance value of the plinth or basement wall detail.

This transformation has the added benefit of enabling a significant reduction in the total number of scenarios in the masonry thermal bridge correction factor's calculation. If we remove the window installation thermal bridges for the three investigated building types we get the much reduced dataset presented in *Tables 9-11*.

			s [m]				
insulation	**details**	R_{wall}	R_{ins}=0	R_{ins} =0.44	R_{ins} =0.88	R_{ins} =1.33	R_{ins} =1.77
internal ins.	bad details	0.608 (44 cm)	0.1356	0.2255	0.3370	0.4343	0.5214
		0.800 (59 cm)	0.1417	0.2143	0.3159	0.4055	0.4907
		0.992 (74 cm)	0.1391	0.2059	0.2889	0.3666	0.4462
	good details	0.608 (44 cm)	0.1356	0.1606	0.2468	0.3225	0.3899
		0.800 (59 cm)	0.1417	0.1591	0.2301	0.3154	0.3731
		0.992 (74 cm)	0.1391	0.1577	0.2196	0.2786	0.3440
			s [m]				
insulation	**details**	R_{wall}	R_{ins}=0	R_{ins}=0.5	R_{ins}=1	R_{ins}=1.5	R_{ins}=2
external ins.	ext. façade	0.608 (44 cm)	0.1357	0.1399	0.1419	0.1432	0.1436
		0.800 (59 cm)	0.1416	0.1409	0.1427	0.1435	0.1439
		0.992 (74 cm)	0.1391	0.1416	0.1429	0.1436	0.1442
	int. façade	0.608 (44 cm)	0.1396	0.2270	0.3252	0.4219	0.5141
		0.800 (59 cm)	0.1459	0.2162	0.3049	0.3930	0.4777

		0.992 (74 cm)	0.1437	0.2078	0.2884	0.3699	0.4498

Table 28 – Summary of s values for the 19th century urban residential building type, without the windows

		s [m]							
masonry	details	R_{ins}=0	R_{ins}=2	R_{ins}=2.5	R_{ins}=3	R_{ins}=3.5	R_{ins}=4	R_{ins}=4.5	R_{ins}=5
aerated c.b.	good	0.1671	0.2598	0.2729	0.2822	0.2943	0.3042	0.3174	0.3265
	bad	0.1673	0.5569	0.6576	0.7602	0.8647	0.9647	1.0666	1.1710
solid brick	good	0.1782	0.3191	0.3373	0.3524	0.3665	0.3838	0.3972	0.4118
	bad	0.1789	0.6645	0.7897	0.9151	1.0376	1.1610	1.2824	1.4069

Table 29 – Summary of s values for the 'cube house' building type, aerated clay brick masonry, without the windows

	s [m]							
details	R_{ins}=0	R_{ins}=2	R_{ins}=2.5	R_{ins}=3	R_{ins}=3.5	R_{ins}=4	R_{ins}=4.5	R_{ins}=5
good	s=0.3779 a=-0.019	s=0.4102 a=-0.018	s=0.4414 a=-0.026	s=0.4611 a=-0.022	s=0.4922 a=-0.031	s=0.5336 a=-0.055	s=0.5504 a=-0.052	s=0.5887 a=-0.075
bad	s=0.3607 a=0	s=0.5629 a=0	s=0.6186 a=0	s=0.6732 a=0	s=0.7292 a=0	s=0.7856 a=0	s=0.8172 a=0	s=0.8703 a=0

Table 30 – Summary of s values for the block house building type, without the windows

Performing the same least square fits on the reduced dataset produces the polynomial coefficient for the equation presented in section 3 as a complete simplified thermal bridge calculation method for the investigated building types and their constructional variants.

ins.	details	p_{00}	p_{10}	p_{01}	p_{20}	p_{11}	p_{02}	p_{21}	p_{12}	p_{03}
int. ins.	good	-0.0109	0.2152	0.2522	-0.0846	-0.1238	-0.0118	0	0	0
	bad	0.0779	0.1524	0.2902	-0.1184	-0.0965	0.0015	0	0	0
ext. ins.	ext. f.	0.1173	0.0477	0.076	-0.0037	-0.0251	-0.001	0	0	0
	int. f.	0.1600	-0.0502	0.2280	-0.0882	0.0319	0.0066	0	0	0

Table 31 – polynomial coefficients in Equation (5) fitted to the data in *Table 9* for the 19th century urban residential building type

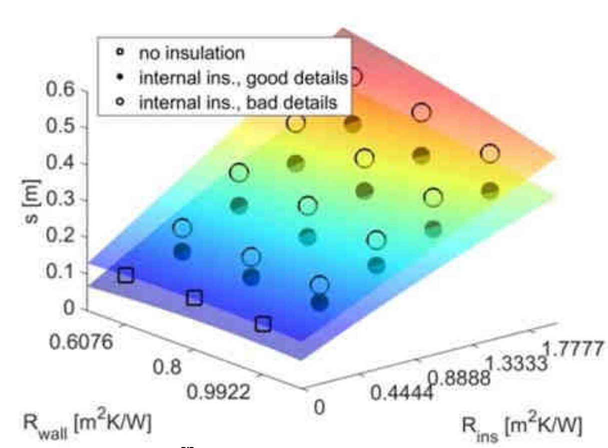

Fig. 101. – 19th century apartment building, internal insulation, no windows, polynomial equations fitted to the calculated data points

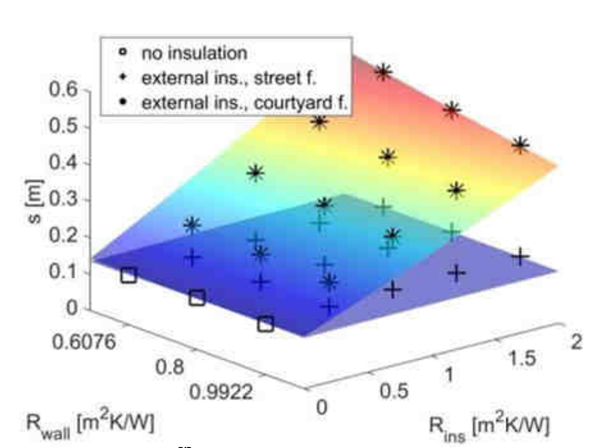

Fig. 102. – 19th century apartment building, external insulation, no windows, polynomial equations fitted to the calculated data points

masonry	details	p_1	p_2	p_3	p_4	R^2
aerated clay brick	good	0.0012	-0.0129	0.0670	0.1672	0.9990
	bad	-0.0004	0.0049	0.1868	0.1672	1.0
solid brick	good	0.0012	-0.0129	0.0670	0.1672	0.9995
	bad	-0.0004	0.0049	0.1868	0.1672	1.0

Table 32 – polynomial coefficients in Equation (6) fitted to the data in *Table 10* for the 'cube house' building type

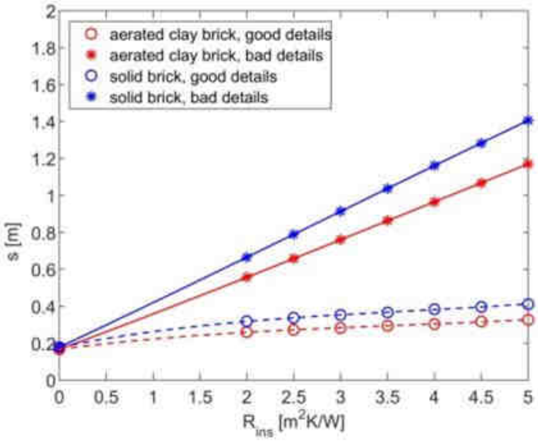

Fig. 103. – 'cube house', no windows, polynomial equations fitted to the calculated data points

details	p_1	p_2	p_3	R^2
good	0.0072	0.0076	0.3755	0.9917
bad	-0.0009	0.1077	0.3583	0.9985

Table 33 – polynomial coefficients for s [m] in Equation (7) fitted to the data in *Table 11* for the 'block house' building type

details	p_1	p_2	p_3	R^2
good	-0.0040	0.0093	-0.0196	0.9335
bad	0	0	0	1.0

Table 34 – polynomial coefficients for a [m] in Equation (8) fitted to the data in *Table 12* for the 'block house' building type

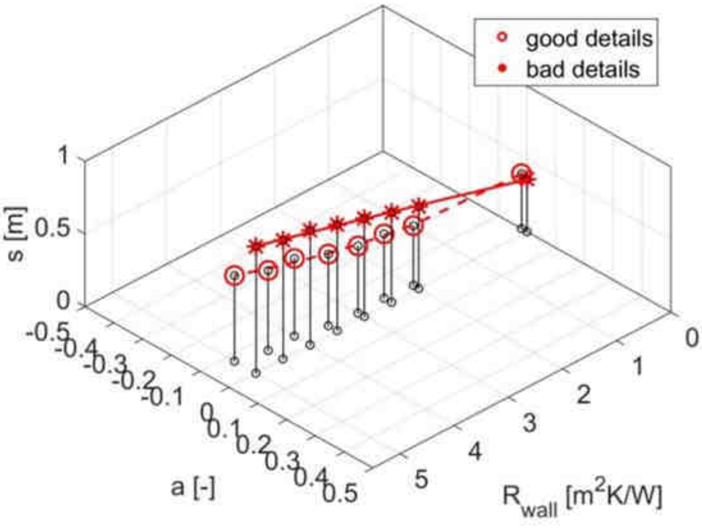

Fig. 104. – 'block building', relationship between R_{wall} and s and a values

4.3.3 The accuracy of the new separated calculation method

The %error in the calculation of the thermal bridge corrected U value of the external wall is presented in the following tables (histogram plots of the error are found in Appendix C).

insulation	details	% Error new, no win. mean	σ
no ins.	-	-0.7911	7.4314
internal ins.	bad details	-1.3091	9.4699
	good details	-0.5581	6.6883
external ins.	ext. façade	-0.6355	6.8861
	int. façade	1.2334	6.4700

Table 35 – Mean and standard deviation of the percentage error of the current Hungarian and the proposed new simplified calculation method for the 19th century urban apartment building type (calculation without windows)

masonry	insulation	details	% Error new, no win. mean	σ
aerated c.b.	no ins.	-	0.5956	9.4359
	external ins.	good details	0.4881	7.2110
		bad details	0.1818	3.1098
solid brick	no ins.	-	0.8313	12.9319
	external ins.	good details	0.4817	7.1329
		bad details	0.3839	4.8255

Table 36 – Mean and standard deviation of the percentage error of the current Hungarian and the proposed new simplified calculation method for the ‘cube house’ building type (calculation without windows)

insulation	details	% Error new, no win. mean	σ
no ins.	-	-0.0230	8.2377
external ins.	good details	-0.2001	17.4097
	bad details	-0.8991	32.2543

Table 37 – Mean and standard deviation of the percentage error of the current Hungarian and the proposed new simplified calculation method (with and without windows) for the ‘block house’ building type (calculation without windows)

It is not possible to compare this error directly to other methods as it has a different definition for the thermal bridge correction of walls (it now excludes window-to-wall interfaces). However the removal of the window-to-wall thermal bridges from the proposed method produces somewhat larger errors than before, especially for the case of the ‘block building’, probably because its poor thermal quality and the larger variability of its façade. The errors could be reduced further by using more complex relationships that fit the generated data better, but these would complicate the calculation method.

5 The heat balance of box type windows

The determination of accurate thermal performance indices for box type windows is an important step, but comparing just these numbers without their constructional and environmental context can be misleading, as it was demonstrated for the subject of thermal bridging in the last chapter. The ultimate measure of a window's thermal performance is its heat balance and influence on the internal thermal environment (i.e. thermal comfort) for the specific climate, local environment, building and orientation it is found in.

As was already demonstrated by the review of fenestration thermal modeling in chapter 2 there are many approaches for calculating fenestration heat balance. However, as it was demonstrated e.g. by Schultze et al. [150] the combination of large solar gains and large thermal mass poses significant challenges for problems with too many simplifications. Historic double-skin box-type windows are usually found in naturally ventilated buildings with thick, good conductance and large thermal mass walls. Instead of using existing commercial or freeware codes a new dynamic building energy simulation program EPICAC BE is introduced.

5.1 EPICAC BE – a dynamic fenestration heat balance simulation program

The new dynamic building-simulation program EPICAC[19] BE [18] was developed in MATLAB for modeling the detailed heat balance and the optimization of single windows or groups of windows and the testing of algorithms not easily achieved in off-the-shelf programs. The aim is not the simulation of complete building, therefore a single-zone or room based approach was chosen, much like the programs COMFEN [151] or the works of Peterson et al. [139] and Reinhart et al [145] reviewed in Chapter 2. This scale is sufficient to account for the main interactions between the building and the energy balance of the windows, but remains tractable and computationally affordable even for a large number of simulation runs. The testing of different retrofit options for different boundary conditions (orientation, external shading, different usage profiles, etc.) is achieved with individual simulations. The sub-models of the program were chosen to best suite the very high thermal mass and naturally ventilated 19th century central-European building stock and their box type windows. The latter requires extra attention due to the window type's inherent difference from contemporary single-skin constructions. The sub-models and algorithms necessary for the task and implementation is introduced in the following section.

5.1.1 Calculating glazing area heat transfer

Both solar/optical and thermal calculation are performed by the program EPICAC ISO (also developed by the author), a MATLAB based code developed for testing center-of-glazing thermal calculation algorithms. The solar-optical calculation for the glazing system is done according the method described in ISO 9050 [93] when only specular layers are present, using data from the International Glazing Database [160], or the matrix layer method of Klems [107] [108] when the shading is active (non specular layers). The necessary Bi-Directional Scattering Distribution Function of the shading layers is generated with the help of the Window 7.3 program [119]. The optical properties of the whole glazing system are precalculated at the beginning of the simulation for all angles of incidence and then the appropriate values are found by interpolation according to the Sun's position and the state of the shading at every time step. The direct solar transmission and the absorbed solar radiation in each layer is calculated at the beginning of each time-step. The thermal calculation is based on the ISO 15099 standard [97] for the calculation of the convective heat transfer coefficients in the cavities and the heat balance equations used in EnergyPlus [67] as it showed better convergence properties when incorporated into the dynamic building energy simulation program.

[19] The program is named after the computer called 'EPICAC' in the fictional short story by the same title of the American writer Kurt Vonneguth Jr. It was inspired by the first electronic general purpose computer ENIAC. The story was published in: Vonneguth, K. (1950) EPICAC, In: Welcome to the Monkey House, Dial Press, Whitmer, Clair., ISBN 0-385-33350-1

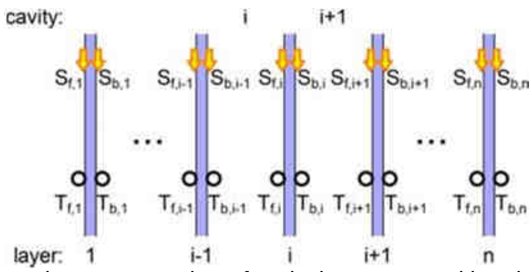

Fig. 105. – schematic representation of a glazing system with only specular layers

The heat balance equations for glazing systems without longwave-infrared transparent or semi-transparent layers (e.g. only glazing layers):

$$q_{lw,e} + h_{gl,1}\left(T_{b,1} - T_{f,1}\right) + h_{c,e}\left(T_{e,air} - T_{f,1}\right) + S_{f,1} = 0 \tag{74}$$

…

$$h_{gl,i-1}\left(T_{f,i-1} - T_{b,i-1}\right) + h_{c,i}\left(T_{f,i} - T_{b,i-1}\right) + \sigma\frac{\varepsilon_{b,i-1}\varepsilon_{f,i}}{1-\left(1-\varepsilon_{b,i-1}\right)\left(1-\varepsilon_{f,i}\right)}\left(T_{f,i}{}^{4} - T_{b,i-1}{}^{4}\right) + S_{b,i-1} = 0 \tag{75}$$

$$h_{gl,i}\left(T_{b,i} - T_{f,i}\right) + h_{c,i}\left(T_{b,i-1} - T_{f,i}\right) + \sigma\frac{\varepsilon_{b,i-1}\varepsilon_{f,i}}{1-\left(1-\varepsilon_{b,i-1}\right)\left(1-\varepsilon_{f,i}\right)}\left(T_{b,i-1}{}^{4} - T_{f,i}{}^{4}\right) + S_{f,i} = 0 \tag{76}$$

…

$$q_{lw,i} + h_{gl,n}\left(T_{f,n} - T_{b,n}\right) + h_{c,i}\left(T_{i,air} - T_{b,n}\right) + S_{b,n} = 0 \tag{77}$$

Eq. (74) and (77) describe the heat balance of the external and internal facing surfaces of the glazing system, while Eq. (75) and (76) the two glazing surfaces facing each other in the internal cavity i (see Fig. 105). The $q_{lw,e}$ external and internal longwave radiation heat flux is described by Eq. (78), and the $q_{lw,i}$ internal longwave radiation heat flux is calculated separately in an iteration loop with the glazing heat balance from the internal surface temperature, and the surface temperature and view factor of all other surfaces in the thermal zone. σ is the Stefan-Boltzmann constant (5.67e-8 [W/m^{2}K^4]), $T_{e,air}$ and $T_{i,air}$ are the absolute external and internal air temperatures [K], $T_{f,i}$ and $T_{b,i}$ the absolute front and back surface temperatures of layer i [K], $h_{gl,i}$ the conductive heat transfer coefficient of layer i [W/m^{2}K], $h_{c,i}$ the convective heat transfer coefficient of cavity i [W/m^{2}K] calculated acc. to ISO 15099, $\varepsilon_{f,i}$ and $\varepsilon_{b,i}$ the front and back longwave infrared emissivity of layer i, while $S_{f,i}$ and $S_{b,i}$ are the absorbed solar radiation in the front and back portion of layer i [W/m^2] (calculated as the half of the total solar radiation absorbed by layer i, according to ISO 9055).

The longwave infrared radiation incident on the external surface is calculated as:

$$q_{lw,e} = f_{sky} I_{atm} + \left(1 - f_{sky}\right)\left(\varepsilon_{terr}\sigma T_{terr}{}^{4} + \rho_{terr} I_{atm}\right) - \sigma T_{f,1}{}^{4} \tag{78}$$

In Equation (78) f_{sky} [-] is the view factor of the window to the sky, I_{atm} [W/m^2] the longwave infrared radiation incident from the sky (taken from the climate file), ε_{terr} the emissivity of the ground [-] (assumed to be 0.9), T_{terr} [K] the absolute surface temperature of the ground (assumed to be equal to the ambient air temperature), and ρ_{terr} [-] the longwave infrared reflectivity of the ground (assumed to be 0.1).

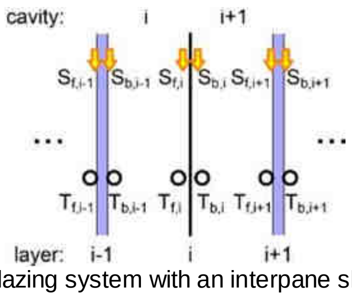

Fig. 106. – part of a glazing system with an interpane shading device (layer i)

The presence of a shading layer with non-specular optical properties switches the calculation of solar-optical properties from the ISO 9055 [93] standard to the matrix layer method of Klems [107] [108]. It also changes the thermal calculation as most shading layers have a non-zero longwave infrared transmittance. Equations (75) and (76) are replaced by (79) (80) (81) and (82) when a shading layer is added in the cavity, and the treatment of the thermal radiation is changed to account for transmittance and multiple reflections across shading layer i according to [67] (see Fig. 106):

$$h_{gl,i-1}\left(T_{f,i-1}-T_{b,i-1}\right)+h_{c,i}\left(T_{f,i}-T_{b,i-1}\right)+\frac{\sigma\varepsilon_{b,i-1}}{1-\rho_{b,i-1}R_i}\left[\frac{\tau_{sh,i}}{1-\rho_{b,i-1}\rho_{f,i+1}}\left(\varepsilon_{f,i+1}T_{f,i+1}{}^4+\varepsilon_{b,i}T_{b,i}{}^4\rho_{f,i+1}\right)+\ldots\right.$$
$$\left.\ldots+\varepsilon_{f,i}T_{f,i}{}^4+\varepsilon_{b,i-1}T_{b,i-1}{}^4R_i\right]-\sigma\varepsilon_{b,i-1}T_{b,i-1}{}^4+S_{b,i-1}=0 \tag{79}$$

$$h_{sh,i}\left(T_{b,i}-T_{f,i}\right)+h_{c,i}\left(T_{b,i-1}-T_{f,i}\right)+\frac{\sigma\varepsilon_{f,i}}{1-\rho_{b,i-1}R_i}\left[\frac{\tau_{sh,i}\rho_{b,i-1}}{1-\rho_{b,i}\rho_{f,i+1}}\left(\varepsilon_{f,i+1}T_{f,i+1}{}^4+\varepsilon_{b,i}T_{b,i}{}^4\rho_{f,i+1}\right)+\ldots\right.$$
$$\left.\ldots+\varepsilon_{b,i-1}T_{b,i-1}{}^4+\varepsilon_{f,i}T_{f,i}{}^4\rho_{b,i-1}\right]-\sigma\varepsilon_{f,i}T_{f,i}{}^4+S_{f,i}=0 \tag{80}$$

$$h_{sh,i}\left(T_{f,i}-T_{b,i}\right)+h_{c,i+1}\left(T_{f,i+1}-T_{b,i}\right)+\frac{\sigma\varepsilon_{b,i}}{1-\rho_{f,i+1}R_{i+1}}\left[\frac{\tau_{sh,i}\rho_{f,i+1}}{1-\rho_{b,i-1}\rho_{f,i}}\left(\varepsilon_{b,i-1}T_{b,i-1}{}^4+\varepsilon_{f,i}T_{f,i}{}^4\rho_{b,i-1}\right)+\ldots\right.$$
$$\left.\ldots+\varepsilon_{f,i+1}T_{f,i+1}{}^4+\varepsilon_{b,i}T_{b,i}{}^4\rho_{f,i+1}\right]-\sigma\varepsilon_{b,i}T_{b,i}{}^4+S_{b,i}=0 \tag{81}$$

$$h_{gl,i+1}\left(T_{b,i+1}-T_{f,i+1}\right)+h_{c,i+1}\left(T_{b,i}-T_{f,i+1}\right)+\frac{\sigma\varepsilon_{f,i+1}}{1-\rho_{f,i+1}R_{i+1}}\left[\frac{\tau_{sh,i}}{1-\rho_{b,i-1}\rho_{f,i}}\left(\varepsilon_{b,i-1}T_{b,i-1}{}^4+\varepsilon_{f,i}T_{f,i}{}^4\rho_{b,i-1}\right)+..\right.$$
$$\left.\ldots+\varepsilon_{b,i}T_{b,i}{}^4+\varepsilon_{f,i+1}T_{f,i+1}{}^4\rho_{b,i}\right]-\sigma\varepsilon_{f,i+1}T_{f,i+1}{}^4+S_{f,i+1}=0 \tag{82}$$

Eq. (79) and (82) describe the heat balance of the glazing surfaces facing the interpane shading layer and Eq. (80) and (81) the heat balance of the front and back facing surfaces of the shading layer itself. The new variables are $h_{sh,i}$ the conductive heat transfer coefficient of shading layer i, $\rho_{f,i}$ and $\rho_{b,i}$, the front and back longwave infrared reflectance of layer i [-], $\tau_{f,i}$ and $\tau_{b,i}$, the front and back longwave infrared transmittance of layer i [-]. The constants R_i and R_{i+1} [-] are defined in Eq. (83) and (84) respectively:

$$R_i=\rho_{f,i}+\frac{\tau_{sh,i}\rho_{f,i+1}}{1-\rho_{b,i}\rho_{f,i+1}} \tag{83}$$

$$R_{i+1}=\rho_{b,i}+\frac{\tau_{sh,i}\rho_{b,i-1}}{1-\rho_{f,i}\rho_{b,i-1}} \tag{84}$$

For every time-step the direct transmission and absorption of solar radiation is calculated only once, while the thermal balance equations of the layers are linearized and solved iteratively to account for the temperature dependence of the convective heat transfer and the interaction with the internal thermal environment via convection and radiation.

During the simulation the boundary conditions of incident direct and diffuse solar radiation, internal and external dry bulb temperatures, external mean radiative temperature and internal net longwave radiation exchange are all taken from the rest of the simulation, and the equations are solved iteratively with the heat balance of the zone. The developed simulation module for the complex glazing system was cross validated to Window 7.3 [120] for several examples with standard boundary conditions and no discrepancies were found for up to two decimals. Using a custom implementation of these algorithms instead of commercial or otherwise hard to modify software allows us to easily explore the effects of model changes such as different choices for the Rayleigh-Nusselt number correlation for the cavity convection coefficients and easily create more complicated controls or automated sensitivity studies.

5.1.2 Control algorithms for shading devices

The simulation of shading devices requires a model describing their operation. The implementation of shading control algorithms in EPICAC BE is very simple, as all the simulation data is available at run time to the shading control logic and no external coupling with other programs or precalculation is necessary, as is the case with many commercial programs. The shading control is called at the beginning of each time-step and the glazing area solar/optical and heat balance calculations are performed according the shading-state.

5.1.3 Calculating whole window heat transfer

The glazing area heat balance is continuously calculated by the program, but values describing the heat transfer through the frame elements are needed to be input and therefore have to be calculated separately. Calculations are performed with the help of LBNL Therm 7.3 [119] according to the standards ISO 15099 [97] and NFRC 100-2010 [135], the area weighted approach for U_w and the modifications to the algorithm introduced at the end of Chapter 3 of this work. Additionally, based on the findings of Chapter 4, an $U_{w,installed}$ value Is calculated for each investigated window and input into EPICAC BE to account for the window-to-wall interface and the effect of various architectural attachments.

As during the simulation the program calculates the heat balance of the glazing area dynamically the $U_{w,inst}$ value can't be used directly. Instead a thermal transmission coefficient $L_{3D,w,frame,inst}$ [W/K] is calculated at the beginning of the simulation: $L_{3D,w,frame,inst} = U_{w,inst} * A_w - U_g * A_g$, where $U_{w,inst}$ and U_g are calculated for standard boundary condition and A_w and A_g are based on the internal dimensions of the window (as internal dimensions are the basis for the zone air heat balance algorithm).

5.1.4 Calculating infiltration and natural ventilation

The infiltration and natural ventilation of historic buildings and windows is the hardest aspect of their energy balance to calculate. A brief summary of the approaches to modelling natural ventilation is found in Caciolo et al. [30]. He highlights that most simulation codes are intended for buildings with mechanical ventilation with preset or dynamically controlled airflow rates augmented by only simple infiltration models. However, most professional simulation programs do offer possibilities for calculating natural ventilation. These can range from simple empirical formulas, through various flow-network models to coupling with full-blown CFD simulations. Unfortunately the computational cost of CFD is still prohibitive in most cases and all simpler models rely heavily on input parameters with high uncertainty, such as pressure coefficients.

Perhaps the biggest challenge lies in the calculation of single sided ventilation. Caciolo et al. [30] demonstrates that both simple empirical calculations and more detailed airflow-network models used in the majority of dynamic building-simulation engines fail to accurately predict the phenomenon. In addition to buoyancy this type of flow is determined by the compressibility of the air and the turbulent fluctuation of the wind speed rather than simple pressure differentials which is the main assumption in most models. Efforts were made to try and correct for this shortcoming in airflow-network model (e.g. Descalaki et al. [38]), but the state of the art is still the use of semi-empirical equations derived by full-scale or wind tunnel measurements (e.g. the models of De Gidds and Phaff [40], Warren and Parkins [166] or Larsen [117]). A good survey of these models is also found in Caciolo et al. [30]. In [33] Carciolo et al. performed a full scale measurement campaign of single sided natural ventilation on a small experimental building, but unfortunately found neither model very accurate.

EPICAC BE is intended for the dynamic simulation of single rooms and therefore needs a model for single sided ventilation for which the model of Larsen [117] was chosen as it is the best documented in the literature. The model uses a form of the orifice equation with the reference wind speed at the building height, wind incidence angle, the temperature difference and some semi-empirical measurement derived coefficients to calculate the airflow rate when the windows are open. The model cannot account for the shielding of the neighboring buildings or the exact position of the opening in the façade, therefore it can only be considered as approximate. For the infiltration calculation (when the windows are closed) pressure coefficients are determined with the help of the CpCalc program[20] [78] and the air permeability of the windows needs to be input.

In all cases a parameters study is recommended to asses the uncertainty of the ventilation and infiltration models. EPICAC BE can also accept a predetermined constant or scheduled ACH (Air Change Rate).

5.1.5 Weather data, models for solar radiation, shading and opaque constructions

The weather data is taken from a climate file derived as a statistical average for Budapest which in addition to basic data contains hourly values of direct and diffuse incident solar radiation on a horizontal plane and values of the longwave atmospheric counterradiation. The diffuse and direct solar radiation incident on a specific surface is calculated with the help of the Perez anisotropic sky model [138]. The external shading of the surroundings, the window reveal etc. is modelled with precalculated shading masks which are taken as an average of a discretized surface to account for partial shading (based on the work of Marsh [125], see: Fig. 107).

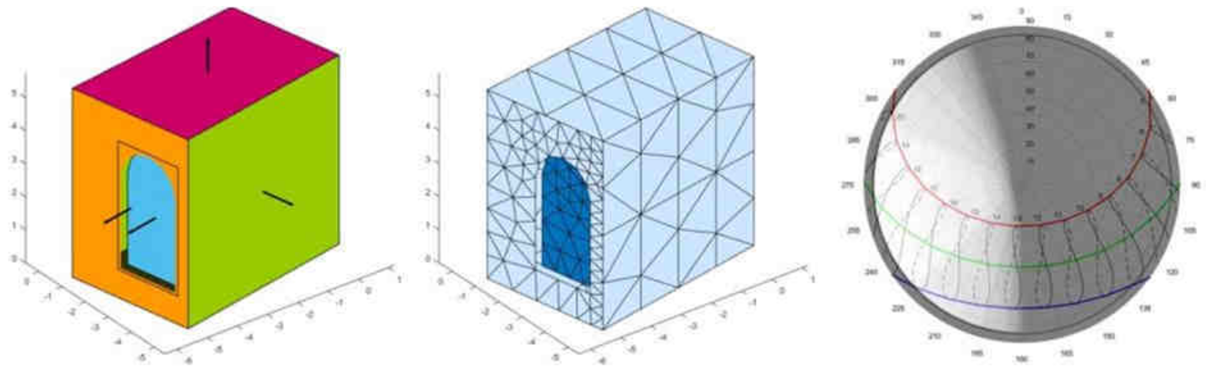

Fig. 107. – The geometrical model of the reference room and thy prototype window (left), the discretization of the surfaces for the shading mask calculations (middle) and an example of the calculated shading mask for the window with partial shadings (right)

To model opaque constructions and accurately represent their thermal mass the simulation uses another proprietary MATLAB program of the author: EPICAC FVM. This code is intended for the heat air and moisture transport modelling (HAM simulation) in one, two or three dimensional constructions, which is based on the work of Künzel [115] and using the finite volume method. EPICAC FVM was validated with the help of the EN ISO 10211 [61] and EN 15026 [65] standards for multi-dimensional stationary heat transfer and transient coupled heat and moisture transfer respectively. The validation is found in Appendix D. In the current form of the building-simulation model EPICAC BE only uses the one dimensional transient heat transport capabilities of EPICAC FVM. Thermal bridge effect are only incorporated with their static heat transfer coefficients, neglecting their dynamic behavior. This is considered acceptable since the solid masonry constructions of the investigated building are pretty homogeneous and the overall effect of thermal bridging is small.

The external longwave radiation exchange for all surfaces is computed based on the surfaces' solid angles to the sky and the ground and the terrestrial and atmospheric counterradiation, after the work of Kehrer and Schmidt [105]. The internal longwave radiation exchange is based on an exchange matrix derived from numerically calculated view factors between all individual surfaces and their emissivities. The calculation is valid for convex room geometries of arbitrary shape. The internal distribution of the transmitted solar load is based on the assumption that all radiation first hits the floor, and the reflections are diffuse and based on the view factors between the floor and the other surfaces. The convective heat transfer coefficients can all be either constant or correlation based. All surface temperatures are calculated iteratively within a time step to account for their interactions.

[20] A program for calculating the pressure coefficients on specific points of building façades depending on building size, shape and environment based on empirical correlations derived from wind tunnel measurements. Developed by Grosso [78].

5.1.6 Calculating zone air moisture balance

The moisture content of the air is needed for calculating thermal comfort indices therefore a transient moisture balance model had to be added to the program. The zone air moisture balance equation is written in terms of the partial vapor pressure and accounts for the moisture storage of the air, ventilation and infiltration, moisture sources and moisture exchange with the internal faces of the enclosure surfaces. Currently the Effective Moisture Penetration Depth (EMPD) model is used to account for the moisture buffering of the enclosure surfaces as described by Janssens et al. in [100]. Internal moisture sources are defined with hourly schedules (occupant moisture generation, potted plants, etc.). The governing equations of the model are:

$$d_{EMPD,j} = \sqrt{\frac{\delta_j p_{sat,j} \tau}{\rho_{dry,j} \xi_j \pi}} \qquad (85)$$

$$\rho_{dry,j} \xi_j d_{EMPD,j} \frac{d}{dt}\left(\frac{p_j}{p_{sat,j}} \right) = \beta_j \left(p_i - p_j \right) \qquad (86)$$

$$\frac{V}{R_v T} \frac{dp_i}{dt} = \sum \dot{m} + \sum n \frac{1}{3600} \frac{V}{R_v T} \left(p_e - p_i \right) + \sum A_j \beta_j \left(p_j - p_i \right) \qquad (87)$$

Equation (85) describes the calculation of $d_{EMPD,j}$ [m], the effective moisture penetration depth of surface j, which is performed for each internal surfaces based on δ_j [kg/msPa] the vapor permeability of the material, $p_{sat,j}$ [Pa] the saturation vapor pressure, τ [s] is the period of the cyclic variation of vapors pressure in the room, $\rho_{dry,j}$ [kg/m3] the dry density of the material and ξ_j [kg/kg] the moisture capacity of the material, defined as the derivative of the moisture storage function. The EMPD is a measure of how deep a theoretical periodic fluctuation of the relative humidity in the internal air of the room causes a vapor flow to penetrate into the surface of the internal constructions. For periods of one day this is on the order od a few millimeters. Equation (86) describes the moisture balance of a d_{EMPD} deep layer at the surface of a solid construction j, where p_j [Pa] is the partial vapor pressure of the surface layer, t [s] the time, p_i [Pa] the partial vapor pressure of the air in thermal zone i to which surface j is adjacent and β_j [kg/m2sPa] is the coefficient for the surface vapor transfer. Finally Equation (87) is the zone air moisture balance, where V [m^3] is the zone air volume, R_v [J/kgK] the specific gas constant of water vapor, T [K] the absolute temperature of the zone air, p_i [Pa] the partial vapor pressure in the zone air, $\dot{m}$ [kg/s] the internal moisture sources, n [1/h] the air change rate, p_e [Pa] the partial vapor pressure of the external air, A_j [m^2] the internal surface area of construction j, β_j [kg/m2sPa] the coefficient for the surface vapor transfer and p_j [Pa] the effective vapor pressure at the surface layer of construction j.

The EMPD model is only a rough approximation of the surface moisture buffering. The values of d_{EMPD} and ξ are derived for moisture variations with a given period τ and around a given relative mean relative humidity. In future iterations of the program a full HAM (Heat Air and Moisture) simulation capability will be added as a more advanced option by coupling the full HAM simulation capability of EPICAC FVM to the zone air moisture balance.

5.1.7 Calculating internal and HVAC loads, zone air heat balance

Internal loads and occupancy are controlled by weekly and hourly schedules.. The modeling of the HVAC system is deliberately kept simple as it is not the primary subject of the program. HVAC loads are modelled either as ideal – to meet the heating or cooling demand exactly – or with simple P type controllers. The convective and radiative fractions of both HVAC and other internal loads the loads are set in the input. Plant systems are not modelled, and only the site energy usage in the room is kept track of.

The zone air heat balance equation takes the following form:

$$V_{zone}C_{p,zone}\frac{dT_{zone}}{dt}=\sum\dot{Q}_{HVAC}+\sum\dot{Q}_{\text{int}}+\sum h_{c,i}A_i\left(T_{s,i}-T_{zone}\right)+\sum L_{3D,w,frame,inst}\left(T_{e,air}-T_{zone}\right)+\dots$$
$$\dots+\sum L_{3D,tb}\left(T_{e,air}-T_{zone}\right)+\dot{m}_{\text{inf}}c_{p,air}\left(T_{e,air}-T_{zone}\right)+\dot{m}_{vent}c_{p,air}\left(T_{e,air}-T_{zone}\right) \quad (88)$$

V_{zone} [m^3] is the internal air volume, $C_{p,zone}$ [J/m^{3}K] the heat capacitance of the zone air, T_{zone} [K] the zone air temperature, $\dot{Q}_{HVAC}$ [W] the convective load of the HVAC system, $\dot{Q}_{int}$ [W] the convective part of the internal thermal loads, $h_{c,i}$ [W/m^{2}K] the convective heat transfer coefficient for surface i (opaqe and glazing surfaces), A_i [m^2] the internal surface area of surface i (opaqe and glazing surfaces), $T_{si,i}$ [K] the internal surface temperature of surface i (opaqe and glazing surfaces), $L_{3D,w,frame,ins}$ [W/K] the thermal transmission coefficient of the window's opaque components as defined earlier, $L_{3D,tb}$ [W/K] the thermal transmission coefficient of the thermal bridges, $\dot{m}_{inf}$ [kg/s] the infiltration mass flow, $\dot{m}_{vent}$ [kg/s] the ventilation mass flow, $c_{p,air}$ [J/kgK] the specific heat capacity of the air entering the zone, $T_{e,air}$ [K] the external air temperature. Like all sub-models the zone air heat balance is solved with a 15 minute time step with the analytical solution scheme described in [67].

5.1.8 Occupant thermal comfort model

The evaluation of the occupant thermal comfort is done by calculating the PMV value for every time-step according to the ISO 7730 standard [92]. The room air and internal surface temperatures are available from the thermal calculation and the zone air partial vapor pressure from the moisture balance equations. The air flow velocity also needed for the PMV calculation is assumed to be constant v=0.05 [m/s] (in lieu of better data), and the mean radiative temperature is evaluated at the middle of the room.

5.1.9 Validation

For validation and as an aide during program development we performed a cross-comparison of EPICAC BE with the IEA BESTEST [101] suite of building energy simulation test cases, which is a widely recognized method to assess the accuracy of building energy simulation programs. In addition to the results originally reported in BESTEST in 1995 more recent validation results were also added to the reference data. We chose the validation data from the programs EnergyPlus 1.1 [82], Design Builder/EnergyPlus 8.1 [5] and IES ApacheSim 5.2 [77] to provide additional comparison with more recent models. We performed all tests in BESTEST, except for the detailed ground contact and sunspace scenarios, as these were not relevant for our program. The comparison of the annual heating and cooling load data for the high-mass test cases is presented in Fig. 108 and Fig. 109, with the selected contemporary programs highlighted in color and EPICAC BE in red. Our results were all within the range of the BESTEST results, and the best agreement is found with the group of recent simulation programs. A complete documentation of the validation is found in Appendix E.

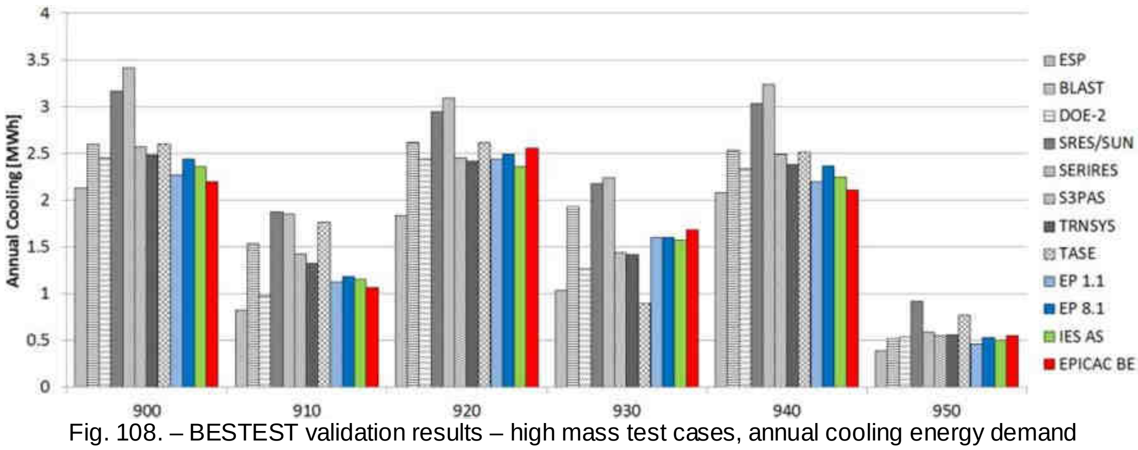

Fig. 108. – BESTEST validation results – high mass test cases, annual cooling energy demand

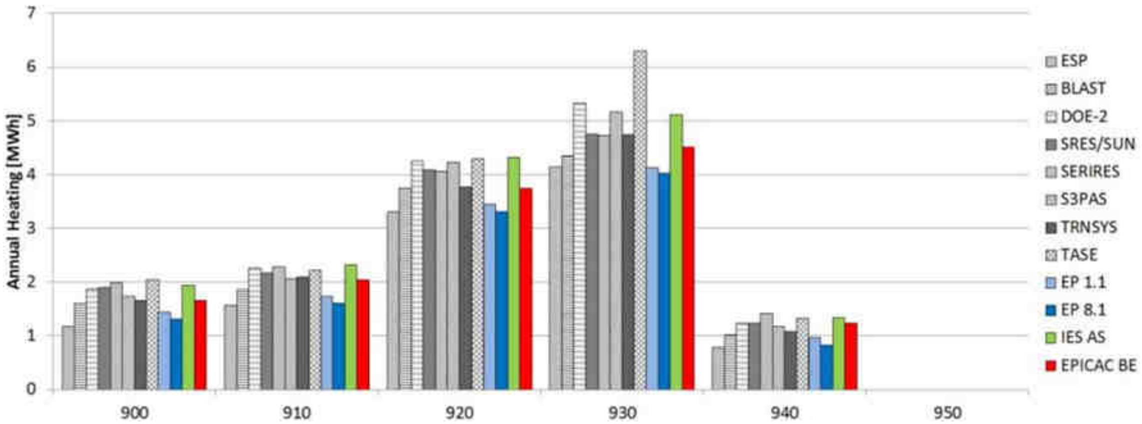

Fig. 109. – BESTEST validation results – high mass test cases, annual heating energy demand

5.2 Case study – the MTA building's windows

In early 2014 the team composed off the 3h architecture studio[21], the Budapest University of Technology and Economics' Department of Building construction[22] and the Artarium studio[23] wood restoration company won a commission to conduct a decision support study analyzing the possibilities of, and then prepare the plans for, the structural and thermal refurbishment of the windows of a very prestigious building: the Palace of the Hungarian Academy of Sciences (Magyar Tudományos Akadémia, henceforth: MTA). The structure, located in the heart of the Hungarian capital Budapest, was designed in the Neo-Renaissance style of contemporary German palaces by the architect Friedrich August Stüler, and built between 1862 and 1865 [106]. The refurbishment of such a national monument is a delicate task, not only because its architectural, historical and societal significance, but also due to its use of noble materials, exquisite detailing and special constructional solutions. The appearance of the windows, and if at all possible the actual window stock had to be preserved. The developed methodology, the use of the simulation program EPICAC BE and the findings that go beyond the scope of the project will be introduced in this section.

Fig. 110. – an old photo of the MTA building at the Danube's embankment

Fig. 111. – An example of the many windows on the MTA building

21 The 3h architecture studio's team: Katalin Csillag, Anna Sára Kiss

22 The Department of Building Costructions' team: Gábor Becker, Gergely Dobszay, Dániel Bakonyi

23 The Artarium studio's teme: Zsolt Kóbor, Péter Zágoni

5.2.1 A brief description of the project

In the MTA building there are more than 200 windows of 23 different size, shape and opening type in rooms of even more varying size and usage. No single solution for their refurbishment can give nearly optimal results for all of them, therefore relying on only simplistic guidelines for the design was clearly inadequate. Instead, a stepwise approach was adapted with the following stages: 1) a detailed architectural survey of all fenestration, 2) cataloging of the structural damages and deficiencies aided with all the diagnostic tools that were available to the team (e.g. Blower Door measurements and IR thermography), 3) a survey of occupants' complaints and wishes regarding thermal comfort 4) the formulation of a well founded refurbishment concept to address the typical structural problems and to demonstrate an optimized thermal solution for a typical single window based on the comparative numerical simulation of a multitude of refurbishment methods, 5) the well documented restoration of this prototype window under constant supervision, and 6) the detailed evaluation of the finished prototype by a long-time monitoring.

During steps 1-4 the 3H architecture studio was the prime contractor, served as the coordinator and was responsible for conducting the architectural surveys, the Department of Building constructions was responsible for giving the professional basis for the job: formalizing the methodology, creating and assessing different design alternatives and performing the necessary calculations presented here. The Artárium studio provided advice and expert's reports for the issues regarding wood restauration. Step 5 was carried out by the Artárium studio with the supervision of the design team (Gergely Dobszay, Dániel Bakonyi), and step 6 is still underway at this moment. The final decision for the rest of the windows will be based on the experiences with the prototype and the use of the design and calculation method developed for its creation. For the prototype refurbishment we chose a typical office room with a single window located at the intermediate floor of the building and oriented towards the west and the embankment of the Danube river (henceforth: the reference room and the prototype window).

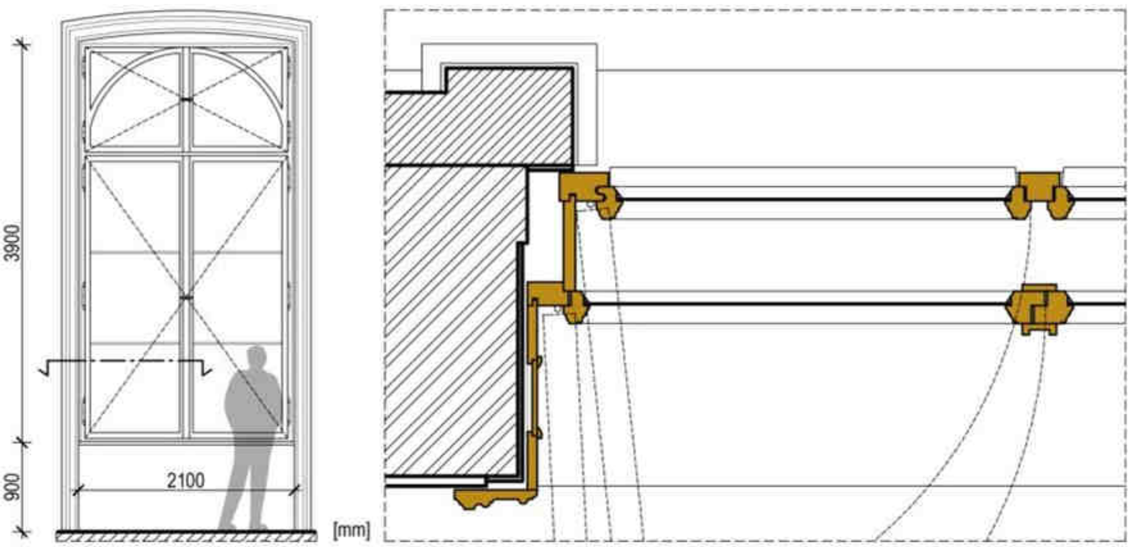

Fig. 112. – the prototype window of the MTA building, internal view with dimensions (left) and horizontal section (right)

The selected prototype window, like the majority of the fenestration in the building, is a double-skin box type window. All of the sashes are inward-opening (see Fig. 112) and an around 20 cm deep casing connects the exterior and interior frames forming sizeable cavity. The peculiarity of the building's windows' is their enormous size, the resulting extreme slenderness of the frame and sash profiles and the use of thin cast iron glazing dividers in an otherwise completely wooden construction. Though these all make the huge windows very elegant, they also limit the possibilities for structural changes to increase their functionality and decrease their heat losses. The 'toolbox' to improve the thermal performance of old but valuable windows (windows that are to be preserved) usually contains three main items:

- the increase of airtightness through a general renovation and the installation of new rubber gaskets to reduce in- and exfiltration, with possible additional modification to the operating hardware to improve the seal

- the modification of the glazing layers to improve its solar-optical and thermal properties, most often with the use of applied films on existing glazing, single-pane hard coated low-e glass, or multi-pane insulating glass (IG) units
- the use of exterior, interpane or interior shading devices or other attachments with the same purpose

The use of IG units is by far the most favored option of the majority of contemporary practitioners, but usually is limited by the fact that even double pane glass can be too heavy and too thick to fit into the small sized sashes and glazing rebates of traditional windows. This problem is often solved by replacing one layer of sashes with larger ones having the necessary size and strength, or the use of extra thin and light insulating glass units made specially to fit into the existing construction (with the compromise of sub-optimal cavity size and reduced mechanical strength due to the small glazing thickness). Due to the building's status as a first class national monument and its architectural quality any noticeable increase of the sash profiles or the complete elimination of the cast iron dividers, in the interest of the use of normal thick and heavy IG units, was ruled out completely. The use of thin double glazing would require the transformation of the iron dividers to a 'fake' grill glued on the internal surface of the glazing. This modification would be irreversible and of a lower architectural quality, but necessary to minimize the thermal bridges that would severely reduce the usefulness of any double glazing. On the other hand, using only single glazing, whilst allows to keep the iron dividers, limits the choice in available coatings. Hard-coatings suitable for single glazing applications are rarely used today, thus their performance is not as well optimized as that of soft-coated glazing products that are only usable in the inside of IG units.

Following the process described earlier the following main scenarios were devised for the refurbishment of the prototype window (listing only the points relevant to the windows' thermal performance) (see also Fig. 113):

- Scenario A - named 'thermally optimal':
  - I. general refurbishment of the frame and sashes, installation of rubber gaskets in the internal opening to increase airtightness, sealing and thermal insulation of the gap between the frame and the masonry
  - II. the installation of special thin double-pane glazing in the external sashes with a good low-e soft coating in the second position and Argon fill-gas, the internal glazing is changed for a hard coated low-e glass with the coating facing outwards to reduce radiative heat transfer in the big cavity between the two sashes
  - III. the transformation of the cast iron glazing dividers in the external sashes into a glued-on grill to allow the IG units to be continuous (only with internal dividers) and reduce thermal bridging
  - IV. the installation of a simple motorized roller shade between the two layers of the window (an external shading was out of the question for this building)

- Scenario B - named 'least intrusive':
  - I. same as Scenario A
  - II. installation of hard-coated single-pane low-e glass into both sashes with the coating facing the cavity and with minimal modification to the window stock
  - III. the installation of a simple motorized roller shade between the two layers of the window

- Scenario C – 'balance of thermal and preservational aspects':
  - I. same as Scenario A
  - II. same as Scenario B
  - III. the installation of a motorized single-cell cellular shade (with a significant thermal resistance in its open state) between the sashes instead of the simpler roller shade
  - IV. the addition of a controller for the shading with the necessary sensors and an optimized algorithm to maximize heat gains and minimize losses during the heating season, and vice-versa in the cooling season

- In addition Scenario O will refer to the original state of the window as a point of comparison for the three refurbishment scenarios.

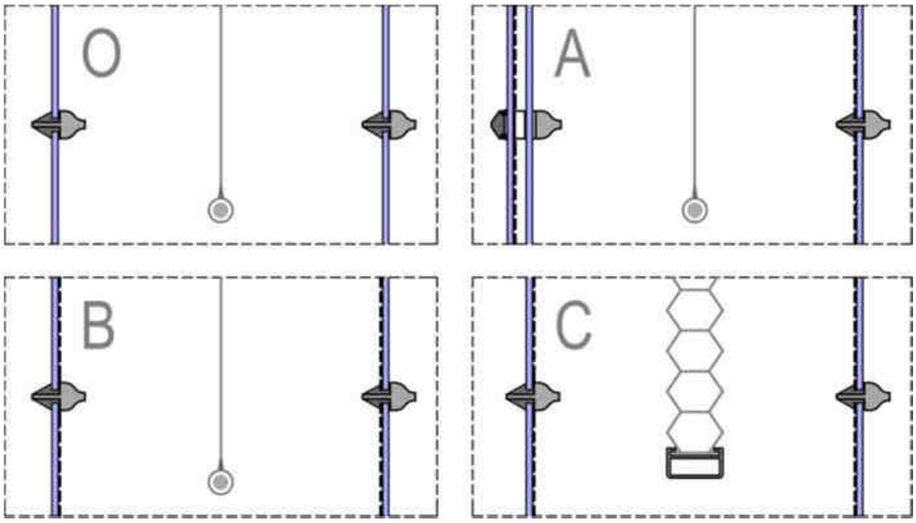

Fig. 113. – schematic view of the different glazing system options (scenarios) drawn though the cast iron glazing dividers

Off course this list of options is far from exhaustive (a much more detailed list of glazing system options for such windows is introduced by Misiopecki and Gustavsen [127] and Bakonyi and Becker [13]), but the scope of this study does not require the detailed analysis of a much bigger set. The point to be demonstrated instead is how to make an informed decision between any possible set of scenarios? Additionally during the design we wanted to investigate whether a combination of a less intrusive refurbishment with only single-pane glazing and an addition of a controlled interpane shading device (scenario C) might yield comparable improvement as a more evident modification that includes double-pane glass (scenario A).

5.2.2 Setting up the simulations

Simulations run with EPICAC BE were the tool used to compare the heat balance and thermal comfort impact of the different refurbishment scenarios during the project. The inputs of these simulation will now be briefly described.

Table 38 shows the center-of-glass performance indices for the different scenarios (see Fig. 113) with and without interpane shading devices and calculated with boundary conditions set by ISO 15099 [97] ($T_{e,air}$=0[°C], $h_{c,e}$=20[W/m^{2}K], $T_{i,air}$=20[°C], $h_{c,i}$=3.6[W/m^{2}K] for the winter and $T_{e,air}$=30[°C], $h_{c,e}$=8[W/m^{2}K], $T_{i,air}$=25[°C], $h_{c,i}$=2.5[W/m$_2$K] and I_s=500[W/m^2] for the summer case, with ambient mean radiative temperatures same as the air temperatures). The shade materials for both the simple roller shades and the cellular shade was chosen to provide a comparatively good performance in the cooling season but still provide a visual transmission of around 10 %. Scenario O is also presented with and without an interpane roller shade. The U_w and $U_{w,inst}$ values calculated for the prototype window based on these glazing system options are summarized in Table 39.

Scenario	Glazing System	Shade up				Shade down			
		U_g [W/m^{2}K]	g [-]	$\tau_{sol,hemi}$ [-]	$\tau_{vis,dir}$ [-]	U_g [W/m^{2}K]	g [-]	$T_{sol,hemi}$ [-]	$T_{vis,dir}$ [-]
O	3 mm float glass* 100 mm air (roller shade)** 100 mm air 3 mm float glass*	2.839	0.799	0.646	0.824	2.301	0.337	0.185	0.185
A	3 mm low-e (ε_b=0.047)*** 6 mm Argon 3 mm float glass* 100 mm air (roller shade)** 100 mm air 3mm low-e (ε_f=0.17)****	1.115	0.494	0.339	0.668	1.064	0.273	0.099	0.156
B	3mm low-e (ε_b=0.17)**** 100 mm air	1.754	0.64	0.456	0.682	1.459	0.297	0.126	0.156

	(roller shade)** 100 mm air 3mm low-e (ε_f=0.17)****								
C	3mm low-e (ε_b=0.17) **** 100 mm air (cellular shade)***** 100 mm air 3mm low-e (ε_f=0.17)****	1.754	0.64	0.456	0.682	0.888	0.234	0.058	0.087

Table 38. – glazing system and center-of-glazing performance indices for all investigated scenarios with and without the shading devices: Ug [W/m2K] the thermal transmittance in winter, g [-] the total solar energy transmittance, Tsol,hemi [-] the hemispherical solar transmittance, Tvis,dir [-] the direct visual transmittance. *IGDB:11100, **white woven shade (τsol=0.25, τvis=0.22), ***IGDB:11333, ****IGDB:4345, *****same textile as for the simple roller shade, single cell, hcell=30 [mm] (τsol=0.11, τvis=0.11)

Scenario	Shade up		Shade down	
	U_w [W/m^{2}K]	$U_{w,inst}$ [W/m^{2}K]	U_w [W/m^{2}K]	$U_{w,inst}$ [W/m^{2}K]
O	2.317	2.452	1.963	2.103
A	1.031	1.204	0.899	1.07
B	1.544	1.699	1.398	1.554
C	1.544	1.699	0.709	0.82

Table 39. – window U_w and $U_{w,installed}$ values of the original window and the refurbishment options, with and without the shading devices

Regarding the control of the shades the maximization of solar gains and the minimization of heat losses in the heating season, and the reverse in the cooling season, was the main objective for our study and our design. The fixed duration of the heating and cooling seasons, the internal and external dry bulb temperatures, the Sun's position (Zenith angle) and the incident global radiation on the window were selected as possible control parameters. Based on the results of Firlag et al. [26] two control algorithms were devise to be investigated: a simple and a more comprehensive option. The first, or simple algorithm relies only on whether the building is in heating or cooling mode, whether it is in the fixed heating or cooling season, and the Sun's position to determine whether it is day or night. Such a basic control has the advantage that it would basically need no sensors to implement. The second, or advanced algorithm tries to decide which position of the shading is actually favorable depending additionally on the temperature difference and the actual incident radiation on the opening. During the heating season the shade is only moved up when the incident radiation exceeds a preset limit where the solar gain increase would outweigh the heat loss increase (this limit was set as 50 [W/m^2]). A further check for the external temperature is added to avoid overheating in the transitional periods when the heating is usually no longer working but the cooling in not jet switched on. During the cooling season the shade is down when the incident radiation is above the preset limit, or the internal temperature is below the external and the increased insulation is still favorable. The two algorithms are summed up in Fig. 114 and Fig. 115 respectively. The implementation of the controls in the program is very simple, as all the simulation data is available at run time to the shading control logic and no external coupling with other programs or precalculation is necessary.

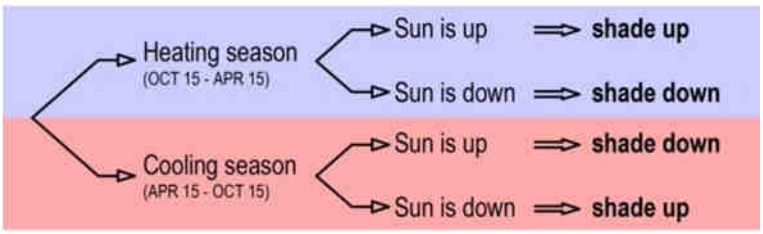

Fig. 114. – our simple shading control algorithm (single column)

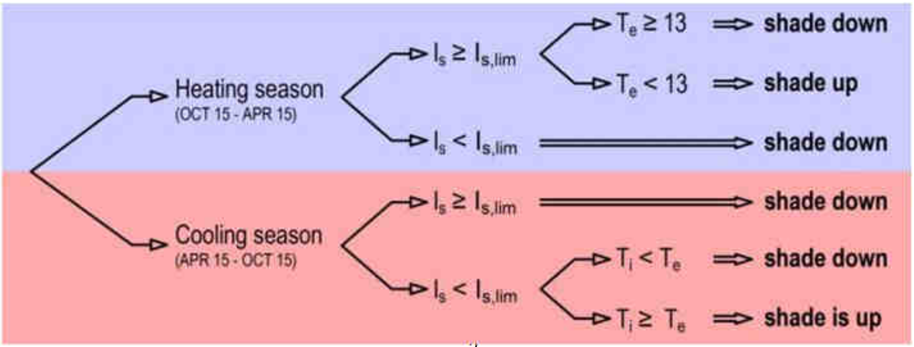

Fig. 115. – our detailed shading control algorithm, I_S [W/m^2] the global solar radiation incident on the window, $I_{s,lim}$ [W/m^2] the limit for the solar radiation, Ti and Te [°C] the internal and external air temperatures (single column)

The prototype window's room in the MTA building is only exposed on a single façade (west), with only small, relatively airtight openings leading to the rest of the building, and therefore the ventilation had to be calculated as single-sided. The pressure coefficients for the infiltration calculation were determined with the help of the CpCalc program [78] and the airtightness of the window in its original state was measured in situ with the help of a Blower Door apparatus. The Blower Door was installed in the only door leading into the room with the prototype window as the only other orifice of significant size while all other cracks, sockets etc. were thoroughly sealed for the duration of the measurement. The prototype window's original air permeability was measured as 32 [m^3/hPa$^{0.695}$] with a flow exponent of 0.695 [-]. This agrees well with data taken from the literature [85]. A realistic target for the refurbishment, also based on the literature, was taken as an airtightness class of 1 to 2 according to the standard ISO 12207 [62]. This roughly corresponds to a flow coefficient between 3.15 and 15.4 [m^3/hPa$^{0.67}$]. A more precise prediction was impossible to make, but the improved airtightness of the refurbished window was since confirmed by repeated Blower Door measurement. The flow coefficient of the window after refurbishment was taken as a = 4.68 [m3/hPa0.667] in the simulations. When measurements are not possible any design decision has to take into account the uncertainties in both the input parameters of the windows and the inaccuracies of the ventilation and infiltration models.

A brief summary of all modeling assumptions and data regarding the simulated reference room is found in Table 40 and the floorplan and cross section of the test room in Fig. 116.

parameter	**value / description**
building type	public building (offices, conference rooms)
location	Budapest, N47.26°, E19.11°, the building is located at the east side (Pest) embankment of the river Danube in a dense urban area
orientation	completely exposed towards the river (west), other orientations calculated for comparison
climate	humid continental
room type	office room for a single person
floor area	23.36 [m^2]
headroom	5.71 [m]
internal heated volume	133.386 [m^3]
room exposure	a single 4.02 [m] long wall is exposed towards the outside with a single window oriented towards the west
external wall	20 cm external limestone cladding, 65 cm solid brick masonry, internal plaster U value: 0.78 [W/m^{2}K]
internal partition walls	29 cm solid brick masonry, plastered
internal floor and ceiling	2 cm parquet, 6 cm concrete screed, ca. 27 cm filling, 14 cm solid brick Prussian vault, 2-4 cm plaster, U value: 1.75 [W/m^{2}K]
thermal bridges	all planar surfaces are calculated with their internal dimensions (except for the window insolation calculation), the total thermal transmittance of all thermal bridges (except the window-wall interface): L_{2D} = 2.37 [W/K]
window	box type window, $A_{w,int}$ = 2.1 x 3.9 [m] internal dimensions, $A_{w,ext}$ = 1.92 x 3.74 [m] external exposed dimensions, 0.78 [-] glazing area fraction on the internal side, l_{inst} =12 [m] installation perimeter length, l_{eg} = 27 [m] edge of glass length, glazing system acc. to Table (1), window U values acc. to Table (2)
external shading	the only external shading is provided by the window reveal (27 [cm] deep due to the pilasters and architrave vault around the opening) and the small hilltop (Buda Castle Hill) located around 0.8 [km] from the building

infiltration	window flow coefficient a = 32 [$m^3/hPa^{0.695}$] for scenario O, and a target flow coefficient of a = 4.68 [$m^3/hPa^{0.667}$] for scenarios A, B and C
ventilation	no mechanical ventilation, the window is opened twice daily for 15 [min] in the morning (8 a.m.) and in the early afternoon (2 p.m.), opening area: 2 [m^2], opening height 2.17 [m]
HVAC systems	a single two pipe fan coil unit located under the window, set either for heating or cooling, with a 100% convective load, modelled as an ideal system. Heating period: October 15 – April 15, cooling period: April 15 – October 15
internal loads	occupancy load = 100 [W] (a single person) typical office usage with a fractional hourly schedule (weekdays 06-07 10%, 07-08 20%, 08-17 90%, 17-18: 70%, 18-20:40%, 20-22: 20%, 22-24: 10%, Saturdays 06-08: 10%, 8-14: 50%, 14-17: 10%, Sundays 0%); plug loads = 5.8 [W/m^2] and lighting load = 10 [W/m^2] with a fractional hourly schedule (weekdays 00-04: 5%, 04-07: 10%, 07-08: 30%, 08-15: 90%, 15-16: 50%, 17-20: 30%, 20-22: 20%, 22-23: 10%, 23-24: 5%; weekends: 00-06: 5%, 06-08: 10%, 08-12: 30%, 12-17: 15%, 17-24: 5%) moisture load – potted plants = 10 [g/h] constant moisture load – occupancy = 50 [g/h] with a fractional hourly schedule (same as occ.)
heating setpoint – day	22 [°C] (between 6 am and 9 pm)
heating setpoint – night	19 [°C] (between 9 pm and 6 am)
heating setpoint – weekends	20 [°C]
cooling setpoint – day	25 [°C] (between 6 am and 9 pm)
cooling setpoint – night, weekends	cooling off

Table 40. – brief summary of modelling assumptions and description of the modelled room

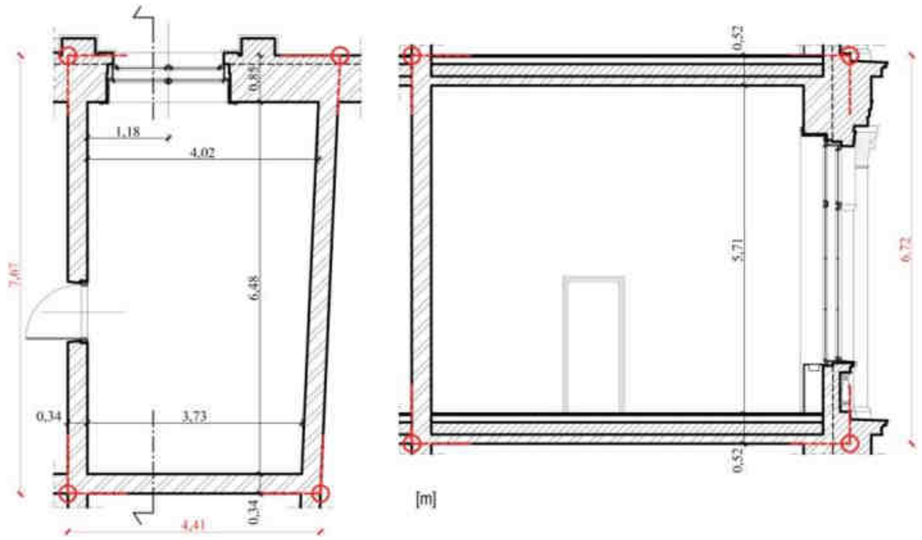

Fig. 116. – the detailed internal and external dimensions of the prototype window's room (1.5 columns)

5.2.3 Simulation Results

Simulation results are presented for the original state of the prototype window and the three investigated refurbishment scenarios. Each refurbishment scenario and the original state is calculated without shading and with either the simple or the optimized shading controls introduced earlier. The actual prototype window and reference room (the office room where the prototype window is located in) is oriented towards the west, but for the sake of this for this work northern and southern orientations are also examined (while keeping all other parameters the same). The infiltration, ventilation, the total heating and cooling energy demand and an analysis of the simulated thermal comfort in both the heating and cooling seasons are the main parameters used for the evaluation of the results.

Examples of the thermal zone's (reference room) calculated monthly heat balance are shown in Fig. 117 and Fig. 118 with all the heat flux component to and from the zone air node. Looking at the monthly heat balance chart of Scenario O in Fig. 117 and Table 41 showing the percentage of the individual heat loss components, it is immediately obvious that with the windows in their original state the heat losses associated with infiltration (38%) and ventilation (18.6%) during the heating season clearly outweighs all other components. This large heat loss corresponds to a calculated average air change rate of n = 0.55 [1/h], which considering the enormous height of the investigated room (5.71 [m]) is clearly excessive compared to the actual ventilation demand for a single occupant. If the ventilation were not single-sided the air exchange would be even larger. Calculating with a desired fresh air supply of 40 [m^3/h/person] the target air exchange rate for the room could be as low as n = 0.1 [1/h] . High levels of airtightness are very hard to achieve with existing windows, especially with such big ones as in the case of the MTA building, but a reasonable increase in seal should clearly be a starting point for all refurbishments.

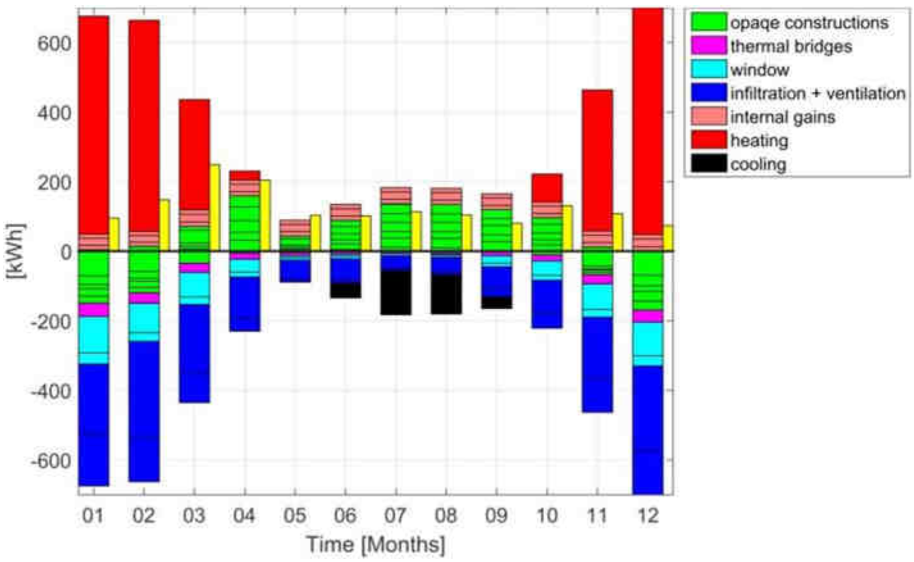

Fig. 117. – Scenario O, no shading – monthly zonal heat balance chart with the different heat flux components to and from the zone air mass (the total direct solar transmittance of the window - yellow bar –effects the air temperature indirectly and is only added for reference)

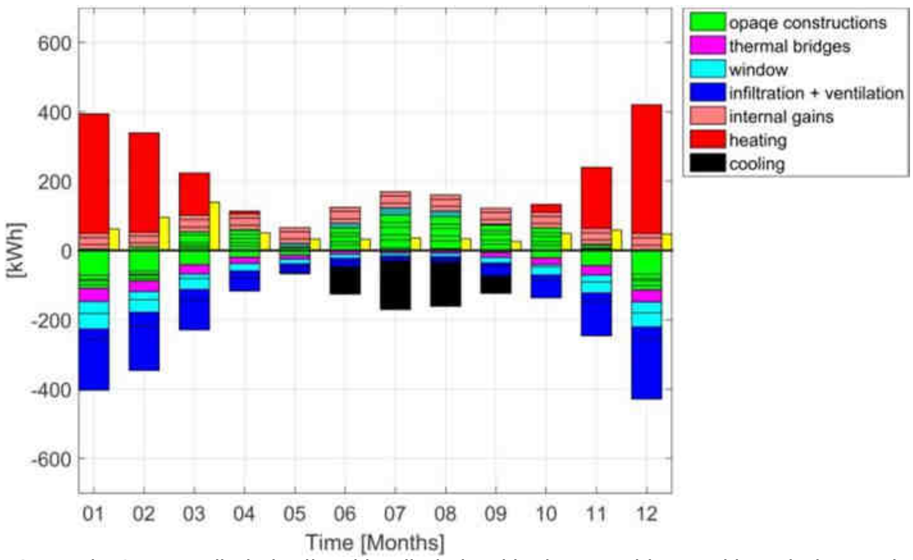

Fig. 118. – Scenario C, controlled shading (detailed algorithm) – monthly zonal heat balance chart with the different heat flux components to and from the zone air mass (the total direct solar transmittance of the window - yellow bar –effects the air temperature indirectly and is only added for reference)

Scenario	Shade	n_{inf} [1/h]	n_{vent} [1/h]	Fraction of total net. heat loss				
				Opaque constr. [%]	Window [%]	T.Bridge [%]	Inf. [%]	Vent. [%]
O	none	0.361	0.184	15.3	22.6	5.5	38	18.6
	simple ctrl.	0.361	0.184	14.2	20.5	5.8	40.1	19.4
	adv. ctrl.	0.361	0.184	15.7	18.6	5.7	39.7	20.3
A	none	0.049	0.178	22.8	22.7	9.8	9.7	35
	simple ctrl.	0.049	0.178	22.5	21.9	10.4	10.3	34.9

	adv. ctrl.	0.049	0.178	23.4	20.7	10.5	10.3	35.1
B	none	0.049	0.179	21.9	26	9.6	9.5	33
	simple ctrl.	0.049	0.178	20.6	24	10.6	10.5	35.3
	adv. ctrl.	0.049	0.178	21.4	22.2	10.7	10.5	35.2
C	none	0.049	0.179	21.9	26	9.6	9.5	33
	simple ctrl.	0.049	0.179	19.9	23	10.8	11	35.3
	adv. ctrl.	0.049	0.178	20.6	20.4	11	11	37

Table 41. – calculated infiltration and ventilation air exchange rates, and the fraction of the individual component's role in the total net. heat loss during the heating season

After refurbishment the air permeability of the window is severely reduced resulting in a calculated average infiltration air exchange rate in the heating season of less than 0.05 [1/h]. The ventilation requirements are no longer met by just uncontrolled infiltration. As the building has no mechanical ventilation the manual airing of the windows is currently the only option. We assumed a twice daily intensive 15 [min] long manual ventilation of the room at 8 in the morning and 2 in the afternoon. The resulting overall ventilation rate is calculated as around n = 0.23 [1/h] in the heating and n = 0.15 [1/h] in the cooling season with very little difference between the different scenarios as seen in Table (4) (the infiltration and ventilation models do not depend on the glazing or the shade). Considering the large volume of the room in winter this is still excessive, but it is doubtful that manual operation could reach much better values and overly optimistic modelling assumptions could skew the results. One must always check whether any increase in airtightness could threaten moisture damage in the interior. Due to the large internal volume and low level of occupancy this was not a major issue for the reference office in the MTA building.

The proportion of the infiltration and ventilation heat loss to the total heating energy demand after refurbishment is only marginally smaller than before (see Table 41): around 40-50 % compared to 55-60%. This indicates that the air exchange related heat loss components are reduced by roughly the same proportion as all of the other components. The increased airtightness is disadvantageous during the cooling season, as there is no possibility for night time ventilation, the users can only operate the window during daytime when intensive ventilation is less desirable. This will increase the cooling energy demand when all other parameters are the same. A hybrid-ventilation with an exhaust fan would clearly be more advantageous for both winter and summer use, preferably incorporated into the same control system as the shading. We did propose such a system, but for the time only the window could be modified, so all calculations are presented with only the natural ventilation introduced here.

The total heating and cooling energy demands of the reference room for all the scenarios (with the actual western orientation) are presented in Table 42 and Fig. 119. Without shading scenario A is the superior with the smallest heating (54%) and cooling (92%) energy demand compared to the baseline case of scenario O. Without shading scenarios B and C are the same, with slightly smaller reduction in heating but an increase in cooling energy demand. It is interesting to note, that despite its U value being considerably lower the heating energy demand of scenario A is only slightly smaller than B and C, because the solar heat gains through the glazing system are also reduced (50% larger total glazing thickness and a different soft coating, see Table 38). The cooling energy demand of the refurbishment cases shows a larger difference. Here the lower SHGC value of scenario A is clearly more favorable and even manages to reduce the cooling load compared to the baseline case despite the lowered air change rate mentioned above. The windows of scenario B and C also have an SHGC value lower than scenario O's, but not sufficiently so to compensate for the reduced infiltration, therefore the cooling energy demand is increased. The need for some form of controlled shade is clearly visible just from this data point alone.

The introduction of a controlled shade changes the results: both heating and cooling energy needs are further reduced and even the relative order of the scenarios is changed. Scenarios A and B show very similar heating and cooling energy needs (within the margin of error) and scenario C is now the best option for both seasons. As demonstrated by the calculations the glazing of scenarios B and C can better utilize useful solar irradiation during the heating season when the shade is moved up by the control, so the additional decrease in transmission heat losses when the shade is lowered during the night achieves a better overall heat balance than scenario A with its lower U and lower SHGC values. The controlled shade reduces the heating energy demand of all scenarios, but with a greater percentage for the ones with a higher baseline glazing U value: 7-8% for scenario A, 10-12% for scenario B and 15-18% for scenario C.

The reduction of cooling energy demand with the shading system is, as expected, more significant than for heating: 46% for A, 55% for B and 66% for C. All the results are smaller than for the unshaded baseline scenario O. However the biggest reduction of cooling energy is achieved by adding controlled shading to the original window (scenario O) (68%), when this shade is not combined with any other measures. This is to be expected since as previously mentioned an intensive natural ventilation can be favorable in the cooling season. The savings in total energy need by only installing controlled shades in the original window is almost as big as with the increase of airtightness and the installation of hard coated low-e glass (scenario B and C) without shading! The increase in airtightness is necessary to reduce heating energy demand, but the results clearly show that the reduction of summer heat gains must also follow.

The energy saving potential of a controlled shading is clearly demonstrated for all scenarios, but the difference between the two investigated shade control algorithms were found to be small with the advanced control being a little better than the simple one. This supports the findings of Firlag et al. [72]. The use of a controlled shading also reduces the relative difference between the three refurbishment scenarios, as the shaded SHGC value was set to be similar for all options and a larger difference in winter heat loss is not to be expected when the ventilation energy demand is still more dominant than the transmission losses.

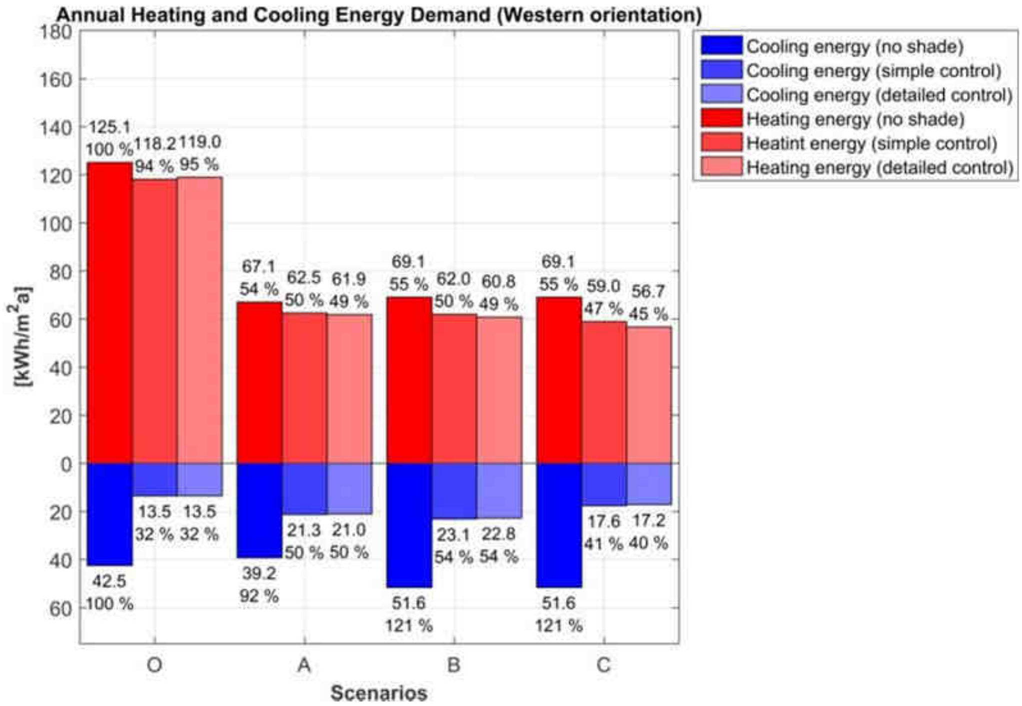

Fig. 119. – Heating and cooling energy demand for the different scenarios, without shade and with two different shading control strategies, original western orientation

value	shading	O	A	B	C
heating energy demand [kWh/m^{2}a]	no shading	125.1	67.1	69.1	69.1
	simple control	118.2	62.5	62.0	59.0
	detailed control	1198.0	61.9	60.8	60.0
cooling energy demand [kWh/m^{2}a]	no shading	42.5	39.2	51.6	51.6
	simple control	13.5	21.3	23.1	17.6
	detailed control	13.5	21.0	22.8	17.2

Table 42. – annual heating and cooling energy demand of all scenarios and shading controls – western orientation

The same results but for a southern and northern orientation (with all other parameters being the same) are presented in Table 43, Fig. 120 and Table 44 and Fig. 121 respectively. The southern orientation is the most favorable for large fenestration in the Central-European climate: in the winter the heat gains are the largest towards the south but the Sun's path is sufficiently high in the summer to increase the angle of incidence and the shading for windows set deeply in the façade. Accordingly, both heating and cooling energy demands are clearly lower than for the western orientation for all scenarios, with and without shading. The relative proportion of the individual results is similar, but even scenario B is noticeably better in heating energy demand than A when a controlled shade is present. Once again, the strategy to have a window with a larger unshaded solar transmission is beneficial if there is enough useful solar gain in the winter, it is possible to compensate for a higher 'unshaded' U value with the lowering of the shade during the night, and the protection against summer overheating is relying mostly on the controllable shade. The heating energy demand is lowered by 9-10%, 16% and 23% by the shading for scenarios A, B and C respectively, and the cooling energy demands by 45%, 55% and 64% compared to their unshaded values.

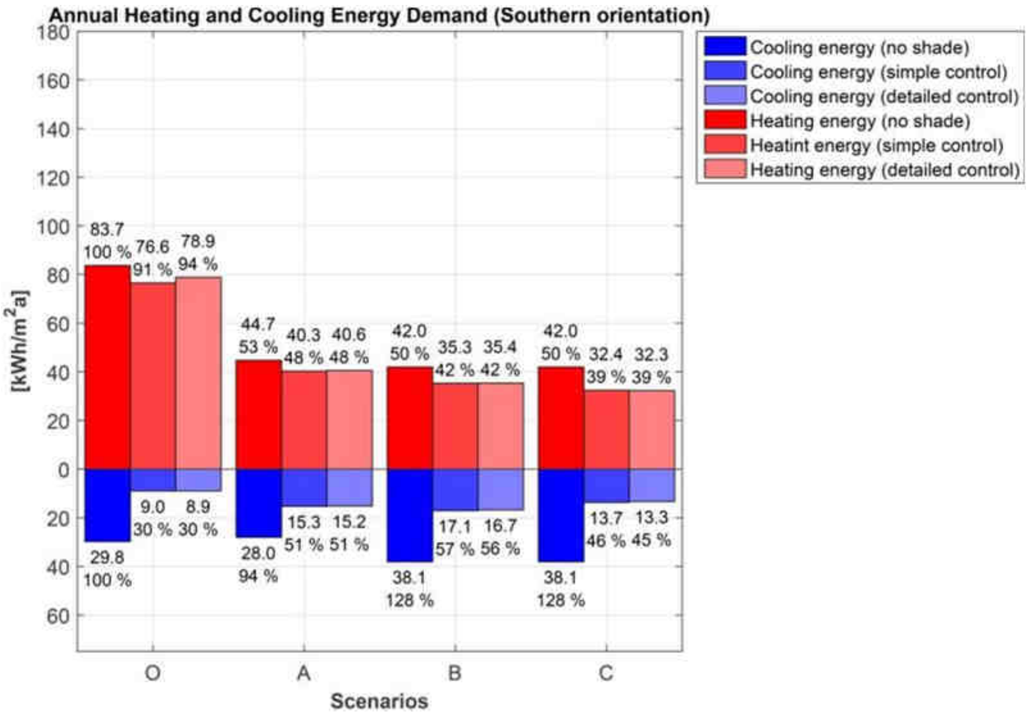

Fig. 120. – Heating and cooling energy demand for the different scenarios, without shade and with two different shading control strategies, southern orientation

value	shading	O	A	B	C
heating energy demand [kWh/m^{2}a]	no shading	83.7	44.7	42.0	42.0
	simple control	76.6	40.3	35.3	32.4
	detailed control	78.9	40.6	35.4	32.3
cooling energy demand [kWh/m^{2}a]	no shading	29.8	28.0	38.1	38.1
	simple control	9.0	15.3	17.1	13.7
	detailed control	8.9	15.2	16.7	13.3

Table 43. – annual heating and cooling energy demand of all scenarios and shading controls – southern orientation

The results for the northern orientation are somewhat different. Both winter and summer heat gains are significantly smaller, and consequently the summer cooling energy demand is small to begin with. Therefore the reduction in heating and cooling energy demand with the use of a controlled shade is, though still significant, somewhat smaller than on the western façade. On the other hand the differences between the simple and advanced shade control algorithms are more significant in heating energy reduction than with the other orientations: the advanced control does a slightly better job. This shows, that on the northern façade it is not always worth to raise the shade during the day in the heating season, because the slight solar gains can't always compensate for the increased heat loss.

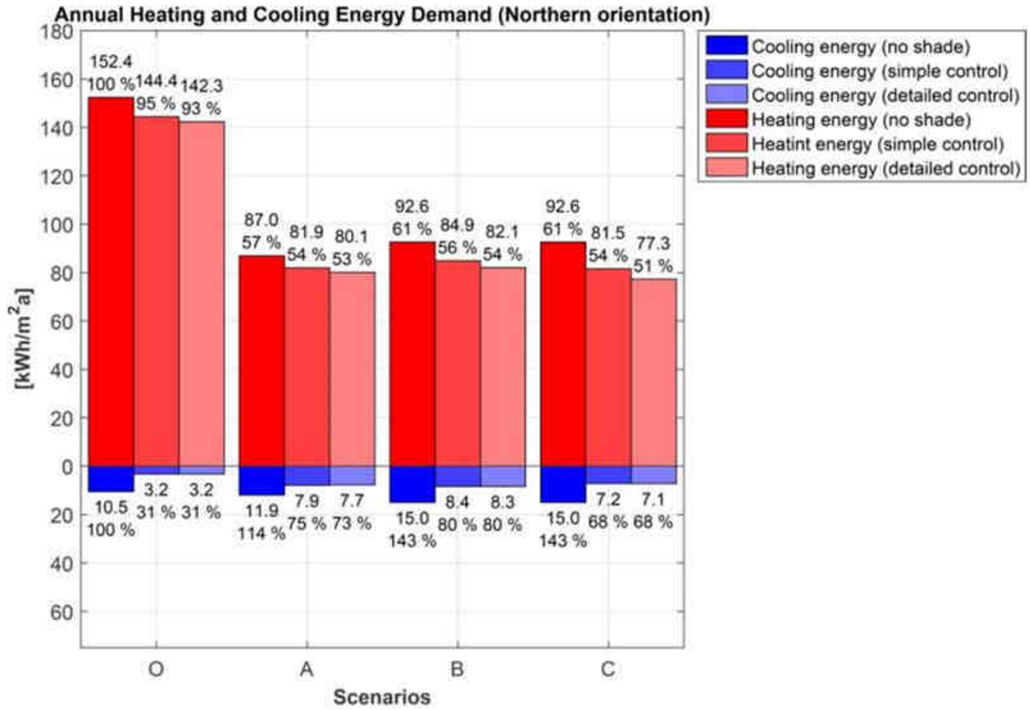

Fig. 121. – Heating and cooling energy demand for the different scenarios, without shade and with two different shading control strategies, northern orientation (1.5 columns)

value	shading	O	A	B	C
heating energy demand [kWh/m^{2}a]	no shading	152.4	87.0	92.6	92.6
	simple control	144.4	82.0	84.9	81.5
	detailed control	142.3	80.1	82.1	77.3
cooling energy demand [kWh/m^{2}a]	no shading	10.5	11.9	15.0	15.0
	simple control	3.2	7.9	8.4	7.2
	detailed control	3.2	7.7	8.3	7.1

Table 44. – annual heating and cooling energy demand of all scenarios and shading controls – northern orientation

The main goal of the refurbishment was the reduction of cooling and heating energy demands, but nevertheless a check of the occupant thermal comfort was added to verify the validity of the refurbishment concepts. The evaluation is based on PMV values calculated for the occupied hours (limited to between 7 and 17 hours) during the simulation run in the heating and cooling seasons (see Table 40). The metabolic rate was taken as 1.2 [met] (sedentary office activity) and the insulation of the clothing as 1.0 [clo] in the heating and 0.8 [clo] in the cooling season (as shorts and short sleeved shirts are not customary in such a building lower values are not likely to occur). The analysis is based on the standardized method described in EN 15251 [66]. Every time-step is put in one of four categories according to Annex A of the standard based on the PMV value: Category I -0.2<PMV<0.2, Category II -0.5<PV<0.5, Category III -0.7<PMV<0.7 or Category IV. The percentage of the working hours spent in each of the four categories is visualized in Fig. 122 and Fig. 123 for the heating and cooling seasons respectively, for every scenario and shading type, as proposed in Annex I of the standard.

In the heating season all refurbishment scenarios improve the thermal comfort compared to the baseline, with or without the addition of controlled shades. The improvement comes from the elevation of the glazing surface temperatures and the reduction in infiltration, which has a much larger positive effect than the negative tendency of the reduction of solar gains. The use of the controlled interpane shading further increases the surface temperature of the glazing and reduces heat losses, especially in the dark hours of the winter nights. The detailed algorithm of the shading control appears to have an even larger effect on the thermal comfort than it had on the energy demand, and the detailed algorithm is clearly superior. Scenario A and the insulating glass has slightly better results without shading but with shading the best results are achieved by Scenario C and the detailed algorithm with more than 50% of the time spent in the best category.

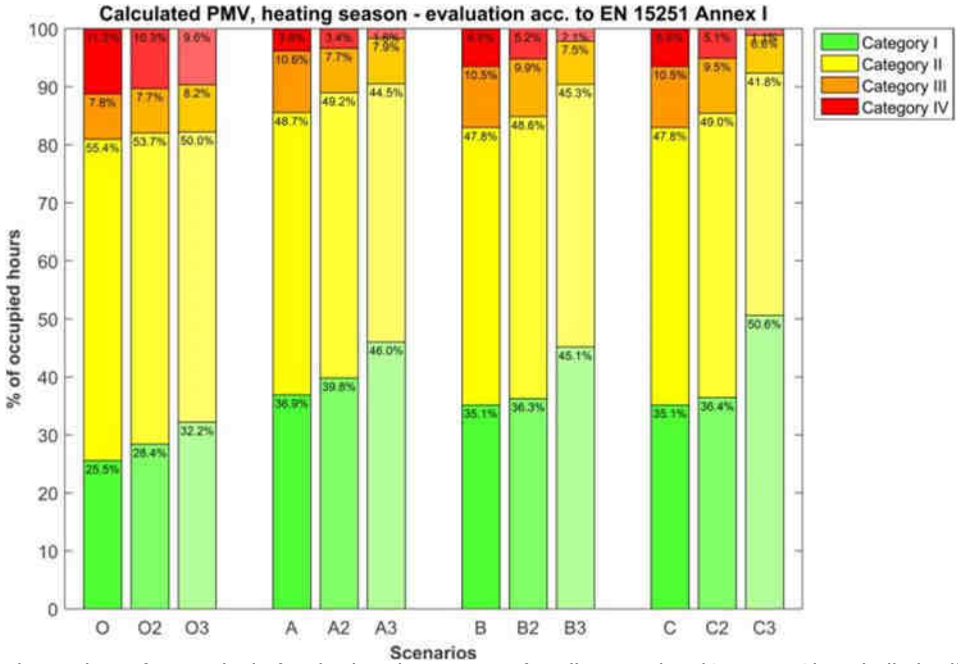

Fig. 122. – Thermal comfort analysis for the heating season for all scenarios (O, A, B, C) and all shading type: no shading / shading with the simple control / shading with the detailed control logic (e.g. O, O2 and O3) (1.5 columns)

The assurance of good thermal comfort in the cooling season is a slightly more difficult task for the westerly oriented test room as we can see in Fig. 123. For the baseline case (scenario O) the majority of the occupied hours is spent in the two worst categories. Category IV gives 33.5% of the time indicating a level of overheating that should only be allowed for a few hours of the year. If the shading is neglected all the refurbishment scenarios exasperate the problem because as seen earlier the reduced g value of the glazing is more than offset in the reduction in the natural ventilation. The addition of the controlled shading improves the situation hugely with only relatively small differences between the two investigated algorithms. The time spent in category IV and the worst overheating is reduced the most to less than a third of the baseline case. The achieved result is still far from ideal, but a further improvement would need other measures that were not in the scope of the current work.

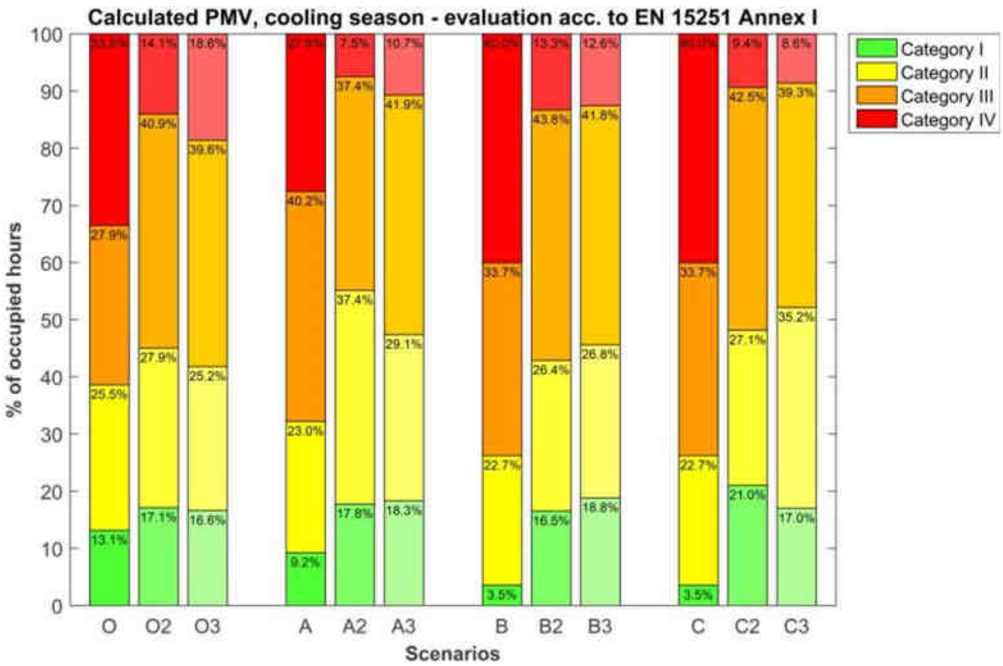

Fig. 123. – Thermal comfort analysis for the cooling season for all scenarios (O, A, B, C) and all shading type: no shading / shading with the simple control / shading with the detailed control logic (e.g. O, O2 and O3)

5.2.4 Discussion

The results show that scenario A and the use of insulating glass units in the refurbishment of historical box type windows is not always the superior option. The use of motorized and controlled interpane shading devices was shown to have a large beneficial effect on the heat balance of traditional windows, especially for higher glazing U and g values. Therefore when the controlled shading is taken into consideration scenario C was found to be the best in all investigated cases, both for energy demand and thermal comfort. Furthermore, and somewhat surprisingly, even scenario B, the least intrusive alteration, gave an at least comparable results to scenario A. The presence or absence of the controlled shading has a huge effect on energy demand. The differences in the investigated shading control algorithms were found to have only small effect on the energy demand but a much more pronounced effect on thermal comfort. The investigation also showed that all refurbishment scenarios can have an adverse effect on summer thermal comfort if they are not paired with the addition of shading devices.

The results depend highly on the fact that the investigated MTA building is mechanically cooled during the summer months when shading systems provide the most benefit. For buildings without mechanical cooling the energy saving potential would clearly be less, though the shading's role in the internal thermal comfort of such buildings is perhaps even more important in such cases. But even in the heating season the inclusion of the shading systems was shown to provide reductions in the heating energy demand by as much as 20% depending on window orientation. The possibility of intensive night time ventilation in the summer (in a residential building or with the addition of a mechanical ventilation system) would also result in different numbers, and the combination of both controlled shading and ventilation would give the best result. The results of the presented calculation can't be simply transferred to other buildings and project but the modelling capabilities of EPICAC BE and its use is well demonstrated. Precise simulations that take building type, building usage, orientation and solar exposures, etc. into account can lead to different results than simple design guidelines and rules of thumb that in this case would have favored the use of insulating glass units.

It is also important to remember, that simulation results and calculated energy savings are still only one, though a very significant input in the actual final design decision. In EU countries our goals regarding the energy usage of buildings is largely determined by the EPBD [70] directive and its recast, where the precise building and component level requirements are determined at state level. In the relevant Hungarian building energy regulation [1], like in the regulations of many other countries, historical buildings are usually exempt from most of the rules. Therefore it becomes the task of the architect or engineer working on a project to define a realistic requirement for energy savings when working on such buildings. This step can itself be aided with numerical simulations. By exploring the possible space of designs and comparing low and high end options we can home in on solutions that provide a reasonable decrease in energy usage without prohibitive costs or the sacrificing of other requirements, such as architectural quality or the preservation of valuable existing constructions.

5.3 Sensitivity study

The models for calculating the specific thermal performance indices of windows and other constructional elements can and must be thoroughly tested and validated with laboratory measurements and by cross comparison with similar as well as more detailed models. However, the same is very hard to achieve with more complex simulations, like the one presented in this chapter and with detailed building energy programs in general. The validation presented for EPICAC BE with the IEA BESTEST suite of test cases [101] is a cross comparison of different programs for the exact same input: climate, material data, operation, certain fixed calculation coefficients, etc. When performing building energy simulations for existing buildings or new realistic designs, in addition to the possible limitations of the different physical models in the program themselves, there are many input parameters and model coefficients that simply can't be determined with complete accuracy. One has to take a 'best guess' for each parameter. The resulting uncertainty in the model output must be taken into account when basing decisions on simulation results.

The uncertainty in the output and the model's sensitivity to the various uncertain parameters (which produces the uncertainty in the output in the first place) can themselves be the subject of study. Identifying the parameters on whose values the output depends the most can aid the further development of models, assist the users of the models by telling which settings to spend more of their time on during input definition and help the design process itself by guiding it to the areas of the most interest.

In their article Eseinhower et al. [46] present a large literature study of various uncertainty and sensitivity analysis techniques. Uncertainty analysis shows how the output changes due to uncertain inputs and tries to establish confidence intervals, while the goal of sensitivity analysis is to determine the relative importance of the influencing parameters for the model output. There are many ways to sort the different sensitivity analysis techniques but Eseinhower et al. used the following main groups: parameter screening methods, local methods and global sensitivity analysis methods. Parameters screening relies on one-at-a-time (OAT) sampling where the value of only one influencing parameter is changed at the same time between its extreme values. Parameters are ranked by their overall effect on the output. Local methods try to approximate the local derivatives of the output for different inputs, but only provide information for a narrow region of the entire range of possible input parameter sets. They may not be suitable for building energy problems which are often multi-modal (have multiple peaks in the output). Global methods try to address this issue by sampling the entire space of possible parameter values. A few examples of global methods are the Morris or elementary effects method, the ANOVA method and the Response Surface Method. The results of a certain technique are either qualitative or quantitative depending whether they only provide ranking of parameters or numerical results that have actual physical meaning. Quantitative methods usually need many more simulation runs and scale badly with increase in the number of of investigated parameters, thus are usually unfeasible for computationally cost intensive simulations. The Morris method is a qualitative method that uses elementary effects which are numerical approximations to partial derivatives of the output, but calculated globally and not just for a local region. It gives a relative ranking of sensitivity and measures of nonlinearity for the different inputs. One main advantage of the Morris method is that it scales only linearly with the number of input parameters and thus it is computationally much less expensive than some other global methods.

After their literature review Eisenhower et al. [46] studied the energy requirements of an American military building (a drill hall) depending on more than 1000 uncertain parameters in the simulation they identified. The thermal modeling was done in EnergyPlus [67] with the help of custom code for the sensitivity analysis and the scheduling of the simulations on a 184 core computer cluster. They used a series of global sensitivity analysis techniques to first reduce the parameter count to around 1/10 before proceeding further with more detailed techniques. Their methodology was aimed at identifying subsystems in the building that could be good targets for energy reduction with monitoring and advanced control strategies.

In Nguyen and Reiter [136] the authors compared many different sensitivity analysis models for use in the field of building energy simulations. They found the best consistency between Fourier Amplitude Sensitivity Test (FAST) and Sobol methods. However, due to the large computational costs of complex dynamic building energy simulations they concluded that the Morris or elementary effects method is perhaps the most suited for performing sensitivity analysis.

Sanches et al. [148] used the elementary effect method for a study and presented a literature review about its use by five other authors in the literature for various problems in building energy simulations. Their study used the program ESP-r [68] for the thermal modeling of an apartment building and the elementary effects method to identify a subset of important parameters amongst a very large selection. These included both architectural/geometrical and constructional details such as material properties. Like Eisenhower et al. [46] they used a ‘best guess’ based approach to get a mean value for the investigated parameters with ±20% intervals if no data could be fined on the distribution of their expected values.

Heisenberg and Brohus [83] used the elementary effects method to identifying the most important parameters for energy usage of a low energy office building’s design. Their aim was to help focus the design process on the most important questions that rank high on the sensitivity scale.

5.3.1 The Elementary Effects Method

Based on the literature the Mooris or elementary effects method was chosen to perform sensitivity analysis for the fenestration heat balance calculations of EPICAC BE. The method was first proposed by Morris [129] and subsequently improved upon by Campolongo et al. in [31] and [32]. It relies on

OAT (one-at-a-time) sampling to rank influencing parameters according to their impact on the model output and to identify nonlinear effects. In its nomenclature y(x) is the output variable of interest which is dependent on the vector x, that contains k elements corresponding to k uncertain real input parameters. We can write x in a dimensionless form, where each element is defined as: $x_i'=(x_i-x_{i,min})/(x_{i,max}-x_{i,min})$. $x_{i,max}$ and $x_{i,min}$ are the maximum and minimum values the i^{th} input parameter can take. The elements of the input vector can be continuous or discrete valued, but for Moor's method every elements is discretized with p levels: $x_i \in \{0,1/(p_i-1),2/(p_i-2),\ldots,1\}$. It is recommended to chose p to be an even number. As Sanches et al. [148] pointed out the domain of x' is a k dimensional hypercube with a p level rectangular grid whose every point corresponds to a unique set of input parameter values. Usually the same p is used for every parameter, but this is not a necessity, as digital parameters (like i.e. the state of a certain system that is either on or off) can have p=2, while better resolution (p>>2) is used only for the continuous parameters.

As a first step an input vector is assembled with random sampling for all of its elements/parameters. This gives a random starting point in the hypercube. The model output is determined with a simulation run. Then in k steps every element of the input vector is changed, one at a time. Every element is changed only once and the order in which they are changed is randomized. To make sure that every value in a parameter's range has an equal probability the change is calculated after Morris [129] as: $\Delta_i=p_i/(2*(p_i-1))$. If the initial random value is $x_i'<0.5$ than the changed value is $x_i'+\Delta_i$, otherwise $x_i'-\Delta_i$. The initial point and the subsequent k steps is called a trajectory, a path through the hypercube. A simulation run is performed at every step along the trajectory (a total of k+1) to get the model output or outputs.

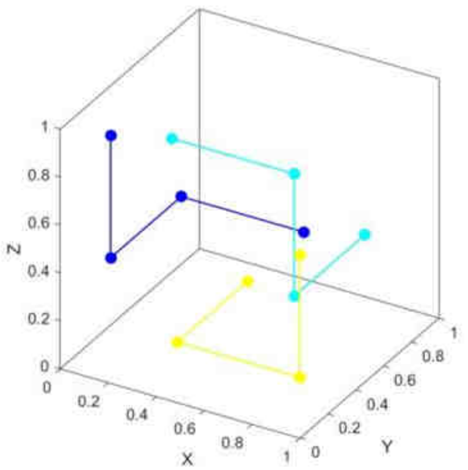

Fig. 124. – An example of three trajectories in a 3 dimensional hypercube

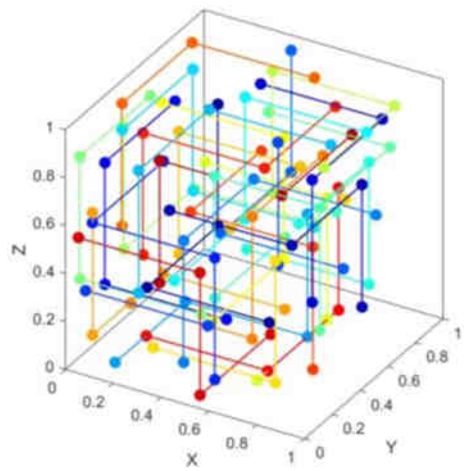

Fig. 125. – An example of 20 trajectories in the same 3 dimensional hypercube showing the near uniform sampling of the complete space of possible states

An elementary effect is defined as:

$$EE_i\left(x'\right)=\frac{Y\left(x'+\Delta_i e_i\right)-Y\left(x\right)}{\Delta_i} \qquad (89)$$

where $EE_i(x')$ is an elementary effect of parameter i, Y is the output of the model. Parameter i is changed from an initial value of x' to $x'+\Delta_i e_i$, where $\Delta i=p_i/(2*(p_i-1))$ as defines earlier and e_i is a vector of zeros except for the coordinate i where it is ±1 (as defined earlier).

An elementary effect is a measure of how big the effect of changing a certain input parameter has on the output, for a given set of other input parameters that were held constant at the time. Each trajectory gives k elementary effects, one for each of the k parameters/elements of x. By running r number of trajectories we get r elementary effects for each of the k parameters at a cost of r*(k+1) simulations. According to the literature r can be as low as 4, but values of one to a few dozen are used in most of the literature. When the simulations are done and the elementary effects have been calculated their mean and the standard deviation is used to assess the sensitivity of the model.

The mean of the elementary effects for parameter i is:

$$\mu_i = \frac{1}{r}\sum_{j=1}^{r} EE_{ij} \tag{90}$$

The standard deviation of the elementary effects for i is:

$$\sigma_i = \sqrt{\frac{1}{(r-1)}\sum_{j=1}^{r}\left(EE_{ij} - \mu_i\right)^2} \tag{91}$$

The value of μ is a measure of how important a certain parameter is for the model: the larger the mean of the elementary effects the larger the model's sensitivity is for the particular parameter. This gives a simple ranking of parameters. Elementary effects with opposite sign may cancel each other out and hide some of their importance, therefore Camolongo et al. [31] suggested using the absolute value of the elementary effect for deriving their mean:

$$\mu_i^* = \frac{1}{r}\sum_{j=1}^{r}\left|EE_{ij}\right| \tag{92}$$

The standard deviation σ_i of a parameter's elementary effects indicates non-linearity: if the standard deviation is high the effect of the parameter's change is dependent on the value of the other parameters.

Sanches et al. [148] suggested a further analysis by plotting the μ_i* and σ_i results on a μ*-σ coordinate system. They pointed out that if the elementary effects are assumed to be normally distributed 95% should lie within ±1.96σ_i. If σ_i/ μ_i* lies below 0.1 than the elementary effect are mostly within ±20% of the mean and they must be almost constant indicating that the input parameter i has a near linear effect on the model output. They also showed that if σ_i/ μ_i* lies between 0.1 and 0.5 the model's sensitivity of the parameter is monotonic, and near-monotonic for 0.5< σ_i/ μ_i* <1. Parameters that are truly non-monotonic and have non-linear interactions lie above 1. Sanches et al. found this test to be justifiable even for elementary effects without standard distribution.

5.3.2 Sensitivity analysis results

Altogether 5 different set of sensitivity analysis runs were performed and evaluated based on the Morris [129] or elementary effects method. The detailed description of all the investigated parameters, their range in the study, and the complete documentation of the results is found in Appendix X. Continuous parameters were discretized with p=10 levels. A wrapper program was written to generate the input files based on the values in the x vector and then autonomously run the EPICAC BE simulations on an ad-hoc cluster of three desktop computers. The test room, test window and the refurbishment scenarios introduced in the case study of the MTA building were used as a basis for the investigations. The main model outputs whose sensitivity was analyzed were the calculated annual heating and cooling energy demand, as well as the infiltration and ventilation air change rates in one of the analysis runs.

The first sensitivity analysis run **SA1** was used to establish an initial list of the most influential parameters for the energy balance of box type windows in their original unrefurbished state. The simulations were run for scenario O, without a controlled interpane shading system. The geometry and the constructions themselves were taken as given. The study focused on parameters describing the building use, user behavior and some uncertain model constants instead. The air change rate was defined with a single parameter (ACH={0.5-2} [1/h]) instead of using infiltration and ventilation models to keep the calculations manageable. Altogether k=18 parameters were defined and investigated with r=20 trajectories requiring a total of 380 independent simulations to be performed.

The results show that for the annual heating energy demand the most influential parameter by far is the air change rate even surpassing the heating setpoint temperature, which was only second. The heat gains of lighting, the nightly and weekend setback of the heating setpoint temperature, the internal convective hat transfer coefficient of the window and the heat gains of the office equipment were the parameters to follow. the rest of the parameters showed quickly diminishing influence and need not be listed here (the full data is found in Appendix F).

For the annual cooling energy demand the cooling setpoint temperature was the number-one factor only followed by the ACH. They were followed by the heat gain of lighting, the weekend state of the cooling system, the external solar absorptance and convective heat transfer coefficient of the masonry and the internal heat gains of occupancy. The rest of the parameters showed negligible influence. The plot of the sensitivity results on the μ*-σ axis is shown in Fig. 126 and Fig. 127 for heating and cooling respectively. For the heating all important parameters are in the linear or near-linear regime while for the cooling the effect of the nightly cooling setpoint setback and the internal convective heat transfer coefficients were in the nonlinear zone.

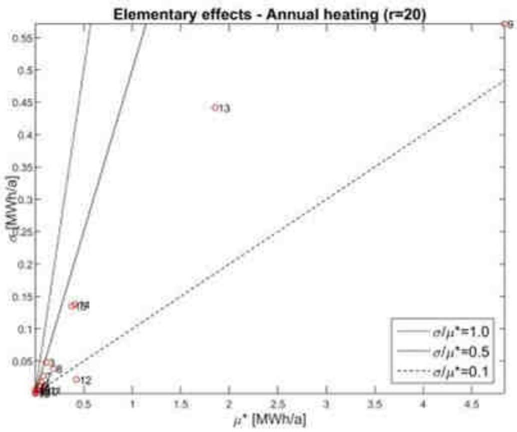

Fig. 126. – SA1 – μ*/σ plot – Annual Heating

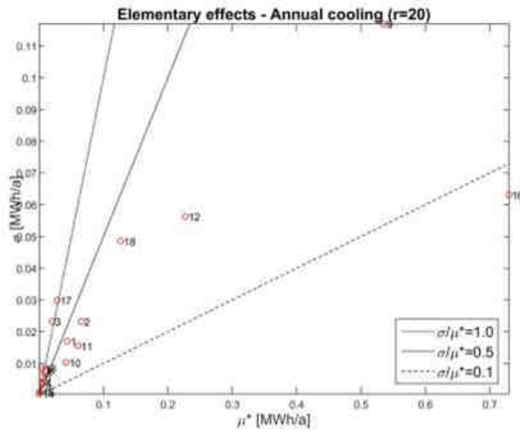

Fig. 127. – SA1 – μ*/σ plot – Annual Cooling

At a later stage it was determined that the air change rate limits set in SA 1 were excessive which could possible skew the results, so **SA1b** was setup the repeat the same calculation but with ACH={0.1,1} [1/h]. The sensitivity ranking of the parameters however did not change at all for the heating energy demand, and only the heat gains of the office equipment's and the external convective heat transfer coefficient changed palaces for the cooling energy demands. The plots are shown in Fig. 128 and Fig. 129.

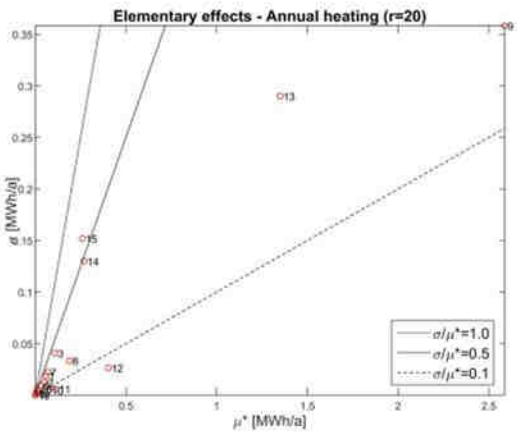

Fig. 128. – SA1b – μ*/σ plot – Annual Heating

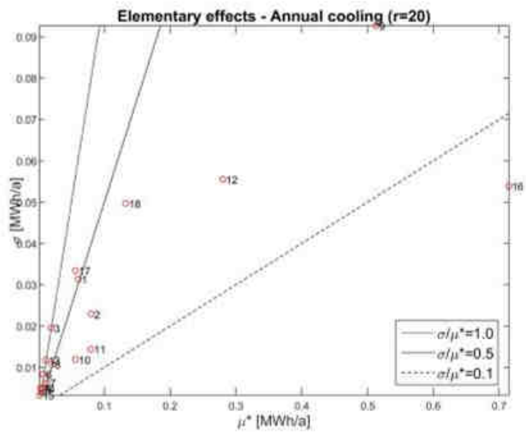

Fig. 129. – SA1b – μ*/σ plot – Annual Cooling

The next sensitivity analysis run **SA2** was dedicated to investigate the infiltration and single-sided natural ventilation models in EPICAC BE. Altogether k=17 input parameters were selected that included the total building height, wind pressure coefficients, the air permeability of the window, the distribution of the airflow paths with regards to the neutral plane, the window's opening area and height as well as the occupants' behavior and the HVAC setpoints. The trajectories numbered the same (r=20) which required 360 independent simulation runs. The calculated air change rate for infiltration was ACH=0.25-0.55 [1/h] and for ventilation ACH=0.05-0.3 [1/h]. The window was the same unrefurbished and unsealed window of scenario O and airing was only performed twice daily for a time described with it's own parameter: t_{open}={5-20} [min].

For infiltration during the heating season unsurprisingly the window's air permeability and flow exponent were the two main influencing parameters. They were followed by c_{p1} (the pressure coefficient when the window is windward), the total building height, de difference between the neutral plane and the flow path, the c_{p2} and $c_{p3,4}$ (the pressure coefficient for leeward and tangential situations). The rest of the parameters showed comparatively low influence. Parameters c_{p2} and $c_{p3,4}$ showed the most non-linearity (see Fig. 130).

For the ventilation air change rate the time for the window opening, the ventilation area, the opening height and the heating setpoint temperature were the only influencing parameters. As mentioned earlier the single-sided ventilation model used is that of Larsen [117], which is a semi-empirical model with inbuilt pressure coefficients (hence the absence of c_{p1}, c_{p2} and $c_{p3,4}$ which were defined only for the infiltration model) based on wind speed and buoyancy (hence the influence of the heating setpoint). All parameters' influence was near-linear.

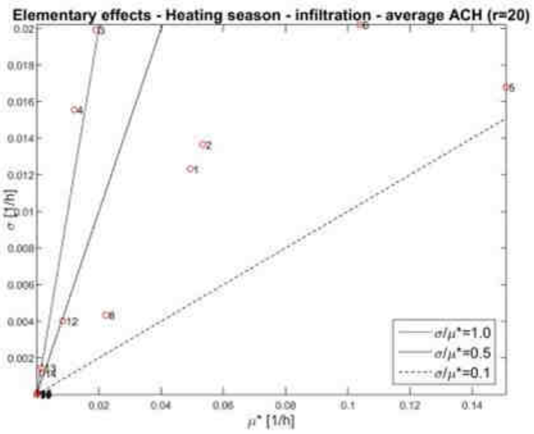

Fig. 130. – SA2 – μ*/σ plot – $ACH_{infiltration}$ in the heating season

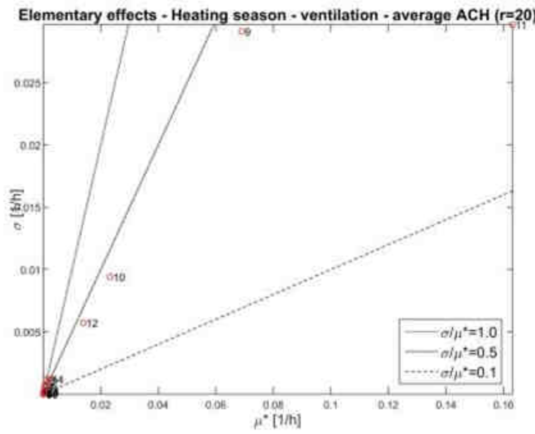

Fig. 131. – SA2 – μ*/σ plot – $ACH_{ventilation}$ in the heating season

The third sensitivity analysis run **SA3** was aimed at studying the sensitivity of the model with the after-refurbishment scenario C and the dynamically controlled interpane shading system combined together with the detailed infiltration and ventilation models. It used k=20 parameters and r=20 trajectories for a total of 420 individual simulation runs.

For the heating energy demand the most influential parameters were the heating setpoint, the window opening time, window air permeability, internal lighting load, office equipment thermal load, weekend temperature setback, nightly temperature setback, internal convective heat transfer coefficient of the walls, the occupancy thermal load, the external heat transfer coefficient of the masonry, the external solar absorptance of the masonry and the internal convective heat transfer coefficient of the window. This result is somewhat different than the parameter ranking of SA1 and SA1b, partly because of the different definition of the air change rate, and partly because of the improved (thermally in in terms of airtightness) windows. The most influential parameters' effect was near-linear (see Fig. 132).

For the cooling energy demand the cooling setpoint temperature, the lighting thermal load, the external surface solar absorption coefficient, the office equipment thermal load, the window air permeability, the external surface convective heat transfer coefficient, the occupancy thermal load and the cooling's state during the weekends were the parameters of significant influence. Like in the case of the heating energy demand the importance of infiltration and air change is reduced as the window airtightness is increased.

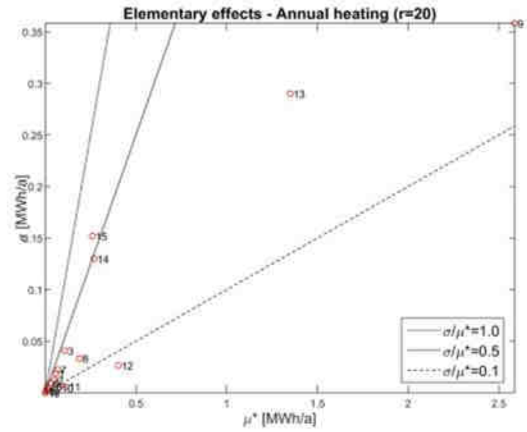

Fig. 132. – SA3 – μ*/σ plot – Annual Heating

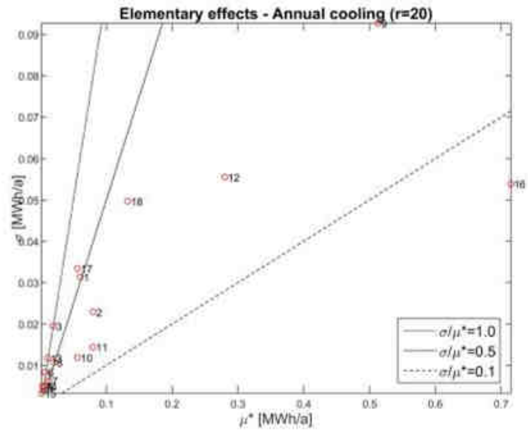

Fig. 133. – SA3 – μ*/σ plot – Annual Cooling

Finally **SA4** was performed on all 4 scenarios of the MTA building in parallel to check whether the uncertainty in the input parameters can change the relative ranking of the various design options. Based on the sensitivity ranking of the parameters determined with the earlier run's only k=12 parameters were selected with a trajectory count of r=40, which for all 4 scenarios meant a grand total of 2080 individual simulation runs. The four individual scenarios were calculated along the exact same trajectories and with the same parameter combinations at each step. At no points was there any change in the relative scenario ranking in either the heating or the cooling energy demand. Histograms of calculated heating energy demand based on the 420 individual simulation runs for the tree refurbishment scenario are shown in Fig. 134 - Fig. 136 and as a percentage of the energy demand of scenario O in Fig. 137. While the overall error in the predicted energy demand can be quite large depending on the uncertain input parameters the relative difference between the different scenarios for the same set of parameters seems remarkably consistent. The same can be seen for the cooling energy demand in Fig. 138 - Fig. 141.

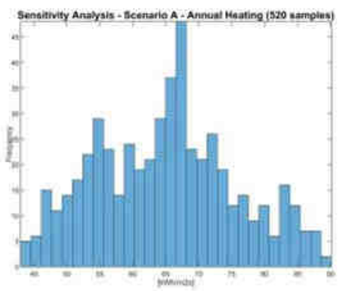

Fig. 134. – SA4 –
scen. A heating E. dem.

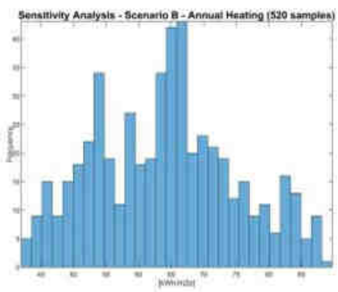

Fig. 135. – SA4 –
scen. B heating E. dem.

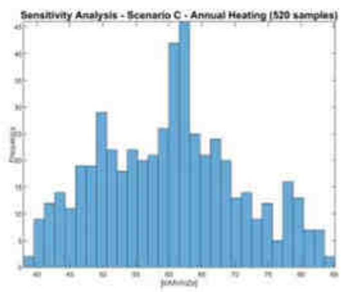

Fig. 136. – SA4 –
scen. C heating E. dem.

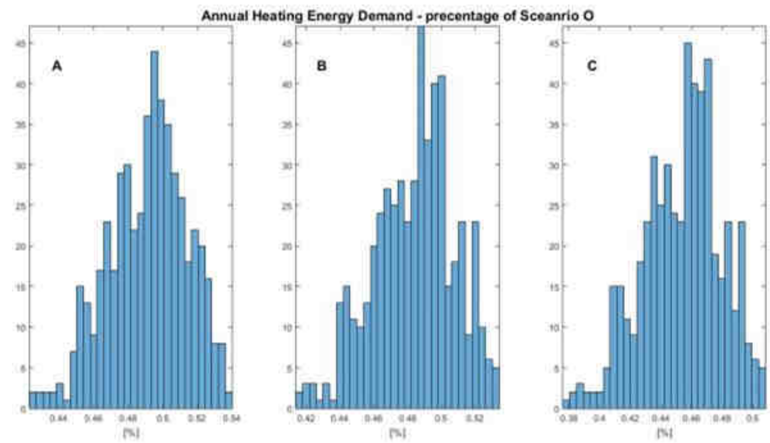

Fig. 137. – SA4 – histogram of heating energy demand as a percentage of scenario O

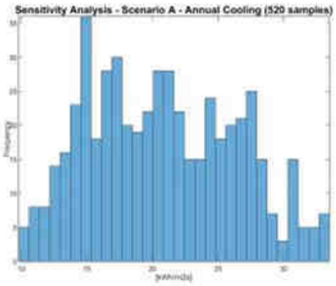

Fig. 138. – SA4 – scen. A cooling E. dem.

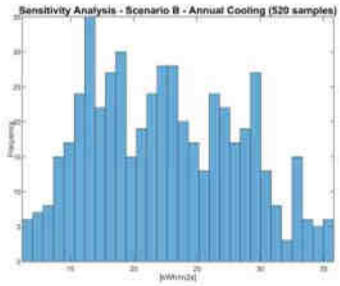

Fig. 139. – SA4 – scen. B cooling E. dem.

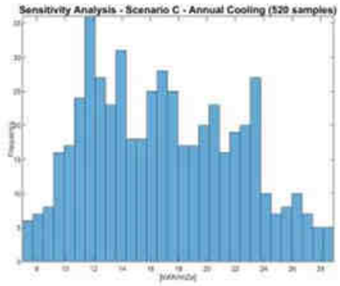

Fig. 140. – SA4 – scen. C cooling E. dem.

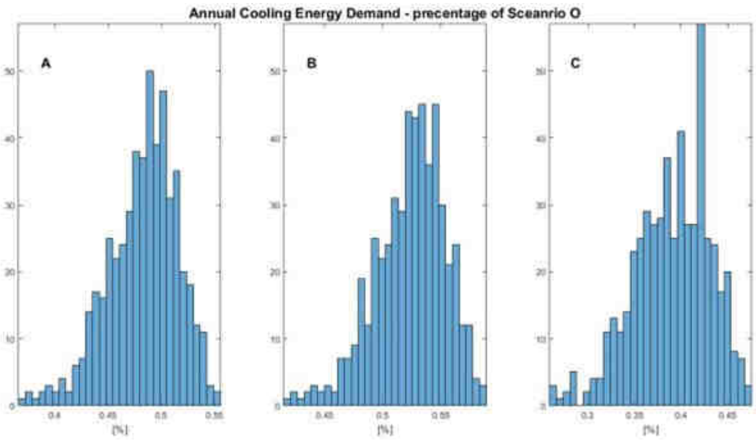

Fig. 141. – SA4 – histogram of cooling energy demand as a percentage of scenario O

5.3.3 Discussion

The results of the extensive sensitivity analysis shows even disregarding the possible errors in the physical models the uncertainty of the model inputs and parameters can cause large deviation in the intermediate calculation results (e.g. air change rate), and in the final numerical outputs of the model (annual heating and cooling energy demand). The uncertainty in the main constructional (window air permeability, opening aperture etc.) and environmental factors (pressure coefficients) determining air change rate, the heating and cooling energy setpoints as well as window opening duration (i.e. user behavior and operation) and the internal heat gains can all cause significant deviations in the predicted energy demand, making exact predictions of energy usage very difficult. The investigated convective heat transfer coefficients show a smaller effect, and the parameters describing infiltration and ventilation loose some relative importance as window airtightness is increased.

The analysis also showed, that the effect of most of the influencing factors is very nearly monotonic and near-linear, especially for the most influential factors like the heating and cooling setpoint. As a result the whole model's behavior is near-linear, and despite the numerous sources of uncertainty the produced ranking of individual investigated refurbishment scenarios as well as the predicted relative reduction in energy demand remains remarkably consistent. Inherent uncertainties focus the main role of building energy simulations on the comparison of different options, the performing of optimization and the discovery of phenomenon that can enlighten the design, instead of on the production of perfectly accurate numerical outputs. These are the intended uses of the developed program EPICAC BE as well. Still, a careful designer/modeler must explore the sources of uncertainty and make efforts to reduce the most important sources. To this end the lessons learned from this study should be incorporated into the preliminary stages of a window refurbishment project. The customary architectural survey of window stock, geometry and damages should always be extended with a survey of typical building use and occupant behavior so that it can be used to improve the accuracy of thermal modeling and be taken into account in the design phase. Non-typical user behavior and building use can't be the main base for a responsible design (even refurbishments are designed for a long life-span and more generation of occupants) but must nevertheless inform the design in the work of a sufficiently reflective designer.

5.4 Proposed methodology

The windows of prestigious monuments are characterized by excellent stock materials, non-standard sizes, shapes, designs and sometimes unique ways of operation. Due to these factors, their shear age and value, their often regrettable current state as well as the unprofessional nature of earlier interventions their repair and retrofit can't be planed based solely on design experience, general guidelines or rules-of-thumb. The buildings may themselves deviate significantly enough from the ordinary (e.g. extremely thick walls, very large internal headroom and volume, special systems of heating) to stress the need for the windows' refurbishment not to be undertaken outside of a much wider context (i.e. the whole building itself). Furthermore, aspects of monuments preservation can often exclude refurbishment techniques that would seem most optimal and straightforward in other circumstances (e.g. swapping parts or complete windows with strengthened replacements that can better suite tight seals, operational needs or the installation of heavy high thermal resistance glazing). Although first class monuments are exempt from many requirements energy usage reduction goals cant be ignored, but right design goals have to be determined with care. Disregarding these special aspects and the lack of a constructive design process can lead to solutions that are unprofessional, uneconomical, unsuited for the building's use or sacrifice cultural value to try to meet rigid goals of building energy use.

Based on the introduced design project and experience gained wit other work, the development, use and testing of the program EPICAC BE I propose the following general methodology for designing the retrofit of valuable historic double-skinned box type windows.

Preliminary phase

- Architectural survey: the documentation of main window dimensions, frame and divider profiles, frame materials and surface treatments, operation, hardware, installation type, constructional context, various attachments (ledge, wooden paneling in the internal reveal, framing, etc.) and shading devices
- Creation of a window typology: the sorting of windows based on age and origin, geometry and construction into groups and sub-groups to later serve as a basis for the customization of the plans
- Survey of damages: general repair, operability, typical faults and their causes, etc.
- Survey of additional influencing parameters: survey of user complaints, typical usage, special operational requirements, characterization of relevant HVAC systems, etc.

Concept creation

- Quantification of the window's performance in the state they are found in: thermal simulation and/or measurements (whenever possible): Blower-Door measurement with the combination of infrared thermography for identifying fault points, etc.
- Determining the design goals and requirements: defining requirements of monument preservation, important user requirements, special operational or constructional requirements posed by the building/room usage, approximate goals of energy reduction
- The creation of a priority list: ranking the individual goals and requirements on a case-by-case basis
- Creating possible refurbishment scenarios to meet the prioritized list of design goals
- Quantifying the possible improvements in thermal performance: comparing the refurbishment scenarios with the help of thermal modeling (e.g. EPICAC BE), determining the range of realistic improvements, possible feedback into the design goals, priority ranking and scenario creation

Design phase

- Synthesis: harmonizing the scenarios for window refurbishment with the current and/or future building use and HVAC systems in cooperation with the HVAC designers and/or operators
- Decision: selection of a refurbishment scenario in consultation with the client
- Plan development: creation of plans, specifications, final documentation of earlier stages

Control and validation phase (optional)

- The control of refurbishment works
- Validation measurements: control of airtightness, if necessary the long-term monitoring of room and/or window hygrothermal behavior
- Creation of as-built plans and final documentation

6 Summary

6.1 New scientific findings

The proposed new scientific findings of the thesis are summed up in the following points:

6.1.1 Finding I.

Fenestration thermal models and sub-models: assessing the range of validity of standardized calculation tools for double skin box type windows

It is a self evident goal to have models for calculating fenestration thermal properties that are as accurate for double-skin box type windows as for contemporary single-skin constructions. Designers have a large number of fenestration thermal design tools at their disposal that are incorporated into two main series of standards, one in the EU and one in North-America. The models in these standards were however initially developed for the single-skin windows of contemporary manufacture. In order to keep the necessary calculations manageable the standards are based on simplifying assumptions enabled by a good knowledge of the thermophysical processes in these contemporary windows. They thus have a series of implicit assumptions that are often not reported in their text, nor do they show the research works they were based on.

I. a) With a detailed survey of the relevant literature I have shown what the implicit simplifying assumption in the fenestration thermal calculation standards are, what is their base in the primary literature and what is their range of validity.

I. b) I have demonstrated that in the cavities of double-skin box type windows, merely due to their different cavity thickness and vertical aspect ratio range, a radically different natural convection flow regime is encountered (a turbulent boundary layer flow instead of a laminar conduction regime flow) which lies outside the validity range of the standardize fenestration thermal models.

Results published in: Bakonyi and Becker [16] and Bakonyi and Dobszay [21].

6.1.2 Finding II.

A new dedicated correlation for calculating the convective heat transfer coefficient in the glazing cavities of double-skin box type windows depending on the vertical aspect ratio and the Rayleigh number.

With the help of CFD model validated based on measurement results found in the literature and a large parameter study I have created a new correlation for calculating the convective heat transfer coefficient in the glazing cavities of double-skin box type windows depending on the vertical aspect ratio and the Rayleigh number, derived explicitly for the windows type. To this end I have performed a Monte Carlo simulation to identify the Rayleigh number and vertical aspect ratio range which are most often encountered in the glazing cavities of box type windows. I performed a further parameter study to study the temperature stratification in the cavity core of box type windows depending on the Rayleigh number and the aspect ratio.

II. a) By fitting a new set of empirical equation to a dataset of convective heat transfer results, derived for the Rayleigh number and vertical aspect ratio range of double-skin box type windows, I created a new correlation for calculating the Nusselt number that better expresses the aspect ratio dependence of convective heat transfer for a given Ra number than other equations found in the literature:

$$Nu = \max \begin{cases} Nu_1 = 0.0776 Ra^{0.3041} \\ Nu_2 = 0.0193\left(1 + Ra^{0.0897} Ar^{-0.0382}\right)^{3.9826} \end{cases} \tag{93}$$

where: Nu [-] – the Nusselt number
Ra [-] – the Rayleigh number based on cavity thickness
Ar [-] – the vertical cavity aspect ratio

II. b) By studying the dimensionless temperature field in the cavities of box type windows it can be concluded that they constitute a transition point between near-rectangular and high aspect ratio cavities. In box windows' cavities with very small aspect ratios the vertical temperature stratification is near linear with the dimensionless height (y/H), while at higher aspect ratios the stratification is significantly reduced in the middle of the cavity and it is mostly constrained to the very top and bottom of the flow (0.1<y/H and 0.9>y/H). I summarized the results of the study in a new correlation for the vertical temperature stratification:

$$f = 0.5 + 0.8963 \cdot b + 0.0159 \cdot b^2 - 1.5771 \cdot b^3 - 0.0341 \cdot b^4 + 5.2452 \cdot b^5 ... \\ -0.0238 \cdot A \cdot b - 0.0010 \cdot A \cdot b^2 + 0.1176 \cdot A \cdot b^3 + 0.0025 \cdot A \cdot b^4 - 0.1282 \cdot A \cdot b^5 \quad (94)$$

$$b = \left(\frac{y}{H} - 0.5 \right) \quad (95)$$

where: f [-] – the dimensionless temperature of the core
A [-] – the dimensionless aspect ratio (A=H/L)
y [m] – the height
H [m] – the total height of the cavity

The same parameters study was conducted for complete glazing systems with typical 3 [mm] thick float glass panes, longwave radiative heat transfer, and simple combined heat transfer coefficients at the internal and external boundaries. The vertical aspect ratio and Ra number range was kept the same. The results showed that the temperature stratification in the core of the cavity causes a stratification of the glazing surface temperature as well that reached ±10% of the total cavity temperature difference on the cold side (the coldest point of the cold size glazing can be up to 10% of the cavity temperature difference colder than its mean temperature), which an important phenomenon when trying to asses the condensation resistance of box type windows. Therefore:

II. c) I have proven that the standard fenestration heat transfer models that rely on one-dimensional calculation for quantifying the heat transfer and temperature field in glazing systems and neglect the temperature stratification can not be used for assessing the condensation resistance of double-skin box type windows as they can not predict minimum surface temperatures.

Results published in: Bakonyi and Dobszay [22].

6.1.3 Finding III.

The accuracy of standard fenestration heat transfer models for predicting overall window thermal transmittance

The standard fenestration heat transfer models in the literature do not take into account the three-dimensional nature of the flow and the radiative heat transfer or the temperature stratification of certain flow regimes when calculating the overall window thermal transmittance. I created three-dimensional models of simplified generic and as a control a realistic complex-geometry box type windows to study the accuracy of said calculation methods. I compared the results of standard fenestration heat transfer calculation, 3D heat conduction calculations based in the standard fenestration models and CFD/conjugate heat transfer simulations for simple and thermally improved versions of the model windows' glazing system. I performed the standard calculation with the both the original and the improved correlation for the cavity Nusselt number I introduced. The inability of the standard models to compute 3D heat flow with only 1 and 2D approximations is clearly demonstrated in the significant errors between the 2 and 3D thermal calculations. I could reduce the errors by increasing the edge-of-glazing area in the 2D thermal calculations compared to the standards thereby capturing more of the multi-dimensional effects in the edge-of-glazing thermal transmittance. I identified the minimum edge-of-glazing width to get a edge-of-glazing width independent window thermal transmittance by observing the calculations' convergence.

III. a) I performed a comparative study of standardize conduction-only fenestration thermal transmittance models with 3D thermal and 3D CFD/conjugate heat transfer models for a set of generic and a realistic box type window geometries, with the help of both standardized and my proposed correlation for the glazing cavity Nusselt number. I have concluded that the standard edge-of-glazing area/width in the NFRC 100-2010/ISO 15099 calculation method is inadequate to capture the fullness of even the 2D heat flow and results in large errors when compared to 3D thermal calculations. I concluded that the edge-of-glass are width must be increased to at least 200 [mm] (from the 63.5 [mm] in the standard) to produce and edge-of-glass width independent result.

When compering the calculated thermal transmittance of standard and CFD simulations the error is dependent on the buildup of the glazing system: unmodified glazing is better, while thermally improved (low-e coated or using insulating glass units) glazing systems is more poorly predicted by the standardized calculations. Changing the Nusselt number correction in the standard method to the new improved correction does not increase the calculation accuracy in every cases. The fact that the removal of the Nusselt number correlation as source of error can, in certain circumstances increase calculation error clearly shows that there are additional sources of error in the standard models. The standard model can't be enabled to accurately calculate box type windows with just simple modification to it's equivalent thermal conductivity approach.

III. b) By comparing the thermal transmittance calculation methods listed above I have demonstrated, that:

- ***the NFRC 100-2010 / ISO 15099 based standard calculations can predict overall thermal transmittance with an accuracy of only ±10%,***
- ***the 3D thermal simulations are generally closer to the CFD results as even the improved 2D calcualtions,***
- ***that the NFRC 100-2010 / ISO 15099 based standard calculation tends to overpredict thermal transmittance***
- ***the NFRC 100-2010 / ISO 15099 based calculation method with the improved correlation for the Nusselt number is more accurate for un-refurbished windows, while it tends to underpredict thermal transmittance for glazing systems with larger thermal insulation,***
- ***the difference in calculated thermal transmittance with hard coated low-e glazing in the internal or external position, which is only predicted by CFD simulation, highlights the importance of three-dimensional infrared radiation effects that are neglected by the standard models.***

6.1.4 Finding IV.

A proposed new methodology for the simplified calculation of non-repeating thermal bridges at external walls

The constructional and thermal properties of windows are in strong connection with the thermal bridge that is created at their interface with the surrounding wall. To study the effect this window installation thermal bridge has on the overall heat transfer I created a new simplified method for the simplified calculation of non-repeating thermal bridges in external walls. I have realized that the simplified thermal bridge correction in the current national building energy calculation method can under- or over-predict the effect of non-repeating thermal bridges in the overall thermal transmittance of external walls. This becomes highly important when governmental grants for energy reduction measures with thermal insulation are awarded based on savings calculated with this unreliable method. With the help of the new method I have demonstrated that it is not possible to create thermal bridge correction factors with acceptable accuracy that are not dependent on the building type and main constructional parameters. I refined the new model with the goal of reducing the number of necessary input parameters to a minimum and to enhance its usability by making it able to interpolate between the different values of constructional an geometrical parameters.

IV. a) I have demonstrated a new method that is capable to calculate the thermal bridge correction factor for the external walls of buildings with well typifyable facades and well specified construction with much higher accuracy than the existing method in the Hungarian national building energy regulation, without increasing the workload of the calculation

considerably. I have derived and tested the method for three distinct, ubiquitous building types: 19th century urban apartment buildings, rural and suburban single storey houses based on type plans ('cube houses') and ca. 1960' urban apartment buildings based on type plans and built with prefabricated wall blocks ('block houses').

It doesn't need any proof that the key to the success of all simplified calculation methods is identifying the most important influencing factors and the reduction of the necessary input parameters to a minimum, without sacrificing too much accuracy when compared to more detailed but time-consuming calculation methods. During the development of my new simplified thermal bridge correction method I have investigated the effect of window installation type and installation thermal bridge on the value of the thermal bridge correction factor, and found it to be significant. The effect is too big to be ignored, but the extremely large space of window and window installation options make it unfeasible to incorporate them all into the calculation. Window and window installation type can't be simply expressed mathematically (unlike e.g. thermal insulation thickness or thermal resistance) and different variants can't simply be interpolated between. These realizations led me to propose that that the window-to-wall interface's thermal bridge is to be accounted for in the windows' thermal transmittance and be removed from the set influencing the walls' average U value.

IV. b) With the help of the proposed new simplified thermal bridge correction method I have demonstrated that account of the window-to-wall installation thermal bridge should not be taken in the wall's thermal bridge correction, but should instead be incorporated into $U_{w,inst}$, the window thermal transmittance coefficient in the installed state, to enable the creation of truly general simplified wall thermal bridge correction methods without sacrificing accuracy. I made the modification on the method for al three building types mentioned above, and demonstrated the possible reduction in influencing parameters and overall complexity, and analyzed its accuracy.

Results published in: Bakonyi [15], Bakonyi and Dobszay [17] and Bakonyi and Dobszay [20]

6.1.5 Finding V.

Fenestration heat balance calculations to support the design decisions in the retrofit of historical double-skin box type windows

V. a) I created a single zone dynamic building energy simulation program package EPICAC BE, explicitly optimized for historic buildings and traditional double-skin windows, to perform fenestration heat balance simulations and test custom algorithms. I performed the validation of the program with the help of the IEA BESTEST suit of simulation test cases which is a method recognized by researchers and software developers alike. EPICAC BE met all of the test requirement.

V. b) With the help of the new program I have demonstrated that in certain situations it is possible for alternate retrofit solutions, such as the use of higher thermal transmittance but higher g value glazing system in combination with dynamically controlled shading devices, to reduce the heating and cooling energy demand of valuable historic box type windows further than it is possible with thin IG units (even with the same shading devices). During the planning of window refurbishments for a prestigious Hungarian national monument this allowed the creation of a design concept that suits the combined building energy and monument preservation goals better than previous design practices.

V. c) A detailed sensitivity analysis of the models for the previously mentioned design project demonstrated that the calculated heating and cooling energy demand in a window heat balance model is highly sensitive, besides constructional and environmental parameters, to a number of building use and occupant behavior factors. I have demonstrated that though this limits the possibilities for very accurate predictions of energy demand the near-linear and monotonic influence of the main uncertain parameters still allow for a very consistent prediction of relative ranking between individual design options as well as the prediction of relative energy savings.

V. d) Based on the experiences gained with the program, the experiences of the introduced

design project and the results of the detailed sensitivity analysis I created a new proposed design methodology for refurbishment projects of valuable historic windows. I have demonstrated that the design methods and guidelines found in the literature and widely used at home and abroad do not necessarily lead to optimal solutions for realistic complex requirements. The use of the proper design methodology and suitable simulation tools can lead to alternate options that do not require the irreversible destruction of even parts of the window stock.

Results published in: Bakonyi and Dobszay [19].

6.2 Avenues for further study

As written at the beginning of this thesis in chapter 1.2, from the long-term research program laid out to refine the modelling of double-skin box type windows the work done here is only the beginning. Further study must focus on the remaining open questions:

- Is it possible to create simplified thermal transmittance calculation methods for box type windows that can significantly improve the accuracy of the current standard methods while avoiding the very large manual and computational workload of 3D CFD simulations?
- A methodology for incorporating the interaction of convective and transmission heat transfer in the cavities of box type windows should be developed, possibly by basing it on the research done on airflow windows.
- Models to predict the condensation resistance of box type windows are very much needed to test the applicability of various retrofit options in high humidity environments and buildings with a mechanical ventilation system. Such a model has to reliably predict both the lowest surface temperature in the main glazing cavity, as well as the highest partial vapor pressure in the cavity. The phenomena involved are highly complex but could be tackled with many approaches: analysis of long term monitoring measurements to create empirical or semi-empirical models, very detailed CFD/Multiphysics simulations or intermediate models informed by both. Additionally a thorough statistical analysis of the new models and the boundary conditions will be needed determine actual reasonable design limits for the prevention of interpane condensation, instead of only focusing on worst-case-scenarios that occur very rarely.
- The effect the stratified boundary layer flow in the main cavity of box type windows has on the hygrothermal behavior of the window-to-wall interface needs to be determined by long-term measurement campaigns. Based on the findings and the findings of this theses a new methodology for incorporating box windows in HAM detail simulation needs to be developed.
- The improvements in modeling techniques thus far and in the future need to be incorporated into the complex room or building level heat balance models.
- Further sensitivity analysis is needed on not just uncertain model inputs, but on constructional inputs and variables, orientations, building geometries etc. to inform the design process with near optimal scenarios for a variety of situations.

As the methodology, not just the results, of this thesis is a product of a long research process that could only crystallize toward its end I have already started some investigation listed here that could not be fully finished and fit into the scope of this work. A hygrothermal monitoring of a box type window was already conducted and another more thorough measurement campaign is currently underway at the MTA building mentioned in Chapter 5.

6.3 Acknowledgements

I would like to thank all of my colleges for their help and support in creating this thesis, with special thanks to my supervisor Dr. Gábor Becker and Dr. Gergely Dobszay.

I would also like to thank Dr. Várfalvi János and Tamás Orbán for their generous help in performing a hygrothermal monitoring of a box window in the university building, which although did not fit into the scope of this work nevertheless help start me in my research and will be the subject of future publications.

I am also obliged to Dr. Árpád Veress at the Budapest University of Technology and Economics' Department of Aeronautics, Naval Architecture and Railway Vehicles for his advice and support with the CFD simulations.

I would also like to thank Imre Papp and Péter Sólyomi at the ÉMI Minőségellenőrző Innovációs Nonprofit Kft. for the access to their Building Constructions laboratory, and their patience and untiring help in the hot box measurements.

For the test windows, materials and manufacture of the hot box apparatus I am also grateful to Károly Vigh and the entire Hofstädter Kft.

For the financial support of the measurements I thank the ODOO+ project (a "SolarDecathlon versenyen eredményes BME ODOOprojekt további hasznosításának vizsgálata " c. projekt, illetve az azt támogató „Új Széchenyi Terv ED_13-1-2013-0005 programja" keretében).

7 Bibliography

[1] 7/2006 (V. 24.) (2006) Decree of Minister without portfolio about the determination of energy efficiency of buildings (in Hungarian) Hungarian Ministerial Decree

[2] Abid, R. (1993) Evaluation of two-equation turbulence models for predicting transitional flows, *Journal of Engineering Science*, Vol. 31, pp. 831-840, DOI: 10.1016/0020-7225(93)90096-D

[3] Aksouh, A., Mataoui, A., Seghouani, N., Haddad, Z. (2010) Assessment of performance of low reynolds turbulence models in predicting natural convection, In: *V. European Conference on Computational Fluid Dynamics ECCOMAS CFD 2010*, Lisbon, Portugal, 14-17 June 2010

[4] Aksouh, A., Mataoui, A., Seghouani, N., Haddad, Z. (2011) Rayleigh number effect on the turbulent heat transfer within a parallelepiped cavity, *Thermal Science*, Vol. 15(2), pp. 341-356, DOI: 10.2298/TSCI110201114A

[5] ANSI/ASHRAE Standard 140-2011 Building Thermal Envelope and Fabric Load Test, DesignBuilder Version 4.2 (incorporating EnergyPlus 8.1.0), 2014

[6] ANSYS FLUENT Theory Guide, Release 13.0, ANSYS, inc. Southpointe, 275 Technology Drive Canonsburg, PA 15317, ansysinfo@ansys.com, http://www.ansys.com, USA, 2010

[7] Ammour, D., Iavocides, H., Craft, T.J. (2011) Model validation od buoyancy-driven flows inside differentially heated cavities, In: *Proc. 12th UK National Heta Transfer Conference, Leeds, UK, 2011.*

[8] Amussen, T. F., Santos, I., Svendsen, S., Vanhoutteghem, L. (2009) Program to Optimize the Selection of Windows in Dwellings: WinDesign, In: *50 years of research and education on thermal insulation of buildings, Department of Civil Engineering*, Technical University of Denmark, DTU Byg Report R2009, pp. 34-35, e-print: http://www.byg.dtu.dk/~/media/Institutter/Byg/publikationer/byg_rapporter/byg_r209.ashx?la=da

[9] Ascione F., Bianco N., de' Rossi F., Turni G., Vanoli G. P. (2012) Different methods for the modelling of thermal bridges into energy simulation programs, Comparisons of accuracy for flat heterogeneous roofs in Italian climates, *Applied Energy*, Vol. 97, pp. 405−418, DOI: 10.1016/j.apenergy.2012.01.022

[10] ASTM E903-12 (2012) Standard Test Method for Solar Absorptance, Reflectance, and Transmittance of Materials Using Integrating Spheres, DOI: 10.1520/E0903-12

[11] ASTM G173-03 (2012) Standard Tables for Reference Solar Spectral Irradiances: Direct Normal and Hemispherical on 37° Tilted Surface, DOI: 10.1520/G0173-03R12

[12] Bakonyi, D., Becker, G. (2010) The building physics consequences of the replacement of box type windows (in Hungarian), In: Horváth Sándor, Pataky Rita (ed.) *I. Épületszerkezeti Konferencia Gábor László professzor születésének 100. évfordulója tiszteletére*, Budapest, Hungary, 2010.11.25, pp. 76-83, ISBN: 978-963-313-017-9

[13] Bakonyi D., Becker G. (2011) The heat transfer coefficient of traditional box type windows respecting the effects of the window-to-wall interface (in Hungarian) In: Horváth S., Pataky R. (Eds.) *II. Épületszerkezettani konferencia: épület- és szerkezetfelújítás, Deparment of Building Constructions*, Budapest University of Technology and Economics, Budapest, Hungary, 21-22. November 2011, pp. 10−18, ISBN: 978-963-313-043-8

[14] Bakonyi, D., Becker, G. (2012) The heat transfer in insulating glass units depending on the incidence angle (in Hungarian) In: Pataky, R., Horváth, S. (ed.) *III. Épületszerkezeti Konferencia: Környezettudatos építés szerkezetei*, Budapest, Hungary, 2012.11.20., pp. 58-63, ISBN:978-963-313-067-4

[15] Bakonyi, D. (2013) The role of thermal bridges in reducing the energy usage of buildings with valuable historical facades (in Hungarian), In Horváth, S., Pataky, R. (Eds.) *IV. Épületszerkezettani konferencia, Vízszigetelések*, Department of Building Constructions, Budapest University of Technology and Economics, Budapest, Hungary, 19 November 2013, pp. 100−107, ISBN: 978-963-313-092-6

[16] Bakonyi, D., Becker, G. (2014) Possibilities of simulations in the planning of the retrofit of historical double skin windows, *Advanced Materials Research Journal*, Vol. 899, pp. 155-160, DOI: 10.4028/www.scientific.net/AMR.899.155

[17] Bakonyi, D., Dobszay G. (2014) A proposed methodology for the improvement of the simplified calculation of thermal bridges for well typified facades, *Periodica Polytechnica, Civil Engineering*, Vol. 58, pp. 309−318, DOI: 10.3311/PPci.7215

[18] Bakonyi, D.; Becker, G. (2014) Building Physics Simulation in Practice (in Hungarian) In: Pataky, R.; Horváth, S. (ed.) *V. Épületszerkezeti Konferencia Épületfizika, Budapest*, Hungary, 2014.11.25., pp. 132-150, ISBN:978-963-313-129-9

[19] Bakonyi, D., Dobszay, G. (2016) Simulation aided optimization of a historic window's refurbishment, *Energy and Buildings*, In Press, Accepted Manuscript, DOI: 10.1016/j.enbuild.2016.05.005

[20] Bakonyi, D., Dobszay, G. (2016) Simplified calculation of non-repeating thermal bridges of the typical Central-European small suburban houses, *Pollack Periodica*, under review

[21] Bakonyi, D., Dobszay, G. (2016) Thermal models for box type windows – Part 1: A review of the flow characteristics and convective heat transfer calculation of very large glazing cavities, *Periodica Polytechnica-Architecture*, under review

[22] Bakonyi, D., Dobszay, G. (2016) Thermal models for box type windows – Part 2: A new dedicated correlation for predicting convective heat transfer in the very large glazing cavities of box type windows, *Periodica Polytechnica-Architecture*, under review

[23] Batchelor, G. (1954) Heat transfer by free convection across a closed cavity between vertical boundaries at different temperatures, *Quarterly of Applied Mathematics*, Vol. 12, pp. 209-233, ISSN: 0033-569X

[24] Berggren, B., Wall, M. (2013) Calculation of thermal bridges in (Nordic) building envelopes – Risk of performance failure due to inconsistent use of methodology, *Energy and Buildings*, Vol. 65, pp. 331-339, DOI: 10.1016/j.enbuild.2013.06.021

[25] Betts, P.L.; Dafa'Alla, A.A. (1996) Experimental study of turbulent natural convection in a tall air cavity, *Exp. Heat Transfer*, Vol. 9, pp. 165-194, DOI: 10.1080/08916159608946520

[26] Betts, P.L.; Bokhari, I.H. (2000) Experiments on turbulent natural convection in an enclosed tall cavity, *International Journal of Fluid Flow*, Vol. 21, pp. 675-683, DOI: 10.1016/S0142-727X(00)00033-3

[27] Blanusa, P., Elmahdy, H., Goss, W., Jensen, C., Roth, H., Svendsen, S., Weitzmann, P. (2007) Comparison between ASHRAE and ISO thermal transmittance calculation methods, *Energy and Buildings*, Vol. 39, pp. 374-384., DOI: 10.1016/j.enbuild.2006.09.007

[28] Brumă B., Moga L., Moga I. (2016) Aspects regarding dynamic calculation of plan building elements having thermal bridges, *Energy Procedia*, Vol. 85, pp. 77−84, DOI: 10.1016/j.egypro.2015.12.276

[29] Burthene, S., Jacob, G. P., Henze, G. P. (2010) Uncertainty analysis in building simulation with monte carlo techniques, In*: SimBuild 2010 - Fourth National Conference of IBPSA*, IBPSA, pp. 419-426, e-print: http://www.ibpsa.us/pub/simbuild2010/papers/SB10-DOC-TS08B-01-Burhenne.pdf

[30] Caciolo, C., Marchio, D., Stabat, P. (2009) Survey of the Exisitng Approaches to assess and design natural ventilation and need for further development, In: *Eleventh International IBPSA Conference*, Glasgow, Scottland, July 27-30, pp. 220-227, e-print: https://hal.inria.fr/file/index/docid/574589/filename/BS09_0220_227-2.pdf

[31] Campolongo, F., Cariboni, J., Saltelli, A. (2007) An effective screening design for sensitivity analysis of large models, *Environmental Modelling and Software*, Vol. 22, pp. 1509–1518, DOI: 10.1016/j.envsoft.2006.10.004

[32] Campolongo, F., Saltelli, A., Cariboni, J. (2011) From screening to quantitative sensitivity analysis. A unified approach, *Computer Physics Communications*, Vol. 182, pp. 978-988, DOI: 10.1016/j.cpc.2010.12.039

[33] Carciolo, M., Stabat, P., Marchio, D. (2011) Full scale experimental study of single-sided ventilation: Analysis of stack and wind effects, *Energy and Buildings*, Vol. 43, pp. 1765–1773, DOI: 10.1016/j.enbuild.2011.03.019

[34] Carlson, W., Eckert, E. (1961) Natural convection in an air layer enclosed between two vertical plates with different temperatures, *International Journal of Heat and Mass Transfer*, Vol. 2, pp. 106-110, ISSN: 0017-9310

[35] Chen, K., Wung, T., Yin, S. (1978) Natural convection in an air layer enclosed with rectangular cavities, *International Journal of Heat and Mass Transfer*, Vol. 21, pp. 307-315, ISSN: 0017-9310

[36] Chen, Q., Xu. W. (1998) A zero-equation turbulence model for indoor airflow simulation, *Energy and Buildings*, Vol. 28, pp. 137-144, DOI: 10.1016/S0378-7788(98)00020-6

[37] Citterio, M., Cocco, M., Erhorn-Kluttig, H. (2008) Thermal bridges in the EBPD context: overview on MS approaches in regulations, ASIEPI, e-print: http://www.buildup.eu/sites/default/files/P064_EN_ASIEPI_WP4_IP1_p3073.pdf

[38] Dascalaki E., Santamouris M., Argiriou T A., Helmis, C., Soilemes A. (1995) Predicting Single Sided Natural Ventilation Rates In Buildings, In: Solar Energy, Vol. 55, pp. 327-341, DOI: 10.1016/0038-092X(95)00057-X

[39] Davidson, L., Nielsen, P.V., Sveningsson, A. (2003) Modification of the V2F model for computing the flow in a 3d wall jet, *Turbulence Heat and Mass Transfer*, Vol. 4, pp. 577-584

[40] De Gids, W., Phaff, H. (1982) Ventilation rates and energy consumption due to open windows: A brief overview of research in the Netherlands, *Air infiltration review*, Vol. 4(1), pp. 4-5.
[41] DIN 4108-2 (2003) Wärmeschutz und Energie-Einsparung in Gebäuden - Teil 2: Mindestanforderungen an den Wärmeschutz
[42] DIN 4108-2 Beiblatt 2 (2006) Wärmeschutz und Energie-Einsparung in Gebäuden - Wärmebrücken - Planungs- und Ausführungsbeispiele
[43] DOE-2 Reference Manual, Lawrence Berkeley National Laboratory, http://doe2.com/doe2/
[44] Durbin, P. A. (1995) Separated Flow Computations with the k-epsilon-v2 Model, In: *AIAA Journal*, Vol. 33, pp. 659–664., DOI: http://dx.doi.org/10.2514/3.12628
[45] D&R International (2013) Residential Windows and Window Coverings: A Detailed View of the Installed Base and User Behavior, D&R International, Ltd., Silver Spring, MD, February 2013
[46] Eisenhower, B., O'Neill, Z., Fonoberov, V. A., Mezic, I. (2012) Uncertainty and sensitivity decomposition of building energy models, Journal of Building Performance Simulation, Vol. 5, pp. 171-184, DOI: 10.1080/19401493.2010.549964
[47] Elder, J. (1995) Laminar free convection in a vertical, *Journal of Fluid Mechanics*, Vol. 23, pp. 77-98, DOI: 10.1017/S0022112065001246
[48] Ellis, P.G., Torcellini, P.A. Crawley, D.B. (2007) Simulation of Energy Management Systems in EnergyPlus, In: *Proceedings of Building Simulation 2007*, Beijing, China, e-print: http://www.nrel.gov/docs/fy08osti/41482.pdf
[49] El Moutaouakil, L., Zrikem, Z., Abdelbaki, A. (20054) Performance of various RANS eddy-viscosity models for turbulent natural convection in tall vertical cavities, *Heat and Mass Transfer*, Vol. 50, pp. 1103-1113, DOI: http://dx.doi.org/10.1007/s00231-014-1322-4
[50] ElSherbiny, S., Hollands, K., Raithby, G. (1982) Effect of thermal boundary conditions on natural convection in vertical and inclined air layers, *Journal of Heat Transfer*, Vol. 104, pp. 515-520, ISSN: 0022-1481
[51] ElSherbiny, S., Hollands, K., Raithby, G. (1982) Effect of the Thermal Boundary Condition on Natural Convection in Vertical and Inclined Air Layers, In: *Transaction of the ASME*, Fla., July 27-30, pp. 96-102
[52] EN 410 (2011) Glass in building. Determination of luminous and solar characteristics of glazing
[53] EN 673 (2011) Glass in building. Determination of thermal transmittance (U value). Calculation method
[54] EN 1026 (2000) Windows and doors. Air permeability. Test method.
[55] EN 1027 (2000) Windows and doors. Watertightness. Test method.
[56] EN 10077-1 (2006) Thermal performance of windows, doors and shutters - Calculation of thermal transmittance - Part 1: General
[57] EN 10077-2 (2012) Thermal performance of windows, doors and shutters - Calculation of thermal transmittance - Part 2: Numerical method for frames
[58] EN 12211 (2000) Windows and doors. Resistance to wind loads. Test method.
[59] EN ISO 6946 (2007) Building components and building elements -- Thermal resistance and thermal transmittance -- Calculation method
[60] EN ISO 8990 (1994) Thermal insulation. Determination of steady-state thermal transmission properties. Calibrated and guarded hot box.
[61] EN ISO 10211 (2011) Thermal bridges in building construcions – Heat flows and surface temperatures – Detailed calculations
[62] EN ISO 12207 (2008): Windows and Doors. Air permeability. Classification
[63] EN ISO 12567 (2010) Thermal performance of windows and doors. Determination of thermal transmittance by the hot-box method. Part 1: Complete windows and doors
[64] EN ISO 13789 (2007) Thermal performance of buildings -- Transmission and ventilation heat transfer coefficients -- Calculation method
[65] EN 15026 (2007) Hygrothermal performance of building components and building elements. Assessment of moisture transfer by numerical simulation.
[66] EN 15251 (2007) Indoor environmental input parameters for design and assessment of energy performance of buildings- addressing indoor air quality, thermal environment, lighting and acoustics
[67] EnergyPlus version 8.0 Engineering Reference, U.S. Department of Energy
[68] Energy System Research Unit (2002)The ESP-r System for Building Energy Simulation, User Guide Version 10 Series, University of Strathclyde
[69] European Research Community on Flow, Turbulence and Combustion Database, http://cfd.mace.manchester.ac.uk/cgi-bin/cfddb/prpage.cgi?79&EXP&database/cases/case79/Case_data&database/cases/case79&c

as79_head.html&cas79_desc.html&cas79_meth.html&cas79_data.html&cas79_refs.html&cas79_rsol.html&1&0&0&0&0

[70] European Parliament (2002) EPBD - Directive 2002/91/EC of the European Parliament and of the Council of 16 December 2002 on the energy consumption of buildings

[71] Evola G., Margani G., Marletta L. (2011) Energy and cost evaluation of thermal bridge correction in Mediterranean climate, *Energy and Buildings*, Vol. 43, pp. 2385−2393, DOI: 10.1016/j.enbuild.2011.05.028

[72] Firląg, S., Yazdanian, M., Curcija, C., Kohler, C., Vidanovic, S., Hart, R., Czarnecki, S. (2015) Control algorithms for dynamic windows for residential buildings, *Energy and Buildings*, Vol. 109, pp. 157-173, DOI: 10.1016/j.enbuild.2015.09.069

[73] Furler, R. A. (1991) Angular Dependence of Optical Properties of Homogeneous Glasses, In ASHRAE Transactions, Vol. 97 (2)

[74] Ganguli, A.A.; Pandit, A.B.; Joshi, J.B. (2009) CFD simulation of heat transfer in a two-dimensional vertical enclosure, *Chemical Engineering Research and Design*, Vol. 87, pp. 711-727, DOI: http://dx.doi.org/10.1016/j.cherd.2008.11.005

[75] Gärtner, M., Gerner, D. (1196) Historische Fenster. Entwicklung, Technik, Denkmahlpflege, Verlag Deutsche Verlags-Anstalt DVA, Stuttgart, ISBN: 3421031045

[76] Gibson, M.M., and B.E. Launder. (1978) Ground Effects on Pressure Fluctuations in the Atmospheric Boundary Layer, *J. Fluid Mech*, Vol. 86, pp. 491-511, DOI: http://dx.doi.org/10.1017/S0022112078001251

[77] Gough, M., Rees, C. (2004) Tests performed on ApacheSim in accordance with ANSI/ASHRAE Standard 140-2001, ApacheSim Version 5.2, IES Ltd., Glasgow, UK

[78] Grosso, M. (1992) Wind pressure distribution around buildings: a parametrical mode, *Energy and Buildings*, Vol. 18, pp. 101-131, DOI: 10.1016/0378-7788(92)90041-E

[79] Gustavsen, A. (2001) Heat Transfer in Window Frames with Internal Cavities, PhD Thesis, Department of Building and Construction Engineering, Faculty of Civil and Environmental Engineering, Norwegian University of Science and Technology, Trondheim, Norway

[80] Gustavsen, A., Arasteh, D., Jelle, B., Curcija, C., Kohler, C. (2008) Developing Low-Conductance Window Frames: Capabilities and Limitations of Current Window Heat Transfer Design Tools, *Journal of Building Physics*, Vol. 32, pp. 131-153, ISSN: 1744-2591, DOI: 10.1177/1744259108097672

[81] Hanam, B., Finch, G., Hayes, S. (2013) Energy Ratings for Windows: Balancing Energy Consumption and Thermal Comfort, In: Thermal Performance of the Exterior Envelopes of Whole Buildings XII International Conference, e-print: http://rdh.com/wp-content/uploads/2014/04/Energy-Ratings-for-Windows-Balancing-Energy-Consumption-and-Thermal-Comfort.pdf

[82] Heinriger, R.H., Writte, J.W. (2003) EnergyPlus Testing with ANSI/ASHRAE Standard 140-2001 (BESTEST). EnergyPlus Version 1.1.0.020., Ernest Orlando Lawrence Berkeley National Laboratory, Berkeley, California, 1028 Busse Highway, Park Ridge, Illinois 60068, USA

[83] Heisenberg, P. K., Brohus, H. (2008) Sensitivity Analysis Applied in Design of Low Energy Office Building, In: The 29th AIVC Conference in 2008, Advanced building ventilation and environmental technology for addressing climate change issues, 14-16 October 2008, Kyoto Japan, Vol. 2, pp. 33-40, e-print: http://vbn.aau.dk/files/16607988/Sensitivity_Analysis_Applied_in_Design_of_Low_Energy_Office_Building

[84] Hollands, K. G. T., Unny, T. E., Raithby, G. D., Konicek, L. (1976) Free Convection Heat Transfer Across Inclined Air Layers, *Journal of Heat Transfer*, Vol. 98, pp. 189-193, DOI: 10.1115/1.3450517

[85] Holste, F., Urban, A., Wilken, M. (1996) *Erhaltung der Kastenfenster durch gezielte Verbesserungsmaßnahmen*, Report: Für das Bundesministerium für Raumordnung, Bauwesen und Städtebau (BM Bau), Bonn, IFT Rosenheim, ISBN: 978-3-8167-4778-9

[86] Homb, A., Uvslok, S. (2012) Energy Efficient Windows with cultural value, Measurements and calculations, Technical Report, SINTEF Byggforsk

[87] Hsieh, K.J.; Lien, F.S. (2004) Numerical modeling of buoyancy-driven turbulent flows in enclosures, *International Journal of Heat and Mass flow*, Vol. 24, pp. 659-670, DOI: http://dx.doi.org/10.1016/j.ijheatfluidflow.2003.11.023

[88] Hutchins, M.G., Topping, A.J., Anderson, C., Olive, F., van Nijnatten, P., Polato, P., Roos, A., Rubin, M. (2001) Measurement and prediction of angle-dependent optical properties of coated glass products: results of an inter-laboratory comparison of spectral transmittance and reflectance, *Thin Solid Films*, Vol. 392, pp. 269-275, DOI: 10.1016/S0040-6090(01)01042-2

[89] IFT Rosenheim: Energy Label Fenster – Einfache Kennzeichnung von Fenstern zur Verbraucherinformation, https://www.ift-rosenheim.de/documents/10180/138181/PI1110103.pdf/9b0e4bb4-654f-4d68-8541-5a20e764fdde, accessed on: March 30, 2016
[90] Ince, N., Launder, B. (1989) On the computation of buoyancy driven turbulent flows in rectangular enclosures, *International Journal of Heat Fluid Flow*, Vol. 10, pp. 110–117, DOI: 10.1016/0142-727X(89)90003-9
[91] International Energy Agency (2011) Issues Paper for Policy pathway for windows and other glazed areas, 6 July 2011, Paris, e-print: https://www.iea.org/workshops/policy-pathways-energy-efficiency-in-windows-and-other-glazed-areas---060711.html
[92] ISO 7730 (2005) Ergonomics of the thermal environment -- Analytical determination and interpretation of thermal comfort using calculation of the PMV and PPD indices and local thermal comfort criteria
[93] ISO 9050 (2003) Glass in building -- Determination of light transmittance, solar direct transmittance, total solar energy transmittance, ultraviolet transmittance and related glazing factors
[94] ISO 9845-1 (1992) Solar energy – Reference solar spectral irradiance at the ground at different receiving conditions – Part 1: Direct normal and hemispherical solar irradiance for air mass 1,5
[95] ISO 10292 (1994) Glass in building. Calculation of steady-state U values (thermal transmittance) of multiple glazing
[96] ISO 13790 (2008) Energy performance of buildings -- Calculation of energy use for space heating and cooling
[97] ISO 15099 (2003) Thermal performance of windows, doors and shading devices - Detailed calculations
[98] ISO 18292 (2011) Energy performance of fenestration systems for residential buildings -- Calculation procedure
[99] Jakob, M. (1967) *Heat Treansfer*, Vol. 1, Wiley, New York, 1967, pp. 536-539.
[100] Janssens, A., De Paepe, M. (2005) Effect of moisture inertia models on the predicted indoor humidity in a room, In: *26th AIVC Conference*, Brussels, 21-23 September 2005, e-print: http://www.kuleuven.be/bwf/projects/annex41/protected/data/UG%20Oct%202005%20BGinf%20A41-T1-B-05-2.pdf
[101] Judkoff, R.; Neymark, J. (1995) Inetarnational Energy Agency Building Energy Simulation Test (BESTEST) and Diagnostic Method, National Renewable Energy Laboratory, Golden, Colorado, NREL/TP-472-6231
[102] Kakasy, L. (2012) Reducing the energy usage of building from the turn of the century with valuable facades (in Hungarian), *Magyar Építőipar*, Vol. 65, pp. 52-58
[103] Karlsson, J., Karlsson, B., Roos, A. (2007) A simplified model for assessing the energy performance of windows, *Energy and Buildings*, Vol. 33, pp. 641–651, DOI: 10.1016/S0378-7788(00)00131-6
[104] Kayne, A.; Agarwal, R. K. (2013) Computational fluid dynamics modeling of mixed convection flows in buildings enclosures, *International Journal of Energy and Environment*, Vol. 4, pp. 911-932, DOI: http://dx.doi.org/10.1115/ES2013-18026
[105] Kehrer, M; Schmidt, T. (2008) Radiation Effects On External Surfaces, In: *Building Physics 2008 – 8th Nordic Symposium*, pp. 207-212
[106] Kemény, M. (2016) A Brief Architectural History of the Palace of the Academy, http://mta.hu/english/about-mta-105677, last accessed on March 03 2016
[107] Klems, J. H.(1993) A New Method for Predicting the Solar Heat Gain of Complex Fenestration Systems – I. Overview and Derivation of the Matrix Layer Calculation, In: ASHRAE Transactions, Vol. 100(1), pp. 1065-1072
[108] Klems, J. H.(1993) A New Method for Predicting the Solar Heat Gain of Complex Fenestration Systems – II. Detailed Description of the Matrix Layer Calculation, *ASHRAE Transactions*, Vol. 100(1), pp. 1073-1086
[109] Klems, J. H.(1995) Measurements of Bidirectional Optical Properties of Complex Shading Devices, *ASHRAE Transactions*, Vol. 101, pp. 791-801
[110] Klems, J. H.(1996) Calorimetric Measurements of Inward-Flowing Fraction for Complex Glazing and Shading Systems, *ASHRAE Transactions*, Vol. 102, pp. 947-954
[111] Korpella, S., Lee, Y. (1983) Multicellular Natural Convection in a Vertical Slot, *Journal of Fluid Mechanics*, Vol. 126, pp. pp. 91-121, DOI: http://dx.doi.org/10.1017/S0022112083000063
[112] Kumar, S.: Investigation of 3D Heat Transfer Effect in Fenestration Products, MSc Thesis, University of Massachusetts Amherst, 2010

[113] Kuntner, F (2011) The possibilities and limits of the internal thermal insulation of buildings with valuable facades, Thesis for the degree of specialist thermal insulation and waterproofing engineer, Budapest University of Technology and Economics, Budapest, Hungary

[114] Künzel, H. M. (2004) Energetische Altbausanierung durch Innendämmung, *WTA Journal*, Vol. 4, pp. 361-374, e-print: http://www.hoki.ibp.fraunhofer.de/ibp/publikationen/fachzeitschriften/WTA_Journal_Innendaemmung.pdf

[115] Künzel, H. M. (1994) Verfahren zur ein- und zweidimensionalen Berechnung des gekoppelten Wärme- und Feuchtetransports in Bauteilen mit einfachen Kennwerten, PhD Dissertation, Lehrstuhl für Bauphysik, Universität Stuttgart, Stuttgart, Germany, e-print: http://www.ibp.fraunhofer.de/content/dam/ibp/de/documents/hk_dissertation_tcm45-30727.pdf

[116] Lam, C. K. G., Bremhost, K. (1981) A modified form of the k-ε model for prediction of wall turbulence, In: *Transactions of ASME, Journal of Fluids Engineering*, Vol. 103, pp. 456-460.

[117] Larsen, T.S., Heiselberg, P. (2008) Single-sided natural ventilation driven by a combination of wind pressure and temperature difference, *Energy and Buildings*, Vol. 40, pp. 1031–1040., DOI: 10.1016/j.enbuild.2006.07.012

[118] Launder, B.E., and B.I. Sharma (1974) Application of the energy dissipation model of turbulence to the calculation of flow near a spinning disk, *Letters in Heat Mass Transfer,* Vol. 1, pp. 131-138, DOI: http://dx.doi.org/10.1016/0094-4548(74)90150-7

[119] Lawrence Berkeley National Laboratory: Therm Finite Element Simulator 7.3.2.0

[120] Lawrence Berkeley National Laboratory: Window 7.3

[121] Lien, F.S., Leschziner, M. A. (1999) Computational modeling of a transitional 3D turbine-cascade flow using a modified low-Re k–ε model and a multi-block scheme, *International Journal of Computational Fluid Dynamics*, Vol. 12, pp. 1–15., DOI: http://dx.doi.org/10.1080/10618569908940812

[122] Mach, T., Grobbauer, M., Götzhaber, W. (2013) Dankmalaktiv I – Sanierung alter, denkmalgeschützter Gebäude auf Aktivhausstandard?, Report, e-print: http://www.get.ac.at/tl_files/Download/Endberichte/Publizierbarer_Endbericht_denkmalaktiv_I_31052013.pdf

[123] Maestre, I.R., Molina, J.L., Roos, A., Coronel, J.F. (2007) A single-thin-film model for the angle dependent optical properties of coated glazings, *Solar Energy*, Vol. 81, Issue 8, pp. 969-976, DOI: 10.1016/j.solener.2006.12.002

[124] Mainini, A. G., Bonato, D., Poli, T., Speroni, A. (2014) Lean strategies for window retrofit of Italian office buildings: impact on energy use, thermal and visual comfort, In: *International conference on Solar Heating and Cooling for Buildings and Industry*, SHC 2014, Energy Procedia, Vol. 70, pp. 719-728, DOI: 10.1016/j.egypro.2015.02.181

[125] Marsh, A. (2005) The application of shading masks in building simulation, In: *Ninth International IBPSA Conference*, Montréal, Canada, August 15-15, pp. 725-732

[126] Michele, G. D., Oberegger, U. F., Baglivo, L. (2015) Coupling dynamic energy and daylighting simulations for complex fenestration systems, In: *Pre-prints of BSA 2015- Building Simulation Application*, e-print: http://www.eurac.edu/en/research/technologies/renewableenergy/publications/Documents/EURAC-RenEne_GDeMichele-UFilippiOberegger-LBaglivo_IBPSA-Italy2015.pdf

[127] Misiopecki, C., Gustavsen, A.: Numerical Simulation of Thermal Performance of Window Retrofit Options for Historic Buildings, In: 3rd *European Workshop on Cultural Heritage Preservation*, EWCHP 2013, pp. 195-202

[128] Menter, F. R. (1994) Two-Equation Eddy-Viscosity Turbulence Models for Engineering Applications, *AIAA Journal*, Vol. 32, pp. 1598-1605, DOI: http://dx.doi.org/10.2514/3.12149

[129] Morris, M. D. (1991) Factorial samplings plans for preliminary computational ex-periments, *Technometrics*, Vol. 33, pp. 161-174, DOI: 10.2307/1269043

[130] Nagy B. (2014) Comparative analysis of multi-dimensional heat flow modelling, In: *Proc. of 2nd Conference for PhD students in Civil Engineering*, Cluj-Napoca, Romania, pp. 468−476.

[131] Nagy B. (2015) Thermal calculation of ground contact structures, Correction factors of environment- and structure-dependent effects on the heat transfer coefficient, *International Journal of Computational and Experimental Science and Engineering*, Vol. 1, pp. 26−29.

[132] Neumann, H., Hinz, D., Müller, R., Schulze, J. (2003) *Fenster im Bestand - Grundlagen der Sanierung in Theorie und Praxis*, Expert Verlag, 1. Edition, ISBN: 3-8169-2203-1

[133] Newell, M. E., Schmidt, F. W.: Heat Transfer by Laminar Natural Convection Within Rectangular Enclosures, *Journal of Heat Transfer*, Vol. 92, pp. 159-165, DOI:10.1115/1.3449616

[134] Nikoofard, S.; Ugursal, V. I.; Beausoleil-Morrison, I. (2012) Effect of window modification on household energy requirement for heating and cooling in Canada, In: *Proceedings of eSim 2012: The Canadian Conference on Building Simulation*, Halifax, Nova Scotia, pp. 324-337

[135] NFRC 100-2010 (2010) Procedure for Determining Fenestration Product U-factors

[136] Nguyen, A-T., Reiter, S. (2015) A performance comparison of sensitivity analysis methods for building energy models, *Building Simulation*, Vol. 8, pp. 651-664, DOI. 10.1007/s12273-015-0245-4

[137] Orosz M., Csanaky J. (2015) Estimating the thermal bridge at wall corners with artificial neural network, *Acta Technica Jaurinensis*, Vol. 8, pp. 230−239.

[138] Perez, R., Ineichen, P., Seals, R., Michalsky, J., Stewart, R. (1990) Modeling daylight availability and irradiance components from direct and global irradiance, *Solar Energy*, Vol. 44, pp. 271–289, DOI: 10.1016/0038-092X(90)90055-H

[139] Petersen, S., Svendsen, S. (2010) Method and Simulation Program informed decision in the early stages of building design, *Energy and Buildings*, Vol. 42, pp.1113-1119, DOI: doi:10.1016/j.enbuild.2010.02.002

[140] Power, J.P., 1999, Finite Element Model of Turbulent Flow and Heat Transfer in a FenestrationSystem, Ph.D. Thesis, Department of Mechanical Engineering, University of Massachusetts Amherst.

[141] Prona AG (2011) Bauphysikgrundlagen zur Fensterkampagne „Fenster sind die Augen eines Hauses“ (in German), Report comissioned by: Heimatschutz Basel, Hardstrasse 45, Basel, Switzerland, e-print: http://www.heimatschutz-bs.ch/uploads/media/Bauphysikgrundlagen_Fensterkampagne.pdf

[142] Quinten J., Feldheim V. (2016) Dynamic modelling of multidimensional thermal bridges in building envelopes: Review of existing methods, application and new mixed method, *Energy and Buildings*, Vol. 110, pp 284-293, DOI: 10.1016/j.enbuild.2015.11.003

[143] Raitby, G. D., Wong, H. H. (1981) Heat transfer by natural convection across vertical air layers, *Numerical Heat Transfer*, Vol. 4, pp. 447-457, DOI: 10.1080/01495728108961803

[144] RDH Building Engineering Ltf. (2013) Review of Window Energy Rating Procedure in Canada, Final Research Report, January 2013, https://hpo.bc.ca/files/download/Report/Window-ER-Full-Report.pdf

[145] Reinhart, C., Bourgeois, D., Dubrous, F., Laouadi, A., Lopez, P., Stelescu, O. (2007) Daylight1-2-3 – A State-of-the-Art Daylighting/Energy Analysis Software for Initial Deisgn Investigations, In: *Proceedings of Building Simulation 2007 conference*, Beijing, China, September 3-6 2007, pp. 1669-1676

[146] Roels, S., Deurnick, M., Janssens, A., Van Orshoven, D. (2011), A pragmatic approach to incorporate the effect of thermal bridging within the EPBD-regulation, In: *Proceedings of the 9th Nordic Symposium on Building Physics - NSB 2011*, Tampere University of Technology, pp. 1009-1016, e-print: https://lirias.kuleuven.be/bitstream/123456789/313428/1/Paper+Nordic+Roels+Staf.pdf

[147] Rubin, M., Powles, R., Von Rottkay, K (1999) Models fort he angle-dependent optical properties of coated glazing materials, *Solar Energy*, Vol. 66, pp. 267-276, DOI: 10.1016/S0038-092X(99)00029-8

[148] Sanches, D. G., Lacarriere, B., Musy, M., Bourges, B. (2014) Application of sensitivity analysis in building energy simulations: Combining first- and second-order elementary effects methods, *Energy and Buildings*, Vol. 68, pp. 741-750, DOI: 10.1016/j.enbuild.2012.08.048

[149] Schrader, M. (2001) *Fenster, Glas und Beschläge als historisches Baumaterial*, Anderweit Verlag GmbH, Suderburg-Hösseringen, ISBN: 3-931824-04-7

[150] Schulze, J., Svendsen, S. (1998) WINSIM: A simple simulation program for evaluating the influence of windows on heating demand and risk of overheating; *Solar Energy*, Vol. 63, pp. 251-258., DOI: 10.1016/S0038-092X(98)00062-0

[151] Selkowitz, S., Mitchell, R., McClintock, M., McQuillen, M., McNeill, A.,Yazdanin, M. (2011) COMFEN 3.0 – Evolution of an Early Design Tool for Commercial Façade and Fenestration Systems, In: *Building Enclosure Sustainability Symposium (BESS) Conference 2011*, April 29-30 2011, Pomona, CA

[152] Sherman, M.H.; Grimsrud, D.T.(1980) Infiltration-pressurization correlation: Simplified physical modeling, *ASHRAE Transactions*, vol. 86, pp. 778-807

[153] Shewen, E. C., Hollands, K.G.T., Raithby, G.D. (1989) The Measurement of Surface Heat Flux Using the Peltier Effect, In: *Transaction of the ASME*, August 1989, Journal of Heat Transfer, Vol. 111, pp. 798-803, DOI: 10.1115/1.3250754

[154] Shewen, E. C., Hollands, K.G.T., Raithby, G.D. (1996) Heat Transfer by Natural Convection Across a Vertical Air Cavity of Large Aspect Ratio, *Journal of Heat Transfer*, Vol. 118, pp. 993–995, DOI: 10.1115/1.2822603

[155] Skou, M. B., Kragh, J. (2009) European energy labelling scheme for windows, In: *ECEEE 2009 summer study,* pp. 877-887, e-print: http://www.eceee.org/library/conference_proceedings/eceee_Summer_Studies/2009/Panel_4/4.150

[156] Sullivan, R., Chin, B., Arasteh, D., Selkowitz, S. E. (1992) RESFEN: A Residential Fenestration Performance Design Tool, In: *ASHRAE Conference*, January 26-29, Anaheim, CA

[157] Szalay, Zs. (2008) Modelling building stock geometry for energy, emission and mass calculations, *Building Research & Information*, Vol. 36, pp. 557-567, DOI: 10.1080/09613210802396429

[158] Talamon, A., Csoknyai, T (2011) Monitoring of a Performance oriented Policy Model for the Retrofit of Buildings Built with Prefabricated Technology, *Environmental Engineering & Management Journal*, Vol. 10, pp. 1355-1362

[159] Theodosius, T.G., Papadopoulos, A. M. (2008) The impact of thermal bridges on the energy demand of buildings with double brick wall constructions, *Energy and Buildings*, Vol. 40, pp. 2083-2089, DOI: http://dx.doi.org/10.1016/j.enbuild.2008.06.006

[160] The International Glazing Database, IGDB Versio 43.0, Lawrence Berkeley National Laboratory, http://windowoptics.lbl.gov/data/igdb

[161] The RADIANCE 4.2 Synthetic Imaging System, Reference Manual, Lawrence Berkeley National Laboratory

[162] TRNSYS 17, a TRaNsient System Simulation program

[163] Urbikain, M.K., Sala, J.M. (2009) Analysis of different models to estimate energy savings related to windows in residential buildings, *Energy and Buildings*, Vol. 41, 2009, pp. 687–695, DOI: 10.1016/j.enbuild.2009.01.007

[164] Van Den Bergh, S., Hart, R., Jelle, B. P., Gustavsen, A. (2013) Window spacers and edge seals in insulating glass units: A state-of-the-art review and future perspectives, *Energy and Buildings*, Vol. 58, pp. 263-280, DOI: 10.1016/j.enbuild.2012.10.006

[165] Verband Fenster und Fassade (VFF) (2003) HO.09 Runderneuerung von Kastenfenstern aus Holz, Report

[166] Warren, P.R., Parkins, L.M. (1985) Single sided ventilation through open windows, In: *Conference proceedings, thermal performance of the exterior envelopes of buildings, ASHRAE*, Clearwater Beach, FL, USA, pp. 209–228.

[167] Wei, F., Grunewald, J., Nicolai, A., Zhang, C., Zhang, J. S. (2012) CHAMPS-Multizone – A combined heat, air, moisture and pollutant simulation environment for whole-building performance analysis, *HVAC & Research*, Vol. 18, pp. 233-251, DOI: 10.1080/10789669.2011.587585

[168] Winklemann, F. C. (2001) Modeling windows in EnergyPlus, In: S*eventh International IBPSA Conference*, Rio de Janeiro, Brazil, August 13-15 2001, pp. 457-464

[169] Wright, J., Sullivan, H. (1989) Natural Convection in Sealed Glazing Units: A Review; *ASHRAE Transactions*, Vol.: 95, pp. 592-603

[170] Wright, J. (1996) A Correlation to Quantify Convective Heat transfer Between Vertical Window Glazings, *ASHRAE Transactions*, Vol.: 102., pp. 940-946

[171] Wright, J. (1998) A Simplified Numerical Method for Assessing the Condensation Resistance of Windows, *ASHRAE Transactions*, Vol.: 104, pp. 1222-1229

[172] Xaman, J., Álvarez, G., Lira, L., Estrada, C. (2005) Numerical study of heat transfer by laminar and turbulent natural convection in tall cavities of façade elements, *Energy and Buildings*, Vol. 37, pp. 787-794, DOI: 10.1016/j.enbuild.2004.11.001

[173] Yakhot, V., and S.A. Orszag (1986) Renormalization group analysis of turbulence, *Journal of Scientific Computing,* Vol. 1, pp. 3-51, DOI: http://dx.doi.org/10.1007/BF01061452

[174] Yang, Y.: Natural convection flow and heat transfer in vertical and inclined glazing cavities; MSc Dissertation: Department of Mechanical and Industrial Engineering, University of Massachusetts Amherst, 2003.

[175] Zhang, Z., Zhang, W., Zhai, Z., Chen, Q. (2007) Evaluation of Various Turbulence Models in Predicting Airflow and Trubulence in Enclosed Environments by CFD: Part-1: Summary of Prevalent Trubulence Models, *HVAC & Research*, Vol. 13, pp. 853-870, DOI: http://dx.doi.org/10.1080/10789669.2007.10391459

[176] Zhang, Z., Zhang, W., Zhai, Z., Chen, Q. (2007) Evaluation of Various Turbulence Models in Predicting Airflow and Trubulence in Enclosed Environments by CFD: Part-2: Comparison with

Experimental Data from the Literature, *HVAC & Research*, Vol. 13, pp. 871-886, DOI: http://dx.doi.org/10.1080/10789669.2007.10391460
[177] Zhao, Y., Goss, W., Curcija, D., Power, J. (1998) Improved Heat Transfer Correlations for Quantifying Laminar Natural Convection Across Fenestration Glazing Cavities, In: *Thermal Envelopes VII*, Clearwater, Florida, December 1998, pp. 397-403
[178] Zhao, Y., Goss, W., Curcija, D., Power, J. (1997) Predicting the Multicellular Flow Regime of Natural Convection in Fenestration Galzing Cavities; *ASHRAE Transactions*, Vol. 103, pp. 1009-1020